# FINAL REPORT

## Assessing the Impact of Maneuver Training on NPS Pollution and Water Quality

## SERDP Project SI-1339

December 2008

James M. Steichen
Kansas State University

Stacy L. Hutchinson
Kansas State University

Naiqian Zhang
Kansas State University

J. M. Shawn Hutchinson
Kansas State University

Charles (Jack) Oviatt
Kansas State University

Alan Anderson
ERDC-CERL

Timothy Keane
Kansas State University

Philip L. Barnes
Kansas State University


Strategic Environmental Research and Development Program

# Assessing the Impact of Maneuver Training on NPS Pollution and Water Quality

**SERDP Project Number: SI-1339**

Final Technical Report
December 2008

**Principal Investigators:**

James M. Steichen
Biological and Agricultural Engineering
Kansas State University

Stacy L. Hutchinson
Biological and Agricultural Engineering
Kansas State University

Naiqian Zhang
Biological and Agricultural Engineering
Kansas State University

**Other Research Scientists:**

J. M. Shawn Hutchinson
Geography
Kansas State University

Charles (Jack) Oviatt
Geology
Kansas State University

Alan Anderson
U.S. Army Corps of Engineers
ERDC-CERL

Timothy Keane
Landscape Architecture
and Regional and Community Planning
Kansas State University

Philip L. Barnes
Biological and Agricultural Engineering
Kansas State University

# REPORT DOCUMENTATION PAGE

*Form Approved*
*OMB No. 0704-0188*



**PLEASE DO NOT RETURN YOUR FORM TO THE ABOVE ORGANIZATION.**

| 1. REPORT DATE *(DD-MM-YYYY)* | 2. REPORT TYPE | 3. DATES COVERED *(From - To)* |
|---|---|---|
| 17-02-2009 | SERDP Final Report | Mar 2003 - Dec 2008 |

**4. TITLE AND SUBTITLE**

Assessing the Impact of Maneuver Training on NPS Pollution and Water Quality

**5a. CONTRACT NUMBER**

DACA 72-03-C-0014

**5b. GRANT NUMBER**

**5c. PROGRAM ELEMENT NUMBER**

**6. AUTHOR(S)**

Steichen, James, M. Hutchinson, Stacy, L. Zhang, Naiqian. Hutchinson, J, M, Shawn. Oviatt, Charles. Anderson, Alan. Keane, Timothy. Barnes, Philip L.

**5d. PROJECT NUMBER**

SI-1339

**5e. TASK NUMBER**

**5f. WORK UNIT NUMBER**

**7. PERFORMING ORGANIZATION NAME(S) AND ADDRESS(ES)**

Kansas State University
2 Fairchild Hall
Manhattan, KS 66506

**8. PERFORMING ORGANIZATION REPORT NUMBER**

**9. SPONSORING/MONITORING AGENCY NAME(S) AND ADDRESS(ES)**

Strategic Environmental Research and Development Program Office
901 N. Stuart Street, Suite 303
Arlington, VA 22203

**10. SPONSOR/MONITOR'S ACRONYM(S)**

SERDP

**11. SPONSOR/MONITOR'S REPORT NUMBER(S)**

**12. DISTRIBUTION/AVAILABILITY STATEMENT**

Approved for public release; distribution is unlimited

**13. SUPPLEMENTARY NOTES**

**14. ABSTRACT**

The objective of this work was to identify sources of nonpoint source pollution resulting from military activities, to assess the impact of this pollution on surface water quality, and to provide information for commanders to lessen the impact of training on water quality. Vehicle tracks prevent sheet flow of runoff to streams. Effectiveness of native grass in reducing nonpoint pollution was assessed on hillslopes. Using LIDAR elevation data, soil, and vegetation information, a GIS tool was developed to identify likely locations of gullies. A sediment concentration sensor was developed for use in streams. Sensor data was recorded using wireless communication technology. Impact of constructed low-water fords on stream stability was assessed. Recommendations for location and design of low-water fords are provided.

**15. SUBJECT TERMS**

nonpoint pollution, sediment concentration sensor, fords, wireless data collection, GIS models, native grass buffer, stream equilibrium

| 16. SECURITY CLASSIFICATION OF: | | | 17. LIMITATION OF ABSTRACT | 18. NUMBER OF PAGES | 19a. NAME OF RESPONSIBLE PERSON |
|---|---|---|---|---|---|
| a. REPORT | b. ABSTRACT | c. THIS PAGE | UU | 231 | 19b. TELEPHONE NUMBER *(Include area code)* |

Reset

**Post-doctoral Fellows and Research Associates:**

Reid Christianson, Biological and Agricultural Engineering, Kansas State University
Amy Good-St. Claire, Biological and Agricultural Engineering, Kansas State University
Ik-Jae Kim, Biological and Agricultural Engineering, Kansas State University
Sanjayan Satchithanantham, Biological and Agricultural Engineering, Kansas State University

**Graduate Students:**

Erik Bowles, Geography, Kansas State University
Tony Davis, Geography, Kansas State University
Wei Han, Biological and Agricultural Engineering, Kansas State University
Melissa Ingrisano, Biological and Agricultural Engineering, Kansas State University
Peng Li, Biological and Agricultural Engineering, Kansas State University
Gilbert Malinga, Biological and Agricultural Engineering, Kansas State University
Quentin Stoll, Biological and Agricultural Engineering, Kansas State University
Thomas J. Vought, Jr., Geography, Kansas State University
Ben White, Geography, Kansas State University
Yali Zhang, Biological and Agricultural Engineering, Kansas State University

**Approved for public release; distribution is unlimited**

This report was prepared under contract to the Department of Defense Strategic Environmental Research and Development Program (SERDP). The publication of this report does not indicate endorsement by the Department of Defense, nor should the contents be construed as reflecting the official policy or position of the Department of Defense. Reference herein to any specific commercial product, process, or service by trade name, trademark, manufacturer, or otherwise, does not necessarily constitute or imply its endorsement, recommendation, or favoring by the Department of Defense.

# TABLE OF CONTENTS

**Page**

# TABLES

**Page**

# FIGURES

## ACRONYMS

| Acronym | Definition |
|---|---|
| 3G | Third generation |
| ADC | Analog to digital convertor |
| AVHRR | Advanced Very High Resolution Radiometer |
| BMPs | Best Management Practices |
| BWA | Broadband wireless access |
| C | cover management |
| c.v. | Coefficient of variation |
| CC | Canopy Cover |
| CDMA | Code-Division Multiple Access |
| CF | Compact flash |
| CRP | Conservation Reserve Program |
| CWSI | Idso-Jackson crop water stress index |
| DAQ | Data acquisition system |
| DEMs | Digital elevation models |
| DGPS | Differential global positioning system |
| EDGE | Enhanced Data-rate GSM Evolution |
| EOS | Earth Observing System |
| EROS | Earth Resources Observation & Science |
| ESRI | Environment System Research Institute |
| FTP | File transfer protocol |
| GAP | Kansas GAP Land Cover data |
| GIS | Geographic Information Systems |
| GLM | General linear model |
| GPRS | General Packet Radio Service |
| GPS | Global positioning system |
| GSM | Global system for mobile communication |
| HEG | HDF-EOS to GeoTIFF Conversion Tool |
| HUC | Hydrologic Unit Code |
| IDW | Inverse Distance Weighted |
| $I_{int}$ | Intensity index |
| $I_p$ | Precipitation intensity |
| IR | Infrared |
| ISM | Industrial, scientific, and medical |
| ITAM | Integrated Training and Management |
| JTAG | Joint test action group |
| K | Soil Erodibility |
| L | overland flow |
| LAN | Local area network |
| LED | Light-emitting diode |
| $L_R$ | Loss ratio |
| LRAM | Land Rehabilitation and Maintenance |
| LS | Slope Length and Steepness |
| LST | Land Surface Temperature |
| LWSC | Low water scream crossing |

MODIS ..... Moderate Resolution Imaging Spectroradiometer
NASA ..... National Aeronautics and Space Administration
NDVI ..... Normalized Difference vegetation Index
NED ..... National Elevation Data
NEPA ..... National Environmental Policy Act of 1969
NHD ..... National Hydrography Dataset
NIR ..... Near infrared
nLS model ..... GIS-enabled kinematic wave model
NPS ..... non-point source
NRCS ..... Natural Resource Conservation Service
$N_S$ ..... Actual number of data packets received during a period
NSF ..... National Science Fundation
$N_T$ ..... Number of data packets theoretically transmitted during a period
OBS ..... Optical backscatter
OPTIMO ..... Optical Technology for Intelligent Monitoring Online
P ..... Support practice factor
PCMCIA ..... Personal computer memory card international association
PDOP ..... Position Dilution of Precision
Plu ..... Prior Land Use
$P_r$ ..... Recorded precipitation
PT ..... Phototransistors
PTE ..... Pollutant trapping efficiencies
r ..... Pearson correlation coefficient
R ..... Rainfall and runoff erosivity
REMM ..... Riparian Ecosystem Management Model
RMSE ..... Root mean square error
RTLA ..... Range and Training Land Assessment
RUSLE ..... Revised Universal Soil Loss Equation
S ..... Sediment concentration
s.d. ..... Standard deviation
$S_c$ ..... Cumulative sediment concentration
SCS ..... Soil Conservation Service
SDDS ..... Seamless Data Distribution System
SERDP ..... Strategic Environmental Research and Development Program
SQL ..... Structured query language
SR ..... Spatial resolution
Sr ..... Surface Roughness
SRA ..... Sustainable Range Awareness
SSC ..... Suspended sediment concentration
SSURGO ..... Soil Survey Geographic
SWAT ..... Soil and Water Assessment Tool
T ..... Turbidity
$T_D$ ..... Duration of the observation period in seconds
TINs ..... Triangular irregular networks
TMDLs ..... Total maximum daily loads
TRI ..... Training Requirements Integration

$T_S$ ..... Sampling interval in seconds
TSS ..... Total suspended solids
TTD ..... Total Training Days
TWR ..... Time of Waiting for Restart
USDA ..... United States Department of Agriculture
USLE ..... Universal Soil Loss Equation
UWB ..... Ultra-wideband
VIT ..... Vegetation Index-Temperature
WDT ..... Watchdog timer
WEPP ..... Water Erosion Prediction Project
WiMAX ..... Worldwide Interoperability for Microwave Access
WLAN ..... Wireless local area networks
WSN ..... Wireless sensor network

## ABSTRACT

The objectives of this work were to identify sources of nonpoint source pollution resulting from military activities, to assess the impact of this pollution on surface water quality, and to provide information for commanders to lessen the impact of training on water quality. Vehicle tracks prevent sheet flow of runoff to streams. Effectiveness of native grass in reducing nonpoint pollution was assessed on hillslopes. Using LIDAR elevation data, soil, and vegetation information, a GIS tool was developed to identify likely locations of gullies. A sediment concentration sensor was developed for use in streams. Sensor data were recorded using wireless communication technology. Impact of constructed low-water fords on stream stability was assessed. Recommendations for location and design of low-water fords are provided.



Key words: nonpoint pollution, sediment concentration sensor, fords, wireless data collection, GIS models, native grass buffer, stream equilibrium.



## ACKNOWLEDGEMENTS

We thank the Department of Defense Strategic Environmental Research and Development Program (SERDP) for the financial support that made this research project possible. Appreciation for technical assistance is extended to Mr. Bradley Smith, SERDP Executive Director and Dr. Robert Holst, Sustainability Infrastructure Program Manager when we started our research. This fine support continued through the end of the project when Dr. Jeffrey Marqusee was SERDP Executive Director and Dr. John Hall was the Sustainability Infrastructure Program Manager. We appreciate the HydroGeoLogic, Inc. staff that provided administrative assistance.

This research also depended upon the support of Fort Riley, especially the Integrated Training Area Management (ITAM) Program and Dr. Philip B. Woodford, the coordinator of ITAM at Fort Riley and the project COR. In addition we recognize Chris Otto, Monte Cales, Troy Livingston, Tony Davis and the rest of the ITAM staff for helping Kansas State University faculty and graduate students conduct field research under realistic conditions on an active Army training post. We appreciate the effort and patience that made this work possible.

We also recognize the assistance of Biological and Agricultural Engineering staff including Darrell Oard, research lab manager and especially Lou Ann Claassen, who produced this final report.

# 1.0 Objectives

The objectives of this work are to identify sources of NPS pollution resulting from military activities, to assess the impact of this pollution on surface water quality and to provide information for commanders to lessen the impact of training on water quality.

This research project was conducted in response to SERDP Statement of Need (SON) number CPSON-03-02: Characterizing and Monitoring Non-Point Source Runoff from Military Ranges and Identifying Their Impacts to Receiving Water Bodies.

The objectives of this SON are to provide tools and/or data 1) to characterize and monitor non-point source runoff resulting from military activities on DoD training and testing ranges, and 2) to identify the impact of these sources on receiving waters. Anticipated products resulting from a proposal responding to this SON include the following:

- Identification of military activities within training and testing ranges that are non-point sources of pollutants.
- Development of tools to assess and diagnose the impairment of aquatic systems from potential military-specific, non-point sources of pollutants.
- Development of field-portable technologies to provide real-time monitoring (including both temporal and spatial variability) of the quantity and quality of non-point source runoff from DoD installations.
- Data and technologies that advance the state-of-knowledge of the development of total maximum daily loads (TMDLs), such as GIS technologies to model the contribution of DoD sources of non-point pollution.

This research project was designed to respond directly to both SON objectives and all four anticipated products. The objectives of this research project are to identify sources of NPS pollution resulting from military activities, to assess the impact of this pollution on surface water quality and to provide information for commanders to lessen the impact of training on water quality.

The technical objectives of this research are:

1. Identify military activities occurring within training ranges at Fort Riley that may cause NPS pollution.
2. Design a field study to develop a complete field data set for evaluating the effectiveness of riparian buffers for mitigating the impacts of military activities.
3. Assess the effectiveness of the LWSC project by conducting the field study including
    a. In-stream water and sediment sampling, and
    b. Channel stability monitoring including bed stability (aggradation/degradation), lateral stability (bank erosion), and bed material size distribution.
4. Evaluate and modify a comprehensive riparian buffer simulation, REMM, for evaluation of ecosystem and NPS pollution control functions of buffer systems.
5. Evaluate the most effective means to cross streams during maneuvers, based on frequency, intensity, and stream stage.
6. Develop a GIS for use with NPS models to model the contribution of NPS pollution on a representative watershed at Fort Riley.
7. Develop improved field-portable technologies to provide timely monitoring of NPS runoff to provide Commanders options during a maneuver exercise to lessen impact on water quality without canceling training

# 2.0 Background

## 2.1. Problem Definition

Maneuver training of mechanized infantry and armor units requires large areas of high-quality training lands. High-quality maneuver lands are necessary to assure the Army meets readiness requirements. The technology of today's military equipment has out stripped land availability to land requirements, creating intense training stress on installations. Training restrictions due to noise, threatened and endangered species habitat protection, water quality requirements, etc. have further reduced available training lands. Since training requirements and rotations to National Training Centers are scheduled several years in advance, tactical units must develop their training timetables based on these master schedules and availability of maneuver land. This results in very little flexibility to change or even delay training maneuvers. These restrictions result in heavier usage of the remaining maneuver areas and place greater stress on the ecological system. It may not be possible to repair and revegetate areas before they must be used again.

These restrictions do not consider the day-to-day weather patterns. Intense rainfall or long periods of saturated soil coupled with regulations concerning non-point source pollution (NPS) and requirements to meet total maximum daily loads (TMDLs) which may result in unforeseen and considerable delays in maneuver training. This loss of a given training window may result in units being improperly trained for their rotation to National Training Centers, reducing the effectiveness of their valuable training at a cost of millions of dollars.

We understand that military maneuver training activities can cause two broad categories of NPS pollution. The first category concerns training activities occurring on the hillsides. Streams are separated from these damaged upslope areas by varying amounts of riparian buffer strips of grass and other permanent vegetation. As NPS runoff passes through the vegetative buffer, sediment and other pollutants are removed. Water quality samples of runoff entering and leaving the buffer strips will be modeled to evaluate the effectiveness of native grass buffers for mitigating the impacts of military activities.

The second category includes vehicles crossing streams and runoff from roads, trails and ditches that carry NPS runoff towards the stream. At Fort Riley a low water stream crossing (LWSC) project was initiated in 1992 to address the stream crossing problem. The LWSC project was successful in supporting training by making steam crossings safer for vehicles and soldiers and improving access to training lands during high flow periods. The streams presumably were protected from frequent random crossings tearing up the stream banks and increasing sediment flow downstream. Some question still exists about whether the LWSCs have affected stream stability. The LWSC design has been adapted and applied at many installations throughout the United States. The Canadian military has also requested the design.

This research is designed to provide two tools to the installations with the objective of preventing reduction in military activities while preserving water quality. First, the installation land management plan can be modified to incorporate NPS and TMDL considerations based on different training scenarios and climatic events. Second, developing field-portable technologies to provide real time monitoring will provide information to Commanders where potentially

critical NPS pollution may occur and where TMDLs would be exceeded. This information would permit Commanders to make instantaneous changes to their battle plans as if in a real conflict.

## 2.2. Study Area

Fort Riley, Kansas is a U.S. Army base encompassing over 40,460 hectares of land in the southwestern Riley and the north central Geary counties. Located in the northern portion of the Flint Hills ecoregion (Omernik 1987), Fort Riley is in a transition zone between tallgrass and mixed grass prairies (Kuchler 1974). Elevations range from a low of 310 to a high of 410 meters above sea level.

Though a variety of landcover types can be found within the installation, approximately 82% of Fort Riley is grassland, specifically tall and shortgrass species (Figure 2.2-1). Oak and hackberry are dominant in woodlands, while big bluestem, indiangrass, and brome are the primary grassland species (Fay 1997). Only 2% of Fort Riley is comprised of urban and built-up areas. Most of these sites are located in the southern portion of the installation and include land uses such as family housing, offices and troop barracks, motor pools, and parking lots. Surface water features are also an important component to the identity and landscape of Fort Riley. The Kansas and Republican Rivers form Fort Riley's southern and southwestern border, respectively. Milford Lake, a U.S. Army Corps of Engineers multipurpose reservoir, is along the western boundary and Wildcat Creek runs along the northeast boundary. Small streams from surrounding agricultural areas enter the installation then connect to larger tributaries originating from within the fort before draining into Timber Creek, Madison Creek, and Wildcat Creek in the north and the Republican and Kansas rivers to the west and south.

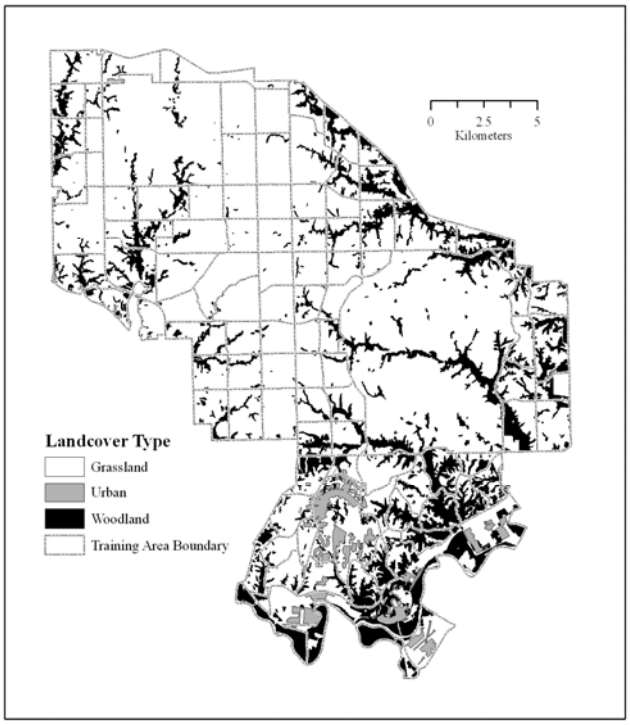


**Figure 2.2-1. Fort Riley landcover and training area boundaries.**

# 3.0. MATERIALS, METHODS, RESULTS, AND DISCUSSION BY TASK

## 3.1. TASK 1: CONTINUOUS SOIL MOISTURE MAPPING USING MODIS NDVI AND LST PRODUCTS

### 3.1.a. INTRODUCTION

Soil moisture is an important storage pool in the hydrologic cycle. The water content of soils impacts a variety of physical and biological processes in the biosphere and links the Earth's surface and atmosphere through its influence on surface energy and moisture fluxes. In addition, antecedent soil moisture conditions affect the hydrologic behavior of land surfaces by controlling, in part, the partitioning of precipitation into runoff and storage terms. Because of this, quantified soil moisture conditions are critical inputs for models in agriculture, biology, climatology, hydrology, and meteorology.

However, our ability to describe and map soil moisture conditions over large geographic areas is complicated by the natural spatial and temporal variability of soils, topography, landuse/landcover, and precipitation patterns (Carlson *et al.* 1995). Generally, soil moisture is measured in the field at specific points. Through a variety of spatial interpolation techniques, point measurements can then be used to create continuous surfaces to better visualize soil moisture conditions over an area of interest. However, this “manual” approach is time consuming and is not an appropriate operational method for rapid and continuous soil moisture monitoring at the regional (or larger) scale. Because of this, remote sensing methods for estimating soil moisture conditions are frequently used in land surface climatology, surface hydrology, and primary production modeling efforts.

The goal of this project is to use readily available, and free, remotely-sensed data products to generate accurate and spatially-distributed estimates of near surface soil moisture conditions on a repetitive basis for Fort Riley, Kansas. This study uses Land Surface Temperature (LST) and Normalized Difference Vegetation Index (NDVI) image products recorded by the Moderate Resolution Imaging Spectroradiometer (MODIS) sensor onboard the TERRA satellite, operated by the National Aeronautics and Space Administration (NASA). When used in conjunction with field measurements of soil moisture, these remotely-sensed data are then used as independent variables in a regression model to estimate soil moisture conditions for the study area.

### 3.1.b. PAST RESEARCH

Remote sensing of soil moisture has been an active field of research for the past 20 years, with investigators utilizing a variety of techniques and wavelengths of electromagnetic energy. In particular, advances in active microwave remote sensing techniques have shown the potential for monitoring soil moisture conditions at the spatial and temporal scales required for large scale modeling efforts (O'Neill *et al.* 1993, Engman and Chauhan 1995, O'Neill *et al.* 1996, Ulaby et al. 1996, Hutchinson 2003).

In the visible and near-infrared spectrum, Tucker (1979) documented the ability to quantify variations in green biomass using plant spectral reflectance characteristics. More specifically, Tucker found combinations of red and infrared (IR) reflectance (*e.g.,* NDVI) to be more effective at monitoring vegetation biomass, leaf water content, and chlorophyll content than similar combinations in the green and red spectrum. Goward *et al.* (1985) concluded that NDVI measurements from the Advanced Very High Resolution Radiometer (AVHRR) series of satellites were useful in the study of vegetation patterns at the macroscale, as the NDVI data agreed very well with known continental patterns of both natural and anthropogenically-modified vegetation.

In studies specifically geared toward the estimation of soil moisture, Carlson (1986), Carlson *et al.* (1994), and Gillies and Carlson (1995) used surface radiant temperature and combinations of thermal infrared and NDVI measurements to define model parameters of soil moisture. Surface temperature was found to have a distinct negative relationship with NDVI measurements, with the slope of the negative relationship proving useful as a proxy for landscape-scale canopy resistance and "wetness" (Nemani and Running 1989 and Nemani *et al.* 1993). Similarly, the Idso-Jackson crop water stress index (CWSI) was created based upon plant foliage temperature (Idso *et al.* 1981 and Jackson *et al.*1981). Using the Vegetation Index-Temperature (VIT) trapezoid, Moran *et al.* (1994) later proved that the CWSI theory could be applied even without *a priori* data on vegetation cover.

### 3.1.c. METHODS

#### Methods

#### Soil Moisture Measurements

Field measured soil moisture data were used to validate satellite estimates. Data were collected during the months of April through August 2004 on approximately a weekly basis at over 80 points within nested sampling grids located in primary training areas across the central part of the installation. At each point during the all sampling periods, three soil moisture readings were taken using a TDR 300 soil moisture probe (Spectrum Technologies, Plainfield, IL). Also at each point, three ground temperature measurements were taken using a Crop Trak noncontact infrared thermometer (Spectrum Technologies, Plainfield, IL). The three sampled values for soil moisture and ground temperature were averaged for each point. The mean of these averaged values was also calculated for each of the sample points located within the same satellite image grid cell.

**Satellite Image Acquisition and Processing**

Satellite image data consisted of MODIS LST and NDVI image products acquired from the NASA Earth Observing System (EOS) Data Gateway (http://edcimswww.cr.usgs.gov/pub/imswelcome/). The LST product (MODIS/TERRA LAND SURFACE TEMPERATURE/EMISSIVITY 8-DAY L3 GLOBAL 1KM SIN GRID V004) was an 8-day composite image with a spatial resolution of 1 km in the x- and y dimensions. The NDVI product (MODIS/TERRA VEGETATION INDICES 16-DAY L3 GLOBAL 1KM SIN GRID V004), was a 16-day composite image with the same spatial resolution of 1 km. Composite LST and NDVI images for the calendar year 2004 were downloaded from the EOS Data Gateway in .HDF format via FTP and converted into .TIF files using the HDF-EOS to GeoTIFF Conversion Tool (HEG) (http://newsroom.gsfc.nasa.gov/sdptoolkit/HEG/HEGHome.html). After converting each of the composites into .tif format, the images were then loaded into the ArcGIS 9.1 (ESRI, Redlands, CA) software and their geographic extent clipped to the Fort Riley installation boundary.

Original digital number values for the LST and NDVI image grids were received in a scaled form. The final data preparation step was to transform these scaled values into "normal" NDVI and temperature units. The LST data was converted from degrees Kelvin x 200 to degrees Celsius using the following equation in the ArcGIS 9.1 raster calculator:

$$LST_R = (LST_I * 0.02) - 273.15 \quad \text{[Eq. 3.1-1]}$$

where:

$LST_R$ = re-scaled LST digital numbers
$LST_I$ = initial, or original, LST digital numbers

NDVI images from the EOS Data Gateway were also scaled, but by a value of 10,000. These grids were re-scaled downwards, again using the ArcGIS 9.1 raster calculator, by:

$$NDVI_R = NDVI_I / 10{,}000 \quad \text{[Eq. 3.1-2]}$$

where:

$NDVI_R$ = re-scaled NDVI digital numbers
$NDVI_I$ = initial, or original, NDVI digital numbers

## 3.1.d. DATA ANALYSIS

Initial data analysis consisted of assessing the association between LST and NDVI image pairs using the Pearson correlation coefficient (r) to verify that the expected negative relationship between temperature and greenness actually exists within the study area. Next, a scatterplot of LST and NDVI data values was constructed from each grid cell where field measurements of soil moisture and ground temperature were taken. Again, this was a validation step to determine whether these data points formed the characteristic Vegetation Index-Temperature (VIT) trapezoid.

A multiple linear regression model was then used to establish the form of the relationship between the dependent variable volumetric soil moisture ($\theta_v$), and the independent variables LST and NDVI:

$$\theta_v = B_C - (B_{NDVI} * NDVI_R) - (B_{LST} * LST_R) \quad \text{[Eq. 3.1-3]}$$

where:

$\theta_v$ = volumetric soil moisture ($cm^3/cm^3$)
$B_C$ = constant beta value
$B_{NDVI}$ = NDVI beta value
$NDVI_R$ = re-scaled NDVI digital numbers
$B_{LST}$ = LST beta value
$LST_R$ = re-scaled LST digital numbers

Individual regression models were developed using SPSS 12.0 (SPSS Inc., Chicago, IL) for each of the nine time periods covered by an individual composite LST/NDVI image. The strength of the regression relationships was evaluated using the coefficient of determination ($R^2$), which represents the ratio of explained variation to total variation in the dataset. The standard error of the estimate was also calculated and used as a measure of the error associated with the soil moisture content predicted for a typical data point. Each of the individual regression models were then applied with the ArcGIS 9.1 raster calculator, using appropriate LST and NDVI composite images as inputs, to generate spatial estimates of volumetric soil moisture content for the entire Fort Riley installation.

### 3.1.e. RESULTS AND DISCUSSION

Examination of Pearson correlation coefficients for a selected time series of 2004 LST and NDVI images shows most dates to have the expected negative relationship between land surface temperature and greenness (Table 3.1-1). However, two dates (August 12 and August 28) show a slight positive relationship between the two datasets. For the remaining dates with negative correlations, the magnitude and significance correlation varies over time, with r-values ranging from a “high” of -0.815 to a “low” of -0.052. For only two composite dates, those ending on May 8 (NDVI050804 and LST050804) and September 13 (NDVI091304 and LST091304), was the negative relationship significant.

**Table 3.1-1. Correlation coefficients for NDVI and LST composite images in 2004.**

| Variable (mmddyy) | Mean | Std. Deviation | N | Pearson Correlation |
|---|---|---|---|---|
| NDVI050804 | 0.61 | 0.06 | 19 | -0.815** |
| LST050804 | 25.08 | 0.85 | 19 | |
| NDVI052404 | 0.75 | 0.03 | 19 | -0.407 |
| LST052404 | 29.47 | 1.09 | 19 | |
| NDVI060904 | 0.76 | 0.04 | 19 | -0.120 |
| LST060904 | 32.91 | 1.36 | 19 | |
| NDVI062504 | 0.78 | 0.04 | 19 | -0.413 |
| LST062504 | 23.37 | 0.42 | 19 | |
| NDVI071104 | 0.75 | 0.04 | 19 | -0.408 |
| LST071104 | 31.24 | 0.82 | 19 | |
| NDVI072704 | 0.78 | 0.03 | 19 | -0.052 |
| LST072704 | 30.85 | 1.38 | 19 | |
| NDVI081204 | 0.73 | 0.04 | 19 | 0.244 |
| LST081204 | 29.15 | 0.92 | 19 | |
| NDVI082804 | 0.69 | 0.03 | 19 | 0.187 |
| LST082804 | 28.42 | 0.73 | 19 | |
| NDVI091304 | 0.66 | 0.03 | 19 | -0.488* |
| LST091304 | 27.67 | 0.37 | 19 | |

**Correlation is significant at the 0.01 level (2-tailed).

* Correlationis significant at the 0.05 level (2-tailed).

The pattern of observed r-values for LST and NDVI appears to be related to air temperatures during the study period. The highest negative correlations coincide with composite image dates during which cooler temperatures were recorded at local weather stations. For example, during the composite period ending on May 24, the r-value between LST and NDVI was -0.407 and the mean daily maximum temperature was 29.4$^{o}$C. For the period ending June 9, the mean daily maximum temperature increased to 33.0 $^{o}$C while the correlation between LST and weakened to -0.120. Moving to the next composite period, June 25, temperatures were unseasonably cool (mean daily maximum temperature = 23.3 $^{o}$C) and the negative relationship between LST and NDVI strengthened to r = -0.413. These preliminary results suggest that very warm temperatures common during the summer months in the Great Plains region of the U.S., may limit the effectiveness of a linear regression-based approach to soil moisture estimation using coarse grain LST and NDVI data sources.

A scatterplot of LST versus NDVI data for grid cells containing at least one field sampling point further illustrates the correlation results (Figure 3.1-2). This visualization also confirms that, for those composite image dates with negative r-values, the 2004 data from Fort Riley closely matches the pattern referred to by Moran *et al.* (1994) as the Vegetation Index-Temperature (VIT) trapezoid. Further examination of Figure 3.1-2, however, also show how this two-dimensional VIT space migrates left and right with temperature and up and down with vegetation development.

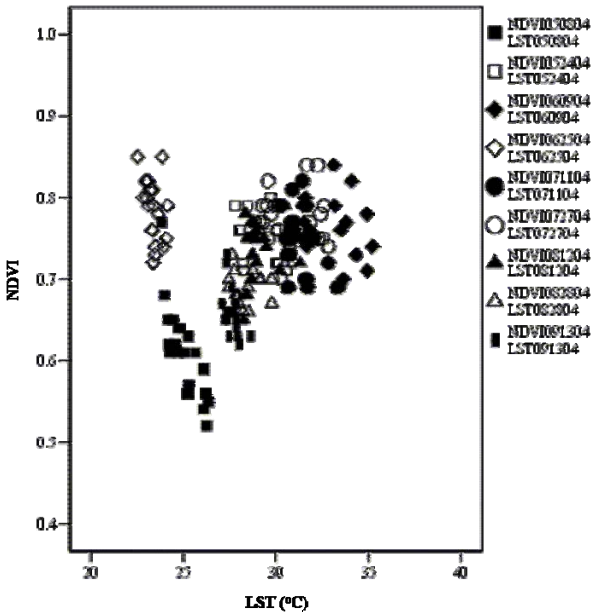


**Figure 3.1-1. Scatterplot of NDVI and LST for selected locations in 2004.**

Early growing season image pairs (e.g., May 8) begin in the lower left portion of the graph. For the remaining dates, their "center of mass" moves generally up and to the right (greener and warmer) until the peak of vegetation development (approx. late July), then back down and to the left (less green and cooler). The exception to this pattern is June 25, the composite period with much cooler than normal air temperatures. What is clear from Figure 3.1-1 is that a single regression model designed to predict volumetric soil moisture based upon the expected negative relationship between LST and NDVI will not be successful for this study area. However, a series of models, based upon the observed LST-NDVI relationship for individual dates, would be a more appropriate strategy for generating a time series of spatial soil moisture estimates. Such regression models were developed for each composite image period during the 2004 growing season. Early results, as might be expected given the correlation analysis, have met with only moderate success. To date, the accuracy of quantitative predictions of volumetric soil moisture varies significantly. Table 3.1-2 shows the regression model results for two "typical" composite image dates, May 24 and June 9. Standard errors of the estimate for these, and the other 2004 composite period dates, are approximately two times higher than what would be preferred given the spatial resolution of the input LST and NDVI data sources.

**Table 3.1-2. Summary of regression model results for May 24 and June 9, 2004**

| Model Date (mmddyy) | R | R Square | Adjusted R Square | Std. Error of the Estimate |
|---|---|---|---|---|
| May 24, 2004 (052404) | 0.199 | 0.040 | -0.080 | 13.097 |
| June 9, 2004 (060904) | 0.085 | 0.007 | -0.117 | 11.511 |

Though numeric predictions of soil moisture cannot yet be reliably obtained using the methods explained here, spatial soil moisture predictions may be used in a relative sense to differentiate moisture conditions between different locations. Figure 3.1-2 shows predicted soil moisture (bilinear interpolation applied to 1 $km^2$ grid cells) during the composite period ending May 24.

Moist soils can be found in the east-central parts of the study area and extending south and west to the installation boundary. Soils tend to be drier in the east and northwest.

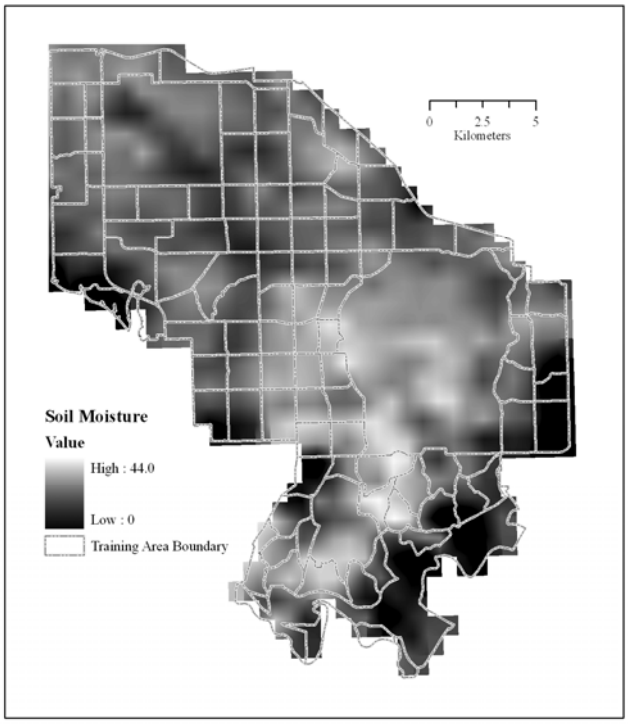


**Figure 3.1-2. Predicted volumetric soil moisture conditions – May 24, 2004.**

Moisture conditions are generally drier during the composite period ending June 9 (Figure 3.1-3). However, moist soils can are common in the east-central, northern, and northwestern portions of the installation. Drier conditions predominate in the more urban and built-up areas in the south and along the southern Kansas River corridor.

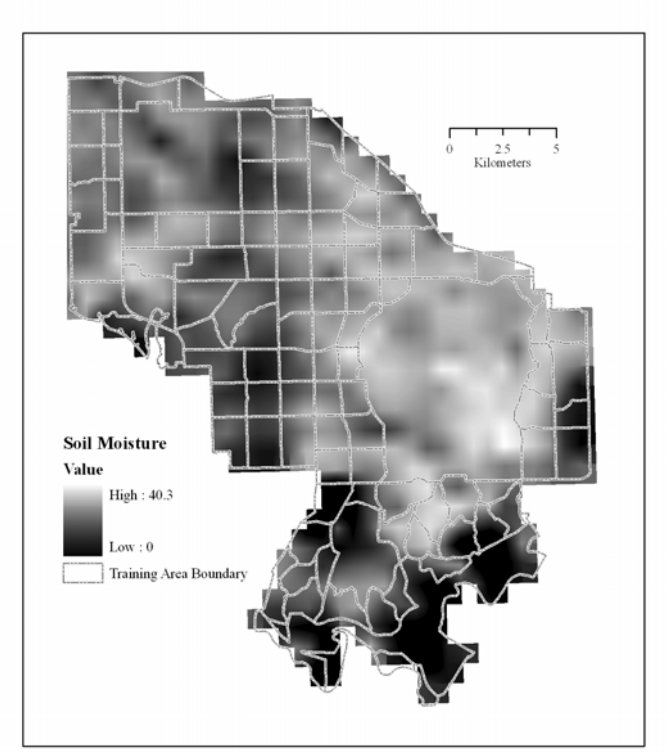


**Figure 3.1-3. Predicted volumetric soil moisture condition – June 9, 2004.**

Image differencing techniques can also be applied to better assess changes in soil moisture conditions between two dates. Figure 3.1-4 shows changes in predicted volumetric soil moisture as determined by subtracting the June 9 prediction from that of May 24. Approximately 59 percent of Fort Riley, primarily the northern and eastern portions of the installation, had wetter soils on June 9 than May 24.

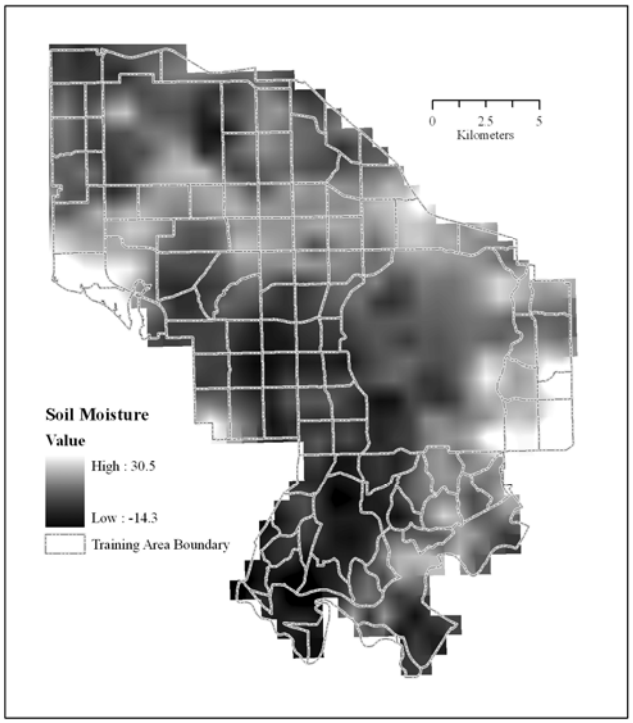


**Figure 3.1-4. Predicted change in volumetric soil moisture condition – May 24 to June 9, 2004.**

## 3.2. TASK 2: QUANTIFY VEGETATIVE IMPACTS

### 3.2.a. INTRODUCTION AND BACKGROUND

Military lands are one of the U.S. Army's most valuable resources. Along with training, the land can provide a variety of uses including timber production, agriculture, livestock grazing, off-road vehicle recreation, and hunting (Warren and Bagely 1992). Technological advances in weapon systems and evolution of combat tactics have increased the need for larger and more versatile weapon ranges, maneuver areas, and impact areas (Houston et al., 2001). Current training requirements place high demands on some training areas, with a potential negative impact on environmental quality and, subsequently, unit readiness. Military land managers now contend with environmental issues whose management often requires a short or long-term reduction in amount of land available for training. Frequent disturbance of soil and flora that accompany military maneuvers can further limit the land area needed to sustain the army's readiness (Houston et al., 2001, Trame, 1997).

Significant impacts on military lands include accelerated soil erosion resulting from ground cover removal and increased run-off due to compaction from military vehicles. An increased rate of soil erosion caused by foot and vehicle traffic negatively impacts the environment. Removal of vegetation can damage key soil properties (e.g., nutrients, organic matter) making large areas less habitable for plants. Less vegetation and lower water infiltration rates due to

compaction increases surface runoff, especially highly erosive concentrated flows (Trame, 1997). Sediments transported down slope can be detrimental to riparian vegetation and if not trapped effectively by that vegetation, enter streams and degrade surface water quality (Bartsch et al., 2002).

According to the 2000 Fort Riley Range and Training Land Development Plan, a total of 29,632 $km^2$ days is needed to train armored or mechanized infantry battalions to successfully perform certain mission essential tasks. The currently available maneuver area at Fort Riley provides for only 12,477 $km^2$ days, which is over 17,000 $km^2$ days short of the mandated requirement. This difference challenges military land managers with frequent scheduling conflicts and the very real danger of over-utilizing maneuver area lands. Sustainable use and management of the land resource are two major challenges for installation land managers, including civilian staff and military leaders, as force readiness must be balanced with environmental protection. To better mitigate against soil erosion, the location and severity of risk areas must be made available.

### 3.2.b. APPROACH

Although soil erosion is a natural occurring process, human activities can accelerate natural rates of erosion to the overall detriment of both military training lands and the environment. This portion of the research project will combine satellite image processing techniques to assess vegetation condition for the purpose of modifying the existing RUSLE soil erosion model to account for military-specific training intensity in determining improved annual estimates of soil erosion. Continued military readiness requires large continuous areas of safe quality training lands. Locating areas of unacceptable rates of erosion will assist military land mangers in their mission to provide quality training areas while minimizing impacts on the environment.

Smith and Wischmier led the efforts to design the first "*universal*" equation for soil erosion. The Universal Soil Loss Equation (USLE), published in ARS Special Report 22-66 (1961), was based upon six contributing factors:

$$A = R * K * LS * C * P \qquad \text{[Eq. 3.2-1]}$$

where,

A = annual soil loss (ton / acre year)
R = rainfall and runoff factor (hundreds of foot·ton force·inch / acre·hour·year)
K = the soil erodibility factor (ton·acre·hour / hundreds of acre·foot·ton force·inch /
L = the length of the slope (dimensionless)
S = the slope steepness (dimensionless)
C = the cover-management factor (dimensionless)
P = the support practice factor (dimensionless)

Since the publication of USDA Agricultural Handbook 282 (Wischmeier and Smith 1965), the USLE has become the most widely used soil erosion model, and foundation for continued research and development of improved empirical, physical, and processed-based erosion models (Bartsch et al., 2002, Quyang and Batholic 2001, Jones et al., 1996).

In 1987, the USLE was revised to improve the soil loss estimation by incorporating additional research and new technology (Renard et al., 1994). The Revised Universal Soil Loss Equation (RUSLE) is used to determine the long-term average annual soil loss carried in runoff from slopes (Renard et al., 1997). Although the RUSLE uses the same factors as USLE, changes were made to the algorithms associated with each of the contributing factors described below.

Both USLE and RUSLE are empirically-based statistical models developed using collected data from long term observations of soil erosion on research plots to determine average annual soil loss (Nearing et al. 1994). These models are popular due to the relative simple calculation, the low number of variables needed to determine each factor in the equation, and the available data of numerical values for each factor. However, it is important to note that USLE and RUSLE were developed to estimate soil loss in agricultural environments, not rangelands or military training lands.

### 3.2.c. RUSLE FACTORS

#### Rainfall-Runoff Erosivity (R) Factor

Rainfall and runoff erosivity (R) is used as a climatic factor for the RUSLE equation. Specifically, it estimates an annualized amount of energy associated with rainfall events for different geographic areas. The total energy, and peak intensity of each individual storm over an historical period is summed to determine total storm energy. This erosivity index is derived from raindrop kinetic energy, number of storms, amount of rain, and intensity of storms (Renard *et al.*, 1997). Most RUSLE implementations use isoerodent maps from empirical data provided by Renard et al. (1997) in the USDA RUSLE Handbook to identify an appropriate R factor value. Using this data, the R factor for Fort Riley was a constant value of 175.

#### Soil Erodibility (K) Factor

The second RUSLE factor, K, is based upon soil properties and soil characteristics and how these relate to soil loss. Specifically, the K factor is calculated using the structure, permeability, and percent of organic matter, sand, and silt properties of specific soil types (Bartsch et al., 2002; Renard et al., 1997; Jantz et al., 1975). This factor value is also related to the rainfall, runoff, and infiltration of water or moisture and is measured in complex units (tons/acre/h(hundreds of acre)/foot-ton force(tonf)/in)-1.

The Natural Resource Conservation Service (NRCS) has calculated soil erodibility for different soil types and associated K factors made these available in soil survey manuals for local areas as well as in digital format via the Soil Survey Geographic (SSURGO) product.

#### Slope Length and Steepness (LS) Factor

Slope length and steepness is determined by the local topography of an area. According to the RUSLE Handbook (Renard et al., 1997), slope length is the horizontal distance from the origin of overland flow to the point of either initial deposition or where concentrated flow begins. The assumption is an increase in length will increase soil erosion.

The slope length and steepness factor was created using the standard USGS NED 30-meter. The LS factor was computed using the technique first reported by Desmet and Govers (1996) and later modified by Mitasova et al. (1996) and Engel (2003). This technique incorporates the concept of unit contributing areas in an attempt to better account for variable topography and improve LS factor estimates as described by the RUSLE Handbook (Renard et al., 1997).

**Cover Management (C) Factor**

The cover management, or C-factor, represents the effects of vegetation, management, and erosion control practices on soil loss. A landcover layer, provided by ITAM, was used to create the cover management (C) factor. This dataset classified landcover into five categories: Grassland, woodland, urban, water and barren. For the urban and water areas, a value of 0.0 was used for the C-factor (Bartsch et al., 2002). This value was adopted because of the assumption that no soil is exposed in these landcover types.

Sub-factors utilized by RUSLE in this category include prior land use, canopy cover, surface cover, surface roughness, and soil moisture. The product of sub-factors (PLU, CC, SC, SR) is used to estimate C based upon different landcover layer categories. The soil moisture subfactor is not used.

**Prior Land Use (PLU) Subfactor**

The first of four subfactors of the C-factor is Prior Land Use (PLU). PLU considers prior landuse and the type of tillage practices applied to agricultural fields. Tillage operations can change the density of soil surface, and increase erosion risk, by breaking soil bonds (Renard *et al*., 1997). A PLU sub-factor value is based on the type of surface disturbance and ranges from 1 (for conventional till operations) to 0 (for undisturbed areas) (Renard, *et al*. 1997). For the purpose of this study, the installation is considered to be an undisturbed, non-agricultural environment and the PLU subfactor will be ignored. To account for soil disturbances that do occur on the installation, a new military intensity factor will be developed and applied in a modified RUSLE to predict annual soil losses.

**Canopy Cover (CC) Subfactor**

The second C sub-factor is the amount of vegetation cover protecting bare soil surfaces. Plant canopies reduce the amount of rainfall reaching the soil and reduce the energy of raindrops that reach the surface. Raindrops fracture upon impact with vegetation creating smaller drops of water with less energy (Renard et al., 1997). CC values range from 0 to 1 and are determined by the fraction of land covered by canopy and the height the raindrops fall after impacting the vegetation. This subfactor was determined from the formula (Renard et al. 1997; Bartsch et al., 2002):

$$CC = 1 - F_c * \exp(-0.1 * H) \qquad \text{[Eq. 3.2-2]}$$

where,

$F_c$ = fraction of land surface covered by canopy (%)
H = canopy height (ft)

Percent canopy coverage was determined from collected LCTA data on percent bare ground observations within established vegetation plots. The average percent bare ground of 135 grassland plots at Fort Riley was 51.3%. Therefore, the value of 48.7% was used as the fraction of land surface covered by canopy value for this landcover type. An average bare ground estimate of 25 woodland plots was 12.7% (87.3% canopy cover). The average height of vegetation was determined from the 2001 LCTA transect data. Grassland and woodland plots had average heights of 0.323 and 3.326 meters, respectively.

**Surface Cover (SC) Subfactor**

An SC subfactor considers the splash erosion reduction capacity of water runoff, which affects erosion by decreasing the soil surface area to exposed raindrop impacts. Reduction of splash erosion includes ponded areas, crop residue, rocks, and nonerodible materials in contact with the soil surface.

Surface cover is calculated using an empirical value for land use, the percentage of land area covered by residue, and the surface roughness:

$$SC = \exp[-b * S_p * (0.24 / R_u)^{0.008}] \quad \text{[Eq. 3.2-3]}$$

where,

b = empirical landuse coefficient (dimensionless); 0.3 (obtained from Kuenstler 1998)
$S_p$ = fraction of land (%) covered by surface cover from LCTA data; 0.487 for grasslands and 0.873 for woodlands (obtained from LCTA 2001 bare ground estimates)
Ru = surface roughness (in.); 0.30 (obtained from Renard et al. (1997)

**Surface Roughness (SR) Subfactor**

Soil surfaces have different roughness characteristics that influence soil erosion. A rough surface contains depressions and barriers for runoff. These depressions and barriers reduce overland flow, which lowers the transport capacity and rate of soil detachment. The SR factor considers the degree of surface disturbance, vegetation roughness, and soil cloddiness.

Values of SR range from 0.25 (in) for California annual grassland to 1.30 (in) for root-plowed rangelands. The random roughness value of 0.30 (in) is an empirical value calculated for tall grass prairie (Renard *et al*. 1997).

**Support Practice Management (P) Factor**

The sixth and final RUSLE component is the support practice factor (P). P factor considers soil loss associated with specific practices such as: strip-cropping, contour farming, terraces, and subsurface drainage in cultivated lands. This factor is used for agricultural practices and is

normally not used with rangelands (Bartsch et al., 2002). Factor P does not consider the practices of no-till, sod-based crop rotations or crop-residue management, as they are part of the C factor. Because Fort Riley is being considered an "undisturbed" site the P factor will not be considered here. Instead an additional factor, Military Training Intensity, will be developed to account for the effect of military training activities, and the intensity of those training events, on installation lands.

**Military Training Intensity**

Various military training activities, and the intensity of those training events, on installation lands will negatively impact vegetation (Quist *et al*., 2003; Houston *et al*., 2001; Trame, 1997; Warren and Bagley, 1992). Vegetation is an important factor to control erosion by minimizing raindrop impacts on the soil and holding soil in place with extensive root systems. To measure the intensity of military training at Fort Riley, data from 2002 was collected from the Range Control Office, which tracks the number of soldiers, the units, and the training areas used on a daily basis at Fort Riley. This raw data was then converted to Total Training Days (TTD) by multiplying the number of days each soldier occupies a training area by the number of soldiers per training area:

TTD = Number of soldiers * number of days [Eq. 3.2-4]

Next, the number of troops in specific training areas was estimated. Military units will reserve training areas but may not utilize them for the entire period or distribute troops evenly across the training lands. The training data provided by Fort Riley Range Control included the total number of soldiers and which areas were open, but it did not identify the specific number of soldiers working in each training area. The procedure used to determine the number of unit soldiers per training area was to divide the number of areas opened by the total number of soldiers reported. For example, if a total of 220 soldiers trained in Maneuver Areas A, B, C, D, and E, then the TTD for each maneuver area would be 220 divided by 5, or 44.

**Imagery Analysis**

Satellite imagery from the Landsat 5/7 TM and MODIS sensors for the year 2002 were used for vegetation analysis. The red and near infrared wavelength bands from each sensor were used to calculate NDVI values for two different sites (control and training area) within the Fort Riley study area in order to determine whether differences in vegetation condition could be inferred for the growing season of 2002.

Specific training area study sites were Maneuver Areas A, B, and D. These areas had the highest number of total training days (TTD) during 2002. Due to the nature of military training activities at Fort Riley, only grasslands were evaluated in this analysis. Woodlands were excluded, as little, if any, major vehicle maneuvers are conducted within forested sites. The Fort Riley Impact Area was selected as a control site for comparison with the maneuver areas. The impact zone is adjacent to Maneuver Areas A, B, and D and share similar physical and weather conditions. However, the impact zone is off-limits for training and can be considered "undisturbed" compared to areas subjected to military training exercises.

LANDSAT 5 TM and LANDSAT 7 ETM+ images were purchased by ITAM from the USGS National Center for Earth Resources Observation & Science (EROS). Acquisition dates of the imagery were April 10, June 29, July 15, August 8, and August 16, 2002. The August 8 image is from the Landsat 5 satellite. Radiometric corrections and georeferencing processes were performed at the EROS Data Center.

MODIS images from 2002 were collected and downloaded from the Earth Observing System Data Gateway website (http://edcimswww.cr.usgs.gov/pub/imswelcome). Image dates were March 28, April 7, April 23, May 9, May 25, June 10, June 26, July 12, July 28, August 13, and August 29. Downloaded image data were already processed for NDVI. MODIS NDVI data were converted from hierarchical data format (.hdf) into georeferenced tagged image format (.tif) files that could be consumed and used within ESRI GIS software.

### 3.2.d. RUSLE SOIL EROSION RISK

Annual soil erosion losses were calculated for Fort Riley using the standard RUSLE model. Individual grid layers representing each of the RUSLE factors were multiplied in a GIS to derive a spatially-distributed estimate of annual soil losses. Estimated soil erosion losses ranged from 0.00 to 235 ton/acre/year. As expected, the majority of flat upland areas on the installation are characterized by very low to low predicted rates of annual erosion. Areas of medium to very high risk are found in the eastern and southern portions of the installation where variable topography is more common.

### NDVI Values

Landsat-derived mean NDVI values for the impact area control and training area study sites followed the same pattern during the study period. In the April 10 image both areas had negative values (Table 3.2-1), with the training area mean NDVI being smaller than that of the impact area control. These negative values suggest, incorrectly, that no vegetation is present. A one-tailed Student's t-test shows that the difference between mean NDVI values for the control and training areas are significant (alpha = 0.01).

**Table 3.2-1. Comparison of mean Landsat 5/7 derived NDVI values for the impact area control and training area study sites for selected dates in 2002.**

| Date | Mean NDVI Control (a) | Mean NDVI Training Area (b) | Difference (a-b) |
|---|---|---|---|
| April 10 | -0.22 | -0.23 | -0.01 |
| June 29 | 0.13 | 0.10 | 0.03 |
| July 15 | 0.04 | 0.01 | 0.03 |
| August 8 | 0.29 | 0.28 | 0.01 |
| August 16 | 0.04 | 0.03 | 0.01 |

Figure 3.2-1 shows that while the impact area control and training area study sites each have a similar temporal pattern in NDVI values, the training area NDVI is consistently lower. Also evident in this figure is a decrease in NDVI values beginning in June followed by an increase in mean NDVI in August.

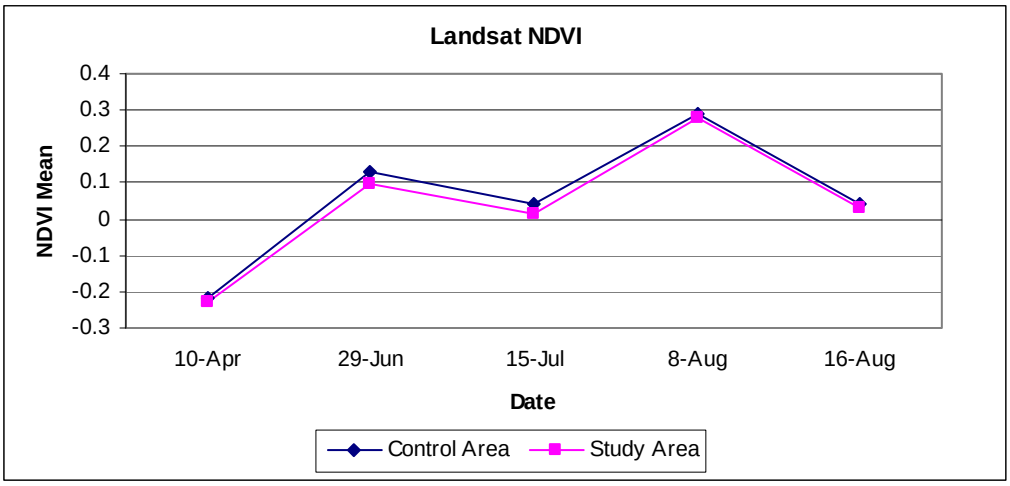


**Figure 3.2-1. Comparison of Landsat 5/7 TM derived mean NDVI values for the impact area control and training area study sites in 2002.**

Historical daily rainfall data collected from the Manhattan, Kansas Regional Airport was examined to determine if variable precipitation was responsible for this "abnormal" trend in NDVI based upon typical tallgrass prairie phenology. The daily precipitation data was summed to generate totals dictated by the image acquisition.

The range of total precipitation during the study period was 0 to 81.03mm (Table 3.2-2). This data reveals a trend of increasing precipitation from 28 March to 25 May with a total during that time span of nearly 172 mm. There shows a sharp decrease in rainfall between June 10 and July 12, which relates to the decrease in NDVI values during this same time period. Precipitation amounts increase once again between July 28 and August 29, which relates to the upturn in NDVI values noted during this same period.

All other image dates show that the training area study site mean value was lower than the impact area control, with the largest difference in mean values being 0.03 during the study period. This could suggest training impacts vegetation health.

**Table 3.2-2. Total precipitation amounts between MODIS image acquisition dates. Precipitation measured at Manhattan Regional Airport, Manhattan, Kansas (Source: National Weather Service).**

| Date | Rainfall (mm) | Cumulative Total (mm) |
|---|---|---|
| March 28 - April 7 | 0.51 | 0.51 |
| April 8 - April 23 | 43.94 | 44.45 |
| April 24 - May 9 | 46.23 | 90.68 |
| May 10 - May25 | 81.03 | 171.70 |
| May 26 - June 10 | 29.46 | 201.17 |
| June 11 - June 26 | 9.40 | 210.57 |
| June 27 - July 12 | 2.54 | 213.11 |
| July 13 - July 28 | 28.96 | 242.06 |
| July 29 - August 13 | 28.45 | 270.51 |
| August 14 - August 29 | 27.18 | 297.69 |

As was the case with NDVI values derived from LANDSAT 5/7 TM data, differences exist between greenness conditions in the impact area control and training area study sites (Figure 3.2-2). MODIS-derived NDVI is also consistently higher in the impact area control during the time period examined and, as compared with TM NDVI values, the difference between the two study sites was much higher. A one-tailed Student's t-test shows that the difference between mean NDVI values for the control and training areas are significant (alpha = 0.01).

Minimum values during the study period was on March 28, with the mean NDVI for the impact area control and training area study sites being 0.25 and 0.27, respectively. Maximum mean NDVI values were recorded on the June 10 image. On this date, mean NDVI for the impact area control site was 0.76 while the training area study equaled 0.70. The maximum difference in mean NDVI values between the two sites (0.08) was observed on the May 9 image (see Table 3.2-3).

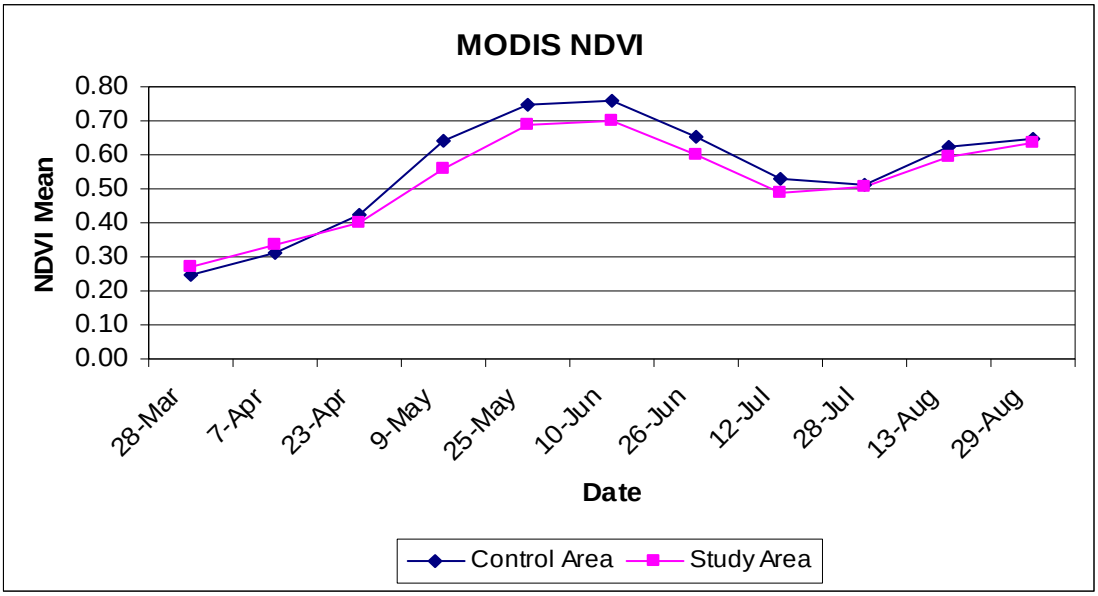


**Figure 3.2-2. Comparison of MODIS-derived mean NDVI values for the impact area control and training area study sites in 2002**.

**Table 3.2-3. Comparison of mean MODIS-derived NDVI values for the impact area control and training area study sites for selected dates in 2002.**

| Date | Mean NDVI Control (a) | Mean NDVI Training Area (b) | Difference (a-b) |
|---|---|---|---|
| March 28 | 0.25 | 0.27 | -0.02 |
| April 7 | 0.31 | 0.34 | -0.03 |
| April 23 | 0.43 | 0.40 | 0.03 |
| May 9 | 0.64 | 0.56 | 0.08 |
| May 25 | 0.75 | 0.69 | 0.06 |
| June 10 | 0.76 | 0.70 | 0.06 |
| June 26 | 0.65 | 0.60 | 0.05 |
| July 12 | 0.53 | 0.49 | 0.04 |
| July 28 | 0.51 | 0.50 | 0.01 |
| August 13 | 0.62 | 0.59 | 0.03 |
| August 29 | 0.64 | 0.64 | 0.00 |

Mean NDVI values for the training area study site was higher than that of the impact area control for the first two image dates (March 28 and April 7). This was likely the result of burning practices in the training area which removes litter and promotes rapid tallgrass prairie growth. Because of the difference in burning practices in the training area and impact area control study sites, and its impact on greenness values, NDVI information for these first two dates were not considered for purposes of estimating a training intensity factor for the modified RUSLE equation.

Excluding the first two MODIS image acquisition dates, the difference in mean NDVI between the training area and impact area control sites ranged from a low of 0.00 (August 22) to a high of 0.08 (May 9). As was the case with the analysis of Landsat-derived NDVI values, these differences suggest that military training activities are negatively impacting above ground vegetation to such an extent that a difference in greenness can be detected from satellite altitudes and at a variety of spatial resolutions, even during periods of relatively high rainfalls.

**Training Intensity Factor**

All TTD data was summarized for each maneuver and training area in 2002 (Figure 3.2-3 and Table 3.2-4). In 2002, TTD summed to 140,023. Of all Fort Riley maneuver areas, MA A, B, and D were those with the highest TTD, ranging from a high of 15,905 to a low of 13,166. Of designated training areas, TA 09 and TA 12 experienced TTD of 2,720 and 1,505, respectively. These were the only training areas with TTD exceeding 889.

This same TTD data was also summarized by month (Table 3.2-5), ranging from a high of 40,136 in November to a low of 1,868 in March. In 2002, five months (January, June, October, November, and December) equaled or exceeded 12,420 TTD and accounted for over 75% of TTD at Fort Riley.

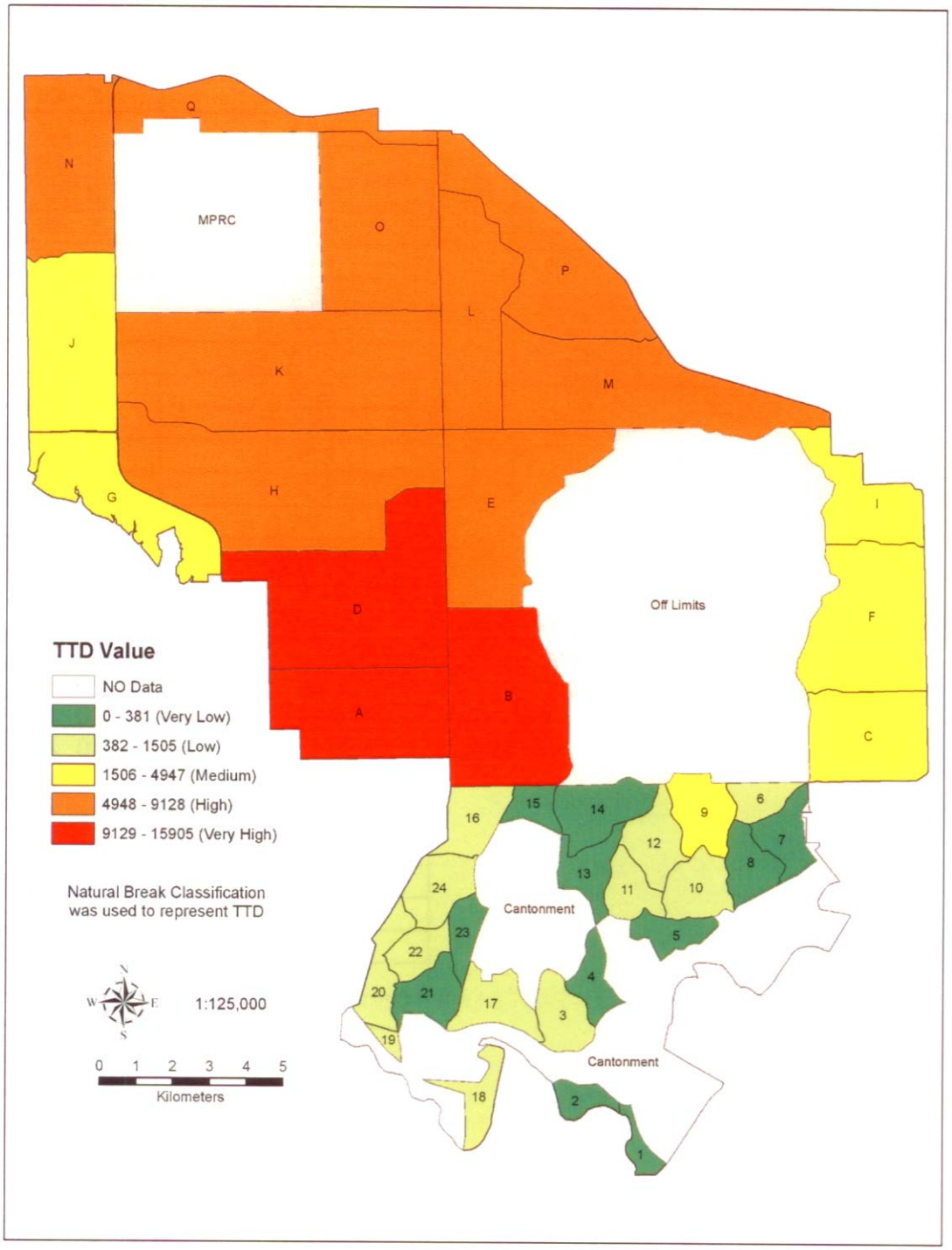


**Figure 3.2-3. Total Training Days (TTD) for Fort Riley, Kansas in 2002 (Source: Fort Riley Range Control Office).**

**Table 3.2-4. Total Training Days (TTD) for 2002 by area. Total TTD = 140,023 (Source: Fort Riley Range Control Office).**

| Area | Training Days | Area | Training Days |
|---|---|---|---|
| MA A | 15,905 | TA 01 | 138 |
| MA B | 13,166 | TA 02 | 138 |
| MA C | 2,924 | TA 03 | 899 |
| MA D | 14,603 | TA 04 | 191 |
| MA E | 9,128 | TA 05 | 308 |
| MA F | 2,624 | TA 06 | 610 |
| MA G | 1,922 | TA 07 | 337 |
| MA H | 7,026 | TA 08 | 381 |
| MA I | 2,147 | TA 09 | 2,720 |
| MA J | 4,947 | TA 10 | 503 |
| MA K | 7,682 | TA 11 | 601 |
| MA L | 6,486 | TA 12 | 1,505 |
| MA M | 8,066 | TA 13 | 77 |
| MA N | 5,650 | TA 14 | 99 |
| MA O | 6,327 | TA 15 | 121 |
| MA P | 8,859 | TA 16 | 825 |
| MA Q | 8,609 | TA 17 | 596 |
| | | TA 18 | 881 |
| | | TA 19 | 717 |
| | | TA 20 | 723 |
| | | TA 21 | 318 |
| | | TA 22 | 561 |
| | | TA 24 | 703 |

**Table 3.2-5. Total Training Days (TTD) for 2002 summarized by month (Source: Fort Riley Range Control Office).**

| Month | Training Days | Month | Training Days |
|---|---|---|---|
| January | 19,451 | July | 9,620 |
| February | 1,937 | August | 5,306 |
| March | 1,868 | September | 6,991 |
| April | 3,734 | October | 12,420 |
| May | 5,203 | November | 40,136 |
| June | 20,023 | December | 13,335 |

From March to August 2002, the non-control study area (MA A, B, and D) had a total of 15,013 TTD (Table 3.2-6). March had the lowest TTD (455) while the month of June had the highest intensity of TTD (7,399). Increase of training was from March to June with a sharp increase from May to June. During July and August, TTD decreases but still has a much higher TTD intensity than the beginning of the study period. The training intensity factor for the modified RUSLE model was derived by combining the difference in NDVI values during March through August with the monthly TTD.

**Table 3.2-6. Total Training Days for Maneuver Areas A, B, D during the months of March through August 2002. (Source: Fort Riley Range Control Office).**

| Month | Training Area | Total Training Days (TTD) |
|---|---|---|
| March | A | 185 |
| | B | 135 |
| | D | 135 |
| | **Total** | **455** |
| April | A | 194 |
| | B | 722 |
| | D | 382 |
| | **Total** | **1298** |
| May | A | 116 |
| | B | 474 |
| | D | 116 |
| | **Total** | **706** |
| June | A | 2659 |
| | B | 1925 |
| | D | 2815 |
| | **Total** | **7399** |
| July | A | 2111 |
| | B | 915 |
| | D | 38 |
| | **Total** | **3064** |
| August | A | 762 |
| | B | 463 |
| | D | 866 |
| | **Total** | **2091** |
| | **Sum of Totals** | **15013** |

The largest difference in NDVI values, as imaged by the Landsat TM and MODIS sensors, was 0.08. Values for the training intensity factor were determined by taking this maximum difference value and dividing it by 5, which was equal to the number of soil erosion loss (annual) classes used. The result of this operation, 0.016, served as the increment by which the final training intensity factor increases in the pixel-level training intensity factor.

In a GIS, a raster layer was generated using 2002 TTD that were organized into five classes into which the following training intensity factor values were substituted: Very Low = 0.016, Low = 0.032, Medium = 0.048, High = 0.064, and Very High = 0.08 (Figure 3.2-4). For purposes of running the modified RUSLE model, a value of one was added to each pixel value (e.g., the five class breaks for the training intensity factor would be equal 1.016, 1.032, 1.048, 1.064, and 1.08) to account for the varying levels of military training in the annualized soil loss prediction.

### 3.2.e. MODEL RESULTS

Each of the RUSLE factors were then combined with the new training intensity factor layer in local raster operation to estimate annual soil loss. Incorporation of a training intensity factor resulted in a difference in estimated annual soil losses of between 0.00 and 5.40 tons/acre/year (Figure 3.2-5) as compared to the unmodified RUSLE (Figure 3.2-5). Adding the training intensity factor increased the maximum soil loss to be over 247 tons/acre year.

A "difference" map was created by subtracting the original RUSLE results grid from the modified RUSLE output to determine the difference in soil loss estimates between the two models and to help better visualize where those differences were located (Figure 3.2-5). The difference map shows areas of increased estimated soil losses on grasslands within training and maneuver areas.

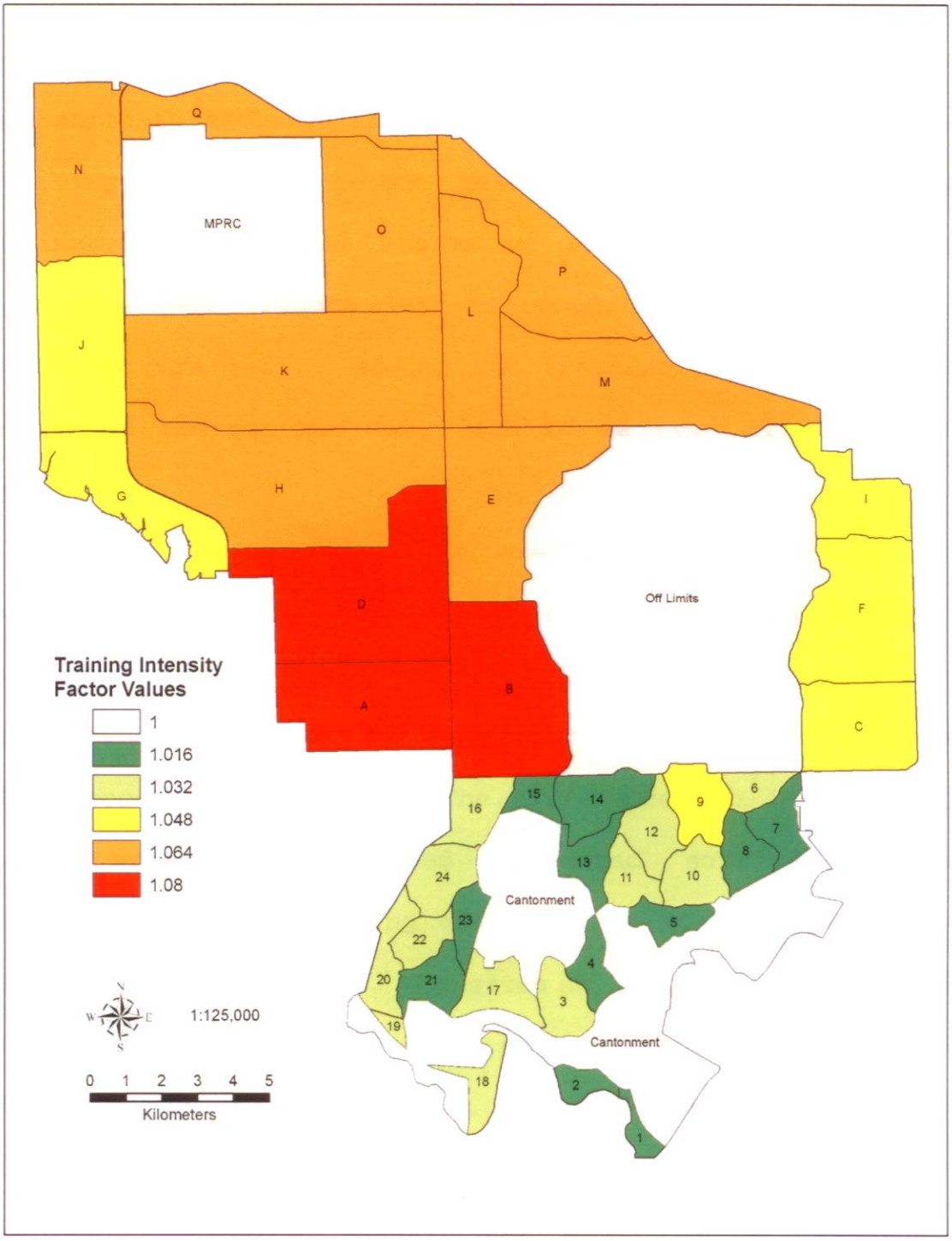


**Figure 3.2-4. Training intensity factor for Fort Riley, Kansas in 2002.**

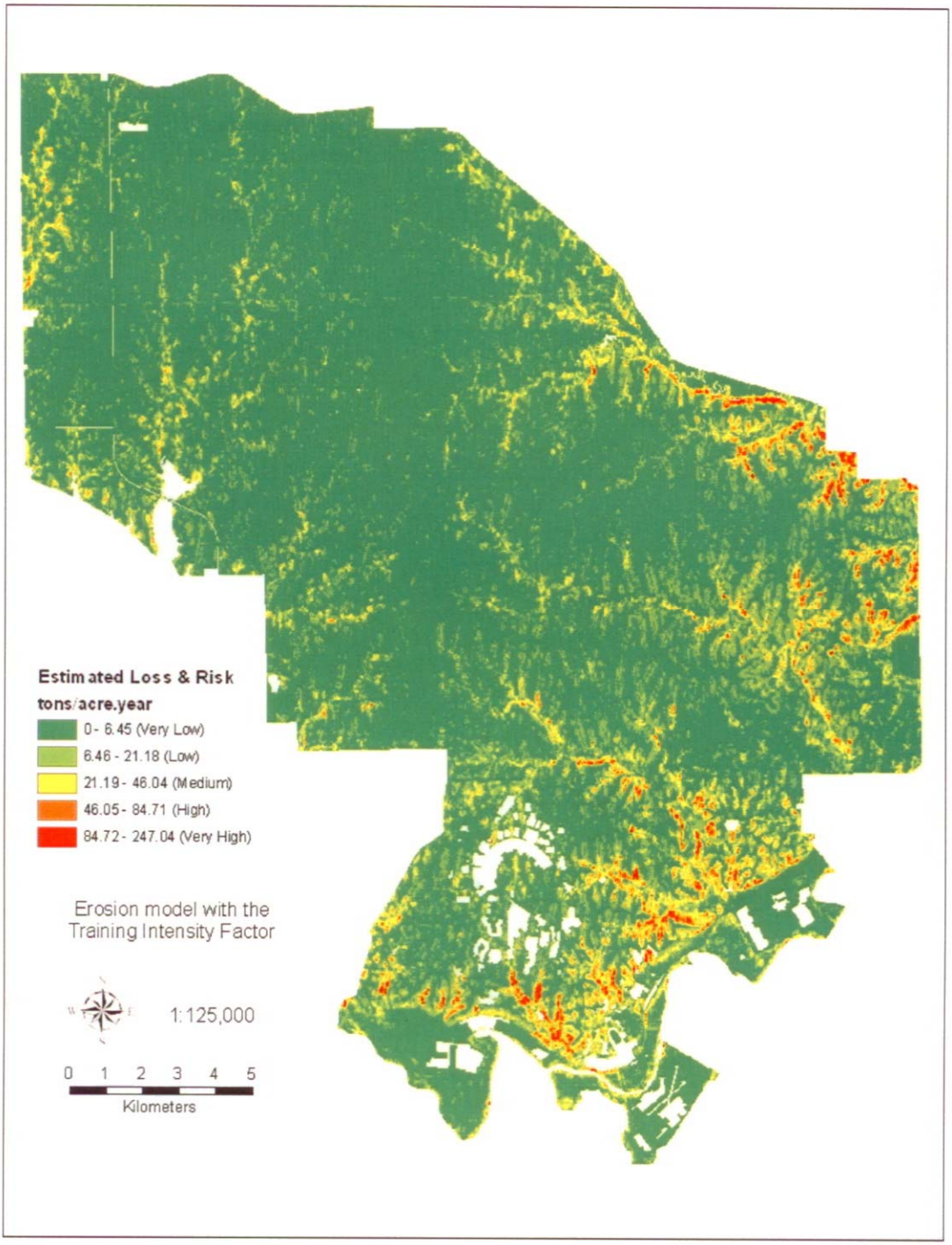


**Figure 3.2-5. Estimated soil loss and risk for Fort Riley, Kansas in 2002.**

The sites of the highest estimated soil erosion losses were found co-located with higher slope values along stream channels. These areas are typically not used for vehicle maneuver exercises due to a number of factors, including safety and environmental awareness regulations. The majority of vehicle-based training is done in areas of very low to moderate soil losses.

Most of the locations exhibiting the highest increase in annual soil erosion losses, as estimated by the modified RUSLE, were the lettered maneuver areas which generally had higher TTD values (Figure 3.2-6 and Table 3.2-7). The numerical training areas tended to have smaller increases in estimated soil losses. The highest average increase in estimated annualized soil losses were identified in four maneuver and two training areas: B, F, I, M, 9, and 17 (Figure 3.2-6). Maneuver areas F, I, and M are found to have both the highest maximum and average difference values. As expected, modifying the RUSLE using a TTD-derived training intensity factor yields increases in increased estimates of annual soil erosion losses. Maneuver areas in the medium and high TTD classes (F, I, and M) were found to have the highest maximum difference in pixel values and the highest average increases in estimated soil loss.

### 3.2.f. SUMMARY

Methods to estimate annual soil erosion losses, and the potential impact of military training activities on soil loss, are very useful to military land managers. This study illustrates the applicability of the RUSLE model for military training lands and how GIS and remote sensing techniques can save time and resources in determining rates of erosion for large spatial extents.

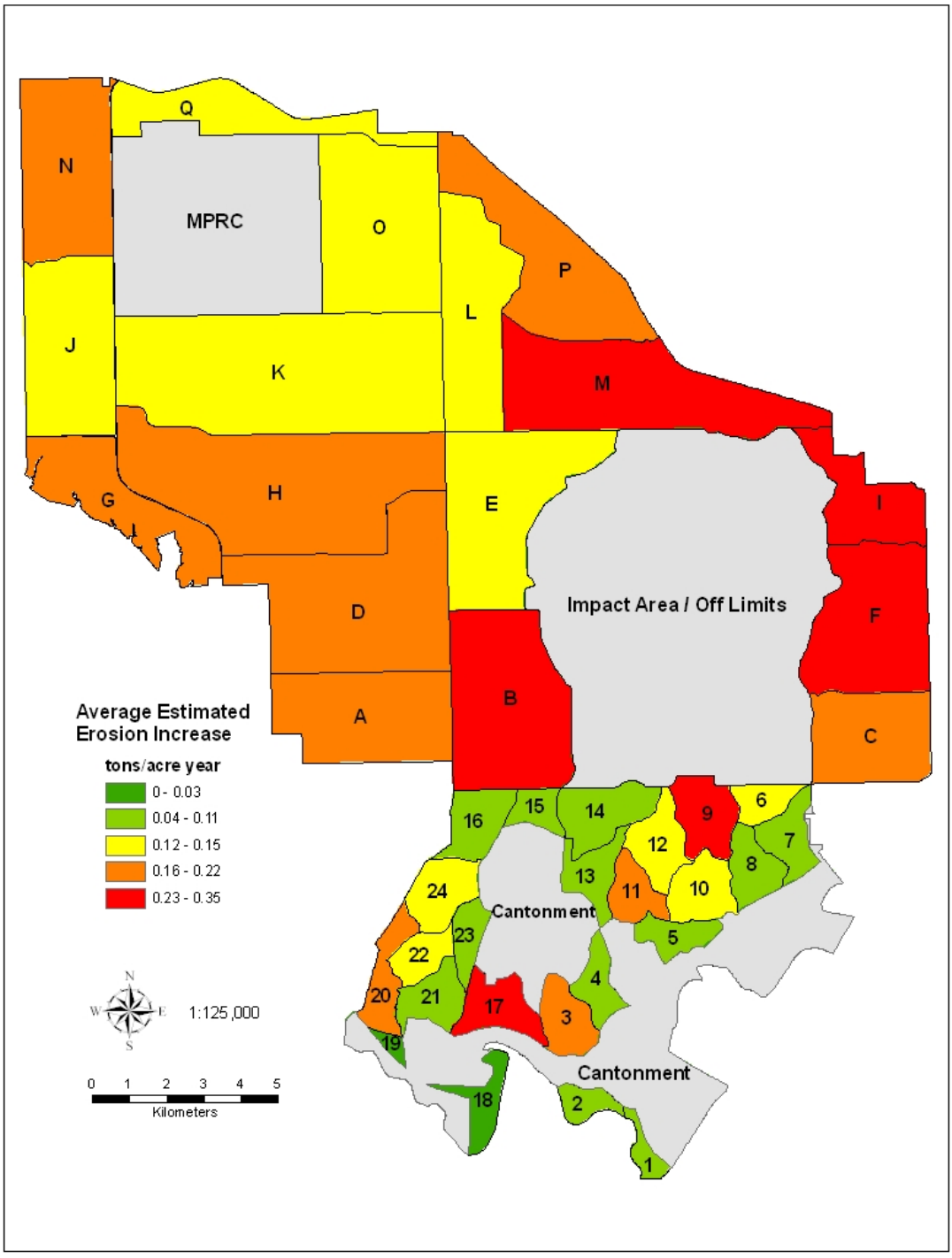


**Figure 3.2-6. Average estimated increase in annual soil erosion in maneuver and training area grasslands at Fort Riley, Kansas based upon application of RUSLE with a training intensity factor.**

**Table 3.2-7. Summary of differences (in tons/acre/year) in estimated annual soil erosion losses at Fort Riley as determined by the modified and unmodified RUSLE models. The COUNT column lists number of pixels included in each training area.**

| AREA | COUNT | MIN | MAX | RANGE | MEAN | STD | SUM |
|---|---|---|---|---|---|---|---|
| A | 11102 | 0.000 | 2.040 | 2.040 | 0.221 | 0.202 | 2451.620 |
| B | 13359 | 0.000 | 2.472 | 2.472 | 0.261 | 0.207 | 3487.830 |
| C | 6292 | 0.000 | 1.375 | 1.375 | 0.192 | 0.163 | 1209.010 |
| D | 19444 | 0.000 | 1.650 | 1.650 | 0.211 | 0.185 | 4100.760 |
| E | 14266 | 0.000 | 3.149 | 3.149 | 0.153 | 0.140 | 2184.910 |
| F | 9218 | 0.000 | 4.341 | 4.341 | 0.264 | 0.238 | 2435.120 |
| G | 7015 | 0.000 | 1.540 | 1.540 | 0.194 | 0.160 | 1360.230 |
| H | 23599 | 0.000 | 2.955 | 2.955 | 0.175 | 0.148 | 4120.130 |
| I | 4628 | 0.000 | 5.398 | 5.398 | 0.347 | 0.311 | 1603.640 |
| J | 11853 | 0.000 | 1.551 | 1.551 | 0.129 | 0.117 | 1528.360 |
| K | 28309 | 0.000 | 1.438 | 1.438 | 0.152 | 0.134 | 4311.940 |
| L | 11183 | 0.000 | 1.423 | 1.423 | 0.145 | 0.128 | 1617.960 |
| M | 13645 | 0.000 | 3.341 | 3.341 | 0.242 | 0.224 | 3303.580 |
| N | 10798 | 0.000 | 3.162 | 3.162 | 0.214 | 0.175 | 2308.140 |
| O | 16465 | 0.000 | 1.162 | 1.162 | 0.121 | 0.106 | 1987.240 |
| P | 9610 | 0.000 | 1.866 | 1.866 | 0.187 | 0.154 | 1798.860 |
| Q | 7542 | 0.000 | 1.046 | 1.046 | 0.148 | 0.126 | 1118.630 |
| 1 | 453 | 0.000 | 0.330 | 0.330 | 0.033 | 0.037 | 14.997 |
| 2 | 6 | 0.002 | 0.123 | 0.122 | 0.070 | 0.049 | 0.417 |
| 3 | 1287 | 0.000 | 2.488 | 2.488 | 0.184 | 0.164 | 236.633 |
| 4 | 808 | 0.000 | 0.314 | 0.314 | 0.074 | 0.055 | 59.469 |
| 5 | 641 | 0.000 | 0.500 | 0.500 | 0.086 | 0.073 | 55.276 |
| 6 | 1242 | 0.000 | 0.589 | 0.589 | 0.133 | 0.097 | 165.078 |
| 7 | 1612 | 0.000 | 0.529 | 0.529 | 0.084 | 0.074 | 134.872 |
| 8 | 1230 | 0.000 | 0.699 | 0.699 | 0.099 | 0.082 | 121.862 |
| 9 | 1526 | 0.000 | 1.438 | 1.438 | 0.247 | 0.204 | 376.880 |
| 10 | 1059 | 0.000 | 1.781 | 1.781 | 0.139 | 0.138 | 147.595 |
| 11 | 1277 | 0.000 | 1.887 | 1.887 | 0.205 | 0.150 | 262.015 |
| 12 | 2571 | 0.000 | 0.715 | 0.715 | 0.148 | 0.111 | 379.951 |
| 13 | 1920 | 0.000 | 0.661 | 0.661 | 0.076 | 0.060 | 145.600 |
| 14 | 3395 | 0.000 | 0.381 | 0.381 | 0.066 | 0.054 | 222.870 |
| 15 | 962 | 0.000 | 0.225 | 0.225 | 0.051 | 0.040 | 49.462 |
| 16 | 1977 | 0.000 | 0.818 | 0.818 | 0.085 | 0.081 | 168.192 |
| 17 | 2295 | 0.000 | 1.582 | 1.582 | 0.234 | 0.233 | 537.777 |
| 18 | 515 | 0.000 | 0.219 | 0.219 | 0.017 | 0.023 | 8.565 |
| 19 | 309 | 0.000 | 0.420 | 0.420 | 0.029 | 0.045 | 9.062 |
| 21 | 2277 | 0.000 | 0.630 | 0.630 | 0.106 | 0.091 | 240.860 |
| 22 | 1781 | 0.000 | 0.645 | 0.645 | 0.127 | 0.090 | 226.329 |
| 23 | 1481 | 0.000 | 0.345 | 0.345 | 0.065 | 0.051 | 96.632 |
| 24 | 2836 | 0.000 | 1.453 | 1.453 | 0.145 | 0.112 | 410.094 |
| 20 | 1589 | 0.000 | 1.060 | 1.060 | 0.181 | 0.151 | 288.134 |

This study shows there is strong evidence of a difference in vegetation condition between areas subjected to varying intensities of military training. This finding is supported by other work on military lands (Anderson *et al*., 1999; Bartsch *et al*., 2002; Houston *et al*., 2001; Quist *et al*., 2003; Trame, 1997; Tweedale *et al*., 2000). The combined use of Landsat TM and MODIS NDVI imagery in this project was able to measure a significant difference in greenness between the training area and impact area control study sites. However, further work is needed to determine the correct biophysical relationship between military training intensity and changes in grassland vegetation health. One example of future work would be the measurement of a vegetation index before and after specific field training exercises using different spatial and spectral resolution remote sensors. Data for the type and number of vehicles used would be useful for further studies.

The addition of a training intensity factor to the RUSLE resulted in increases in estimated annual soil loss on the installation. The use of field experiment plots to study actual soil loss in training areas would provide evidence in validating the estimated soil loss value. Assuming future research can validate the accuracy of this approach; this technique may serve as a better tool for land managers in prioritizing land rehabilitation activities, as well as scheduling military training events.

## 3.3 TASK 3: BUFFER FIELD STUDY

### 3.3.a. BACKGROUND

Military activities can change the natural environment and make the soil vulnerable to erosion. When heavy military vehicles, such as tanks and artillery guns, are operated, they damage the soil cover extensively and expose the surface to rainfall and runoff water, thus increasing the potential for erosion. Other than tank maneuvering areas and artillery firing ranges, land development due to cantonments also contributes to non-point source (NPS) pollution. As a result, all army installations are required to have NPDES permits with $SWP_3$ (Schmid, 1996). There are several ways to control NPS pollution and they are collectively called Best Management Practices (BMPs). BMPs are designed to reduce the amount of pollutants that are generated and/or transported from the source to the receiving water body. They can be either structural (e.g. waste treatment lagoons, vegetated grass waterways) or managerial (e.g. conservation tillage, nutrient management) (Dressing, 2003). Normally BMPs are used in combination to achieve maximum benefits. The mechanisms by which BMPs reduce NPS pollution include reducing available pollutants at the source, preventing the transport of pollutants, and remediating by chemical or biological means (Dressing, 2003).

Since NPS pollution and soil erosion are interrelated, most BMPs tend to reduce soil erosion by reducing soil detachment, reducing sediment transport, and trapping sediment before it enters a surface water body. BMPs also reduce the volume of water reaching water bodies by increasing infiltration of water into soil. Some BMPs increase retention time and reduce peak flow to reduce the in-channel erosion.

The Natural Resources Conservation Service (NRCS) defines a VFS as “a strip or area of herbaceous vegetation situated between cropland, grazing land, or disturbed land (including

forestland) and environmentally sensitive areas" (USDA-NRCS, 2003). VFS are used to reduce sediment and dissolved contaminants in runoff and to improve the quality of stormwater before it reaches a water body (Clar et al., 2004).

VFS serve several purposes, such as reducing sediment, particulate organics and sediment adsorbed pollutants in runoff, reducing dissolved pollutants in runoff, and improving wildlife habitat (USDA-NRCS, 2003). Sediment deposition, infiltration and plant uptake are the major mechanisms for pollutant removal. Filter strips are more effective in trapping sediment bound nutrients than dissolved nutrients (Leeds et al.,1994).

Deposition is the most important pollutant removal process in VFS, and it occurs within the first few meters of a VFS. The velocity of the runoff is reduced when it enters the VFS; with lower velocities, sediment, especially larger particles such as sand and silt sized particles and soil aggregates, start to deposit. Depending on the runoff velocity, smaller particles such as clay may take longer to settle and travel further than larger particles. Trapping of sediments also reduces the sediment bound nutrients and chemicals (Leeds et al., 1994).

Infiltration of runoff within a VFS is increased by two factors, reduced runoff velocity from vegetation resistance and increased porosity from plant roots and organic matter. Reduced velocity helps to increase the time available for infiltration. By increasing infiltration the amount of runoff is reduced. Infiltration also provides additional filtration. Dissolved nutrients and chemicals in the infiltrated runoff will enter into soil so that pollutants in the runoff will be reduced (Leeds et al., 1994).

Nutrients and chemicals trapped in the VFS may be taken up by the vegetation, degraded, or transformed in the soil. A VFS's long term effectiveness may be affected by biological and chemical process such as volatilization, degradation, adsorption, and absorption of pesticides, and N and P transformation (Leeds et al., 1994). Other processes that may take place within a VFS are uptake of nutrients, denitrification and assimilation. (Helmers et al., 2006)
Native tallgrasses, such as big bluestem (*Andropogon gerardii*), Indiangrass (*Sorghastrum nutans*), switchgrass (*Panicum virgatum*), and little bluestem (*Schizachyrium scoparium*), have extensive, deep root systems. Native tallgrasses have greater below ground biomass compared to turf grass. Deep root systems help these plants survive extreme conditions such as fire, drought, floods or cold. The above ground biomass of the plants can absorb the erosive energy of rainfall and runoff, thus reducing erosion. Roots bind the soil together and stabilize it to prevent washed off with the runoff. Deep penetrating roots also help to enhance infiltration. Finally, sediment can be filtered out from runoff and runoff velocity is slowed by the vegetation. Overall native tallgrasses have greater potential as VFS than any other vegetation. Native tallgrasses also possess more habitat value for wildlife (USDA-NRCS, 2004).

Several factors, such as topography, climate, and field conditions, affect the performance of a VFS (Helmers et al., 2006). Specific factors that affect the VFS's performance are flow rate, drainage area, development conditions, soils, infiltration rate, topography, depth of water table, vegetation, climate, sediment characteristics and characteristics of the pollutants being attenuated. (Clar et al., 2004)

Several studies have been conducted to evaluate the ability of VFS to attenuate pollutants coming from feedlots and croplands (Abu-Zreig et al., 2004; Barfield et al., 1998; Blanco-Canqui et al., 2004; Dillaha et al., 1989; Gharabaghi et al., 2001; Helmers et al., 2005; Hubbard et al., 2003; Komor and Hansen, 2002; Lee et al., 1999; Lim et al., 1998; Mendez et al., 1999; Sanderson et al., 2001;Schmitt et al., 1999). However, there is minimal work on VFS effectiveness for reducing pollutants resulting from military activities (Kim, 2005; St Clair, 2006). Additionally, there is only limited information on the effect of different management practices on VFS performance.

### 3.3.b. STUDY AREA APPROACH

VFS experiments were conducted at Fort Riley, located in northeastern Kansas. Mean annual precipitation, maximum and minimum temperature are 850 mm, 19°C, and 6°C, respectively (Daly et al., 2002; 1971- 2000). Elevations on Fort Riley range from 301 and 420 m above sea level, and steep slope variations are delineated along the stream channels in subwatersheds (Seven
Mile Creek, Three Mile Creek, and Wildcat Creek) and the Kansas River. The level III ecoregion (Omerink, 1995) for Fort Riley is the Flint Hills, encompassing northeastern Kansas to the border of Kansas-Oklahoma (25,339 $km^2$), which contains the largest continuous areas of uncultivated tallgrass prairie in the U.S. The three major landcover groups on Fort Riley are grasslands in wide hillslope areas, shrublands, and woodlands (Egbert et al., 2001).

Eight ha of hillslope area (39.15°N, 96.82°W), part of the Three Mile Creek watershed on Fort Riley, was chosen for the two VFS field sites. Riparian buffer zones in the downslope were not included to avoid training disturbance that occurs between maneuver stream crossings and the buffer zones. The hillslope area was covered with native tallgrasses (i.e., big bluestem, little bluestem, Indian grass, and switch grass); switch grass was the dominant species.

The experiments were conducted from August 2005 to November 2007 on two blocks of three vegetated filter strips (6 total), each 20 m x 3 m (3.1). The VFSs were laid along the slope of the land to facilitate the flow of water through the VFS and minimize cross flow. Vegetated filter strips in each block shared a common (longitudinal) boundary among them. To prevent cross flow between VFSs, metal sheets were buried along each boundary. The metal sheets created barriers 5-8 cm above and below the ground surface. The filter strip blocks were located approximately 110 m apart. The average slope of the study area was 3.9%.

Artificial precipitation events were applied to the site using Xcel wobbler irrigation nozzles (high angle $24^o$) (Senninger Inc., Clermont, Florida) with 69 kPa (10 psi) pressure regulators. The experimental set up is shown in Figure 3.3-1. The water source for the experiments was a fire hydrant located approximately 500 m from the filter strips. Each block of VFS had 10 nozzles on two laterals (5 nozzles per lateral). The laterals were spaced 3 m apart along the VFS boundary. Nozzles within each lateral were 3.3 m apart. Each nozzle was attached to a 1.8 m riser. The risers were anchored to the ground by iron bars. Each lateral had a ball valve to control the water flow which was connected to the main pipeline by a manifold. A pressure meter and ball valve on the main pipeline were used to regulate pressure and flow.

A 1230 L (325 US gallons) plastic tank was used as a reservoir to mix and store water treated with pollutants prior to application. A ball valve was fixed on the outlet of the tank for flow control. A screen was fixed inside the tank to keep big soil particles out of the pipelines. Polluted water from the reservoir was applied to the VFS as overland flow through spreaders to encourage sheet flow emulating VFSs design specifications and providing proper function (Clar et al., 2004; Blanco-Canqui et al., 2006). The spreaders were constructed from 1.5 m long and 7.6 cm diameter PVC pipe. Water was discharged through 14 holes, 0.95 cm diameter and 6.5 cm apart. Both ends of the spreaders were sealed.

The spreaders and reservoir were placed upslope from the VFS site. One spreader was placed across the slope of the land at the upslope end of each VFS. They were connected, using plastic hoses, to another manifold which distributed the polluted overland flow from the reservoir. The manifold had three outlets each with a ball valve, 41.1 kPa (6 psi) pressure regulator and a number 9, 3.57 mm (9/64 in) diameter Senninger irrigation nozzle to regulate flow. A water pump was used to pressurize the water as well as to mix the polluted water in the reservoir. A hose from the pump carried the return flow back to the reservoir creating turbulence keeping the polluted water well mixed.

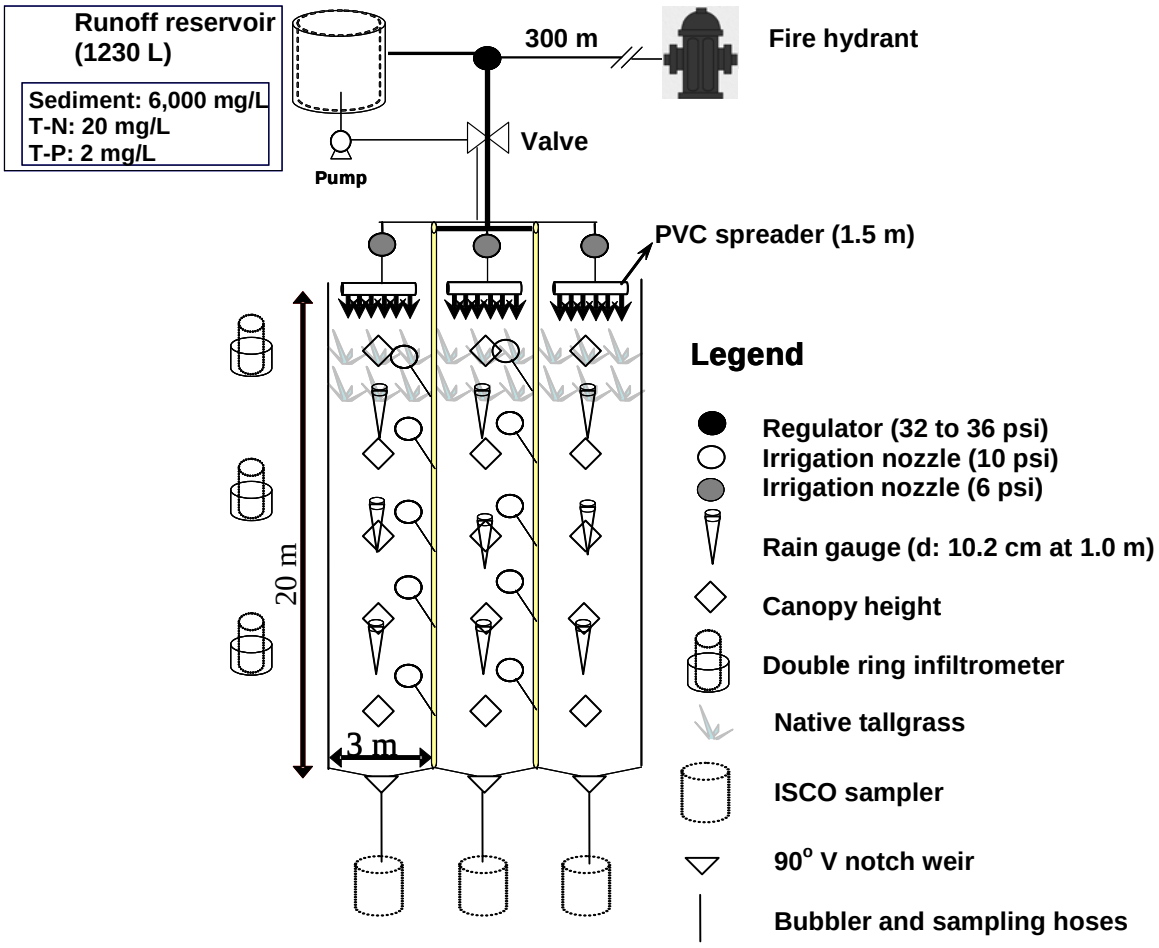


**Figure 3.3-1. Diagram showing the experimental set up at a VFS site in Fort Riley. (The entire site is covered with native vegetation.)**

At the lower end of the VFS, a 90$^o$ V-notch, sharp-crested weir anchored in concrete was used to measure outflow from the VFS. Metal sheets were installed to route outflow over the weir. In 2006 and 2007 an ISCO automatic sampler (model 6712 or 6700, Teledyne ISCO, Inc., Lincoln, Nebraska, USA) was assigned to each VFS in order to measure the depth of water flowing over the weir and take water samples at given time intervals. In 2005, a pump and bucket system was used. Polluted runon from upland area was simulated with overland flow applications from the reservoir. Soil (8kg), urea (55g) and diammonium phosphate (5.5g) were mixed in the reservoir (1230 L) to simulate overland runoff carrying sediment, N and P. The primary concern at this military installation is sediment and overland erosion; however nitrogen and phosphorus were added to gain a better understanding of overall VFS function for the major NPS pollutants in Kansas. Other than sediment nutrients like nitrogen and phosphorous cause eutrophication and pollution in Kansas water bodies, especially in the case of lakes reservoirs and ponds nutrients are the topmost pollutants (KDHE, 2006). Air-dried soil from the site was sieved using a 2 mm sieve before adding it to the reservoir to simulate sediment in runoff. The diammonium phosphate was premixed with about 200 ml of water because of low water solubility and added to the polluted reservoir.

Number of experiments conducted during each year and range of the inputs used are tabulated in the Table 3.3-1. Even though experiments were conducted in same plots, there were some differences in methods used and conditions exist. ISCO samplers were not available during the year of 2005. Year 2007 received more rainfall than other two years.

**Table 3.3-1. Details about the experiments conducted during the three growing seasons.**

| Year | Number of experiments | Simulated rainfall (mm) | Applied overland flow (mm) |
|---|---|---|---|
| 2005 | 7 | 11-121 | 7-42 |
| 2006 | 15 | 21-118 | 2-37 |
| 2007 | 15 | 12-141 | 4-17 |

During each experimental run, several samples and measurements were recorded including infiltration, vegetation canopy height, runoff flowrate, runon flowrate, and applied rainfall. Nine rainfall gauges were used to measure rainfall uniformity during the simulated event. Soil, water (runon and runoff) and vegetation samples were collected in order to measure soil moisture, pollutant concentration and biomass density. Using the measured data, water retained, applied rainfall, rainfall intensity, time of concentration, time to runoff and pollutant trapping efficiencies were calculated. Pollutant trapping efficiency (PTE) (%) was the main parameter used to evaluate the effectiveness of the VFS and was calculated based on a mass balance (Equation 3.3-1) (Barfield et al., 1998):

$$PTE = \frac{M_i - M_o}{M_i} * 100 \qquad \text{[Eq. 3.3-1]}$$

where

$M_i$ is the mass (g) coming in and $M_o$ is mass (g) going out from the VFS.

### 3.3.c. RESULTS AND DISCUSSION

A water balance was done using measured inputs and outputs. Table 3.3-2 shows the average proportion of different inputs and outputs for all three years and individual years. Interception, surface detention and evapotranspiration were assumed to be negligibly small, and were dropped out in the water balance calculations, thus the infiltration volume became equal to the volume of water retained. On most of the days infiltration was the significant component of the outputs.

**Table 3.3-2. Average water balances for all three years (overall), and individual years.**

| | | Rainfall | Runon | Runoff | Water retained |
|---|---|---|---|---|---|
| | | mm | mm | mm | mm |
| Overall | Mean | 54.1 | 14.3 | 10.4 | 56.3 |
| | SD | 28.5 | 10.8 | 12.9 | 33.1 |
| | CV | 0.53 | 0.75 | 1.24 | 0.59 |
| 2005 | Mean | 42.5 | 25.7 | 5.8 | 51.4 |
| | SD | 31.5 | 12.3 | 4.0 | 26.0 |
| | CV | 0.74 | 0.48 | 0.69 | 0.51 |
| 2006 | Mean | 60.1 | 14.4 | 1.9 | 72.7 |
| | SD | 27.0 | 10.3 | 2.1 | 33.6 |
| | CV | 0.45 | 0.72 | 1.15 | 0.46 |
| 2007 | Mean | 53.8 | 8.5 | 21.2 | 42.1 |
| | SD | 26.9 | 3.1 | 14.1 | 27.7 |
| | CV | 0.50 | 0.37 | 0.66 | 0.66 |

Travel time, which is considered for purposes of this study to be equal to the time of concentration, is theoretically a function of the overland flow velocity and the length of travel. The addition of flow resistance in the form of vegetation will slow the observed velocity and increase time of concentration. This phenomena was observed in a correlation between biomass density ($g/m^2$) and time of concentration (min) in the data collected for both filter blocks in 2007 ($P<0.0001$) (Figure 3.3-2). These two parameters are positively correlated; however, the degree of scatter in the data indicates other factors are also involved, which could include concentration of flow on the individual VFSs.

Time of concentration is a parameter which can affect the performance of the VFS. The mechanisms by which pollutants are attenuated are time dependant. In other words, increased residence time gives the VFS more time to trap pollutants and increase infiltration of the water flowing through. So it can be expected that the VFS will have greater pollutant trapping efficiencies (PTE) with increasing above ground biomass density.

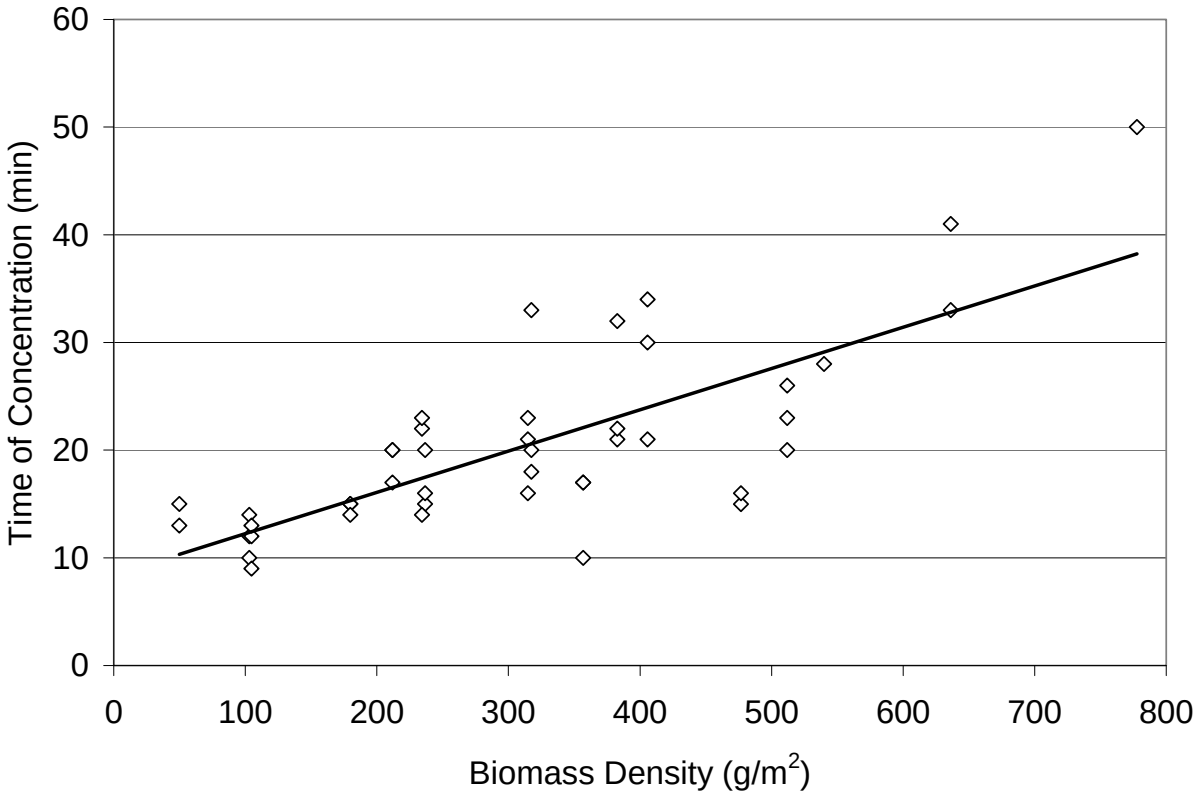


**Figure 3.3-2. Correlation between biomass density and time of concentration over the 2007 growing season (P < 0.0001). Both blocks of filter strips are included.**

This trend can be also explained by using Manning's coefficient (Jin et al., 2000). Manning's coefficient is a measure of surface roughness and changes with the growth stages of the vegetation. The higher the value of Manning's coefficient is, the greater the roughness of the surface and the greater the friction it renders to the flowing water. With the growth of grass, surface roughness increases, thus providing more friction to flowing water. Increasing friction reduces the velocity of the flow and increases the time of concentration. The reduced velocity also enhances settling of sediment.

By using the Manning-kinematic solution for travel time suggested by the TR-55 model for overland flow (Equation 3.3-2) (Soil Conservation Service, 1986), with appropriate rearranging, a Manning's n value can be calculated with measured data (Equation 3.3-3).

$$T_t = \frac{0.93(nL)^{0.6}}{i^{0.4} s^{0.3}} \qquad \text{[Eq. 3.3-2]}$$

$$n = \left( \frac{i^{0.4} s^{0.3} T_t}{0.93 L^{0.6}} \right)^{1.67} \qquad \text{[Eq. 3.3-3]}$$

where

$T_t$ (min) is travel time, n is Manning's n, L (ft) is the length of travel, i (in/hr) is the average rainfall excess intensity for a storm of duration $T_t$, which equals the time of concentration, and s (ft/ft) is slope.

Rainfall excess intensity is generally assumed to be rainfall intensity in small urban catchments due to the large amount of impervious area; however, in this instance rainfall excess is calculated by using the corresponding runoff rates and dividing by the area of concern. This method is a direct measure of rainfall excess.

A seasonal trend can be seen in the resulting Manning n values with low values after burning increasing through the growing season (Figure 3.3-3). Mowing seems to have no effect on the resulting roughness coefficient, which supports the theory that vegetation spacing (stem density) controls flow resistance (Hayes, et al., 1978; Tollner et al., 1976). Roughness decreases again after the system is burned in the fall to near early spring values indicating the roughness coefficient was reset to bare ground values.

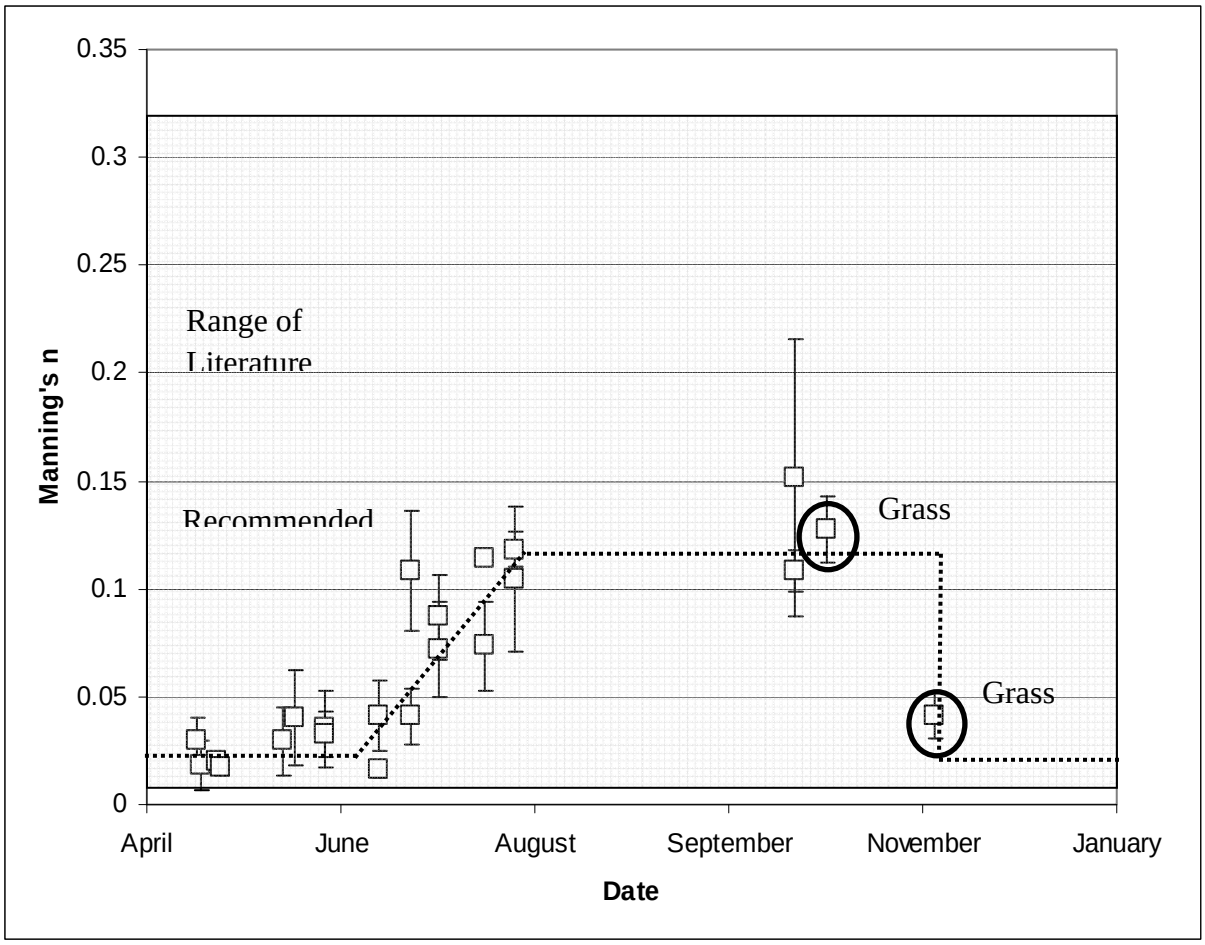


**Figure 3.3-3. Calculated Manning's n values using the Manning-kinematic solution suggested by the TR-55 model and measured flowrates and measured time of concentrations. (This is 2007 data and the site was mowed on October 19, 2007 and burned on November 15, 2007.)**

Differences in initial soil moisture were found to play a significant role in time to runoff. Conceptually the time to runoff is a function of the length of travel, slope, and, the initial soil water content. Although not originally intended for estimating runoff potential, an equation developed by the Soil Conservation Service (SCS) (1975) to estimate lag time (Equation 3.3-4) encompasses the appropriate parameters if the curve number is varied based off of antecedent moisture conditions.

$$t_L = \frac{L^{0.8}(S+1)^{0.7} Y^{-0.5}}{1900} \qquad \text{[Eq.3.3-4]}$$

where $t_L$ (hr) is lag time, L (ft) is flow length, S (in) is the maximum soil water retention parameter in the SCS Curve Number runoff method, and Y (%) is the land slope. This equation was modified (Equation 3.3-5) based on measured data to estimate time to runoff with an $R^2$ value of 0.76 ($P<0.0001$). Exponents were calculated using an iterative method and comparing resulting sum of squares of the differences in observed data and predicted values.

$$t_R = L^{5.35} * V_{WC}^{-2.70} * i^{-0.61} * Y^{-0.5} \qquad \text{[Eq. 3.3-5]}$$

where $t_R$ (min) is the time to runoff, L (m) is length of the VFS, $V_{WC}$ (%) is initial volumetric water content of the soil, i (mm/hr) is the rainfall intensity, and Y (%) is the slope of the VFS.

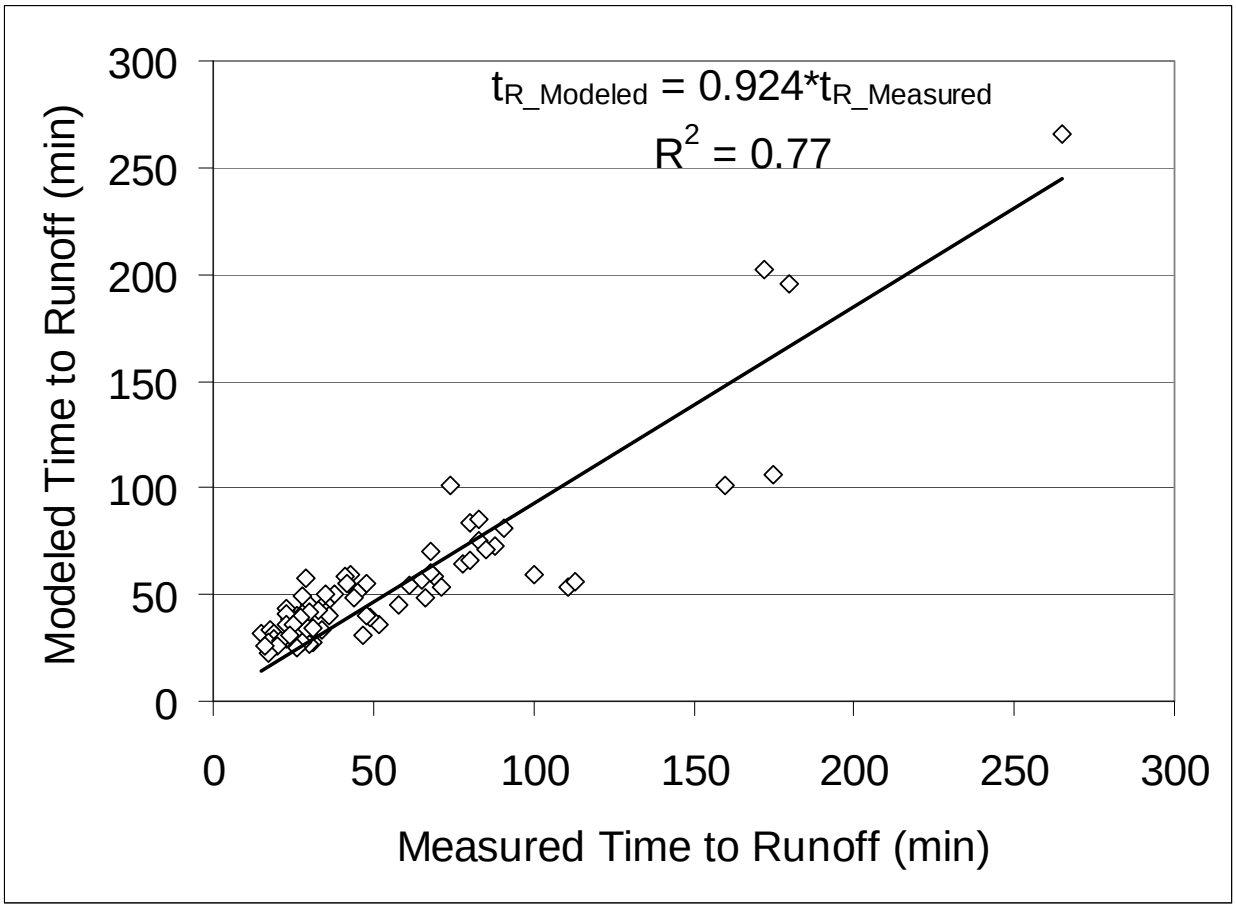


**Figure 3.3-4. Comparison of estimated time to runoff ($t_R$) and measured $t_R$ using equation 5 - 2007 growing season only (P <0.0001 and $R^2$=0.77).**

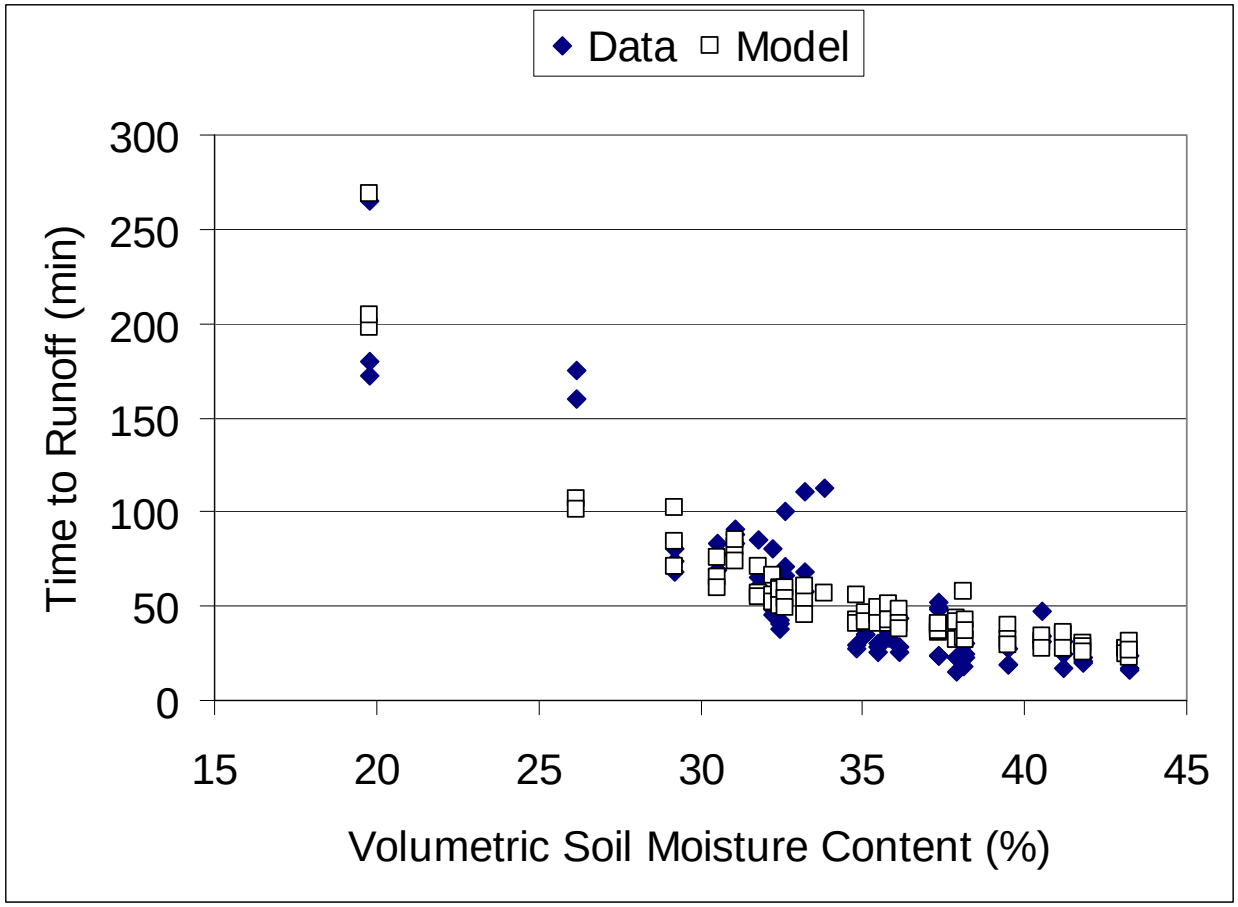


**Figure 3.3-5. Comparison of estimated time to runoff ($t_R$) and volumetric soil moisture content.**

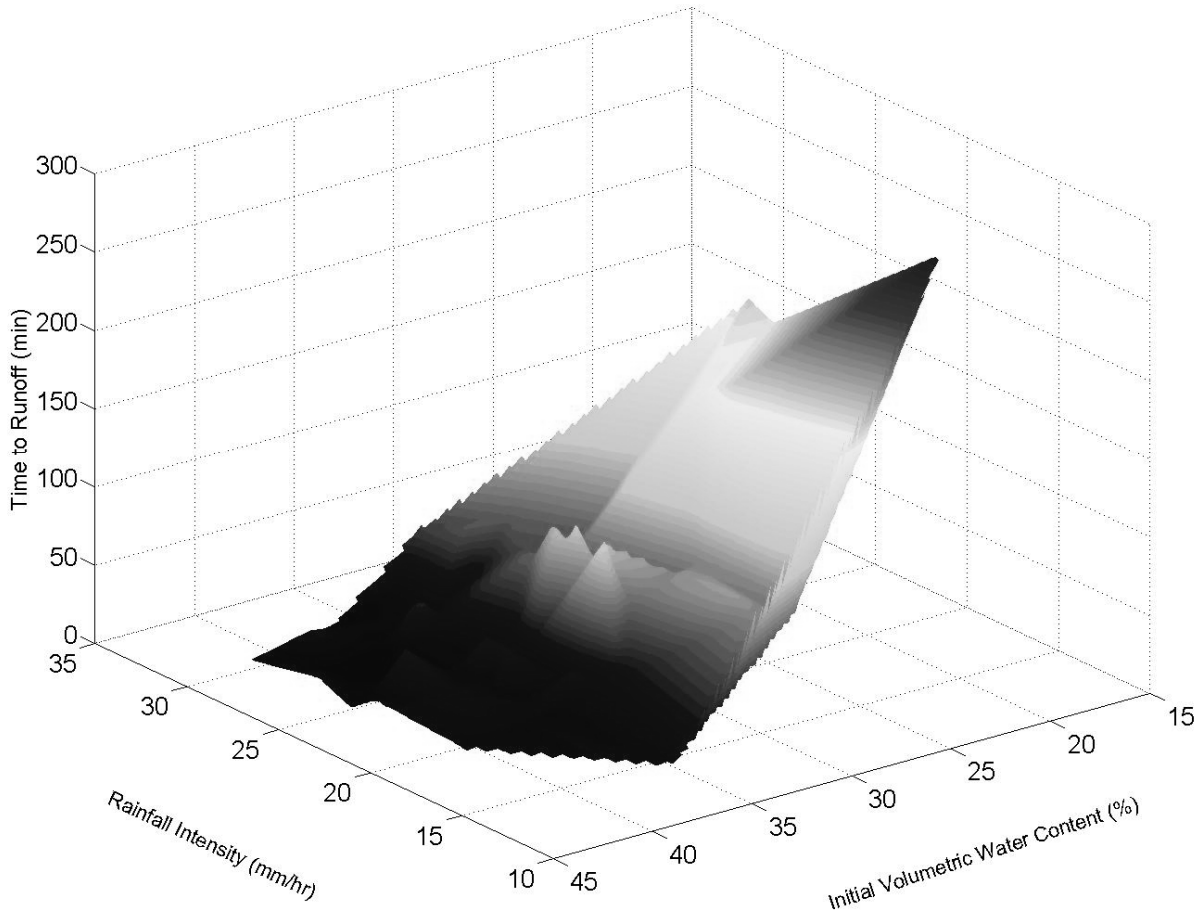


**Figure 3.3-6. Relationship between rainfall intensity, initial volumetric water content of the site, and the time to runoff.**

Dry soils have the ability to abstract more water than moist soils before runoff starts because more water would be required to bring the dry soils to a point where rain intensity exceeds infiltration rate and runoff is initiated (Figure 3.3-5 and 3.3-6). If a VFS has greater time to runoff during a storm due to low soil moisture, it will remove more pollutants from the runoff since time to runoff is correlated with the length of the filter strip and soil moisture. PTE also depends on the same factors. That means military training has to be done beyond a certain distance from water bodies of concern based on the antecedent moisture condition. It is possible to predict the minimum width of the buffer strip for a set of conditions such as soil moisture and slope to have a minimum time to runoff for the desired pollutant attenuation. If the soil is wet, tanks have to stay further away from the water bodies and if the soil is dry, they may maneuver a bit closer to the water bodies.

Runoff initiation is delayed in dry soils due to higher storage capacity during the first portion of each test. Furthermore, the amount of water that infiltrated, or retained during a particular simulation greatly depended on the initial soil moisture. The relationship between soil moisture

and water retained was significant (P<0.0001) (Figure 3.3-7). From the relationship between initial soil moisture with time to runoff and water retained, it is clear that initial soil moisture plays a crucial role in VFS function. It can be expected that a VFS with lower moisture content has the capacity to reduce more pollutants than with wet soil conditions due to the fact that more polluted water enters the soil.

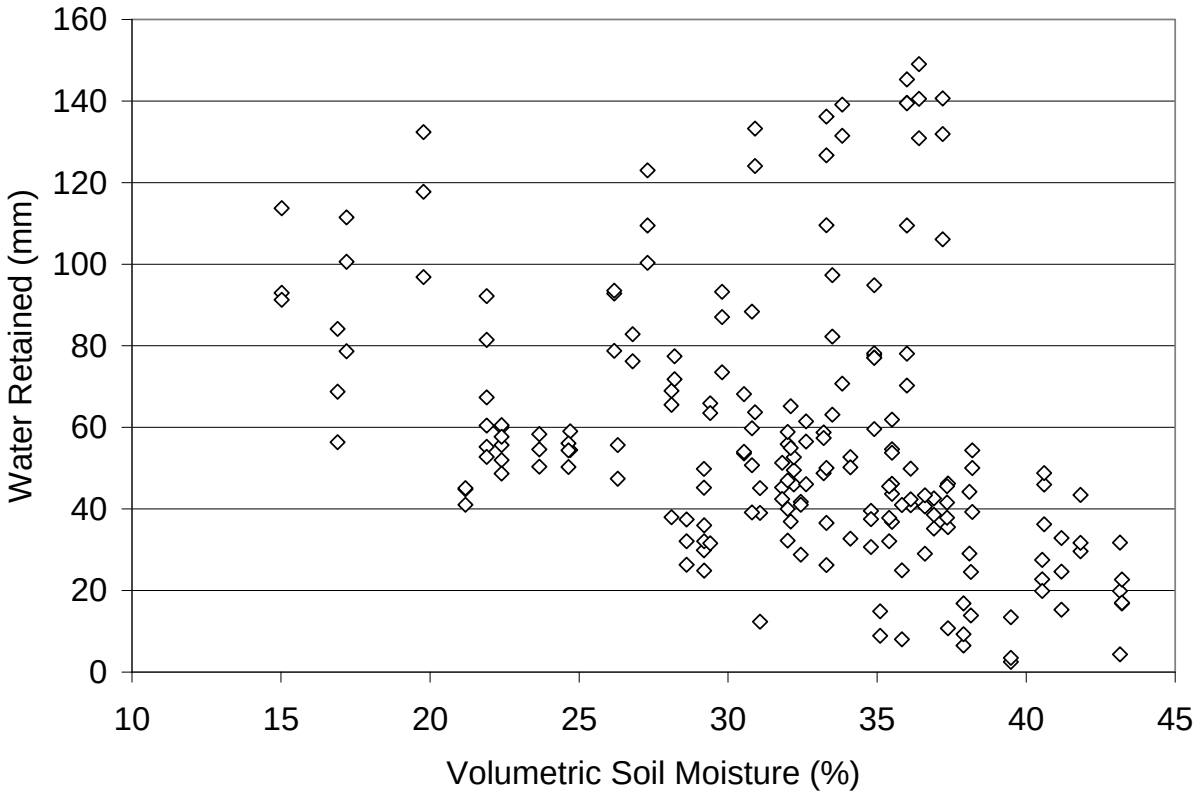


**Figure 3.3-7. Correlation between soil moisture and water retained (P<0.0001).**

Native grasses have extensive root systems (USDA-NRCS, 2004, Tufekcioglu et al., 1999) which improve infiltration. A regression model was fit for total infiltration volume with biomass density (measured as the total mass of vegetation per square meter of surface area) to see if there was any relationship (Figure 3.3-8). The relationship was significant with a P value of 0.00382. This trend agrees with literature that the infiltration is influenced by the root systems of the native grass (Leeds et al., 1994). But it should be also noted that, it was soil moisture which had a greater impact on infiltration volume.

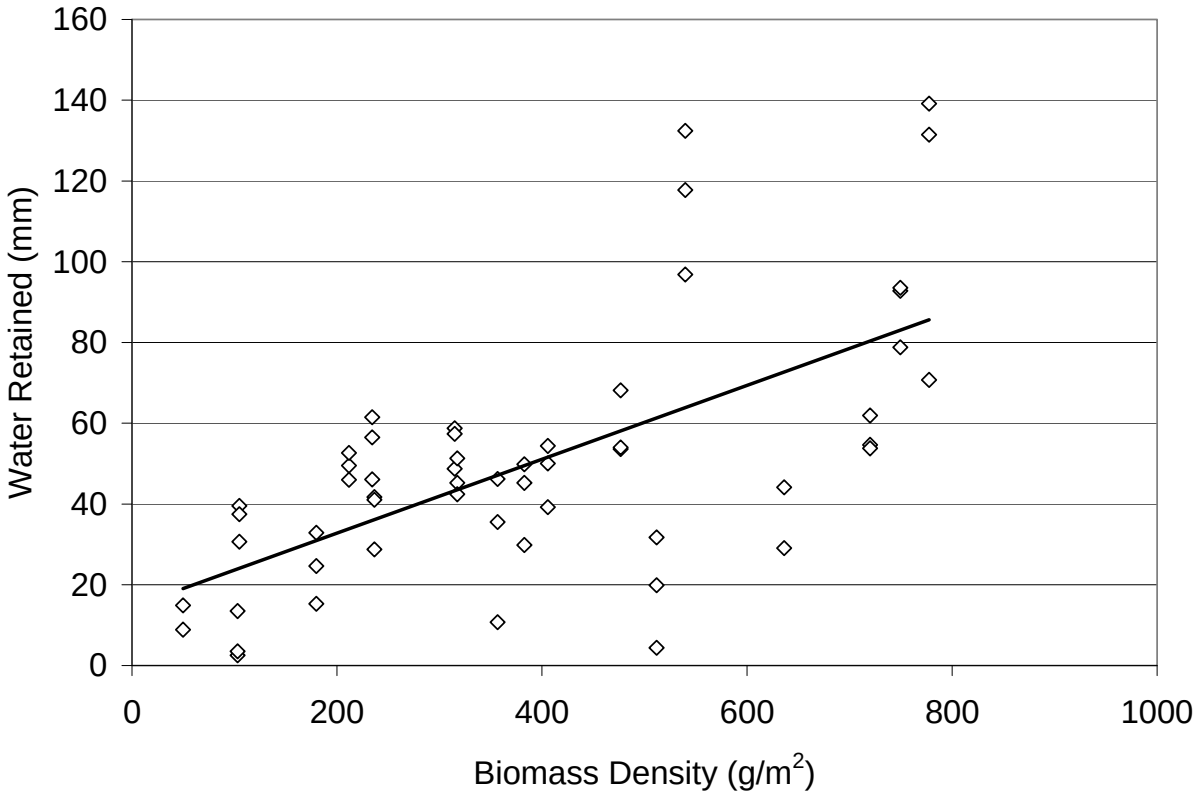


**Figure 3.3-8. Change in water retained in relation to change in biomass density (P=0.00382).**

To better understand the effects soil moisture and biomass density have on water movement, a three-dimensional plot was constructed (Figure 3.3-9). The general trend shows an increase in time to runoff with a decrease in initial soil moisture and an increase in biomass density. The presented data represents the 2007 growing season; however, the experimental procedure was temporarily changed for two tests in July, which were not included. Two additional points were removed due to a low rainfall intensity on one plot.

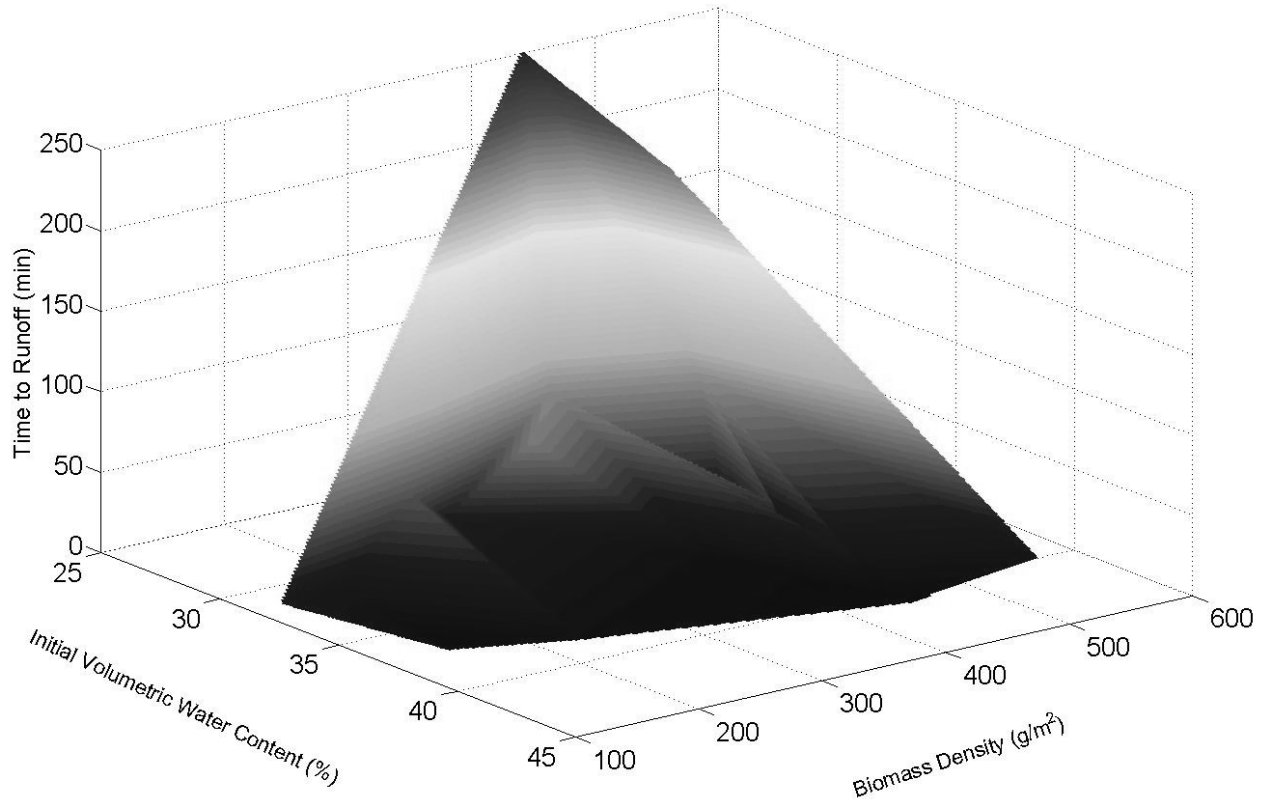


**Figure 3.3-9. The influence of biomass density and initial soil moisture on the time it takes water to runoff.**

### 3.3. d. POLLUTANT TRAPPING EFFICIENCIES

Pollutant trapping efficiency (PTE) was used as a scale to measure the performance of the VFS. Higher PTE implied better performance by the VFS. In general, PTE values for P varied drastically while TSS and N stayed relatively consistent. It should be noted that 100% PTE efficiencies were obtained when there was very little runoff from the sites and/or due to analytical detection limits. For example, several runoff samples had total suspended solids (TSS) concentrations below the detection level (1 mg/L). Summary statistics of the initial soil moisture, biomass density, and PTE are given in Table 3.3-3.

**Table 3.3-3. Summary statistics of biomass, soil moisture and pollutant trapping efficiencies**

| | | Biomass | Soil moisture | Trapping efficiencies (%) | | |
|---|---|---|---|---|---|---|
| | | gm^-2 | g/g | N | P | TSS |
| Overall | Mean | 446.3 | 31.4 | 89.6 | 56.3 | 97.4 |
| | SD | 255.2 | 7.0 | 15.1 | 56.2 | 5.2 |
| | CV | 0.57 | 0.22 | 0.17 | 1.00 | 0.05 |
| 2005 | Mean | 689.5 | 19.8 | 94.7 | 76.9 | 98.6 |
| | SD | 219.6 | 3.9 | 4.8 | 21.1 | 1.4 |
| | CV | 0.32 | 0.19 | 0.05 | 0.27 | 0.01 |
| 2006 | Mean | 336.9 | 32.0 | 99.3 | 98.6 | 99.7 |
| | SD | 194.9 | 5.0 | 1.5 | 1.5 | 1.3 |
| | CV | 0.58 | 0.16 | 0.01 | 0.02 | 0.01 |
| 2007 | Mean | 384.7 | 34.8 | 80.4 | 16.6 | 95.3 |
| | SD | 220.7 | 5.2 | 17.8 | 60.1 | 6.9 |
| | CV | 0.57 | 0.15 | 0.22 | 3.62 | 0.07 |

Pollutant trapping efficiency for N varied from 14% to 100% while PTE for P ranged from -196% to 100%. For TSS, PTE was within the limit of 67-100%. Values for TSS were more consistent throughout the whole study with the majority in the range of 90-100%. For P, negative values were observed when large quantities of runoff occurred. This was also noticed in earlier research and Dillaha et al. (1989) hypothesized that this might have been caused by the re-suspension of the phosphorous particles that were adsorbed to soil particles in the previous simulations.

Since pollutants were carried with water and infiltration was the main mechanism by which pollutants were attenuated, regression models were also fit for PTE with water retained (Figure 3.3-10). As expected, increases in infiltration generally increased the PTE for each constituent. All relationships had a P value of <0.0001. These results confirm that infiltration plays a major role in the pollutant attenuation as reported in literature (Barfield et al., 1998).

Runoff volume influenced the amount of pollutants that were transported in the runoff and its effect was analyzed with regression models (Figure 3.3-11). The more the runoff volume, the higher the amount of pollutants transported, thus the PTE was reduced. These relationships were significant with P values of <0.0001

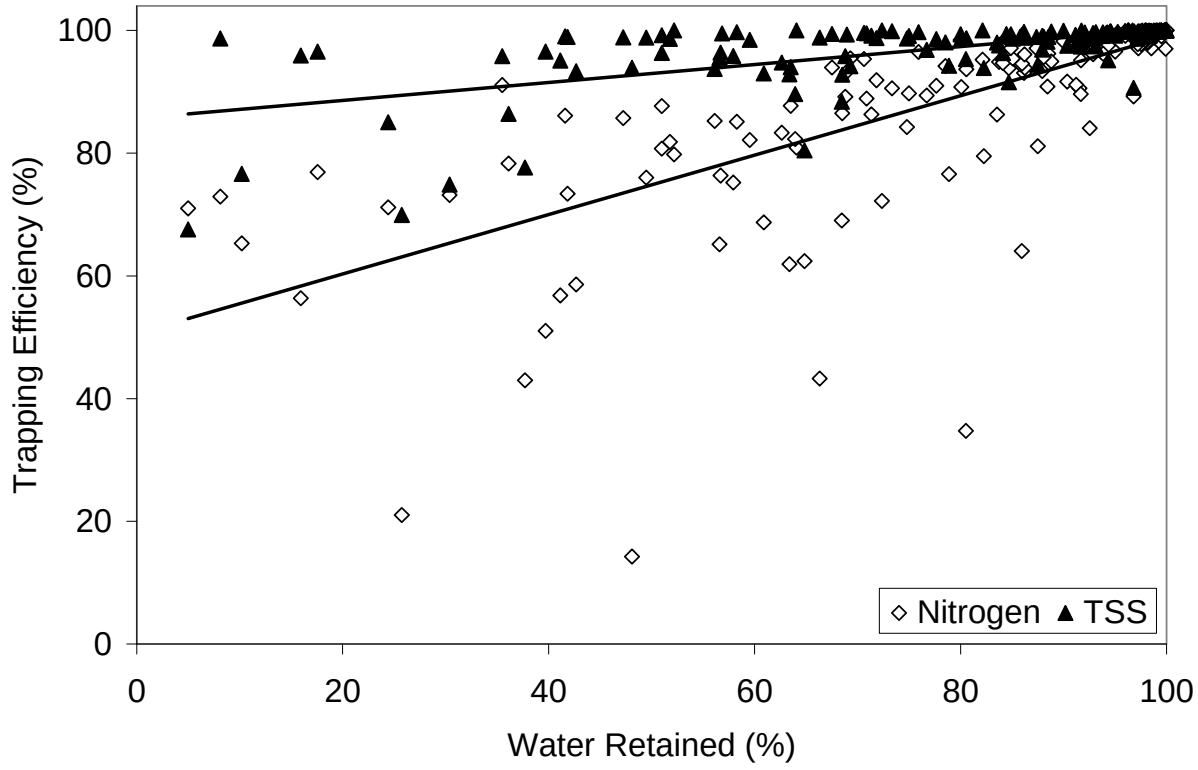


**Figure 3.3-10. Correlation between water retained percentage and pollutant trapping efficiencies (P< 0.0001).**

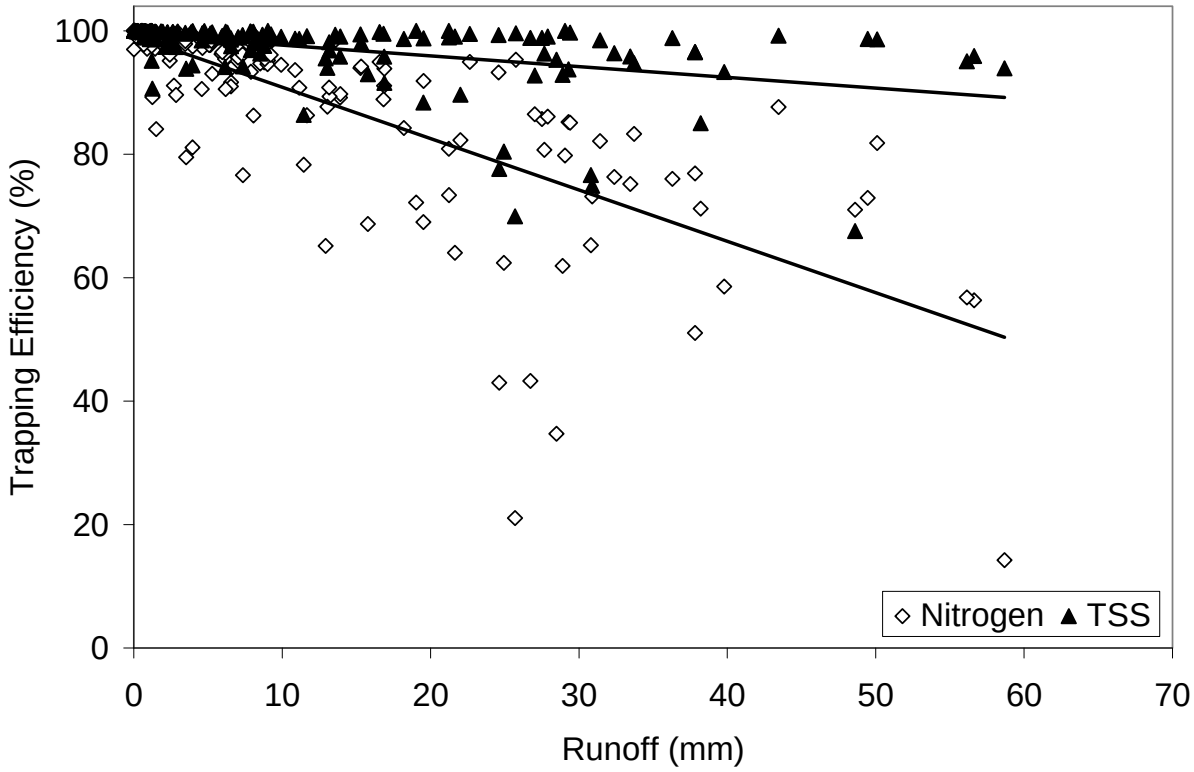


**Figure 3.3-11. Correlation between runoff volume and pollutant trapping efficiencies (P<0.0001).**

Biomass is an integral part of every VFS. The performance of a VFS depends on how dense the vegetation is both aboveground and belowground because biomass alters the hydrological variables such as evapotranspiration, interception and infiltration making VFS performance dynamic throughout the growing season. Infiltration tends to improve with the development of roots, due to formation of macropores and a lowering of bulk density. Also, vegetation at different growth stages may uptake different levels of nutrients. Pollutant trapping efficiency increases with the increasing aboveground biomass density for all constituents. P values for the relationships were 0.0025, 0.009 and 0.0001 for N, P and TSS, respectively.

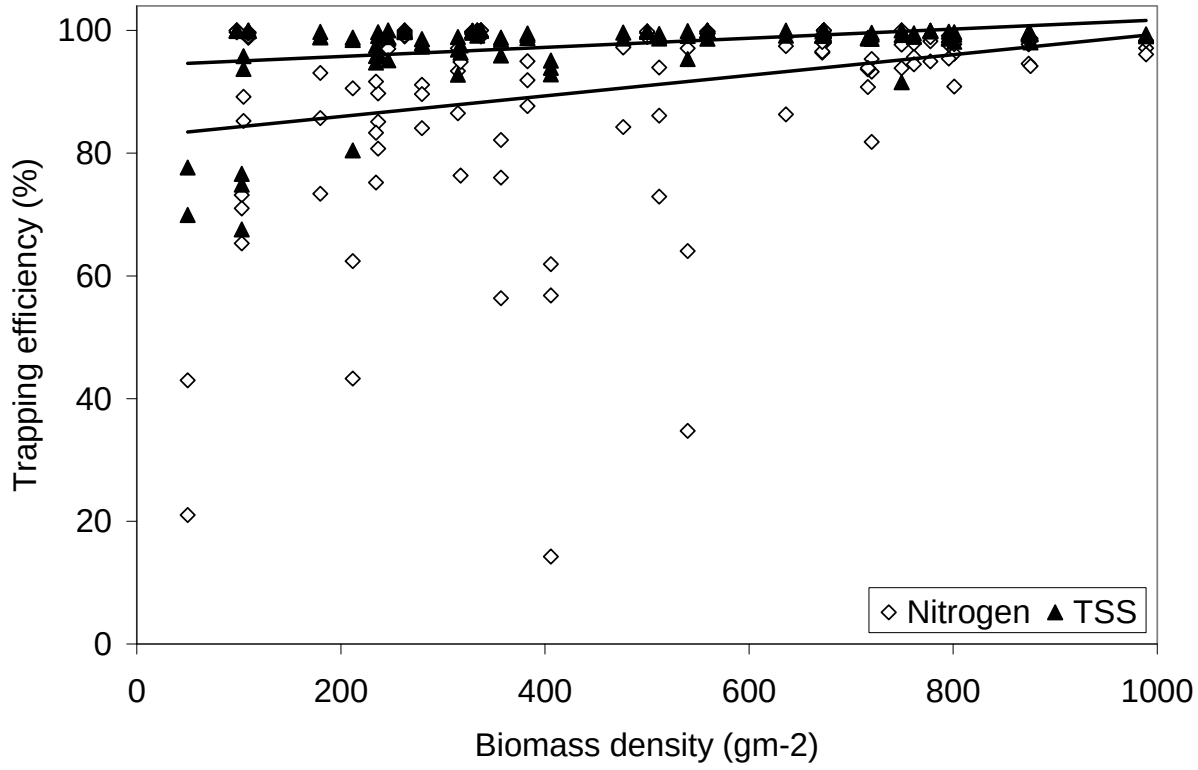


**Figure 3.3-12. Correlation between biomass density and pollutant trapping efficiencies (P values: 0.0025.**

## 3.4. TASK 4: NPS POLLUTION MODELING

### 3.4.a BACKGROUND

In soil erosion modeling there are increasing demands for analysis of local overland flow processes that transport sediments as nonpoint source (NPS) pollution. Routines that evaluate the effectiveness of best management practices (BMPs) on NPS pollution reduction require important overland flow characteristics including flowpath delineation and travel time (Jenson and Domingue, 1988; Sharpley and Kleinman, 2003). Additionally, understanding the transition between varying overland flow regimes is important because erosion potential increases as flow evolves from overland sheet flow to concentrated flow. As overland flow concentrates, concentrated erosion, such as ephemeral gully erosion, is established; this may develop into permanent gully erosion unless proper management is implemented.

In gully formation, the gully head, where concentrated flow begins, is an important feature to identify when assessing erosion potential. Although there are many properties that contribute to erosion evolution, the relationship between the two factors of slope and contributing area has been primarily evaluated to predict gully head locations in past studies. These two parameters (i.e., slope and contributing area) are commonly computed using digital elevation models (DEMs) that are constructed from field survey data or photogrammetric processes in relatively small drainage areas. DEMs coupled with a geographic information system (GIS) are not only used for estimating topographic properties, but also to calculate important hydrologic variables including traveling time, stream order, and drainage area boundaries which are fundamental inputs for quantitative erosion modeling (Roo, 1998).

Predicting locations of water erosion in a given drainage area is made difficult because it is hydraulically related to a flow regime (i.e., sheet flow and concentrated flow), whose transition point may be difficult to identify (Meyer et al., 1999). The kinematic wave theory is a useful tool for assessing the processes of overland flow transport at varying flow regimes (Laguna and Giraldez, 1993; Wong and Chen, 1999; Singh, 2001). One of the initial purposes behind the development of kinematic theory was to explain the movement of flood waves (Singh, 2001). A common practical application of kinematic wave theory is calculating the time of concentration within a drainage area as a shock wave runoff hydrograph (McCuen and Spiess, 1995; Willgoose and Kucera, 1994; Jaber and Mohtar, 2002). The kinematic wave model used to calculate the time of concentration for overland flow is commonly combined with Manning's surface roughness coefficients, expressed as (Ragan and Duru, 1972; McCuen and Spiess, 1995; Wong, 2005):

$$t_c = \frac{a}{i^{0.4}}\left(\frac{nL}{S^{0.5}}\right)^{0.6} \qquad \text{[Eq. 3.4-1]}$$

where $t_c$, the time of concentration for sheet flow (min); $i$, the rainfall intensity (mm/hr); $n$, Manning's coefficient for overland flow; $L$, the length of sheet flow (m); $S$, the slope (m/m); and $a$, a constant (i.e., 7 in metric unit; Wong, 2005). The following assumptions are inherent in kinematic wave implementations: 1) No local inflow within a given area, 2) applicable only for

the downward stream on a plane, 3) no effect of water detention volume, 4) non-concentrated sheet flow, and 5) excess flow rate is a function of depth (McCuen and Spiess, 1995; Willgoose and Kucera, 1995; Wong and Chen, 1999; Liu et al., 2004; Singh, 2001). Because of these unrealistic assumptions, additional information on the utility of kinematic wave models is required for their accurate application under different flow regimes in heterogeneous (topography, soils, and landcover) drainage areas.

McCuen and Spiess (1995), however, reported that the value of $nL / S^{0.5}$ (abbreviated hereafter as nLS) should be less than 100 when calculating accurate times of concentration if sheet flow is dominant. In this study, we hypothesized that a range of nLS values slightly greater than 100 can be utilized to determine the overland flow transitional area such as gully head locations. In contrast to the threshold methods applied in the S-A relationship, nLS provides a combined relationship between surface cover, topography, and hydrology.

The objectives of this study were to develop and apply a GIS-enabled kinematic wave model (nLS model) to identify where overland flow transitions from sheet to concentrated flow, and to evaluate the performance of this model compared to WTI and $AS^2$ approached. A third objective was to assess the benefits of incorporating critical shear stress, an additional soil erosion factor, into the basic nLS model.

### 3.4.b. APPROACH

The study was conducted in the Cheney Reservoir watershed located in south central Kansas near the city of Wichita. This watershed is approximately 160 km south southwest of Fort Riley and was selected due to the large gully data set developed as part of a separate study conducted by the USDA. The contributing drainage area of the reservoir is approximately 2,423 $km^2$ including the tributary streams of the North Fork Ninnescah River (Mau, 2001). Using the 14 digit hydrologic unit code (HUC-14), 19 subwatersheds were determined (Figure 3.4-2). The Cheney Reservoir (40 $km^2$) has been the primary drinking water source (60 to 70% daily basis) for the city of Wichita, Kansas and the surrounding area since construction in 1965 (Pope and Milligan, 2002). Mean annual temperatures (1971-2000) range from 5.9 °C to 20.8 °C (Daly et al., 2002). Mean annual precipitation (1971-2000) increases from west to east with an average of 673 mm at the west (upstream) end of the watershed and 798 mm at the east (downstream) end of the watershed. Elevations in the watershed vary from 397 m to 669 m above sea level with slope ranging from 0% to 24.6% using the USGS 30-m DEMs. According to local county soil survey (Rockers et al., 1966) and Soil Survey Geographic (SSURGO v2.1) data (USDA-NRCS, http://soildatamart.nrcs.usda.gov/), soils in the watershed mainly consist of sandy loam, loamy fine sand, and fine sandy loam (Table 3.4-1). There are 25 landcovers classified in the watershed using Kansas GAP landcover data (Table 3.4-2). Land in the watershed is typically used for agricultural production (54%). Agricultural land and CRP (Conservation Reserve Program) are relatively evenly distributed throughout the watershed. Although CRP areas are typically planted with prairie grasses (Egbert et al., 2001), it is not obvious when agricultural land are converted to CRP. Mau (2001) reported that the major crops are wheat (63%), sorghum (24%), corn (10%), and soybeans (3%) within the Cheney Reservoir watershed.

**Table 3.4-1. Soil texture and its area percent in Cheney Reservoir watershed.**

| Soil texture | Area% | Soil texture | Area% |
|---|---|---|---|
| sandy loam | 25.8 | clay loam | 9.3 |
| loamy fine sand | 17.5 | loamy sand | 3.2 |
| fine sandy loam | 15.9 | silt loam | 2.2 |
| Loam | 13.3 | silty clay loam | 0.2 |
| fine sand | 12.5 | variable | 0.1 |

(source: SSURGO v2.1)

**Table 3.4-2. Landcover and its area percent in Cheney Reservoir watershed.**

| Landcover | Area% | Landcover | Area% |
|---|---|---|---|
| Cultivated Land | 53.9 | Sandsage Shrubland | 0.3 |
| CRP[(1)] | 17.1 | Urban Areas | 0.3 |
| Mixed Prairie | 9.1 | Cattail Marsh | 0.1 |
| Tallgrass Prairie | 7.5 | Deciduous Woodland | 0.1 |
| Sand Prairie | 4.1 | Shortgrass Prairie | 0.03 |
| Cottonwood Floodplain Woodland | 1.8 | Freshwater Marsh | 0.01 |
| Water | 1.6 | Low or Wet Prairie | 0.01 |
| Cottonwood Floodplain Forest | 1.4 | Willow Shrubland | <0.01 |
| Bulrush Marsh | 0.8 | Pecan Floodplain Forest | <0.01 |
| Ash/Elm/Hackberry Floodplain Forest | 0.8 | Playa Lake | <0.01 |
| Non-Native Grassland | 0.5 | Salt Cedar or Tamarisk Shrubland | <0.01 |
| Weedy Upland | 0.3 | Western Wheatgrass Prairie | <0.01 |
| Mixed Prairie – Disturbed | 0.3 | | |

(1) Conservation Reserve Program, (source: Kansas GAP landcover data)

**Description of Erosion Models**

Table 3.4-3 summarizes the equations of the evaluated erosion models and the source of spatial data including DEMs, soils, and land cover used in this study.

**Table 3.4-3. Summary of the evaluated erosion models and the source of spatial data in GIS.**

| Model | Equation | Parameters | Data source (SR*) |
|---|---|---|---|
| nLS[(1)] | $\frac{3.3nL}{\sqrt{S}}$ | -Manning's coefficient (n) | Kansas GAP (30 m) |
| | | -The length of overland flow(L, m)<br>-Slope (S, m/m) | USGS National Elevation Data (30 m) |
| nLSCSS[(2)] | $\frac{3.3nL}{\sqrt{S}}\frac{1}{CSS}$ | -Critical shear stress (CSS, Pa) | SSURGO ver. 2.1 (30 m) |
| WTI[(3)] | $\ln\left[\frac{A}{C \times S}\right]$ | -Contributing area (A, $m^2$)<br>-Unit contour line (C, m)<br>-Slope (S, m/m) | USGS National Elevation Data (30 m) |
| AS[2(4)] | $AS^2$ | -Contributing area (A, $m^2$)<br>-Slope (S, m/m) | USGS National Elevation Data (30 m) |

*SR: spatial resolution, Readers should refer to additional information for each model in the following references: [(1)] McCuen and Speciess (1995), [(2)] CSS was measured using the method of Elliot et al. (1989), [(3)] Moore et al. (1988), and [(4)] Montgomery and Dietrich (1989 and 1992).

**Input Parameterization of Erosion Models in GIS**

**Manning's Coefficient from Land Cover**

Input values for Manning's coefficients in the model of nLS were estimated using Kansas GAP Land Cover data (GAP). GAP determined 40 vegetation classes with several non-vegetative classes in Kansas using the multitemporal bands of Landsat TM data (Wardlow and Egbert, 2003). The minimum mapping unit is 30 m.

**Table 3.4-4. The percent of land cover class in Kansas GAP data and Manning's coefficients (*n*) for Cheney Reservoir watershed.**

| Land cover | *n* | Land cover | *n* |
|---|---|---|---|
| Cultivated Land | 0.045 | Sandsage Shrubland | 0.06 |
| CRP[(1)] | 0.045 | Urban Areas | 0.01 |
| Mixed Prairie | 0.03 | Cattail Marsh | 0.05 |
| Tallgrass Prairie | 0.03 | Deciduous Woodland | 0.07 |
| Sand Prairie | 0.03 | Shortgrass Prairie | 0.03 |
| Cottonwood Floodplain Woodland | 0.1 | Freshwater Marsh | 0.05 |
| Water | 0.0001 | Low or Wet Prairie | 0.03 |
| Cottonwood Floodplain Forest | 0.1 | Willow Shrubland | 0.06 |
| Bulrush Marsh | 0.05 | Pecan Floodplain Forest | 0.1 |
| Ash/Elm/Hackberry Floodplain Forest | 0.1 | Playa Lake | 0.0001 |
| Non-Native Grassland | 0.23 | Salt Cedar or Tamarisk Shrubland | 0.06 |
| Weedy Upland | 0.03 | Western Wheatgrass Prairie | 0.03 |
| Mixed Prairie – Disturbed | 0.04 | | |

(1) Conservation Reserve Program.

The percent areas for each class and the Manning's coefficient (*n*) for overland flow were shown in Table 3.3-4 (Engman, 1983; Foster et al., 1985; McCuen, 1995). The Manning's coefficient used for CRP was the same as cropland. This estimate was supported in the result of gully location identification as described later. In a GIS, the table of Manning's coefficients was joined to each of the GAP landcover and then converted into a raster grid.

**Overland Flow Length and Topography**

A 1-arc-second (approximately 30 m) DEM from the National Elevation Data (NED) was downloaded from USGS Seamless Data Distribution System (http://seamless.usgs.gov/) for surface analyses. Zhang and Montgomery (1994) reported that 10-m DEMs offered more reliable hydrologic assessments than 30-m DEMs. However, 10-m DEMs were not available for the entire watershed at the time of the study. Seven floating-point grid format files of DEM encompassing the area from 37.58°N, 99.13°W to 37.78°N, 97.73°W were merged after reprojecting from geographic coordinate system (GCS NAD83) to UTM (NAD83 14N) using a bilinear interpolation technique that is the recommended method for DEM resampling method (ESRI, 2002). The merged DEM was then clipped using the Cheney Reservoir watershed coverage file.

The deterministic eight direction (D8) method (O'Callagham and Mark, 1984) was used to compute slope and to determine flow direction and flow accumulation grids. The process of pit removal was not used in this study. Pit removal is artificially applied to adjust the published elevation value in the adjacent neighbor cells that have lower elevation than that of the central cell. This manual process is commonly used when delineating surface channel networks or drainage area boundaries with respect to an accumulating threshold in hydrologic modeling. However, transitional erosion areas may be removed and gradual or abrupt erosion features may be filled using this method.

Other topographic factors, including aspect and surface curvature, were computed to evaluate the relationship between gully formation and local surface topography. Aspect was measured clockwise in positive degrees from 0 (North) to 359.9. Surface curvature values range from -1 to 1 to describe the direction of maximum rate of elevation change for neighboring cells. A positive value of curvature represents a convex-upward surface, a negative value of curvature represents a concave-upward surface and zero indicates a flat area (Zeverbergen and Thorne, 1987). Meyer and Martínez-Casasnovas (1999) addressed that surface curvature is one of the factors highly correlated to existences of gully erosions in an agricultural watershed. Flowpath delineation processes are influenced by local maximum curvature characteristics (Hutchinson, 1989).

In the D8 method, the flow direction from the central cell in a 3x3 cell window is determined by the steepest slope gradient in one of eight directions in 45° intervals. For a given cell, the numbers of upstream cells that flow into that cell are summed and that value stored in a flow accumulation grid. The smallest measurable distance between two cells is the same as the spatial resolution (SR) of the raster layer in used the D8 method. Therefore, multiplying the flow accumulation number by the SR is the same as calculating the length of overland flow for each grid cell. For example, if the flow accumulation value in a given cell is 10, and a 30-m DEM

was used to compute flow direction, the length of overland flow would be 300 m. Because the criterion of nLS was developed in English Units (i.e., feet), the length of flow was converted into this unit system. The three layers, Manning's coefficient, slope percent, and overland flow length, were processing using ArcGIS raster calculator (ESRI, Redlands, CA). The parameters used for WTI and $AS^2$ models were developed in the same manner.

**Soil Critical Shear Stress**

Juracek and Wolock (2002) examined the spatial and statistical differences between two published soil digital databases: State Soil Geographic (STATSGO, 1:250,000-scale) database and Soil Survey Geographic (SSURGO, 1:24,000-scale) database. They examined the soil attributes in twelve basins in Kansas. Similar values in three attributes (soil permeability, percent clay, and hydrologic group) were produced for areas larger than 25 $km^2$, but they obtained mostly different results in small areas, especially those along stream networks. Soil critical shear stress (CSS, Pa) for cropland was determined in the following way (Elliot et al., 1989):

$$CSS = 2.67 + 6.5\ clay - 5.8\ vfs \text{ (if sand\% > 30)} \quad \text{(Eq. 3.4-2)}$$

$$CSS = 3.5 \text{ (if sand\% < 30)} \quad \text{(Eq. 3.4-3)}$$

CSS for rangeland was obtained in the following way:

$$CSS = 3.23 - 5.6\ sand - 24.4\ OM + \frac{0.9\rho_b}{1000} \quad \text{(Eq. 3.4-4)}$$

where *clay* is the fraction of clay in the surface soil; *vfs* is the fraction of very find sand; *sand* is the fraction of sand; *OM* is the fraction of organic matter content of the surface soil; and $\rho_b$ is the bulk density ($kg/m^3$). However, if clay and very fine sand content is lower than 0.4 in equation 3.4-2, 0.4 was used for each parameter.

The SSURGO version 2.1 soil tabular and spatial data for Cheney Reservoir watershed was downloaded from the USDA-NRCS Soil Data Mart (http://soildatamart.nrcs.usda.gov/). The tabular soil data was in database file format (Microsoft Access) and the soil spatial data was in the shape file format of Environment System Research Institute (ESRI). Five database files of SSURGO and shape files for five counties in Cheney Reservoir watershed were incorporated in a file, respectively. Queries in the database program were established to export the mean values for each input parameter. These values were joined based upon the table attribute (i.e., mukey) in the shape file and queried to create each soil parameter layer in a raster file. The applied soil depth to derive soil properties was one meter. Representative soil texture was queried within the same depth in the database program.

In order to estimate the soil critical shear stress across the watershed, the land classes in Table 3.3-4 were aggregated into agriculture or rangeland class. All non-cultivated vegetation cells (e.g., prairies and woods) were reclassified as rangeland. Cultivated land remained in the agriculture class, which was dissected into the two areas based on the percent of sand. For water and urban classes, CSS was assumed to be zero.

**Identifying the Locations of Gully Head and Drainage Density**

High-resolution (1-m) aerial photography was used to identify the location of gully heads. Most photographs were taken during, or right after, the growing season. Gully head locations were manually input using "heads-up" digitization and saved in a point shape file. Hence, minimum evaluated size of gully heads in this study was equal to, or greater than 1 $m^2$.

In this study, the 19 HUC-14 subwatersheds were used as a unit drainage area. The three HUC-11 subwatersheds (i.e., upstream, midstream and downstream) were used to select different geographic subwatershed locations and test an applicability of the nLS model at other watersheds (Figure 3.4-4). Integer numbers (1 to 19) were used for easy indication of subwatersheds rather than the HUC-14 identifier. Selected calibration and validation subwatersheds were determined based on the relationship between drainage density and the number of gully heads. The total stream lengths (km) and drainage areas ($km^2$) were determined from National Hydrography Dataset (NHD, http://nhd.usgs.gov/) of Cheney Reservoir watershed at 1:24,000-scale. The coordinate system for all GIS layers was adjusted to UTM NAD83 (14N), as needed.

**Evaluating the GIS-Based Erosion Models**

Figure 3.4-1 presents the methodological diagram used to evaluate the performance of the GIS-enabled kinematic erosion model. After the erosion model layers were developed and the erosion model was run, the point shape file of gully head locations was applied to extract an erosion value for each location. These values were used to determine the overall relationships between topography, drainage density, precipitation, and the locations of the gully heads. Because surface environments are assumed to be homogeneous within a cell in raster files, the coarser resolution data may not sufficiently represent an accurate point of the gully head identified using 1-m aerial photography. Therefore, some gully head locations were relocated in the calibrating process prior to conducting the statistical analyses. Relocation was based on the assumption that gully heads are generated along the first-order stream networks (Montgomery and Dietrich, 1989). The first-order stream networks were delineated from 30-m DEMs with a threshold value of 900 $m^2$. If a gully head was positioned along a higher-order stream or had an nLS value lower than 100, the gully head point was moved to the nearest cell that includes the first-order stream line and nLS greater than 100. In this modification, the direction of relocation among surrounding cells was based on upstream direction.

The three erosion statistical intervals of mean ($\mu$) and standard deviations ($\pm 0.5\sigma$, $\pm 1.0\sigma$, and $\pm 1.5\sigma$) of erosion values were developed using the extracted nLS values on the gully head points. Next, all lengths of the first-order stream networks that were queried by the intervals of nLS values were selected as transitional erosion areas. Because the shapes of stream networks and gully heads were lines and points, a circle-rounded buffer (15-m in radius), was applied to intersect the two files. The assessment of error matrix was performed to evaluate the model accuracy, which represents the probability in determining gully head locations correctly (Jensen, 1996; Meyer and Martínez-Casasnovas, 1999). Information of total subwatershed areas and buffered (or modeled) transitional erosion areas was estimated in cell-basis (30-m resolution). The numbers of gully head points were the same as the number of gully head cells in the analysis.

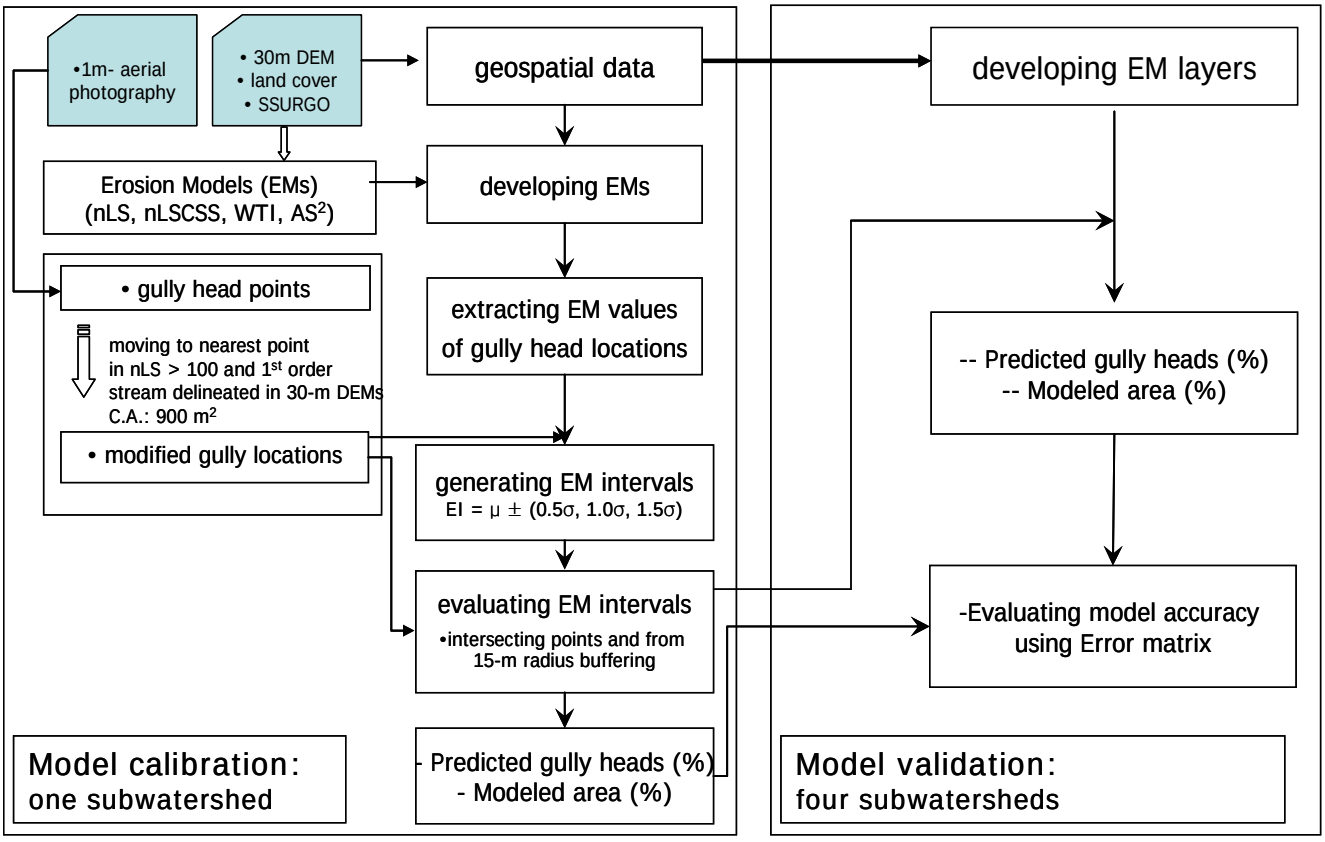


**Figure 3.4-1. The methods flow diagram applied in GIS to develop, calibrate, and validate erosion models. C.A. indicates contributing area to apply a flow accumulation grid in the first-order stream delineation.**

## 3.4.c RESULTS AND DISCUSSION

### Overall Characteristics of the Gully Head Locations

### Drainage Density and Precipitation

Figure 6 shows the locations of digitized gully heads (n = 983) and a map of drainage density ($D_d$, km/km$^2$) at the HUC-14. The number of gully heads varied from 130 in subwatershed 8 to 7 in subwatershed 19. More gully heads were found in the lower reaches of watersheds and drainage density also increased toward the Cheney Reservoir watershed outlet. Figure 3.4-3 shows the linear relationships between the number of gully heads and $D_d$ ($R^2$ = 0.82) and the mean annual precipitation (PPT, 1971-2000, $R^2$ = 0.73) (Daly et al., 2002) in each subwatershed. If the number of gully heads in subwatershed 6 was ignored as an outlier in the plot, the $R^2$ improved to 0.92 for $D_d$ and 0.84 for PPT, respectively. The increase is likely because greater tallgrass landcover was found in subwatershed 6 than other subwatersheds. More details about the impact of land cover are described below.

Subwatershed 14 (n = 122, Dd = 2.10) was selected to calibrate four erosion models such that the model performance could be compared using a large number of gully heads.

Subwatershed 8 (n = 130, Dd = 2.04) was chosen as the validation subwatershed. Three more subwatersheds, 7 (n = 124, Dd = 1.73), 16 (n = 59, Dd = 0.89, and 11 (n = 17, Dd = 0.27) were also used to assess the impact of drainage density on model performance.

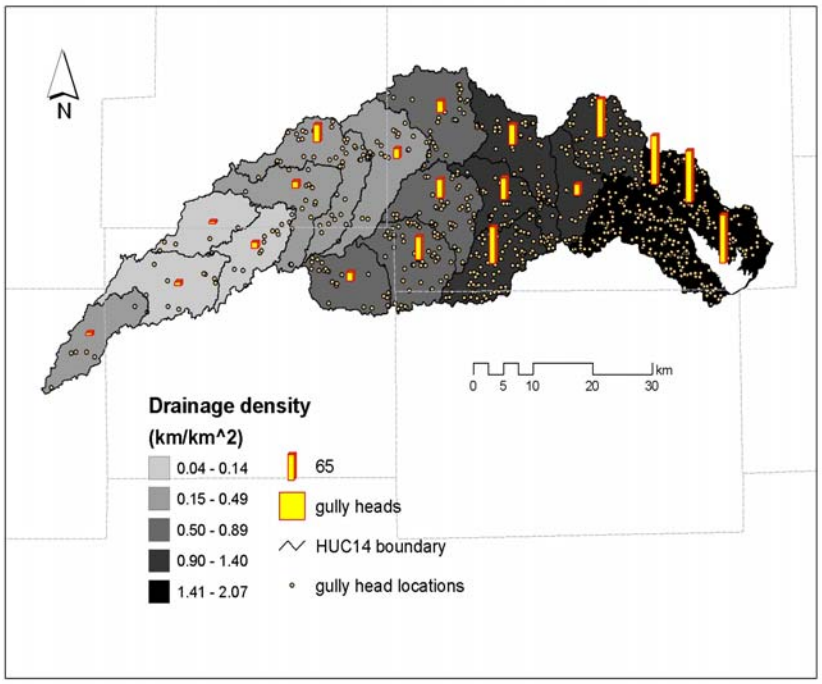


| HUC 11 | HUC 14 | n | $D_d$(km$^{-1}$) |
|---|---|---|---|
| Upstream | 1 | 30 | 0.60 |
| | 2 | 51 | 1.20 |
| | 4 | 25 | 0.39 |
| | 5 | 44 | 0.49 |
| | 11 | 17 | 0.27 |
| | 12 | 6 | 0.07 |
| | 13 | 16 | 0.14 |
| | 18 | 9 | 0.04 |
| | 19 | 7 | 0.35 |
| Mid-stream | 9 | 55 | 1.04 |
| | 10 | 47 | 0.66 |
| | 15 | 93 | 1.26 |
| | 16 | 59 | 0.89 |
| | 17 | 22 | 0.63 |
| Downstream | 3 | 97 | 1.31 |
| | 6 | 28 | 1.40 |
| | 7 | 124 | 1.73 |
| | 8 | 130 | 2.04 |
| | 14 | 122 | 2.10 |

**Figure 3.4-2. Locations and numbers of gully heads (n=983) in HUC-14 and choropleth map of drainage density at Cheney Reservoir watershed. Left table describes the numbers of gully heads for subwatersheds (1 to 19) in Figure 3.4-4.**

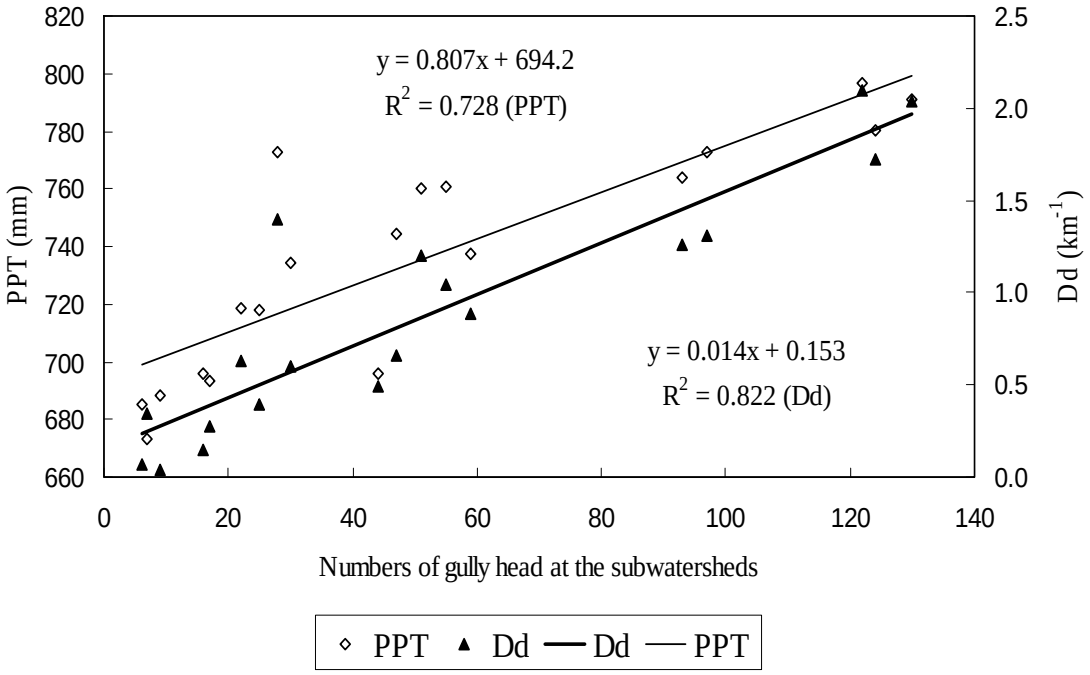


**Figure 3.4-3. The linear relationships between the numbers of gully heads and the drainage density ($D_d$), and the mean annual precipitation (PPT) for each HUC-14 subwatershed.**

**Land Cover and Soil Texture**

Cultivated agricultural land had the largest number of gullies, and CRP had the second largest number of gully heads (Table 3.4-5). About 93% of the gully heads were located in former and current agricultural land, while only 6% of gully heads were found in prairie land areas. The percentages of gully head cells per the total cells (30-m resolution) of each landcover in the Cheney Reservoir watershed were 0.051 for cultivated lands, 0.022 for CRP, and 0.025 for entire prairie areas. As a result, agricultural lands were a major contributor for gully formation. In addition, CRP had less impact than cultivated land on gully head formation, but greater than native prairie area.

The results show that the prairie systems more effectively maintained overland sheet flow than agricultural lands. However, all gully heads in the wooded or forest areas might not have been identified in the aerial photography because of dense vegetation cover.

About 46% of gully heads formed in sandy loam soil (Table 3.4-6), which covers the largest area in the watershed (Table 3.4-1). A significant number of gully heads formed in loam and clay loam soils despite their relative low percent of occurrence. The percentages of gully head cells per the total cells of each soil texture were 0.061 for sandy loam, 0.047 for loam, 0.054 for clay loam, and 0.040 for silt loam, indicating that silt loam was also susceptible to gully head formation.

**Table 3.4-5. The percent of gully heads in landcover**

| Land cover | Numbers of gully head | Gully head % | Cumulative Gully head % | Gully head per a class area (%)[1] | Rank in total area % |
|---|---|---|---|---|---|
| Cultivated land | 803 | 81.7 | 81.7 | 0.051 | 1 |
| CRP | 111 | 11.3 | 93.0 | 0.022 | 2 |
| Mixed Prairie | 29 | 2.9 | 95.9 | 0.011 | 3 |
| Tallgrass Prairie | 27 | 2.8 | 98.7 | 0.012 | 4 |
| Cottonwood Floodplain Forest | 6 | 0.6 | 99.3 | 0.014 | 6 |
| Ash - Elm - Hackberry Floodplain Forest | 2 | 0.2 | 99.5 | 0.014 | 5 |
| Sand Prairie | 3 | 0.3 | 99.8 | 0.002 | 10 |
| Weedy Upland | 1 | 0.1 | 99.9 | 0.011 | 12 |
| Deciduous Woodland | 1 | 0.1 | 100.0 | 0.049 | 17 |

[1] Each gully head point and the total area of each class were estimated in 30-m cell basis.

**Table 3.4-6. The percent of gully heads in soil texture**

| Land cover | Numbers of gully head | Gully head % | Cumulative Gully head % | Gully head per a class area (%)[1] | Rank in total area % |
|---|---|---|---|---|---|
| Sandy loam | 451 | 45.9 | 45.9 | 0.061 | 1 |
| Loam | 178 | 18.1 | 64.0 | 0.047 | 4 |
| Clay loam | 144 | 14.6 | 78.6 | 0.054 | 6 |
| Fine sandy loam | 78 | 7.9 | 86.6 | 0.017 | 3 |
| Loamy fine sand | 59 | 6.0 | 92.6 | 0.012 | 2 |
| Fine sand | 26 | 2.6 | 95.2 | 0.007 | 5 |
| Silt loam | 25 | 2.5 | 97.8 | 0.040 | 8 |
| Loamy sand | 22 | 2.2 | 100.0 | 0.024 | 7 |

[1] Each gully head point and the total area of each class were estimated in 30-m cell basis.

**Slope, Aspect, Surface Curvature, and Critical Soil Shear Stress**

There was no important relationship between slope, aspect, CSS, and gully head locations (Figure 3.4-3). However, curvature analysis suggests that 59% of gully heads (n = 590) were developed in concave shapes of land, 39.5% (n = 388) in convex shapes and 0.5% (n = 5) in flat areas (Figure 3.4-3). This suggests that accelerated concentrated flow on concave planes may generate greater erosion energy than on convex or flat areas.

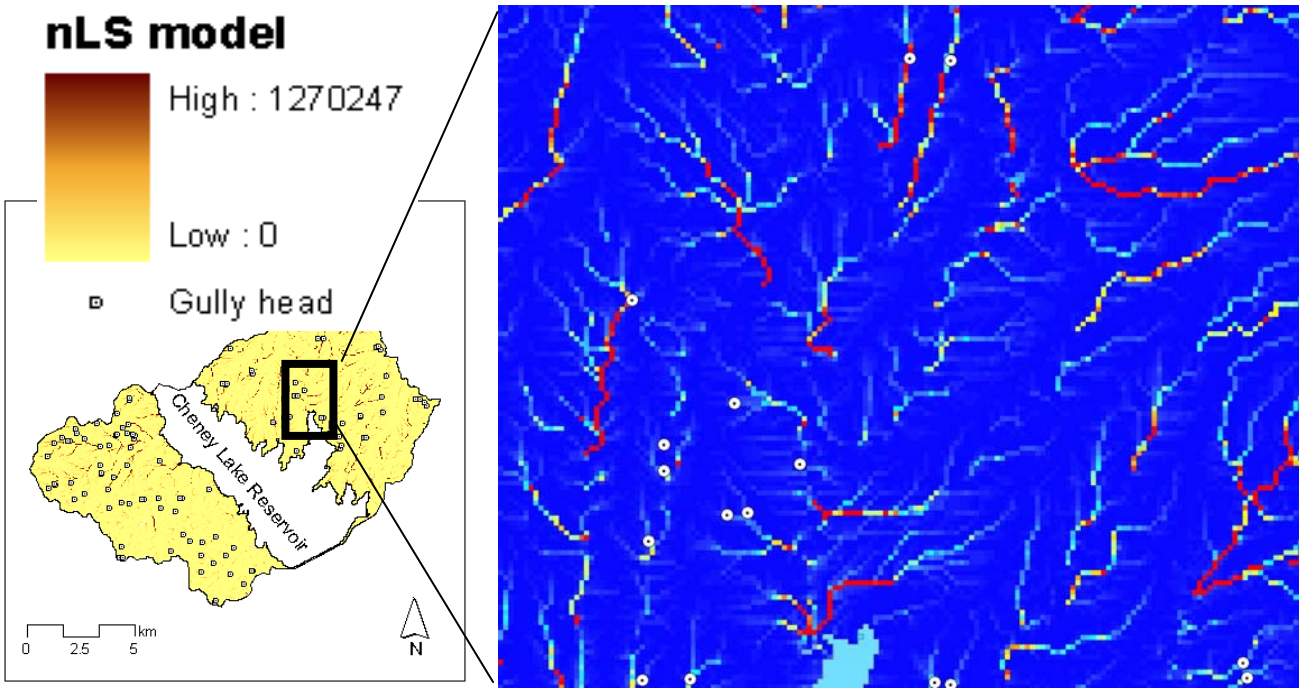


**Figure 3.4-4. An erosion value grid of nLS model and the gully head locations (circles) in the subwatershed 14.**

**Model Calibration and Validation**

Table3.4-7 summarizes the statistics of the four erosion models for all gully head locations in Cheney Reservoir watershed and for the gully head locations in the calibrated subwatershed. Because the lengths of overland flow varied greatly, nLS and nLSCSS had the larger erosion values, while WTI showed the least standard deviation because of natural logarithm transformation. The mean of WTI were greater than the threshold value (6.8) reported in the previous study (Moore et al., 1988). The mean of $AS^2$ was 3.9, indicating a very low value compared to the threshold of 16.7 as determined by Montgomery and Dietrich (1992) using 30-m spatial resolution data. Differences in threshold values in this subwatershed as compared to the previous study may be the result of different soil structure, vegetation, climate, and agricultural practices in the tested areas. The maximum and standard deviation of nLSCSS were greater than that of nLS in the both drainage boundaries; but the mean of nLSCSS was less than that of nLS, suggesting that CSS below zero (e.g., sand loam; Elliot et al., 1989) resulted less distribution of erosion values. Because the standard deviation of $AS^2$ was greater than the mean, this model was excluded from further analyses.

**Table 3.4-7 Statistics of the four erosion models to predict gully head locations in Cheney Reservoir watershed (1-19) and the calibrating subwatershed 14.**

| Number of Subwatershed / Statistics | nLS | | nLSCSS | | WTI | | $AS^2$ | |
|---|---|---|---|---|---|---|---|---|
| | 1-19 | 14 | 1-19 | 14 | 1-19 | 14 | 1-19 | 14 |
| Maximum | 191,631.0 | 189 | 275,363.5 | 295.8 | 20.3 | 14.4 | 191.3 | 66.8 |
| Mean | 2,807.8 | 131.0 | 1,994.3 | 92.48 | 10.4 | 9.4 | 3.9 | 3.8 |
| Standard deviation | 10,895.7 | 22.6 | 13,505.2 | 53.3 | 2.3 | 1.6 | 13.5 | 9.8 |

Of the total number of gully heads (n =122) in the calibration subwatershed 14, 114 were relocated based on the previously discussed methodology. The mean distance for point relocation was 39 m (maximum 131 m), approximately 1 cell. The modified locations in the calibration subwatershed showed variability and improved the statistical intervals for the calibration and validation processes.

Total cell count (30-m resolution) of the calibration subwatershed area was 137,703 (123.9 $km^2$) (Table 3.4-8). In the analysis of overall model accuracy, modeled areas and predicted gully head locations were also calculated in 30-m resolution. Although WTI showed the best performance for predicting actual gully head cells, it also had largest modeled cells (model simulated 34.7, 40.0, and 40.9% of possible transitional erosion cells for each interval). On the other hand, nLS model simulated 12.9, 21.8, and 27.8%. These differences strongly affected in assessing the model overall accuracy. The combination of CSS with nLS model did not improve overall model accuracy. However, the user accuracy of WTI decreased and that of nLSCSS was constant as the range of erosion values was expanded, indicting that all models over-predicted gully head locations, but that of nLS slightly increased. As a result, the best overall model accuracy was founded in nLS model simulation in all statistical ranges.

**Table 3.4-8. Overall model accuracy of WTI, nLSCSS, and nLS in the calibration subwatershed 14.**

| Interval | subwatershed | Total modeled cells | Predicted gully head cells | User accuracy for gully head (%) | Overall accuracy (%) |
|---|---|---|---|---|---|
| | WTI | 47,817 | 85 | 0.23 | 65.3 |
| $\mu \pm 0.5\sigma$ | nLSCSS | 33,436 | 60 | 0.14 | 66.5 |
| | nLS | 17,747 | 33 | 0.19 | 87.1 |
| | WTI | 55,170 | 108 | 0.20 | 60.0 |
| $\mu \pm 1.0\sigma$ | nLSCSS | 46,191 | 79 | 0.14 | 66.5 |
| | nLS | 30,040 | 65 | 0.22 | 78.2 |
| | WTI | 56,427 | 120 | 0.19 | 59.1 |
| $\mu \pm 1.5\sigma$ | nLSCSS | 52,034 | 90 | 0.14 | 66.5 |
| | nLS | 38,337 | 85 | 0.22 | 72.2 |

The mean accuracy of nLS model in the validation process was 88.6% at $\mu \pm 0.5\sigma$, 78.9% at $\mu \pm 1.0\sigma$, and 74.6% $\mu \pm 1.5\sigma$. The best accuracy (92.4% at $\mu \pm 0.5\sigma$) was found in subwatershed 7, which had the lowest drainage density and gully head locations. CSS negatively affected the overall model accuracy in the calibration and validation processes. As a result, the model performance of nLS was not affected by values of drainage density, implying that the nLS model effectively predicted transitional erosion areas and had a wide-applicability in the agricultural watershed. In general, the ranges of $\mu \pm 0.5\sigma$ provided better overall model accuracy, suggesting that these least modeled areas may be used for practically evaluating the nLS model prediction through ground proofing. However, the user accuracy for each interval was still low. The reasons for low model accuracy of the nLS model should be recognized in the discrepancy of spatial resolution as well as in uncertainty of GIS data (Roo, 1998).

**Table 3.4-9. Overall accuracy of nLS and nLSCSS model in the four validation subwatersheds**

| nLS | Sub-watershed | Total cells | Total modeled cells | Predicted gully head cells | User accuracy for gully head (%) | Overall accuracy (%) |
|---|---|---|---|---|---|---|
| μ±0.5σ | 8 | 150,967 | 19,019 | 12 | 0.06 | 87.3 |
| | 7 | 139,898 | 19,612 | 19 | 0.10 | 85.9 |
| | 16 | 164,240 | 18,122 | 9 | 0.05 | 88.9 |
| | 11 | 160,562 | 12,127 | 4 | 0.03 | 92.4 |
| μ±1.0σ | 8 | 150,967 | 32,619 | 21 | 0.06 | 78.3 |
| | 7 | 139,898 | 32,950 | 32 | 0.10 | 76.4 |
| | 16 | 164,240 | 31,624 | 13 | 0.04 | 74.8 |
| | 11 | 160,562 | 22,068 | 5 | 0.02 | 86.3 |
| μ±1.5σ | 8 | 150,967 | 41,960 | 35 | 0.08 | 72.2 |
| | 7 | 139,898 | 42,410 | 41 | 0.10 | 69.7 |
| | 16 | 164,240 | 41,264 | 18 | 0.04 | 74.8 |
| | 11 | 160,562 | 29,416 | 7 | 0.02 | 81.7 |
| μ±0.5σ | 8 | 150,967 | 37,475 | 33 | 0.09 | 75.1 |
| | 7 | 139,898 | 33,933 | 38 | 0.11 | 75.7 |
| | 16 | 164,240 | 32,098 | 13 | 0.04 | 80.4 |
| | 11 | 160,562 | 25,409 | 6 | 0.02 | 84.2 |
| μ±1.0σ | 8 | 150,967 | 51,104 | 44 | 0.09 | 66.1 |
| | 7 | 139,898 | 44,893 | 50 | 0.11 | 67.9 |
| | 16 | 164,240 | 44,069 | 23 | 0.05 | 73.1 |
| | 11 | 160,562 | 36,523 | 7 | 0.02 | 77.3 |
| μ±1.5σ | 8 | 150,967 | 57,242 | 52 | 0.09 | 62.1 |
| | 7 | 139,898 | 49,039 | 51 | 0.10 | 64.9 |
| | 16 | 164,240 | 48,274 | 24 | 0.05 | 70.6 |
| | 11 | 160,562 | 40,385 | 7 | 0.02 | 74.8 |

## 3.5. TASK 5: CHARACTERIZATION OF STREAM SEDIMENT

### Stream Mapping and Comparison

In order to assess the effects of surface runoff on the ephemeral streams on Fort Riley, we undertook a study of the channel geometry of streams on Fort Riley and compared them to similar streams outside the Fort that have had different land-use histories.

### 3.5.a. METHODS

### Study Areas

The Fort Riley study areas were chosen based on the accessibility, use by military vehicles, and presence of low-water stream crossings. Many low-order streams are found along the major routes used by tanks moving to the firing ranges. The study sites impacted by military maneuvers were chosen to overlap a larger study evaluating the effectiveness of low-water stream crossings in preserving stream water quality. Three sites located on second-order streams at Fort Riley (Figures 3.5-1) were chosen, each having a constructed low-water stream crossing. The three sites are located on Seven Mile Creek and Three Mile Creek watersheds and are numbered FR1, FR2, and FR3. FR1 is located on Three Mile Creek while FR2 and FR3 sites are located on Seven Mile Creek. The drainage areas of FR1, FR2 and FR3 are 1.28 $km^2$, 1.83 $km^2$and 2.36 $km^2$ respectively.

The comparison sites to the Fort Riley study areas are located in Marlatt Park and the Konza Prairie Biological Station (KPBS) in Kansas (Figure 3.5-1). The size of drainage areas of the Marlatt Park and Konza study sites are 0.10 $km^2$ and 1.67 $km^2$, respectively. These comparison sites are located in the same physiographic province using the principle that streams in the same physiographic province will create similar landforms (Leopold et al., 1964). The same physiographic province implies that certain extrinsic factors are likely to be similar. These factors include plant communities, climate trends, major soil association or group of major soils, drainage densities, geology, and geologic history. Intrinsic factors such as drainage area and slope were measured at all sites and found to be similar to the Fort Riley sites.

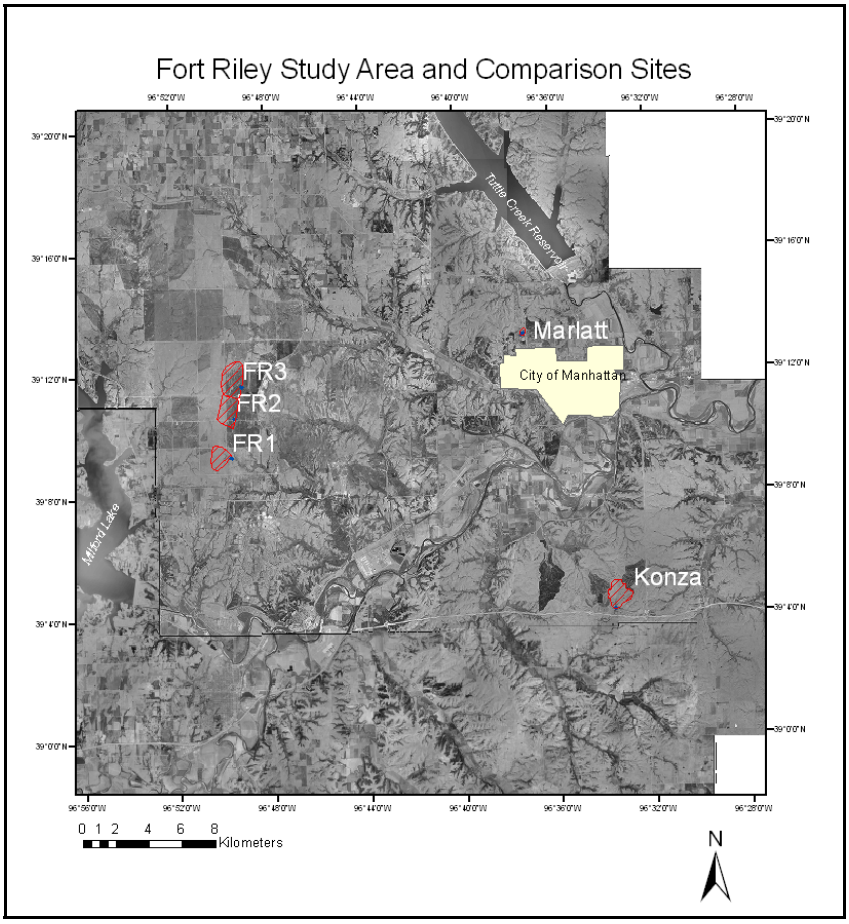


**Figure 3.5-1. Map showing study sites on Fort Riley, Marlatt Park and Konza Prairie. Drainage areas marked with diagonal red stripes.**

The two sites chosen for comparison with the Fort Riley sites are King's Creek on the Konza Prairie Biological Station and the east branch of a tributary to Little Kitten Creek on Marlatt Park. Each stream channel cuts through alluvial material and is of the same order.

**Stream Surveys**

Stream reaches for each study site were surveyed (using standard techniques, USFS, 1994) and classified using the Level II Rosgen Classification Scheme (Rosgen, 1996). This classification sets up a series of commonly used measurements to depict fluvial morphological features and measurements in a uniform way. The resulting observations and measurements place stream reaches into a classification scheme for a means of summarizing characteristics.

Each reach was between 180 and 250 meters in length. The reaches begin and end with a relatively stable portion of the stream, generally between two meander bends. The Fort Riley stream reaches have low-water stream crossings at roughly the center of the reach and encompass improvised low-water stream crossings upstream and downstream from the low-water stream crossing.

Longitudinal profiles were taken for each site using a total station (Topcon GTS-229) to measure x, y, z coordinates along the reach. Measurements taken along the longitudinal profile include right bank, left bank, and thalweg, or the deepest portion of the stream channel, measured at the same distance along the reach. Other measurements include bankfull indicators found through field observations, the entrance of tributaries, occurrence of meander cut-offs, depositional features, improvised stream crossings, and low-water stream crossings.

Longitudinal profiles start and end at the location of a cross section used to represent a stable point on the stream channel. The profile begins with the upstream end of the reach designating right and left banks from a downstream perspective. Measurements along the reach were taken at changes in channel slope and did not exceed 20.9 meters between measurements. A proxy measurement of water surface slope was taken from profile data between two riffle features. Channel sinuosity is another measurement taken from profile data by using the total length of the stream reach measured along the thalweg divided by the valley length.

Cross-section measurements were also taken using a total station (Topcon GTS-229) starting with the right bank benchmark pin and ending with the left bank benchmark pin. Points were taken in 0.5 m horizontal increments outside the active stream channel and 0.2 m within the active channel. Stream cross sections on Fort Riley sites were taken upstream and downstream from military vehicle fording sites and at a stable point at the beginning and ending of each reach (USFS, 1994; Rosgen, 1996). Six cross-sections were measured at FR1 and FR2 and five cross-sections at FR3. In addition, cross sections were taken at designated locations along the study sites on Konza and Marlatt Park. Resurveying cross sections over time can depict changes in channel position and form. Cross-section measurement is also used to measure channel area for an estimation of stream discharge (USFS, 1994).

Monumented benchmarks were created to mark the position of cross sections. Benchmarks were constructed by filling a 1-foot deep (30 cm), 8-inch diameter hole (20 cm) with concrete and placing an 8-inch long piece of concrete reinforcement bar or an 8-inch long carriage bolt in the center with ½ inch extending above the surface of the concrete. A measurement of the benchmark's location was then recorded using a Global Positioning System (GPS) unit (Garmin GPS II Plus). The GPS measurements all have a horizontal error margin between 4 to 6 m. Photographs of each cross section were taken standing in the middle of the channel at the cross section aiming upstream and downstream.

In a survey of bed material called a "pebble count" one hundred samples are taken of the surface bed materials in the active stream channel. These samples are taken in both riffles and pools along the stream reach in proportion to the percent of riffles to pools present in the reach. These data are used to determine the $D_{50}$ (average diameter of the stream bed materials) for the stream reach and is measured at the median axis of the pebble (Wolman, 1954).

Hydraulic variables required for stream classification were determined for each study site. These variables include bankfull depth, width, discharge, and water surface slope. Velocity is a function of flow per unit of time. Factors in streams affecting velocity include channel roughness, boundary of the wetted perimeter, slope, and depth of flow (Leopold et al., 1964).

Using the Manning's equation (Equation 3.5-1) a more accurate portrayal of kinetic energy available to move sediment can be determined (Dunne and Leopold, 1978). The roughness coefficient, n, was chosen from a list of modified roughness coefficients for Rosgen stream types (Rosgen, 1996). The Manning's roughness coefficient is an empirically derived variable whose accuracy can be improved by considering the dimensions of similar stream types taken at a bankfull stage. Stream discharge at bankfull flow was calculated using the general relationship between velocity and channel cross-sectional area (Equation 3.5-2) at the stream's bankfull stage. Bankfull flow is based on the recurrence interval of 1.5 years to estimate duration and magnitude of the one-hour storm producing the given discharge.

$$U = (R^{2/3} S^{1/2})/ n \qquad \text{[Eq. 3.5-1]}$$

$$Q = U A \qquad \text{[Eq. 3.5-2]}$$

Where:

U- Bankfull Velocity (m/s)
R-Hydraulic Radius (m)
S-Water Surface Slope (m/m)
n- Manning's Roughness Coefficient
A-Bankfull Channel Area ($m^2$)
Q-Bankfull Discharge ($m^3/s$)

**Stream Fording Characterization**

Fording sites on the Fort Riley stream reaches were characterized by measuring the vegetation coverage and communities present, the width and slope of fording approaches, the area of stream channel influenced by stream fording, and the presence and character of rills on fording approaches. Approach slope and active channel slope were measured using the clinometer of a Brunton compass. The area of stream channel influenced by stream fording was measured as the length of channel traversed by vehicles and the width of the channel at approximately bankfull height. Rills were characterized by recording average rill depth and general location on the fording approach. Rills are erosion features in smallest channels that only carry water during storms (Leopold et al., 1964). Rills are between 1-200mm in depth and width. These rills usually enlarge in size to form gullies. The fording sites examined included improvised stream crossings and constructed low-water stream crossings. Photographs were taken of right and left bank approaches, rill features, sample vegetation, and other notable features.

**Stream Stability**

Bank stability was measured using the modified Pfankuch channel stability rating (Pfankuch, 1975, Rosgen, 1996). This stability assessment examines the condition of stream banks. The rating is modified by Rosgen (1996) to incorporate width/depth channel dimensions and the resulting score is then applied to the Rosgen stream classification scheme providing an appropriate stability picture for various stream types. Myers and Swanson (1992) also found a correlation between the Pfankuch evaluation and Rosgen stream types suggesting that stream type has a great impact on the susceptibility of streams to agents of erosion.

The Pfankuch evaluation uses a series of 15 measurements that are mostly qualitative in nature. Exceptions to this qualitative data include the average of bank slopes, width/depth ratio, and bottom material size distribution. This method was chosen over bank stability methods since it has been adopted by the U.S.D.A. Forest Service and is well cited in stream assessment literature (Pfankuch, 1975).

### 3.5.b. RESULTS

The first of the three objectives was to describe the fluvial geomorphic features of three stream reaches at Fort Riley This was done using the classification scheme created by Rosgen (1996) and using methods set forth by the United States. Forest Service (USFS, 1994).

#### Stream Classification

Data gathered from cross section measurements include the estimation of a bankfull measurement, representing the level of water in the channel during a flow event that is said to have a recurrence interval of about 1.5 years (Rosgen, 1996). This is also the flow that is responsible for the "formation, maintenance, and dimensions of the channel" and is used by fluvial geomorphologists as a consistent marker for channel measurements. Bankfull measurements for this report were compared against regional figures for the Flint Hills Physiographic Province collected by Emmert (2004). The maximum bankfull depth, mean depth of the channel at the bankfull stage, and bankfull width are used to determine the flood prone width, entrenchment ratio, and width/depth ratio, where the flood-prone width is the width at two times the maximum depth at bankfull. The entrenchment ratio is the flood prone width divided by the width at bankfull, and the width/depth ratio is the bankfull width divided by the mean bankfull depth (Rosgen, 1996). Channel geometry measurements collected for each of the Fort Riley sites are listed in Table 3.5-1. The stream variables used for classifying reach of the Fort Riley study sites are presented in Table 3.5-2.

**Table 3.5-1. Channel Geometry Measurements for Sites on Fort Riley.**

| Site ID | $D_{maxbkf}$ (m) | | $D_{bkf}$ (m) | | $W_{bkf}$ (m) | | FPA (m) | |
|---|---|---|---|---|---|---|---|---|
| | US | DS | US | DS | US | DS | US | DS |
| FR 1 | 0.35 | 0.40 | 0.28 | 0.34 | 2.14 | 3.34 | 3.15 | 4.57 |
| FR 2 | 0.31 | 0.68 | 0.29 | 0.54 | 2.26 | 2.20 | 3.30 | 4.50 |
| FR 3 | 0.54 | 0.45 | 0.45 | 0.39 | 4.10 | 2.30 | 4.05 | 4.20 |

$D_{maxbkf}$: maximum bankfull depth, $D_{bkf}$: mean bankfull depth, $W_{bkf}$: bankfull width, FPA-flood prone area.
US: upstream and DS: downstream.

The stream type for each of the three Fort Riley sites was determined using the Rosgen classification scheme. Each reach was found to be a G6c, which is defined as being an entrenched stream, in that its flood-prone width/bankfull width ratio greater than 1.4, which is the threshold set by Rosgen (1996). This means that as an entrenched stream the potential width of a flood prone area is not much greater than its width at bankfull and therefore the stream is not in contact with its floodplain and is unable to dissipate the energy of higher flows. This stream

type also has a low width/depth ratio of <12, which in comparison to most streams, is deep in relation to its width. The Fort Riley sites are also cutting through alluvial material composed of silt and clay sized material with some chert gravel, a characteristic of a G6c stream type. The bank materials of these streams are typically derived from shale parent material and loess deposits. Rosgen (1996) cites this stream type as being easily disturbed and in a "near continuous degradational process."

**Table 3.5-2. Stream Classification Data for Fort Riley Study Sites.**

| Site ID | ER (m/m) | | W/D(m/m) | | K(m/m) | S (%) | $D_{50}$ (mm) |
|---|---|---|---|---|---|---|---|
| | US | DS | US | DS | | | |
| FR 1 | 1.47 | 1.37 | 7.64 | 9.82 | 1.19 | 1.30 | <0.062 mm |
| FR 2 | 1.46 | 2.05 | 7.85 | 4.06 | 1.26 | 0.86 | <0.062 mm |
| FR 3 | 0.98 | 1.83 | 9.13 | 5.90 | 2.39 | 0.36 | <0.062 mm |

ER: entrenchment ration, W/D: width-depth ratio, K: channel sinuosity S:water surface slope, D50, median grain size

Tables 3.5-3 and 3.5-4 show data used for classifying each of the comparison study sites. Using the same methods for stream classification as were used at the Fort Riley sites, the comparison stream reaches (on Marlatt Park and Konza) were found to be G4c for the Konza site and G6 and C6b for the Marlatt site. The Marlatt reach was separated into two stream types based on the difference in stream character above and below a head cut migrating upstream.

The pebble counts at the Konza and Marlatt sites have a greater percentage of chert gravel. The overall rating for the average bed material ($D_{50}$) for the Konza site is medium gravel approximately 11mm at the median axis. The Marlatt site bed materials have a $D_{50}$ size in the silt/clay-sized fraction, with a higher percentage of gravel-sized material than the Fort Riley sites.

**Table 3.5-3. Channel Geometry Measurements for Sites on Konza and Marlatt Park.**

| Site ID | $D_{maxbkf}$ (m) | | $D_{bkf}$ (m) | | $W_{bkf}$ (m) | | FPA (m) | |
|---|---|---|---|---|---|---|---|---|
| | XS 1 | XS 2 | XS 1 | XS 2 | XS 1 | XS 2 | XS 1 | XS 2 |
| Konza | 1.01 | 1.11 | 0.88 | 0.86 | 6.01 | 6.97 | 11.0 | 11.16 |
| Marlatt Park | 0.84 | 0.60 | 0.69 | 0.42 | 3.16 | 10.15 | 4.85 | + |

$D_{maxbkf}$: maximum bankfull depth, $D_{bkf}$: mean bankfull depth, $W_{bkf}$: bankfull width, FPA-flood prone area. XS 1: cross section 1, XS 2: cross section 2., + implies value results in an ER value of 2.2.

**Table 3.5-4. Stream Classification Data for Study Sites on Konza and Marlatt Park.**

| Site ID | ER (m/m) | | W/D(m/m) | | K(m/m) | S (%) | $D_{50}$ (mm) |
|---|---|---|---|---|---|---|---|
| | XS 1 | XS 2 | XS 1 | XS 2 | | | |
| Konza | 1.83 | 1.60 | 6.83 | 8.10 | 1.86 | 1.1 | <0.062 mm |
| Marlatt Park | 1.53 | 2.2 | 4.58 | 24.17 | 1.13 | 2.9 | <0.062 mm |

ER: entrenchment ration, W/D: width-depth ratio,, K: channel sinuosity S:water surface slope, D50, median grain size

The character of bank materials evaluated at the comparison sites found the bank material at the Konza site rated as "good" using the Pfankuch test and "poor" for Marlatt Park. This difference provides two ends of a spectrum for bank stability

**Bank Stability**

Bank stability measurements were taken using the Pfankuch channel stability evaluation modified by Rosgen (1996). Scores using the Pfankuch test were then used with riparian vegetation considerations to provide a thorough picture of the variables affecting bank protection. Table 3.5-5 shows the Pfankuch scores and ratings for the study sites on Fort Riley and comparison sites (Marlatt Park and Konza).

**Table 3.5-5. Pfankuch Channel Stability Evaluation for Study Sites on Fort Riley and Comparison Sites.**

| Site ID | Score | Rating |
|---|---|---|
| FR 1 | 108 | Fair |
| FR 2 | 109 | Fair |
| FR 3 | 113 | Fair |
| Konza | 100 | Good |
| Marlatt Park | 123 | Poor |

**Bankfull Velocity and Discharge**

An estimate of stream velocity was calculated using the Manning's equation (Equation 3.5-1). This estimation is based on channel dimensions and character in the absence of actual water flow. The roughness coefficient (n) is based on the Rosgen G6 stream type. Discharge was calculated by multiplying velocity and cross section area at bankfull stage. A summary of the variables used to calculate bankfull velocity and discharge are listed in Table 6. Bankfull velocity and discharge measurements for each site are also shown in Table 3.5-6.

**Table 3.5-6. Hydraulic Variables at Study Sites on Fort Riley, Konza and Marlatt Park.**

| Site ID | $W_{bkf}$ (m) | P (m) | R (m) | S (m/m) | n | U (m/s) | $A_{bkf}(m^2)$ | $Q_{bkf}$ ($m^3$/s) (m3/s) |
|---|---|---|---|---|---|---|---|---|
| FR 1 | 4.06 | 4.57 | 1.42 | 0.0130 | 0.067 | 2.15 | 6.47 | 13.90 |
| FR 2 | 6.30 | 6.59 | 2.37 | 0.0086 | 0.067 | 2.47 | 15.59 | 38.37 |
| FR 3 | 4.32 | 4.50 | 1.63 | 0.0036 | 0.067 | 1.24 | 7.33 | 9.09 |
| Konza | 6.97 | 7.22 | 2.64 | 0.0110 | 0.067 | 3.00 | 19.08 | 57.22 |
| Marlatt | 3.16 | 4.15 | 0.94 | 0.0290 | 0.067 | 2.44 | 3.92 | 9.59 |

$W_{bkf}$: bankfull channel width, P:channel wetted perimeter, R: hydraulic radius, S: channel slope, n: Manning's roughness coefficient, U: bankfull velocity,$A_{bkf}$: bankfull area, $Q_{bkf}$: bankfull discharge.

The value of velocity and discharge are compared with regional curve figures created in Emmert's (2004) study on regional curve estimates for physiographic provinces in Kansas. Using formulas from regression analysis on Flint Hills streams for bankfull discharge, stream width, mean depth, and cross-sectional area for a watershed of a given size are provided in Table 3.5-7. The values found for Fort Riley and the comparison sites, based on field measurement, can now be examined.

**Table 3.5-7. Hydraulic Variables Calculated Using Regional Curves for Flint Hills Region**

| Site ID | $W_{bkf}$ (m) | $D_{bkf}$(m) | $A_{bkf}$ ($m^2$) | $Q_{bkf}$ ($m^3$/s) |
|---|---|---|---|---|
| FR 1 | 6.0 | 0.27 | 1.62 | 1.68 |
| FR 2 | 6.8 | 0.30 | 2.07 | 2.19 |
| FR 3 | 7.4 | 0.33 | 2.46 | 2.64 |
| Konza | 6.6 | 0.29 | 1.95 | 2.05 |
| Marlatt | 2.5 | 0.12 | 0.29 | 0.26 |

$W_{bkf}$: bankfull channel width, $D_{bkf}$: bankfull depth,,$A_{bkf}$: bankfull area, $Q_{bkf}$: bankfull discharge

### 3.5.c DISCUSSION

#### Fluvial Geomorphology of Fort Riley Sites

The Rosgen stream type, bank stability rating, and riparian vegetation condition summarizes the overall fluvial geomorphic features of the Fort Riley sites. Stream type G6c is considered an entrenched stream in a nearly continuous degradational process. According to Rosgen (1996),

this stream type can be easily disturbed and will respond quickly to changes in the watershed. With this erosive potential in mind, the bank stability rating is considered to be "fair" and the amount of mature vegetation provides added protection to the stream length as a whole.

Local areas of deposition and scour are present at all Fort Riley sites. Through field observation, sediment bars composed of fine silt/clay material were found along 30 to 50% of the channel. As described by Rosgen (1996) the evolutionary sequence of a G6c stream leads to a continued broadening and shallowing of the stream to form a new F6 stream type and then evolving back to a stable E6 or C6 stream type as a smaller, more sinuous channel is cut into the old F6 channel. Schumm and Rea (1995) support a similar evolution for incised channels, going through a deepening, broadening, fill, and creation of a new channel within this fill.

Channel measurements leading to velocity and discharge calculations were compared to regional curve calculations. The most obvious difference is in the estimated value for discharge at all the sites and the value of discharge calculated from actual measurements. The actual measurement is much higher than the estimated value. This difference is due to the difference in channel cross-sectional area. The actual shape of the bankfull cross-sectional area is not "u" shaped. Mathematical calculation of cross-sectional area uses the area of a semicircle and potentially overestimates discharge.

Other differences in regional curve estimates of channel dimensions and actual measurements are the stream bankfull width of Fort Riley streams. The Fort Riley streams all have stream width slightly wider than regional curve figures. This difference has two potential sources, one being the formula derived from the regional curve itself that was created using Rosgen stream types that included few G type streams. The other possibility for the difference is in the nature of instability of the Fort Riley streams themselves. The Fort Riley streams may be departing from the regional trend. This interpretation requires further study to validate measurements of bankfull and regional information on G type streams.

**Comparison of Fort Riley Sites to Konza and Marlatt Sites**

The Rosgen stream type was found to be similar for the Fort Riley sites and the Konza and Marlatt comparison sites. Differences found were related to variations in entrenchment ratios, width/depth ratios, and the abundance of limestone/chert gravel.

Looking strictly at watershed area, the Fort Riley sites increase in size from FR1 (1.28 $km^2$) to FR3 (2.36 $km^2$). The stream channel dimensions increase accordingly for the most part with this increase in watershed area. An exception to this trend in size is the Konza comparison site. The Konza site had the largest values of mean bankfull depth (0.88 m), bankfull width (6.01 m), and flood prone width (11.0 m and 11.2 m) even though its watershed size is smaller than FR2 and FR3. This larger channel shape is reflected in the velocity measurement with the Konza site having the highest velocity. The Konza site has the highest value of valley slope (2.6) compared to the other sites and this may be the reason for the difference in velocity and channel size to accommodate that flow. The Konza site was also found to have a "good" bank stability rating whereas the Fort Riley and Marlatt sites were rated as "fair" and "poor" respectively.

Differences in these findings may be a sign of differences in watershed history and current management. Myers and Swanson (1992) examined many different Rosgen stream types, all with bank damage from livestock grazing. Bank stability varied with stream type validating that some stream types are more sensitive to grazing than others. In this case the stream types are the same and the difference in management leads to more erosion of the stream banks and possibly the streambeds at Fort Riley.

The Konza comparison site was found to be a Rosgen stream type of G4, which is described as being easily disturbed and susceptible to changes in watershed activities (Rosgen, 1996). Like the Fort Riley streams, this reach has the potential for degradation, but little watershed disturbance and a healthy riparian zone moderate this erosive tendency. Portions of the Konza site are beginning to establish a smaller channel within the large channel, which fits in the evolutionary sequence for this stream type. The floodplain that now exists in the old channel is the site of established cottonwood trees.

The Marlatt Park comparison site also varies from the Fort Riley watershed size trend in that it has a significantly smaller watershed and higher values for bankfull channel depth and a very low width/depth ratio with a similar Rosgen stream type. A lowering of width/depth ratio in this case indicates incision by this stream (Rosgen, 2001). The accelerated erosion of tributaries entering the Marlatt stream segment also confirms incision. Using the bank stability analysis, the Marlatt reach was found to be "poor" and this difference can also be attributed to watershed history and use.

The Marlatt Park comparison site is located along Seth Child Road, a four-lane highway that truncates a portion of the Marlatt Park watershed. Other watershed disturbances occurred during the late 1960's through the 1980's with the grazing of cattle in the immediate watershed (Owensby, C.E., Kansas State University, Department of Agronomy, written communication, 2005). The effects of these disturbances have caused the stream channel slope to increase and degradation to dominate.

**Anthropogenic Impacts on Fort Riley Sites**

Fording sites located along the Fort Riley stream reaches are areas of change in stream width. This local widening of the channel causes the flow of water to slow and suspended material and smaller saltated material to drop out of suspension. The best example of this scenario is at the second improvised crossing at site FR2. This crossing is 5-½ times wider than the average undisturbed stream width of this reach and the left bank now is the site of a large sediment bar that is 6.7m long and 1m wide. To the right of this sediment bar is a deep ponded area.

Fording sites are also the location of concentrated flow, forming rills in the track scars left by vehicles. The summary data of rill occurrence II finds rill depth of improvised crossings to be 5-½ times deeper than those found on the low-water stream crossings. The distribution of those rills are about the same with an average of 28% the approach being dissected by rills and most often located in the wheel tracks left by military vehicles. These rill features are signs of persistent/active erosion, and a good example of a rill feature is found at the second improvised crossing of site FR3.

Comparing the anthropogenic impact of low-water stream crossings to improvised stream crossings, the area of direct stream impact on channel shape is greater for low-water stream crossings than improvised stream crossings. Stream widths for low-water stream crossings are two times wider than for improvised crossings. The lengths of affected stream channels are two times longer for low-water stream crossings than for improvised stream crossings.

Little vegetation is present on the low-water stream crossing approaches to filter and slow the transport of sediment to the stream. Improvised crossings have 3 times more vegetation on their approaches than low-water stream crossings and the lack of vegetation for low-water stream crossings is magnified by an increase in slope of approach for these sites with low-water stream crossings having a slope 1-½ times steeper than improvised crossing approaches. At the low-water stream crossings the lack of vegetation on the crossings is not a cause for additional erosion on the approach area since the construction of low-water stream crossings included the installation of geotextile fabric and limestone gravel (Sample et al., 1998). The presence of vegetation along the improvised stream crossings, however, is seen as a stabilizing feature with many studies pointing towards riparian vegetation reducing the rate of bank erosion (Zaimes et al., 2004; Abernethy and Rutherfurd, 2000; Myers and Swanson, 1992). Without thick riparian vegetation, low-water stream crossings act as conduits for soil eroded from watershed slopes.

Improvised stream crossings will continue to heal as channel width is narrowed by deposition and as riparian vegetation matures, but rill features will persist. In examining aerial photographs of Fort Riley from 1956 to orthophotos taken in 2003, most streams are dissected with improvised crossings and hillslopes are braided with vehicle trails. It is the goal of Fort Riley land managers to reduce the number of improvised crossings with the installation of low-water stream crossings, but hillslope disturbance will still affect stream stability (Sample et al., 1998).

While the anthropogenic impact is obvious at tank fording sites, the compounded influence on channel migration is more difficult to gauge. The meander cut-off is forming on the FR3 reach along the left bank of the LWSC causing the abandonment of the channel just downstream of the LWSC. This LWSC is also located just downstream from a tributary that enters the main stream channel and the total impact of the LWSC on the formation of the meander cut-off is complicated by the additional volume of water that tributary delivers.

The stability of constructed low-water stream crossings at Fort Riley can be improved by placing the crossing site perpendicular to the stream channel, at a stable portion of the stream channel. This stable section would be the site of a riffle feature, which is a shallow portion of the channel that is a site of deposition. Riffle features are generally found at the inflection point between two meander bends and exhibit a slower rate of lateral migration (Dunne and Leopold, 1978). Low-water stream crossings should not be placed directly downstream of tributaries or other features that have the potential for channel erosion.

Water quality at site of low-water stream crossings can be improved by mitigating the amount of sediment being allowed to wash down the approach slope. Improvised crossings that are abandoned should no longer be used, allowing the natural processes already taking place to continue moving them towards a steady state.

### 3.5.d CONCLUSIONS

Fort Riley sites studied in this project were found to be Rosgen stream type G6c and have a Pfankuch bank stability rating of "fair." These are streams that have a high potential for erosion of bank and/or bed material making them naturally susceptible to watershed anthropogenic activity. The many fording sites along the FR1, FR2, and FR3 stream reaches are locations of local channel widening, which causes a reduction in stream velocity and deposition of sediment at the fording site. Fort Riley improvised stream crossings will continue to heal though the rills present in vehicle track scars will continue to persist. Low-water stream crossings will continue to affect the shape of the local channel.

The comparison sites at the Konza Prairie Biological Station and Marlatt Park were found to be similar Rosgen stream types with the Konza site being a G4c and the Marlatt Park site being a G6 and C6b. These two comparison sites were also examples of stream reaches that have both more stable banks and less stable banks than the Fort Riley sites. The difference in anthropogenic influence is attributed to the varying bank stability ratings and observed geomorphic characteristics at each site.

Future work that could confirm these findings might include the use of bank erosion pins to calculate bank erosion rates. This method was used by Zaimes et al. (2004) to quantify differences in erosion between sites with different land management and erosion pins are common tools used for measuring erosion (Dunne and Leopold, 1978; Rosgen, 1996). Stream cross sections are also good indicators of lateral migration over time and can be resurveyed accurately from benchmarks installed for this study.

Historic channel movement through comparison of aerial photographs was attempted in this study, but proved difficult with dense riparian vegetation obscuring exact stream channel location. Image enhancement and additional photos may prove useful in improving the visibility and measurement of stream channels over time providing a sense of lateral migration rate.

Validation of field observations may be conducted with more detailed analysis of factors such as stream suspended load through water samples and streambed load through measurement of depositional bars. Validation through comparison of regional trends proved promising in this study and can be continued with comparisons of meander width and radius and shear stress.

### 3.5.e. Fort Riley Hardened Crossing Monitoring Study

A separate component of Task 5 was to sample water quality including sediment loads in streams during storm runoff events. During 2006, a monitoring plan was setup to examine both temporal and spatial patterns of contaminants in a stream reach in an upper sub-watershed of Three Mile Creek located in training area 36 of Fort Riley, Kansas. During the monitoring performed for this study, two event stations were located up and down stream of a hardened crossing. These event monitoring sites measured stream flow rate and collected event based water quality samples. Using that flow data, samples near those gauges were collected for contaminant analysis. Figure 3.5-2 shows the sub watershed draining 1.58 $km^2$ of tall grass prairie used for

tank training. ISCO event samplers were located up and down stream of a hardened crossing in this sub watershed and were capable of measuring stream flowrates and collecting water samples during a runoff event. This report presents information collected during 2006-2007.

**Figure 3.5-2. Three Mile Creek watershed monitoring site showing the location of the far eastern (downstream) monitoring ISCO sampler (located in the blue box at the far right of the figure). The up-stream sampler was located 30 meters west of the outlet of the watershed on the upstream side of the hardened crossing. The orange line indicates the watershed drainage area.**

**Sampling Frequency and Interval**

It is important to estimate early in a monitoring program the number and frequency of samples required to meet the monitoring objectives. Spooner et al. (1991) reported that the sampling frequency required at a given monitoring station is a function of the monitoring goals and the response to changes in pollutant sources. Sherwani and Moreau (1975) stated that the desired frequency of sampling is a function of several considerations associated with the watershed to be studied and include, response time of the watershed and seasonal fluctuation based on the

climate. Thus, sampling frequency will usually be greater for streams and rivers compared to other water resource types. Some parameters such as total suspended solids can be highly variable in stream systems dominated by nonpoint sources. These highly variable parameters generally require more frequent sampling. Some parameters vary considerably with season, particularly in watersheds impacted primarily by nonpoint sources. Examination of the KDHE 1998 303(d) list and water quality impairments would indicate that the source of the contamination is related to spring and summer runoff events. To calculate daily loading required by the Total Maximum Daily Load (TMDL), the daily stream flow and contaminant concentration needs to be known or estimated. By comparing the daily loading at current conditions with the loading if the stream met standards shows the load reduction needed to meet the standard. This type of program requires a rigorous monitoring program to measure or estimate the daily data needs.

The sub watershed flow is ephemeral and sampling will include samples taken at each sampling location during the flow event. The rest of the year the stream is dry or during the winter months the stream is frozen if water is present.

**Monitoring Parameters**

The following parameters were monitored during monitoring study at each sampling site:

- Stream flow,
- Total Suspended Solids, and
- Total Phosphorus and Nitrogen.

**Stream Flow (Ward and Elliot, 1995)**

Stream flow at the main stream sites will be acquired from the U. S. Geological Survey. Flow in a stream is a function of many factors including precipitation, surface runoff, interflow; the cross sectional geometry and bed slope of the channel, the bed and side slope roughness; meandering, obstructions, and changes in shape; hydraulic control structures and impoundments; and sediment transport and channel stability. Generally, flow in streams and impoundments are classified as open-channel flow because the surface of the flow is open to the atmosphere. Stream flow can be classified several ways. For example, it can be turbulent in steep rocky areas or following severe storm events. Typically, stream flow is tranquil and is considered to be a steady uniform flow. The calculated stream flows for sites without USGS gauges in this study assume this condition where the stream depth does not change during the flow measurement and the same depth at every section along the stream.

The stream flow is:

$$q = va \qquad \text{[Eq. 3.5-3]}$$

where: q = stream flow ($m^3$/sec),
v = average stream velocity (m/sec), and
a = cross-sectional area of flow ($m^2$).

For uniform flow in a stream, the average stream velocity, v, can be estimated by Manning's equation.

$$v = \frac{1}{n} R^{2/3} S^{1/2} \qquad \text{[Eq. 3.5-4]}$$

where: v = average stream velocity (m/sec),
n = Manning's roughness coefficient of the stream channel,
R = hydraulic radius (a/p, p = wetted perimeter), and
S = channel bed slope (m/m).

Flow measurement and sample collection at the event sample sites was made at road crossings at bridges or culverts using an ISCO 6700 sampler instrumented with an ISCO 730 bubble flow module stage recorder. The cross sectional area and hydraulic parameters needed to estimate stream flow through these structures were measured.

Analysis of composite samples produced mean contaminant concentrations for an entire storm. Using these concentrations and recorded flow volumes, contaminant mass transport was computed. The method of computing the flow-weighted volume of each discrete sample to be included in the composite sample was based on the mid-interval method of subdividing as described by Porterfield (1977). A similar method of discrete and composite sampling was used by Pope and Devans (1987) and Pope and Hess (1989).

Samples were collected at the monitoring sites on a stratified fixed-frequency basis. Samples were collected in 340 ml glass jars with Teflon-lined lids. These samples were stored at 4.5°C until analyzed. These samples were analyzed at the Kansas State University Water Quality Laboratory and the Kansas State University Soil Testing Laboratory.

**Total Suspended Solids Parameter**

Total suspended solids (TSS) include all particles suspended in which will not pass through a filter. Nonpoint sources of suspended solids are typically associated with soil erosion in surface runoff and stream bank erosion.
As levels of TSS increase, a stream begins to lose its ability to support a diversity of aquatic life. Suspended solids absorb hear from sunlight, which increases water temperature and subsequently decreases levels of dissolved oxygen.

TSS can also destroy fish habitat because suspended solids settle to the bottom and can eventually blanket the riverbed. Suspended solids can smother the eggs of fish and aquatic insects, and can suffocate newly hatched insect larvae. Suspended solids can also harm fish directly by clogging gills, reducing growth rates, and lowering resistance to disease. Changes to

the aquatic environment may result in diminished food sources, and increased difficulties in finding food. Natural movements and migrations of aquatic populations may be disrupted.

The procedure used in this study to measure the total suspended solids parameter is described the Standard Methods for the Examination of Water and Wastewater Method 209C (Clesceri et al., 1998). Total suspended solid concentrations less than 20 mg/l are considered to be clear. Water with TSS levels between 20 and 80 mg/l tend to appear cloudy, while TSS levels greater than 150 mg/l appear to be dirty and are considered impaired.

**Total Nitrogen and Phosphorus Parameter**

The growth of aquatic plants is stimulated principally by nutrients such as phosphorus and nitrogen. Nutrient-stimulated plant production is of most concern in lakes, because primary production in flowing water is thought to be controlled by physical factors, such as light penetration, timing of flow, and type of substrate available, instead of by nutrients (McCabe et al., 1985).

Generally, phosphorus (as orthophosphate) is the limiting nutrient in freshwater aquatic systems. That is, if all phosphorus is used, plant growth will cease, no matter how much nitrogen is available. The natural background levels of total phosphorus are generally less than 0.03 mg/l. The natural levels of orthophosphate usually range from 0.005 to 0.05 mg/l (Dunne and Leopold, 1978).

Many bodies of freshwater are currently experiencing influxes of phosphorus and nitrogen from outside sources. The increasing concentration of available phosphorus allows plants to assimilate more nitrogen before the phosphorus is depleted. Thus, if sufficient phosphorus is available, elevated concentrations of nitrates will lead to algal blooms. Although levels of 0.08 to 0.10 mg/l orthophosphate may trigger periodic blooms, long-term eutrophication will usually be prevented if total phosphorus levels and orthophosphate levels are below 0.5 mg/l and 0.05 mg/l, respectively (Dunne and Leopold, 1978).

Water samples from this study will be analyzed for total phosphorus at the Kansas State University Soil Testing Laboratory, Manhattan, Kansas. The technique used involves sample digestion with a Potassium Persulfate Reagent in an autoclave and then analyzed using a Technicon AutoAnalyzer 11 (Hosomi and Sudo, 1986).

**Quality Assurance**

Analytical quality assurance consisted of duplicate analyses of selected stream samples, analysis of standard-reference samples, and analysis of blank-water samples. Precision and reproducibility of the analysis were evaluated by duplicate analyses on randomly selected stream samples. An analytical method with a high degree of precision generally produces similar results on duplicate samples. If the concentrations of samples and their duplicate are essentially the same, the variances will be similar, and the correlation coefficient between the two groups should be near one.

**Fort Riley Monitoring**

Rainfall and runoff during this 2 years study represent a dry and a wet year as shown in Figure 3.5-2. The month of May 2007 had several very large storms creating several severe runoff events. This rainfall data was input into a Penman Monteith evapotranspiration model (Allen et al., 1998). Using a tall grass prairie as the crop, soil water balances were calculated for both years shown in Figures 3.5-4 and 3.5-5.

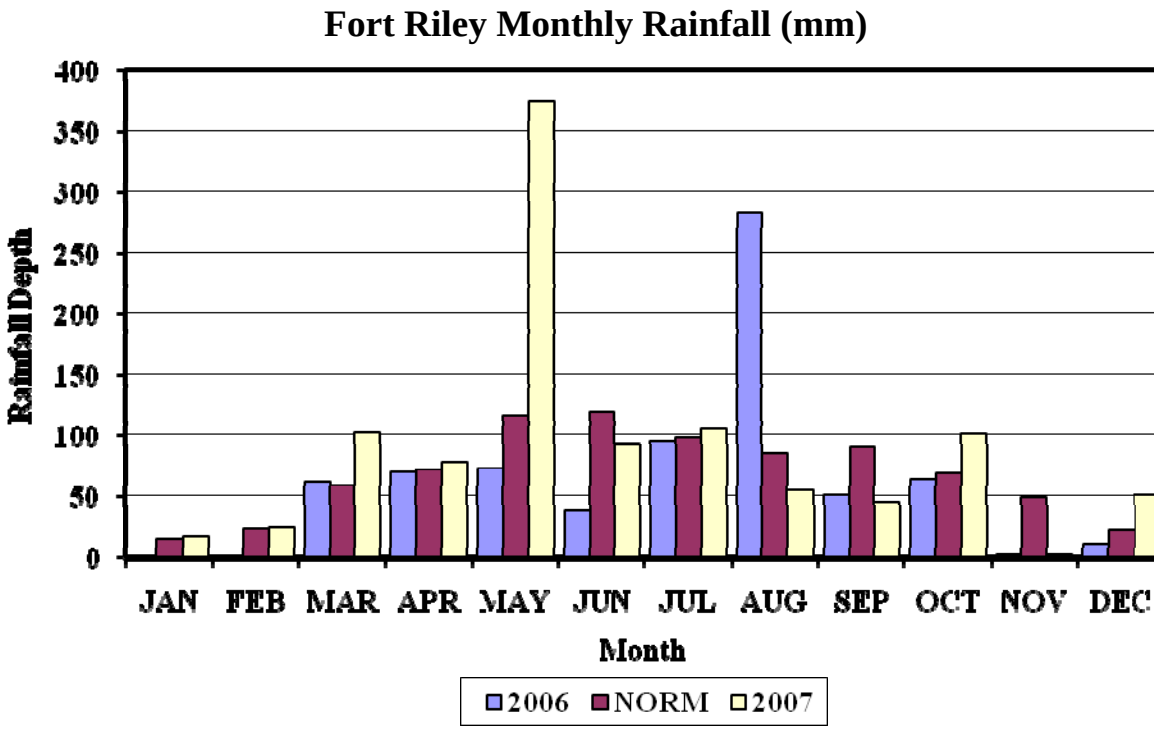


**Figure 3.5-3 Rainfall comparison at Fort Riley between 2006 (747 mm), 30 year average (NORM = 815 mm), and 2007 (1045 mm).**

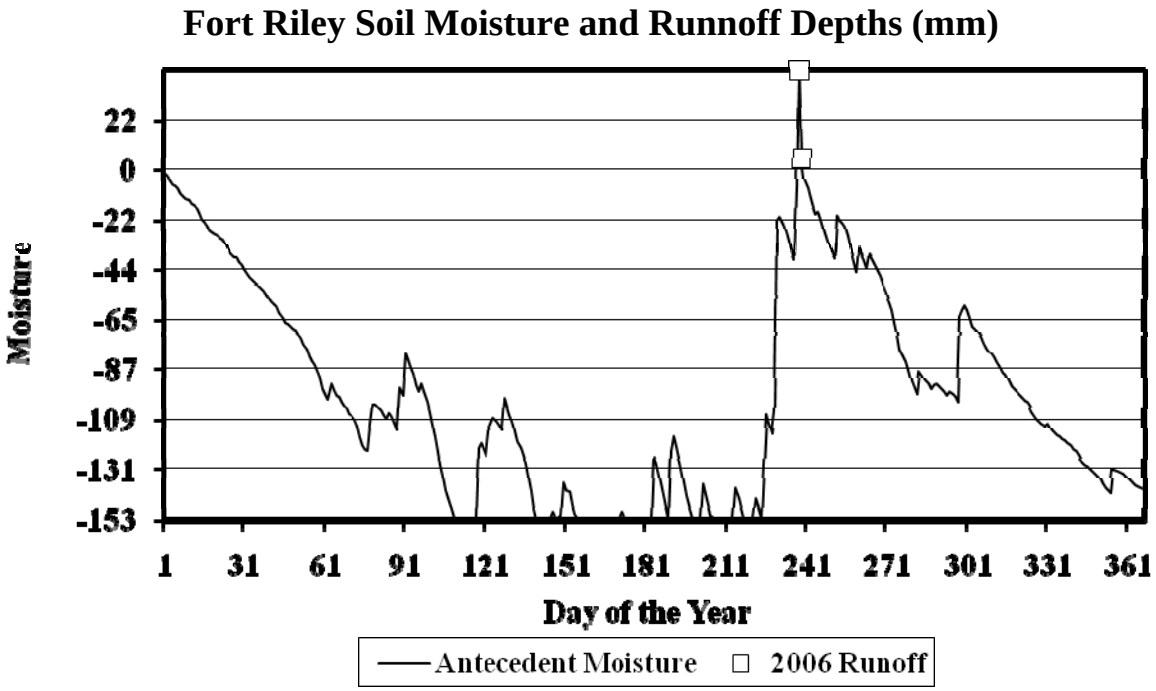


**Figure 3.5-4. Soil moisture balance for 2006 calculated for the Three Mile Creek watershed.**

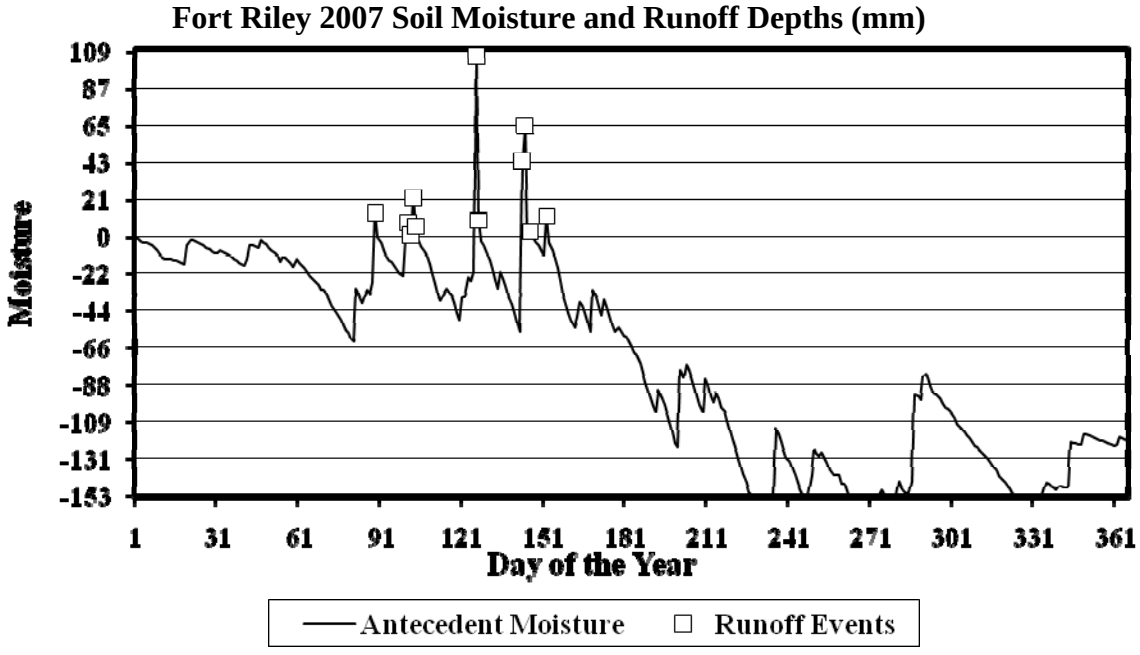


**Figure 3.5-5. Soil moisture balance for 2007 calculated for the Three Mile Creek watershed.**

These figures show the periods of time that the rainfall created excess soil moisture that produced runoff. During 2006, only one event occurred in late August (up stream of the crossing shown in Figure 3.5-6 and down stream shown in Figure 3.5-7).

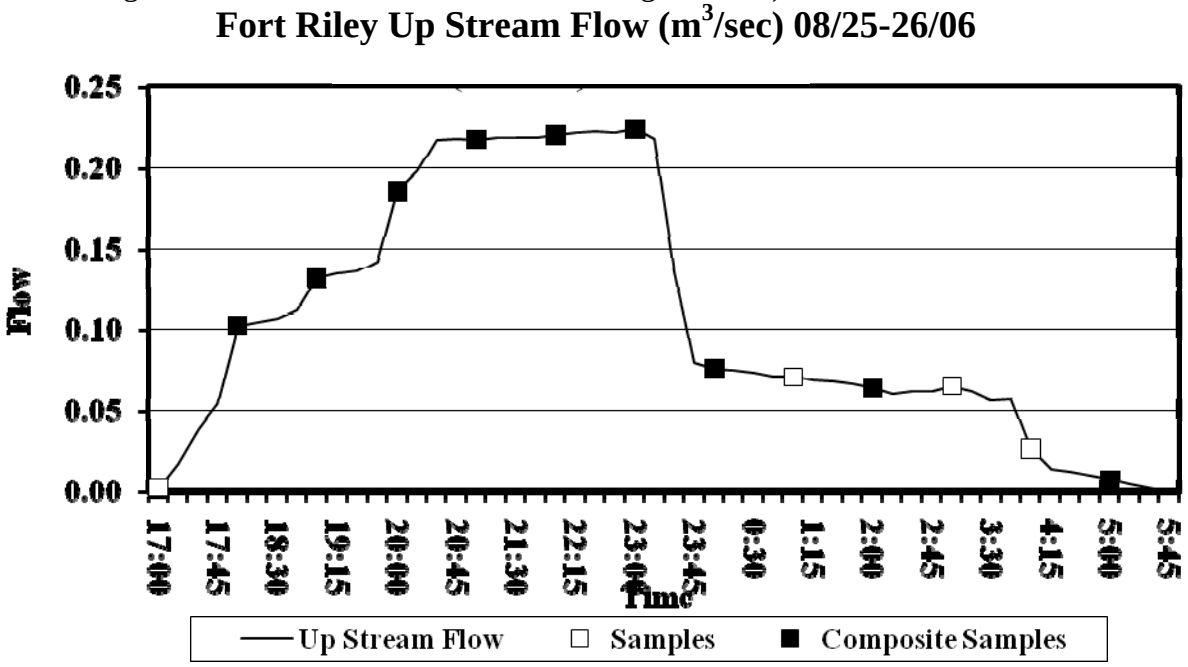


**Figure 3.5-6. Up stream hydrograph during the late August 2006 runoff event at Three Mile Creek monitoring site.**

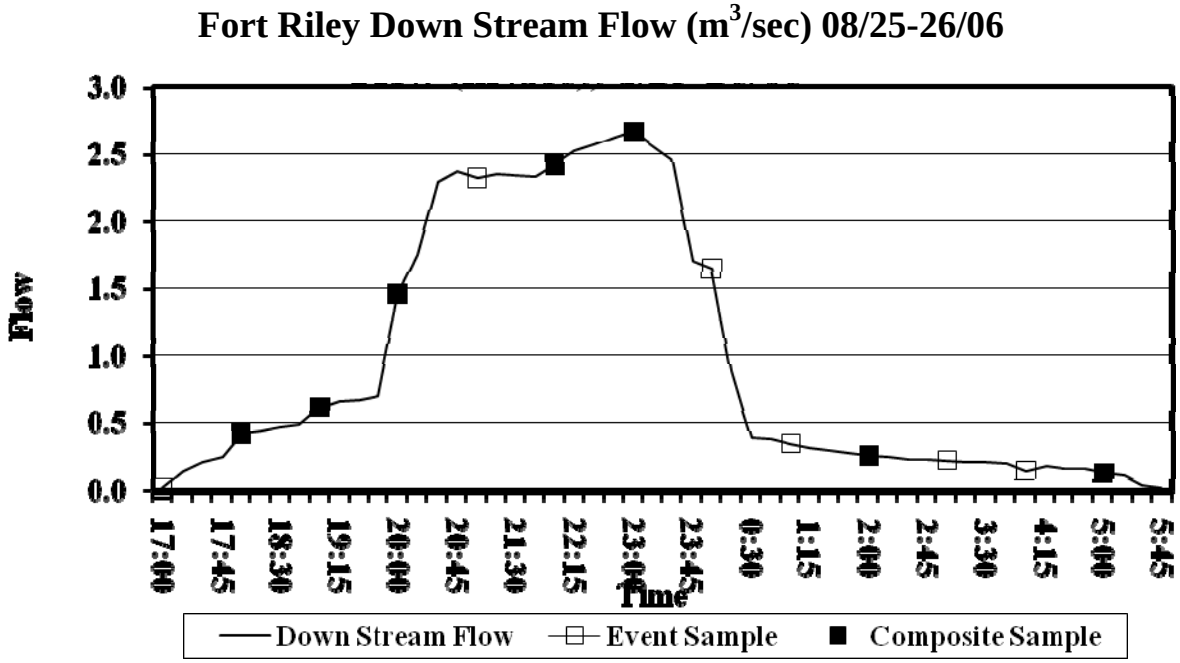


**Figure 3.5-7. Down stream hydrograph during the late August 2006 runoff event at Three Mile Creek monitoring site.**

Figures 3.5-8 through 3.5-17 show the up and down stream hydrographs for the wet periods in late March through early June of 2007.

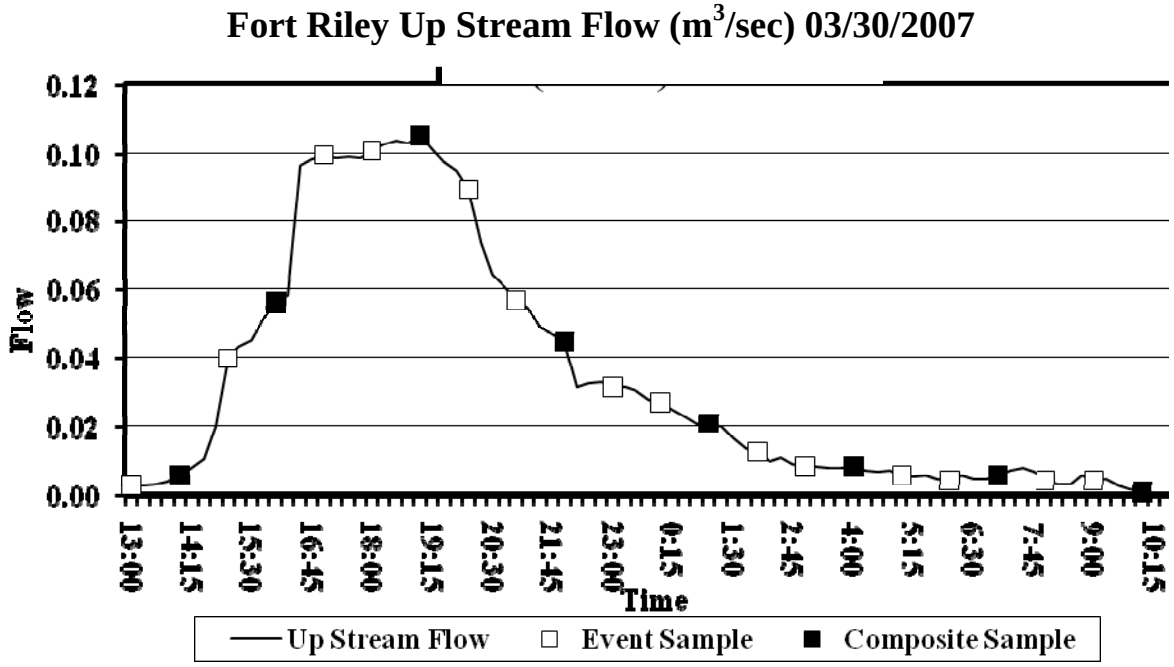


**Figure 3.5-8. Up stream hydrograph during March 30, 2007 runoff event at Three Mile Creek monitoring site.**

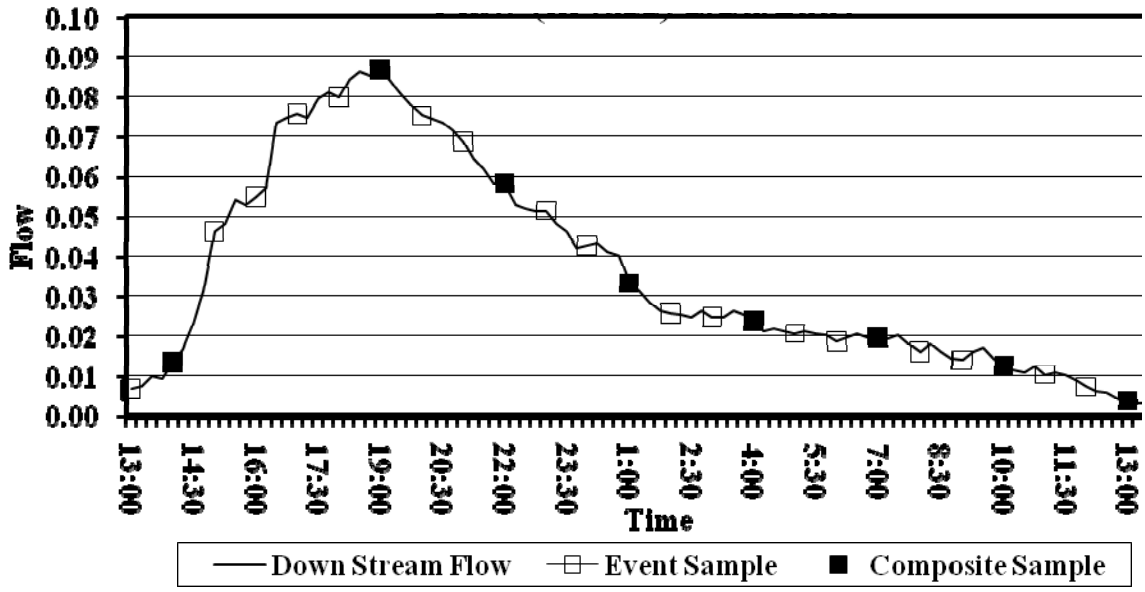


**Figure 3.5-9. Down stream hydrograph during March 30, 2007 runoff event at Three Mile Creek monitoring site.**

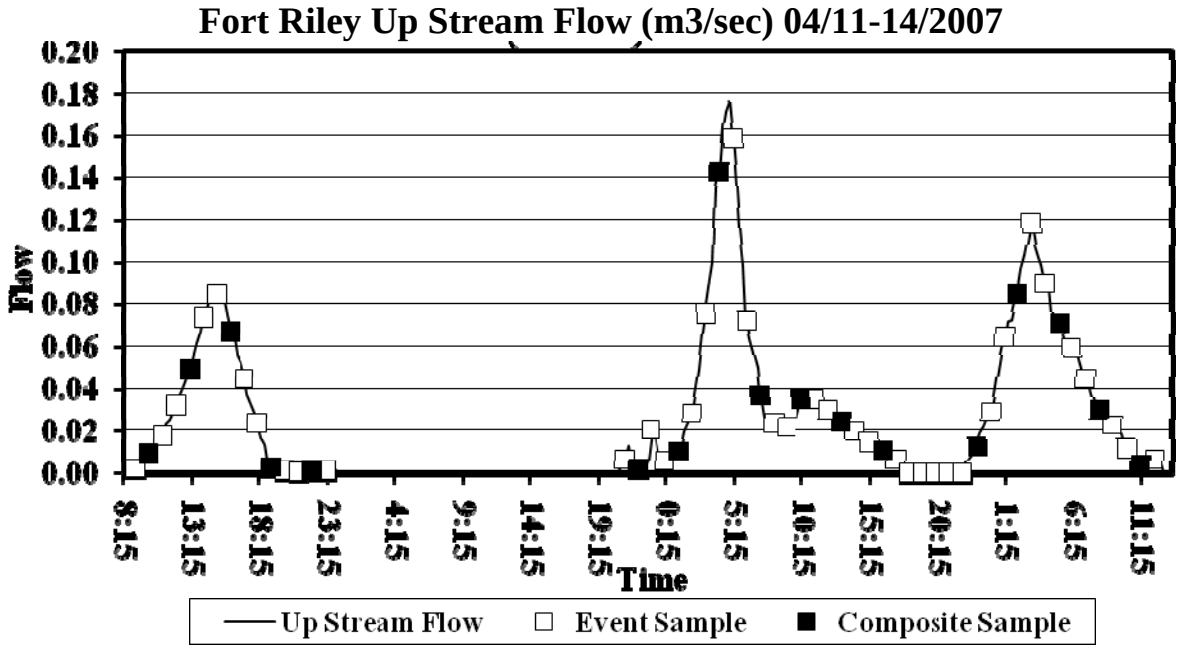


**Figure 3.5-10. Up stream hydrograph During Aril 11 through 14, 2007 runoff event at Three Mile Creek monitoring site.**

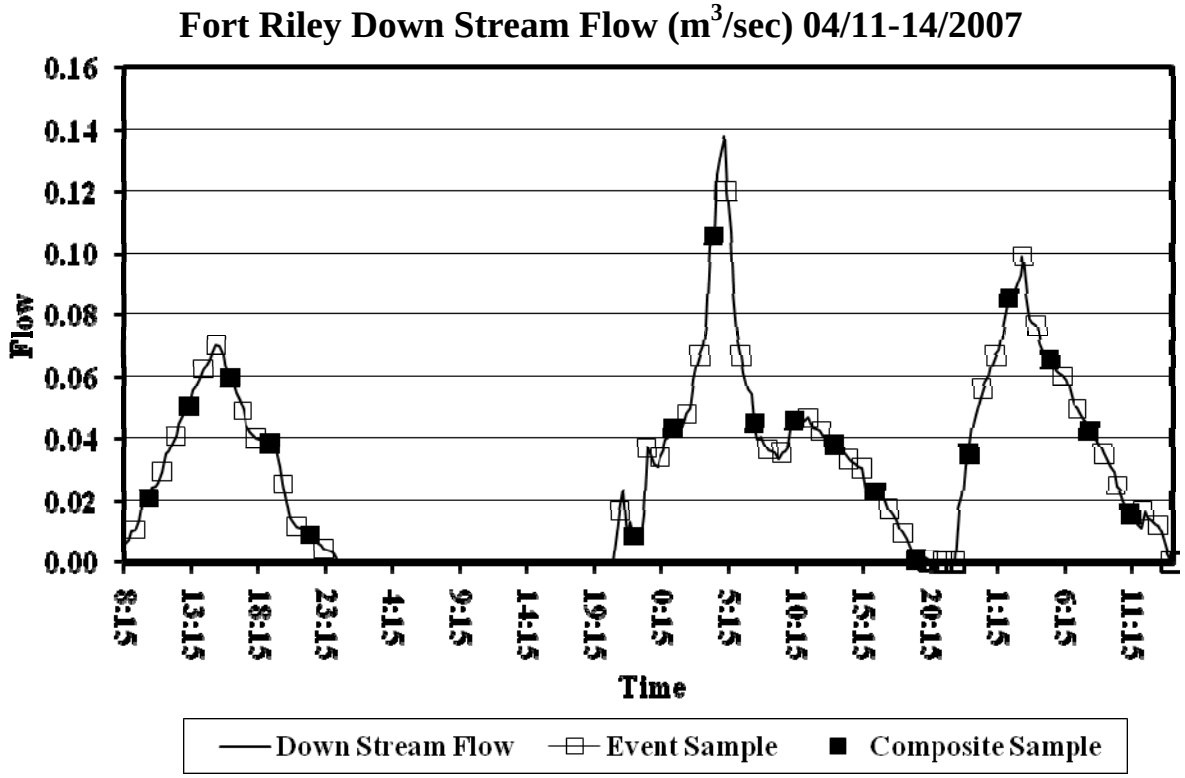


**Figure 3.5-11. Down stream hydrograph during April 11 through 14, 2007 runoff event at Three Mile Creek monitoring site.**

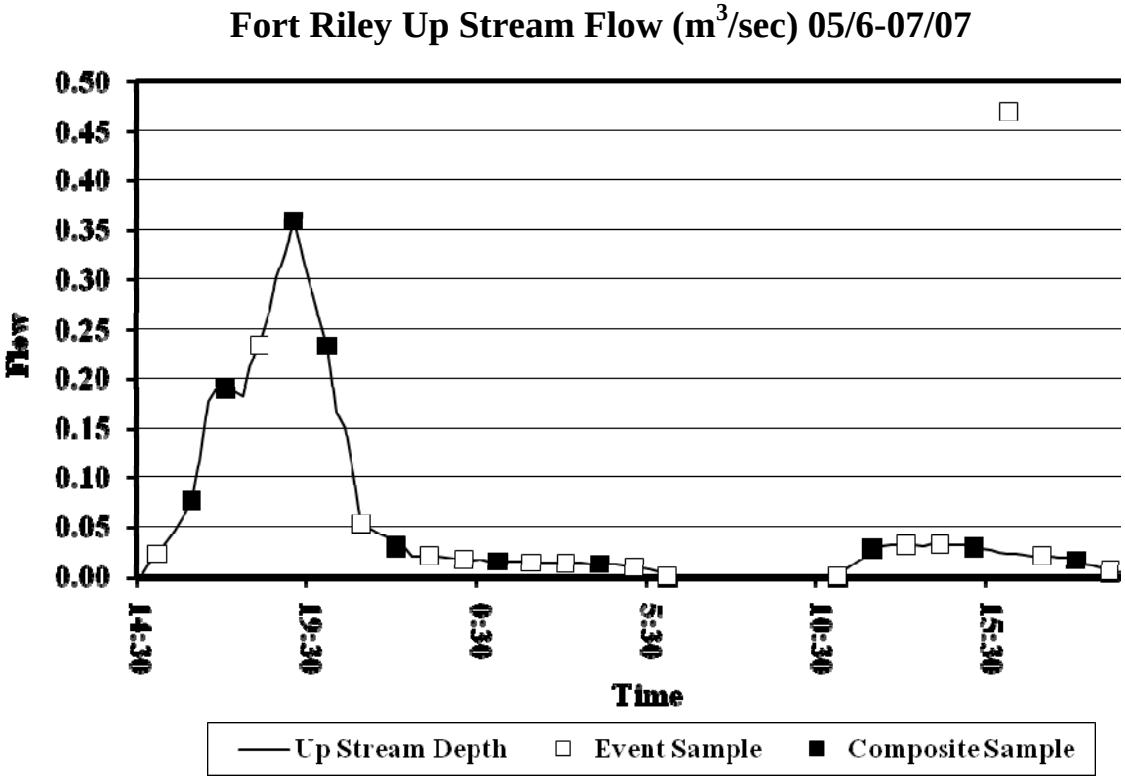


**Figure 3.5-12. Up stream hydrograph during May 6 through 7, 2007 runoff event at Three Mile Creek monitoring site.**

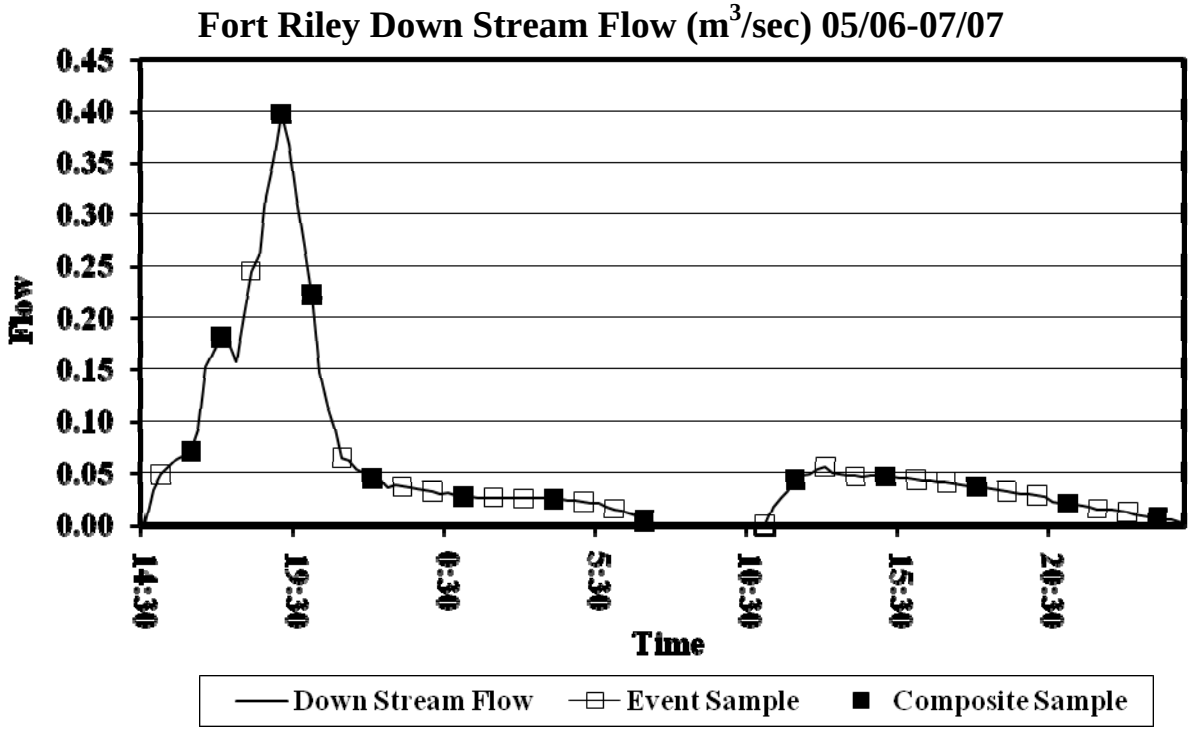


**Figure 3.5-13. Down stream hydrograph during May 6 through 7, 2007 runoff event at Three Mile Creek monitoring site.**

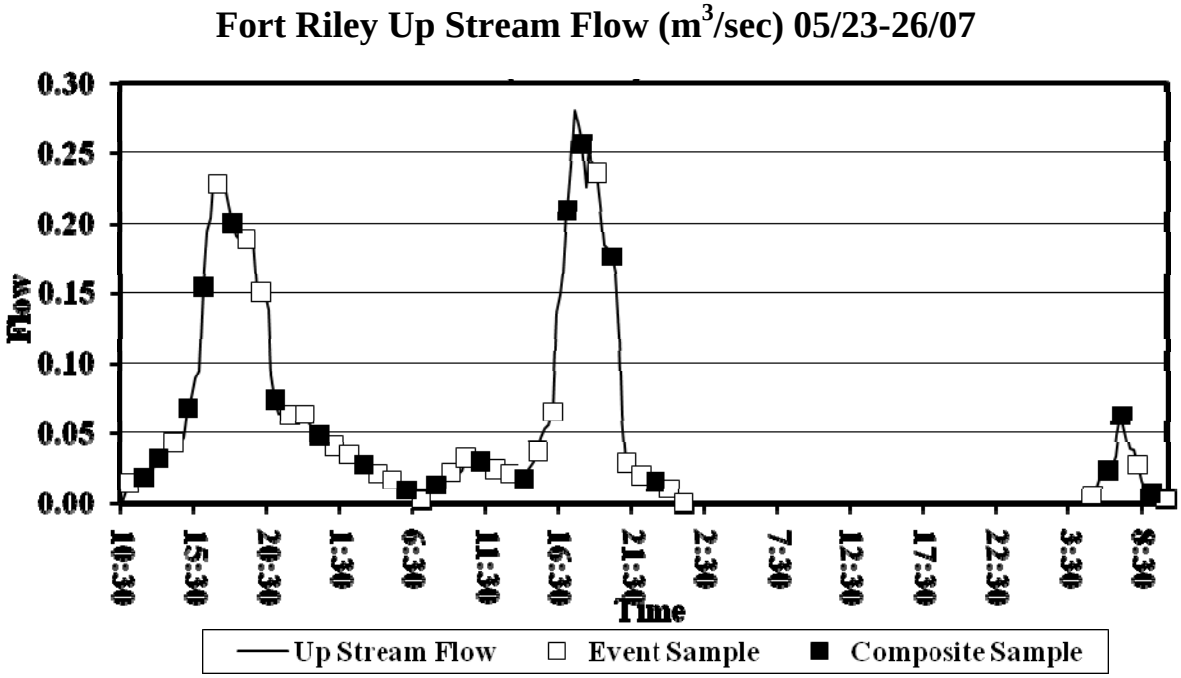


**Figure 3.5-14. Up stream hydrograph during May 23 through 26, 2007 runoff event at Three Mile Creek monitoring site.**

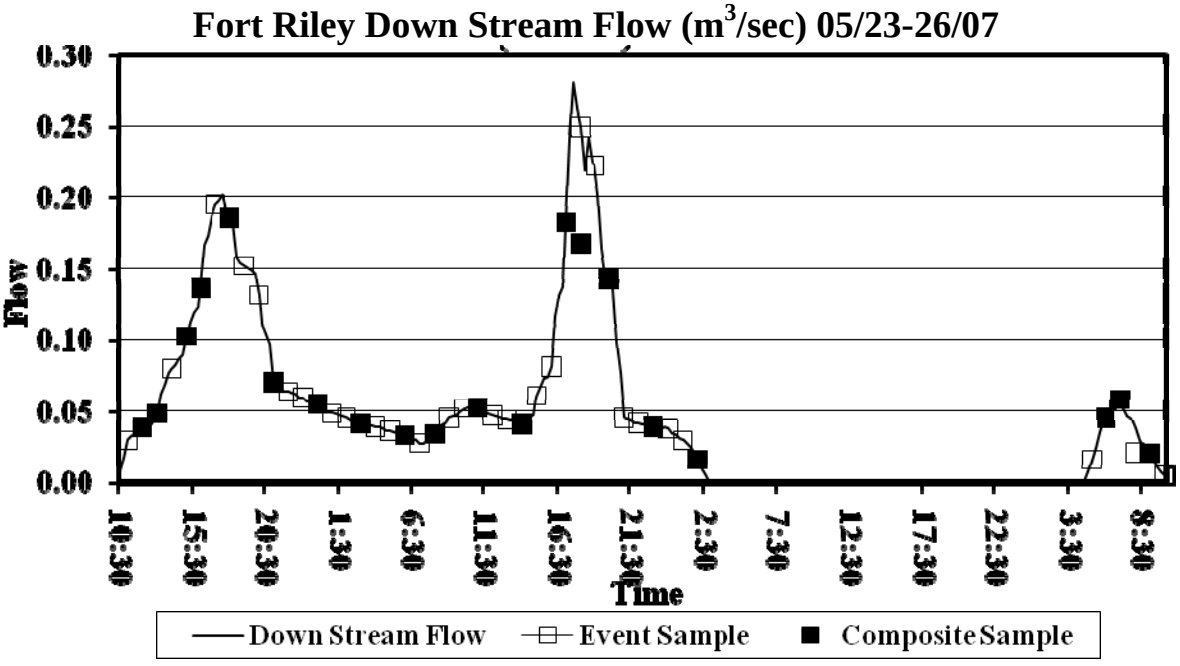


**Figure 3.5-15. Down stream hydrograph during May 23 through 26, 2007 runoff event at Three Mile Creek monitoring site.**

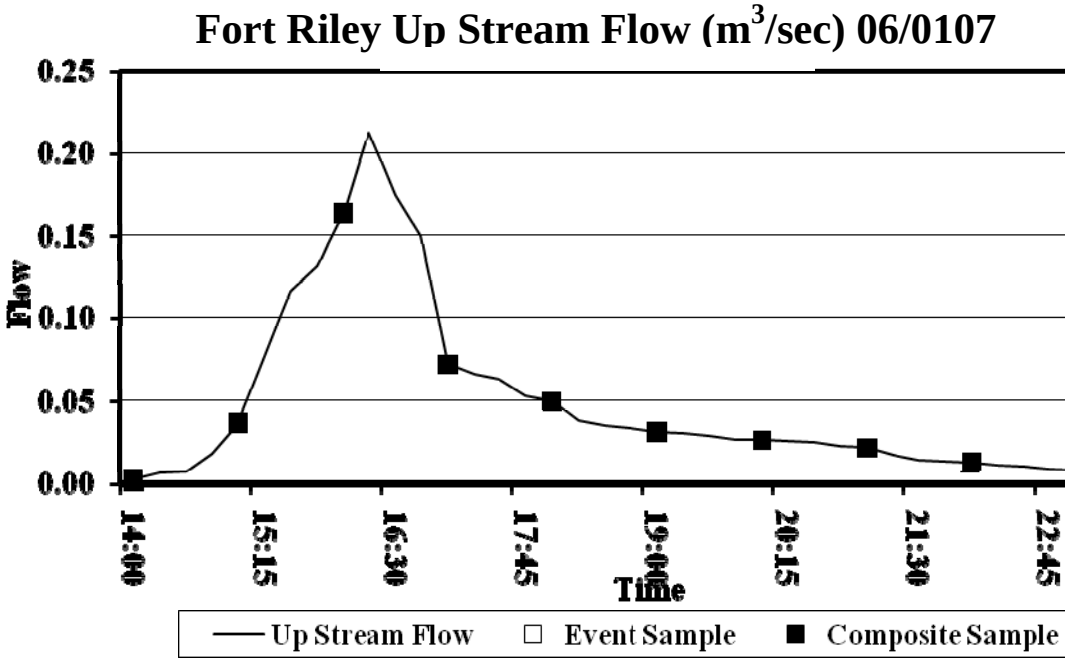


**Figure 3.5-16. Up stream hydrograph during June 1, 2007 runoff event at Three Mile Creek monitoring site.**

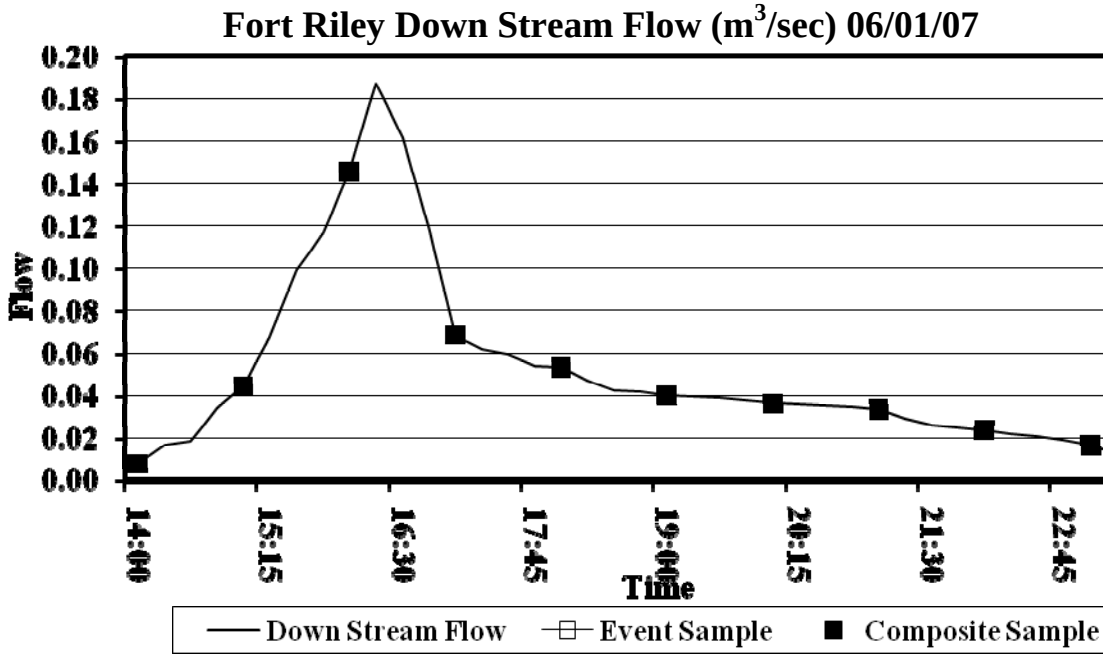


**Figure 3.5-17. Down stream hydrograph during June 1, 2007 runoff event at Three Mile Creek monitoring site.**

Cross sections were surveyed and the cross sectional area and hydraulic radius for increasing depths was calculated by method 1 (Figures 3.5-18 and 3.5-19).

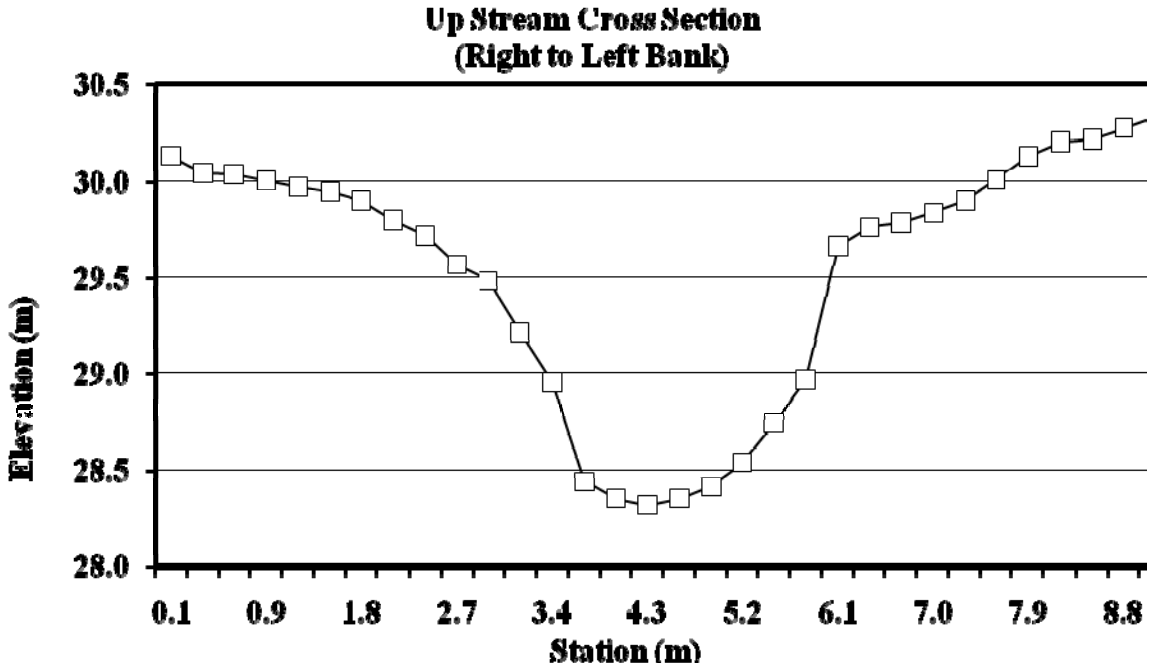


**Figure 3.5-18. Up stream cross section at Three Mile Creek monitoring site.**

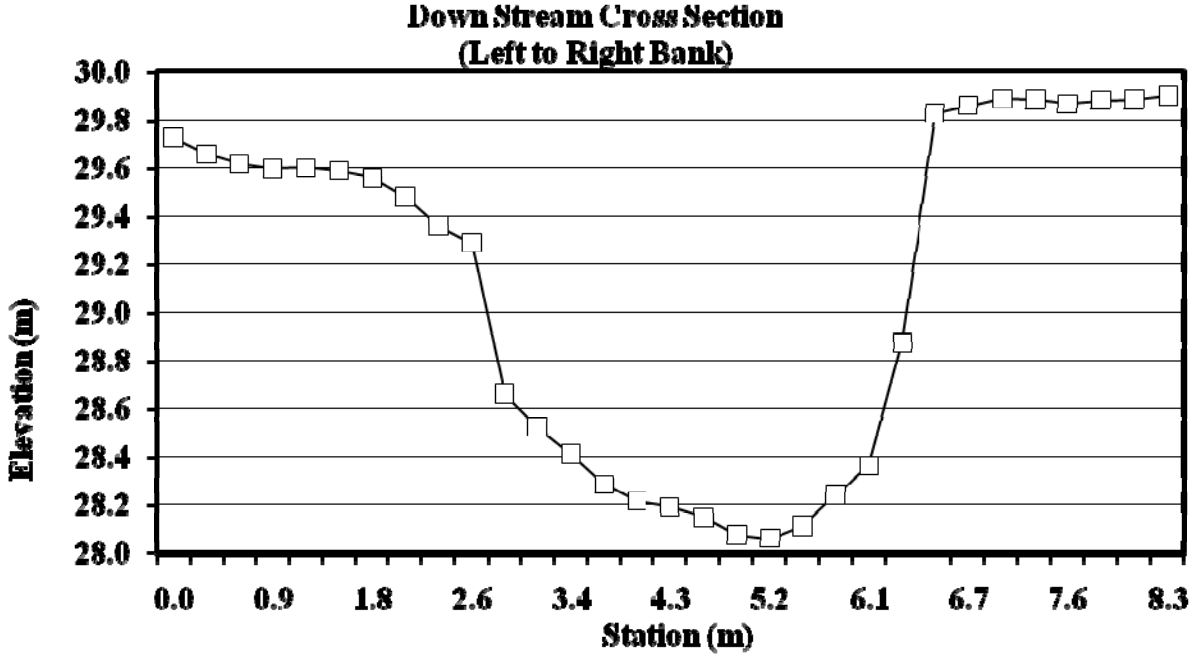


**Figure 3.5-19. Down stream cross section at Three Mile Creek monitoring site.**

The Manning equation calculation was then used to calculate the flow rates for those depths and a rating equation was developed for each cross section (Figures 3.5-20 and 3.5-21).

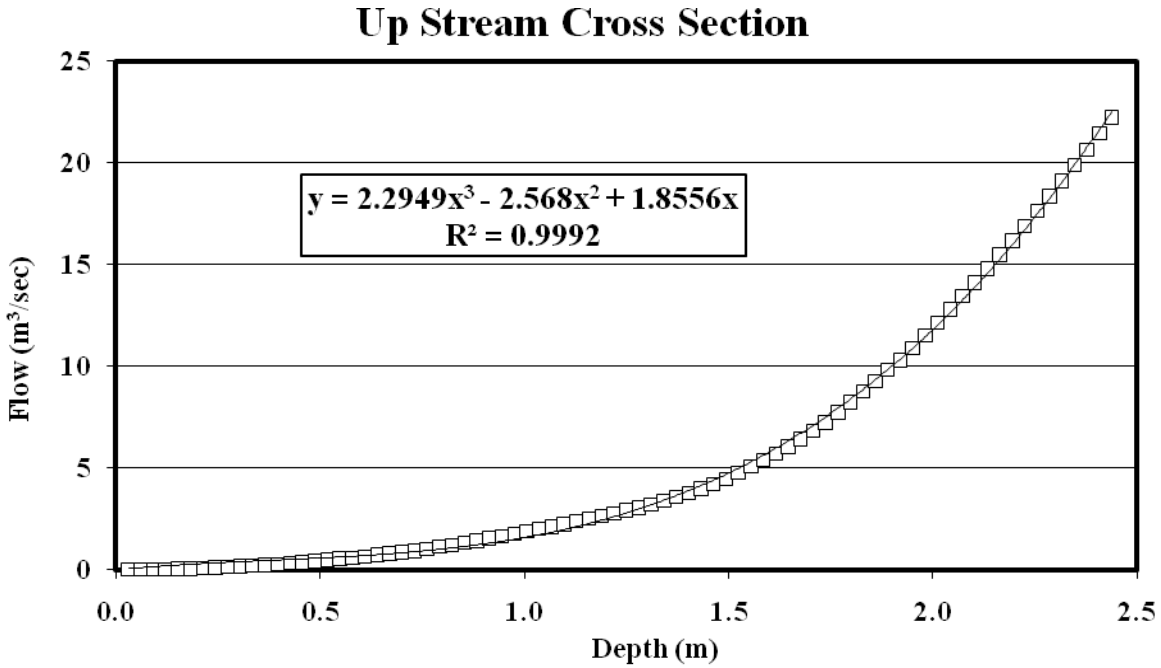


**Figure 3.5-20. Calculated flow rate and rating equation for the up stream cross section.**

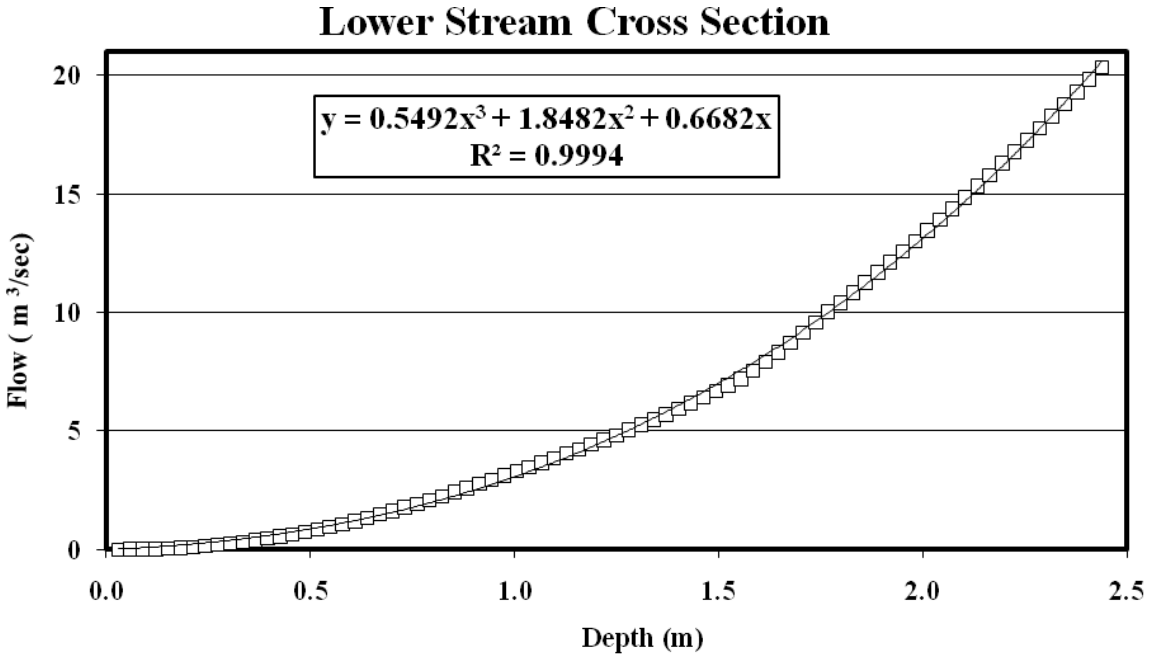


**Figure 3.5-21. Calculated flow rate and rating equation for the down stream cross section.**

With these flow depths, flow rates can be calculated and averaging these flow rates over an interval of time the flow volume can be calculated. For each sampler and runoff event a time and flow weighted sample was analyzed that represented the runoff event. Multiplying the flow volume by the contaminant concentration, the total load for the event can be calculated (Table 3.5-8).

**Table 3.5-8. Summary of Flow Volumes and Contaminant TSS, TN, and TP Concentrations and Loads for a Hardened Crossing at Fort Riley.**

| Year | Event | Sampler | Flow Volume (cu. m) | TSS Conc. (mg/l) | TN Conc. (mg/l) | TP Conc. (mg/L) | TSS Load (kg) | TN Load (kg) | TP Load (kg) |
|---|---|---|---|---|---|---|---|---|---|
| 2006 | 8/25-26/06 | Up Stream | 79027 | 211 | 0.85 | 0.15 | 1041 | 4 | 1 |
| | 8/25-26/06 | Down Stream | 94070 | 249 | 0.89 | 0.21 | 1462 | 5 | 1 |
| | | | | | | | | | |
| 2007 | 3/30-31/07 | Up Stream | 20242 | 89 | 0.28 | 0.06 | 1804 | 6 | 1 |
| | | Down Stream | 26470 | 94 | 0.32 | 0.08 | 2492 | 8 | 2 |
| | 4/11-14/07 | Up Stream | 56087 | 301 | 0.31 | 0.11 | 16907 | 17 | 6 |
| | | Down Stream | 67960 | 359 | 0.37 | 0.15 | 24434 | 25 | 10 |
| | 5/6-7/07 | Up Stream | 179885 | 742 | 0.89 | 0.19 | 133674 | 160 | 34 |
| | | Down Stream | 219644 | 911 | 1.26 | 0.34 | 200395 | 277 | 75 |
| | 5/23-26/07 | Up Stream | 179885 | 548 | 0.57 | 0.17 | 98724 | 103 | 31 |
| | | Down Stream | 211401 | 866 | 0.88 | 0.27 | 183347 | 186 | 57 |
| | 6/1/2007 | Up Stream | 17930 | 58 | 0.18 | 0.16 | 1041 | 3 | 3 |
| | | Down Stream | 21929 | 71 | 0.23 | 0.19 | 1559 | 5 | 4 |

**TSS = Total Suspended Sediment**
**TN = Total Nitrogen**
**TP = Total Phosphorus**

### 3.5.f. CONCLUSIONS

This study examined the impact of a hardened stream crossing on an upper sub-watershed of Three Mile Creek in training area 36 of Fort Riley Kansas. Figure 3.5-22 show the total differences between flow volume and the contaminant loading in this water. The downstream sampler showed an increase of 16.9% total flow volume, 38.2% increase in total suspended sediment loading, 39.1% increase in total nitrogen loading and 46.8% total phosphorus loading. The hardened crossings and the roads leading to them appear to be a conduit for increased contaminants to the stream water.

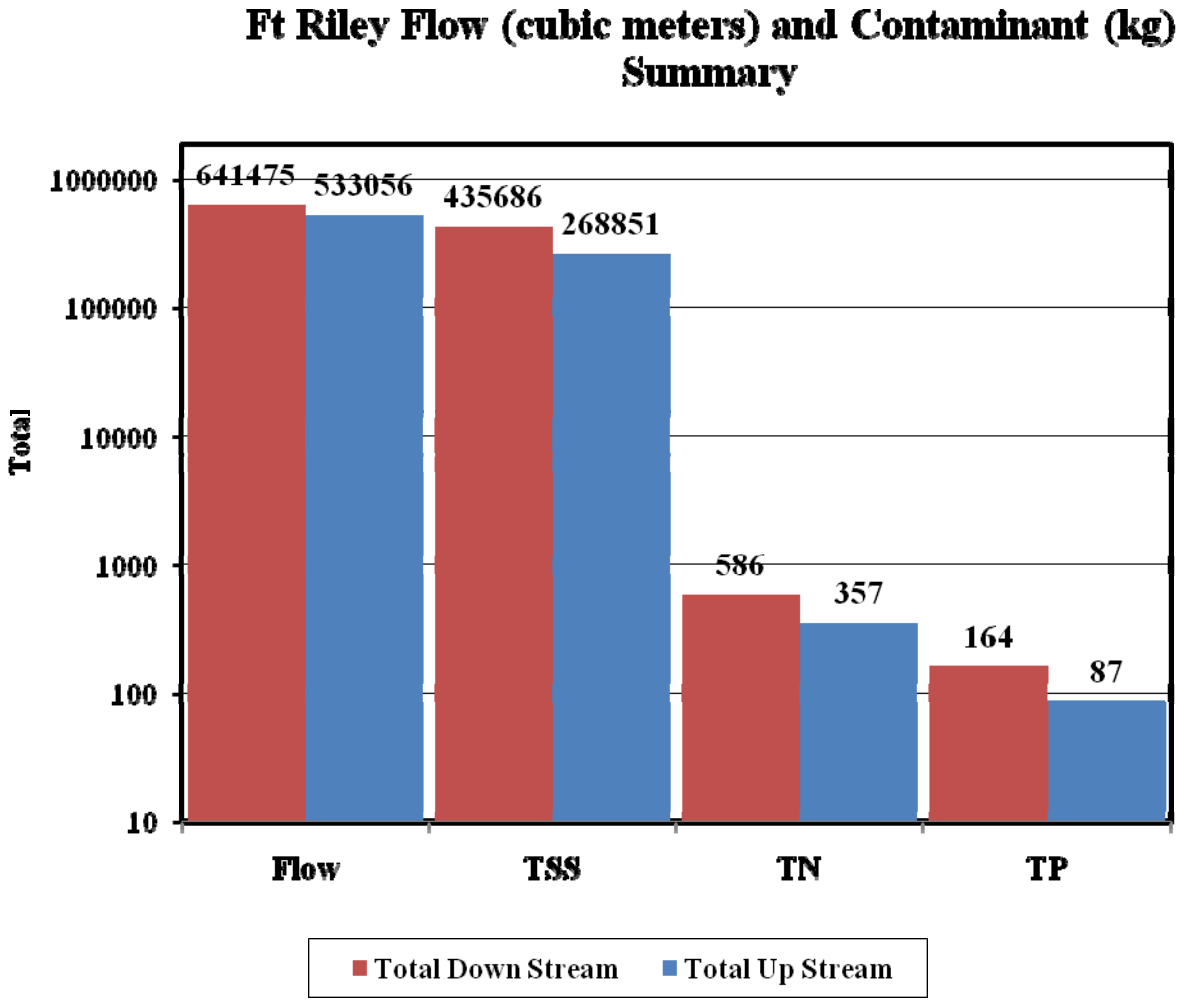


**Figure 3.5-22. Total flow volume and contaminant loading for the 2006-07 study period.**

## 3.6 TASK 6: SEDIMENT LOAD SENSOR

### 3.6.a. IDENTIFYING APPROPRIATE SENSING PRINCIPLE

Non-point source (NPS) pollution is a great concern in various agricultural lands, construction sites, and military training areas. Due to the large impact of military training maneuvers on land surfaces leading to NPS pollution, some military training areas have failed to meet water quality standards. Suspended sediment concentration (SSC) in water bodies, such as streams and lakes, is commonly considered one of the greatest contributors to NPS pollution and poor water quality. Increased turbidity also has negative effects on fish and other aquatic life (Newcombe and MacDonald, 1991).

The conventional method for determining SSC involves manual grab sampling. Water samples taken from a lake or stream are filtered, dried, and weighed in a laboratory to determine the sediment concentration. Although this manual approach remains the best method for accurate measurement of SSC, it is time-consuming, expensive, and labor intensive, especially when multiple samples at different times, depths and locations are required for accurate representation. In many situations, automatically collected real-time data is preferable to discrete samples (Davies-Colley and Smith, 2001).

Turbidity sensors indirectly estimate sediment concentrations by measuring optical properties of water. Thus, suspended or dissolved non-soil materials in water have an adverse effect on the measurement. However, since other fast, direct sediment measurement techniques are not available, the turbidity sensor remains the best tool for real-time estimation of sediment concentration. An improved optical sensor that is capable of removing the effects of non-soil materials on sediment measurement may find broad applications not only in military training areas, but also in areas where runoff from agricultural fields or construction sites is a concern.

Most commercially available turbidity sensors utilize a light source and light detector(s) to measure the amount of light transmitted or scattered within a water sample. For this type of sensor, multiple types of suspended or dissolved non-soil objects in water, including algae, organic matter, various microorganisms, colloidal material, or dissolved molecules, can affect the readings (Sadar, 2002).

The overall objective of this subtask is to develop a real-time sediment sensor to measure suspended soil sediment concentration in water. Specific objectives are 1) modifying the optical structure of conventional turbidity sensors based on spectral characteristics of sediments and non-soil materials in water and 2) developing regression models that are insensitive to water color and soil texture composition to accurately measure pure soil-sediment concentration.

#### Existing Technologies

There are two types of designs used among in-situ turbidity sensors. One design is a flow-through design. This refers to the fact that the sample to be measured flows between a light-emitting and a light-detecting element. This design is normally used in low turbidity

applications. The second type is a surface scatter design. This design is typically used for higher turbidity situations. The light source and light detector are placed next to each other along a single flat surface. Light is emitted into a water sample and the scattered and reflected light intensities are measured.

Many turbidity sensors use infrared light sources to make the sensors less responsive to color within the sample. An example is an optical backscatter (OBS) sensor. This sensor uses a pulsed infrared light, which is transmitted through an optical window and then scattered by particles present in the water in a 165-degree conical zone. Some of the dispersed and reflected light returns to the optical window where a receiver transforms the light into an electric signal. The output voltage is directly related to the suspended solids concentration in the column of water (Buchanan et al., 2001).

The use of both infrared and visible light sources may be helpful in sediment measurement. Infrared turbidity sensors are less susceptible to influences of organic particles, while turbidity sensors using visible light are more sensitive to scattering from finer particles (Gippel, 1989). Thus, a sensor that incorporates both methods may be desirable.

Due to the high cost and large size of many commercial turbidity sensors, much research has been conducted on creating inexpensive and compact sensors. One such sensor utilizes a fiber-optic link and a 670 nm laser-diode light source. Two photodiodes are placed at 180 and 90 degree angles from the incident light, respectively. Test results show low sensitivity to water color changes (Papadopoulou et al., 1998).

A standard procedure has been used for commercially available turbidity sensors to correlate the turbidity measurement with actual suspended-solids concentration. This procedure requires dilution of the sample while taking turbidity readings. At each dilution point, gravimetric solids content is determined. A correlation is then drawn between turbidity and SSC (Sadar and Engelhardt, 2003). This procedure can lead to a good estimation of SSC for stream samples, but the results are limited to the particular stream sampled. Therefore, the procedure would need to be repeated at different locations due to the variation in water properties.

Gippel (1995) stated that turbidity could be used as an adequate indicator of total suspended sediment in most cases. However, turbidity remains highly influenced by the presence of organic particles. Organic particles tend to cause more attenuation in turbidity readings than soil particles (Gippel, 1995).

Hayes, et al. (2001) conducted research on three soil types common to land resource areas in the southeastern United States and combinations of these soil types in an attempt to relate turbidity readings more closely to sediment concentration. Each soil type and soil combination was tested at different concentrations. Measurement of turbidity using a turbidity meter and known sediment concentration were compared. It was found that soils with the highest clay content had the highest turbidity reading at each concentration level. The relationship between turbidity (T) and SSC of each soil type can be expressed as

$$T = a * SS^b \quad \text{[Eq. 3.6-1]}$$

where a and b are constants.

Garg and Chaubey (2003) measured changes in spectral reflectance of suspended sediment as it settles in a container. The sample used was a silty loam soil. A spectro-radiometer measured the reflectance from 346 to 1000 nm. Test results indicated that the distribution of suspended sediment particles differed at various depths, while sediment volume remained unchanged. Larger variations in spectral reflectance were found near the following three wavelengths: 407, 576 and 807nm.

Spectral reflectance has been used in remote sensing to estimate both suspended sediment concentration and chlorophyll levels in surface water bodies. Han et al. (1994) found that red and near infrared (NIR) wavelengths could be used to determine algal chlorophyll levels at varying suspended sediment concentrations. Curran and Novo (1988) reviewed remote sensing of suspended sediment and concluded that the optimum wavelength for estimating suspended sediment concentration depends on the sediment concentration. Reflectance becomes saturated as suspended sediment concentration increases and the saturation point is dependent upon wavelength (Ritchie and Cooper, 2001). However, remote sensing using spectral reflectance does not accurately distinguish between suspended sediment and chlorophyll when suspended sediment concentration is high (Ritchie et al., 1994). Because remote sensing relies only on surface imagery, it is impossible to estimate concentrations at depths within a water body. Moreover, because optical properties of suspended particles vary notably within a stream or lake and among different water bodies (Davies-Colley and Smith, 2001), it is not feasible to measure sediment concentration in small streams using remote sensing. For these applications, in-situ sediment sensors may be more desirable.

"Optical Technology for Intelligent Monitoring Online" ("OPTIMO") technology has been used to assist in solving the issue of ambiguity in turbidity measurement. The technology employs multiple light sources with varying wavelengths and multiple detectors at various angles to help characterize particle size, shape and distribution (Gareth, et al., 2002). Early research on OPTIMO has indicated that small particles produce higher turbidity readings than larger particles among equal volumes. Large changes in color were observed when particle size changed, while no relationship was found between colour and concentration (OPTIMO, 2004). Using this advanced technology, more accurate sediment concentration measurement can be achieved within various water bodies (Gareth, et al., 2002).

Research concerning spectral reflectance has not completely addressed the effects of varying suspended sediment concentrations, particle size distributions, and non-soil particles on turbidity measurement. A review by Davies-Colley and Smith (2001) found that the relationship between turbidity and suspended sediment concentration is not well defined. More definitive research is needed to distinguish suspended sediment concentration from turbidity.

**Spectral Analysis of Water Samples**

Spectral properties of water samples were analyzed using an Oriel spectrometer (Oriel Instruments, Stratford, Connecticut, U.S.A.). The purpose of this study was to identify wavelengths that can be used to reduce the effects of dissolved particles in water on sediment measurement.

Light from the spectrometer light source passed through a fiber optic cable to a water sample (Figure 3.6-1(a)) where it was scattered and then detected at angles of 180, 90, and 45° from the incident light (Figure 3.6-1(b)). Data were taken and recorded using Oriels' Runes II software at wavelengths of 300-800nm in 2nm increments.

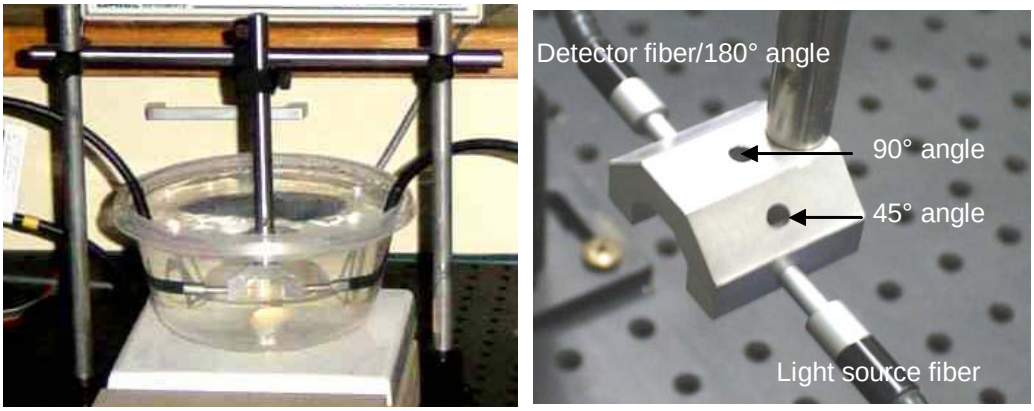


(a) (b)

**Figure 3.6-1. (a) Sensor in water sample, (b) Transmitted, scattered, and backscattered lights detected in 180$^o$, 90$^o$, and 45$^o$. for the spectrometer test.**

Two experiments were conducted.

**Water Test**

The objective of the water test is to select feature wavelengths that may help reduce the influence of water color on sediment measurement. Two types of water, distilled water and water from Tuttle Creek Lake north of Manhattan, KS, were tested. Each water sample was mixed with certain amounts of dried silty clay loam soil with an approximate texture of 16% sand, 46% silt and 38% clay. A stir plate and a stir bar were used to keep the soil particles suspended during the test. Samples were placed in a black cardboard enclosure to avoid the effect of external stray light on the measurement.

For each water sample, tests were run at eight sediment concentrations (50, 100, 150, 200, 400, 600, 800, and 1000 mg/l) and measurements were done from three different angles (45$^o$, 90$^o$, and 180$^o$). Three replications were conducted for each water type. A sample of the Tuttle Creek water sent to the Agronomy Soil and Water Analysis Laboratory at Kansas State University was found to have 44.2 mg/L of total suspended solids and 275.8 mg/L of dissolved solids. The initial SSC was used to determine how much dried soil to add in order to achieve the desired SSC.

The spectral data were preprocessed using a base-line removal method, which subtracts a "baseline" – the spectral data derived from testing of the clean water samples - from the spectral

data. The preprocessed data were then used for statistical analysis. A stepwise selection method (the "Stepwise" procedure in SAS) (SAS Institute, 2002) was used to select feature wavelengths that would help distinguish different water types.

**Soil Texture Test**

The objective of this test was to study the possibility of using specific wavelengths or data taken from different angles to reduce the influence of soil texture on concentration measurement. The test was run using the same spectrometer setup. This time, a single water type (distilled) was used in combination with three different soil textures. The sand-silt-clay contents for the three textures were 50%- 42%-8%, 40%-38%-22%, and 16%-46%-38%, respectively. The corresponding soil texture classifications were sandy loam, loam, and silty clay loam, respectively. Samples with four sediment concentrations – 400, 600, 800 and 1000 mg/L – were used in the test.

The GLM procedure in SAS (SAS Institute, 2002) was performed with multiple combinations of independent variables using data from the soil texture tests at the three wavelengths selected from the water test. For angle, SAS was run with and without texture information included in the model as an independent variable. For texture, SAS was run with and without the angle information included in the model as an independent variable.

In addition, measurements from different angles were combined to form "angle indexes". Equation 3.6-2 gives an example of the "angle index".

$$Index_{BG180\_90} = (BG_{180} - BG_{90})/(BG_{180} + BG_{90}) \qquad \text{[Eq. 3.6-2]}$$

where $BG_{180}$ is the signal detected by a phototransistor installed $180^o$ from a blue-green LED, and $BG_{90}$ is the signal detected by a phototransistor installed $90^o$ from the blue-green LED,

The GLM procedure in SAS was run with individual angle indices and with all three indices included in the models. For these runs, texture was not included in the models.

**3.6.b. RESULTS**

**Wavelength Selection**

Wavelengths were selected based on the results from the stepwise selection process in SAS. Wavelengths of 500, 760, and 620nm were selected at the first three steps, giving $R^2$ values of 0.91, 0.92, and 0.94, respectively, when every $10^{th}$ wavelength sampled was included in analysis. When all wavelengths sampled within a ±20nm range of these three wavelengths were included in another stepwise-selection analysis, wavelengths of 508, 768, 612, and 600nm were selected with $R^2$ values of 0.91, 0.92, 0.95 and 0.95, respectively. Only the first three wavelengths (508nm, 768nm and 612nm) were selected for the final sensor design because 600nm was the last variable entering the model and it had the least contribution to the model.

Three LED emitting lights at the three wavelengths and phototransistors responsive to a wide range of the light spectrum were used in the sensor design. LED with 505nm and 610nm peak emission ratings were found for two of the three, yet LED emitting light in the 700nm range were found to be very expensive and difficult to obtain. Therefore, an 880nm infrared LED, which was readily available, was used in the sensor design.

**Soil Texture Analysis**

When prediction models were established for individual soil types at single angles, lower $R^2$ values were observed for the sandy loam soil in comparison to the loam and silty clay loam soils across all angles of measurement. This indicated a greater variability in measurement for the sandy loam soil. This increased variability may be related to the higher concentration of larger sized particles. A single particle of larger size may block or scatter more light than a smaller particle; therefore, a sand particle passing the sensing area would cause a higher variation in readings compared to a clay particle.

When texture was included in the model as an independent variable, the prediction model established across all three soil texture types resulted in $R^2$ values of 0.91, 0.82 and 0.84 for the 180°, 90° and 45° angles, respectively. When texture was excluded from the model, the $R^2$ values decreased to 0.59, 0.50 and 0.39 for the 180°, 90° and 45° angles, respectively. This result clearly demonstrated that soil texture played an important role in prediction accuracy.

When angle was included in the model, the $R^2$ values were 0.61, 0.58 and 0.74 for the sandy loam, loam and silty clay loam soils, respectively. When angle was excluded from the model, the $R^2$ values reduced to 0.43, 0.39 and 0.67 for the three soils, respectively. This result indicated that measurements obtained at different angles might help reduce the effect of soil texture type on sediment measurement accuracy when soil type in the water is unknown.

This conclusion was validated by running models with normalized angle indices between $180^o$ and 45°, 180° and 90°, and 90° and 45° (Equation 2). These models achieved $R^2$ values of 0.84, 0.84 and 0.84, respectively. This gives a clear indication of the importance of measuring light intensities from different angles when sediment texture is unknown.

**3.6.c. DESIGNING AND TESTING THE SENSOR**

**Sediment Sensor Design and Testing**

A sediment sensor was designed with three LED emitting lights at 505, 880, and 610nm, corresponding to colors of blue-green, infrared and orange, respectively. These LED were selected based on the results from the spectral analysis. Nine phototransistors (PT) were placed at three angles of 180, 90 and 45° from the incident light for each of the three LED (Figure 3.6-2).

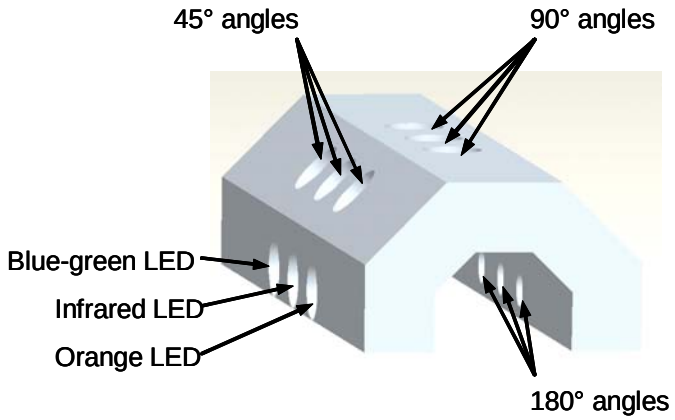


**Figure 3.6-2. Alignment of LED and Phototransistors.**

**Signal Conditioning and Processing**

Current signals from the phototransistors were converted to voltage signals using op-amp based, current-to-voltage converters. The voltage signals were sent to a Campbell Scientific CR5000 datalogger. The datalogger was also used to sequentially pulse the three LED, while reading the PT outputs during both the on and off phases of the LED. This light modulation scheme allowed the use of signal indexes to reduce the effect of ambient light on measurement. A timing diagram showing the LED pulsing sequence is displayed in Figure 3.6-3.

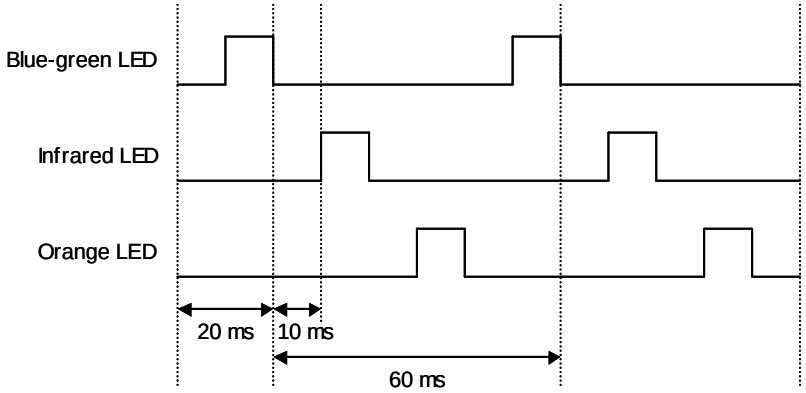


**Figure 3.6-3. Timing Diagram for LED Pulsing.**

**Sensor Test**

The sensor test was performed in a laboratory environment. A round plexi-glass container (26.8 cm inside diameter by 13.0 cm inside depth) was used for the water-soil mixture during testing. The inner walls of the container were painted using a flat black enamel to avoid reflection of light from the container and to minimize the entrance of stray light through the container walls. A variable speed, mechanical mixer (ARROW model 1750) was placed at the center of the container with the mixing blades set just above the bottom surface of the container. The blades and shaft of the mixer were painted using the same flat black enamel. The mixer was used to initially intersperse the soil and water in the container and to suspend the soil particles between each test.

The sensor was placed along one side of the container using a 1.28 cm spacer to keep the sensor from resting on the bottom surface of the container, allowing more space for a uniform mixture of soil particles and water to flow past the sensor elements.

The sensor was tested using three types of water and five types of soil to determine the sensor's ability to measure concentration of sediment with various texture compositions and within different types of water. Texture compositions of the five soil types are given in Table 3.6-1.

**Table 3.6-1. Texture Compositions for Five Soil Types.**

| Soil type | % Sand | % Silt | % Clay |
|---|---|---|---|
| Sandy loam$_1$ | 73 | 16 | 11 |
| Sandy loam$_2$ | 50 | 42 | 8 |
| Loam | 30 | 49 | 21 |
| Clay loam | 20 | 50 | 30 |
| Silty clay loam | 16 | 46 | 38 |

The three water sources were distilled water, Tuttle Creek Lake spillway (Manhattan, KS) and Three Mile Creek (Fort Riley Military Base, KS). Each soil type was tested in combination with each water type. For each soil-water combination, ten concentrations were tested. These concentrations were attained for each soil-water combination by adding soil to water in ascending order. At each concentration, three repeated tests (three "trials") were conducted. Prior to each repeated test, the soil-water solution was mixed to ensure uniform distribution. Readings were taken immediately after agitation ceased.

The SAS 9.0 software package was used for statistical analysis of the results. The stepwise selection method of the general linear regression procedure was used to create a model for predicting the sediment concentration. Model parameters included water type, soil texture, angle of measurement, and color of light source (LED).

Four main groups of analysis were performed on the data in an attempt to examine two assumptions. One assumption was that effect of water color on SSC measurement could be reduced using LEDs of different colors. The second assumption was that measurements obtained at different angles could be used to correct for measurement errors of SSC caused by changes in particle size and size distribution.

The first two groups of analysis were directly based on these assumptions. The first group of analysis was referred to as "color vs. water" analysis, where measurements obtained under multiple LEDs and normalized "color indexes" were the only independent variables in the regression models for predicting sediment concentration. An example of normalized color index is given in Equation 3.6-3.

$$Index_{BG\_IR} = (BG_{180} - IR_{180})/(BG_{180} + IR_{180}) \quad \text{(Eq. 3.6-3)}$$

where

$BG_{180}$ = Signal from the PT placed 180° from the blue-green LED, and
$IR_{180}$ = Signal from the PT placed 180° PT for the infrared LED.

The second group of analysis was referred to as "angle vs. texture" analysis, where measurements obtained from multiple angles and "angle indexes" (Equation 3.6-2) were the only independent variables in the regression models. For these analyses, SSC was the only dependent variable in the regression models.

**"Color vs. Water" Analysis**

For the "color vs. water" analysis, only the transmitted signals (signals of PT placed 180° from the LED) were used so that angle of measurement would not be introduced as a factor. The measurements entered the regression models in three different forms: "original readings", "calculated values" and "color indices". An "original reading" was simply the average value of 20 voltage readings recorded by the CR5000 datalogger during each measurement. A "calculated value" was calculated by subtracting from the "original reading" the average of three repeated measurements in original water sample, when no soil was added. Equation 3.6-4 gives an example of the "calculated value" for signals measured by a PT placed 180° for the blue-green LED. The "calculated values" were introduced to reduce the effect of suspended and dissolved materials in the original water sample on sediment measurement.

$$BG_{180calc} = BG_{180} - BG_{180\_0} \qquad \text{[Eq. 3.6-4]}$$

where

$BG_{180}$ = Signal from PT placed 180° from the blue-green LED, and
$BG_{180\_0}$ = Signal from PT placed 180° from the blue-green LED, when sensor in the original water sample (without added soil)

For the "color vs. water" analysis, three (3) types of regression models were tested. The first type used the original readings as the independent variables. The second type replaced the original readings with calculated values. The third type had both calculated values and color indices in the independent variable list. For each model type, six (6) models were tested. Five of the six models used data from only one soil texture type so that soil texture could be excluded as a factor and the relationship between water color and color LED readings could be more explicitly demonstrated. For the sixth model, data from five individual texture types were combined. Thus, the total number of regression models tested was 18 (3x6). In all these models, data from all water types were included and SSC was used as the only dependent variable.

**"Angle vs. Texture" Analysis**

The second main group of analysis - "angle vs. texture" - was performed in a similar fashion with three (3) types of regression models using "original readings", "calculated values", and "calculated values" plus "angle indices" as independent variables, respectively. Four (4) models were tested for each model type. This included three models for three individual water types, respectively, and one model for combined water types. Thus, the total number of models was 12

(3x4). Data for different texture types were not separated so that texture was not involved as a factor. Data used for each group of analysis were signals from each individual LED measured at the 180°, 90° and 45° angles.

**"Color vs. Texture" Analysis and "Angle vs. Color" Analysis**

The objective of "color vs. texture" analysis was to determine if LEDs of multiple colors would help reduce the effect of particle size or size distribution on SSC measurement. Similarly, the "angle vs. water" analysis was conducted to determine if signals measured at different angles would help reduce the effect of water color on SSC measurement.

These two groups of analyses were performed in the same general fashion as the first two groups except that the independent variables in the regression models switched. For these two groups of analyses, only two types of models were tested. The first type used "calculated values" and the second used "calculated values" together with indices (color indices or angle indices). Therefore, the numbers of models run for the "color vs. texture" and "angle vs. water" analyses were 8 (2x4) and 12 (2x6), respectively.

During the test, it was observed that the range of the voltage readings within the 1.2 sec sampling period was consistently lower for the soils with a higher sand content than soils with lower sand content and higher clay content. This led to an assumption that sand particles settled in the water sample after the mixer was turned off and before the measurement was completed. This may have affected the measurement results. It was also possible that the mixer never suspended many of these heavier sand particles. As a result, sediment concentration in the mixture was not uniform when high sand content was present, and the actual sediment concentration at the location of the sensor may have been different from the "nominal" concentration values, which were calculated from the weight of added soil.

To verify these observations, standard deviation (s.d.) and coefficient of variation (c.v.) for 20 readings recorded for each PT at each concentration value during the 1.2 second test period were calculated. A linear regression analysis was then run with c.v. for the blue-green and orange LED measured at 180° and 45° angles added to the model as independent variables.

For the next regression analysis, c.v. values were replaced with the differences between the last and first data points in each of the 20 original readings. The goal of this analysis was to study the possibility of using soil particle settling time in water to correct for the measurement error caused by particle size distribution.

For the final prediction models, it was desired to maximize the $R^2$ value for the prediction models, while simplifying the sensor design and the prediction model. For this purpose, analysis was performed using only the blue-green and orange LED and the 180° and 45° angles. The GLM procedure in SAS was used to develop a linear model for each set of soil texture data. Data from trial 1 were used for modeling whereas data from trials 2 and 3 were used to validate the models. .

### 3.6.d. RESULTS

**Sediment Sensor Test Results**
**"Color vs. Water" Analysis**

For "color vs. water" analyses, Signals from PTs measured from LEDs of different colors and color indices were the only independent variables in the prediction models. Measurements obtained for all three water types were used in the training data set. An overall improvement can be observed when "calculated values" were used to replace the "original readings" ($R^2$ increased from 0.82 to 0.85). This result suggested the necessity of initial calibration when the sensor is used in an unknown water type. This calibration can be accomplished simply by obtaining a set of measurements from each PT before the water is disturbed by runoff or other events. Values of these measurements can then be subtracted from subsequent measurements to derive the "calculated values".

When color indices were added to the independent variable list, the $R^2$ value was further improved from 0.85 to 0.87. This result clearly demonstrated the effectiveness of the color indices.

When analyses were run on individual soil types, $R^2$ values of 0.99, 0.97, 1.00, 1.00, and 0.99 were achieved for sandy $loam_1$, sandy $loam_2$, loam, clay loam and silty clay loam, respectively. However, when data from all textures were combined, the $R^2$ value reduced to 0.87. This is an indication that the color indices were incapable of addressing the difficulty in sediment measurement caused by differences in soil texture.

During the stepwise selection procedure for models that included both the "calculated values" and color indices as independent variables, it was noticed that the "calculated value" for the infrared LED and color indexes involving infrared were selected the fewest number of times. This gives an indication that the infrared LED does not play as important role as blue-green and orange LED in correcting for various dissolved particles and microorganisms present in the water. This could, however, be due to the use of an 880nm infrared LED instead of 768nm that was chosen from the spectrometer tests. Better results may have been achieved if the chosen wavelength was used.

**"Angle vs. Texture" Analysis**

When angle of measurement and angle indices involving only the blue-green LED were used as independent variables in the models and data across all texture types were used in the training data set, final $R^2$ values of 0.87, 0.90 and 0.92 were achieved for distilled, Three Mile Creek and Tuttle Creek water, respectively. When all water types were combined, the $R^2$ value was 0.87.

Similar results were obtained from the same analysis for the orange and infrared LED, respectively. The results all indicate that angles of measurement were not very effective in reducing the effect of soil texture difference (particle size or size distribution) on sediment measurement, as opposed to our assumption. Another observation was that the 180° vs. 45° angle index was chosen more often than either of the indexes involving the 90° readings through the

stepwise selection procedure, indicating that the 90° angle of measurement does not play as important of a role in determining differences among texture as the 180° and 45° measurement angles do.

Plots of voltage readings vs. concentration for each test were then examined. These plots indicate a large variation in readings for the 90° angle measurement for each color LED. One possible cause for this large fluctuation is the larger amplification gains required for the 90° signals due to smaller signal amplitudes, which resulted in a lower signal-to-noise ratio. From these figures it can also be seen that the fluctuation occurs more often at higher concentrations (above 1000 mg/l), indicating that, for lower concentrations, the 90° angle of measurement may still be useful.

The infrared LED data gave the highest overall $R^2$ value for distilled water, while the blue-green LED data gave the highest overall $R^2$ value for the Three Mile Creek and Tuttle Creek water. This result may be related to the green color of the water, probably due to algae, which was not present in the distilled water.

**"Color vs. Texture" Analysis**

When "color vs. texture" analyses were run, the results were surprisingly better than that of the "angle vs. texture" analyses. The $R^2$ values achieved across five soil texture types were 0.93, 0.90, and 0.91 for distilled, Three Mile Creek and Tuttle Creek water, respectively, and 0.87 for all water combined. This indicates that color may actually be more helpful than measurement angle in determining differences in texture. More research is needed to search for wavelengths that can help reduce the effect of sediment texture on SSC measurement.

**"Angle vs. Water" Analysis**

The $R^2$ values obtained from "angle vs. water" analyses were slightly lower overall than those from "color vs. water" analyses. Values of 0.87, 1.00, 0.98, 0.99, 0.99 and 0.99 for all textures combined, sandy $loam_1$, sandy $loam_2$, loam, clay loam and silty clay loam, respectively, were compared to values of 0.87, 0.99, 0.97, 1.00, 1.00 and 0.99 for the same respective soil textures.

**Models Including Color and Angle Indices**

Statistical analysis was performed on models including all color indices and angle indices that do not involve the infrared LED and the 90° measurements. The rationales for removing the infrared LED and 90° measurements were (1) Previous statistical analyses have indicated that the infrared LED and 90° measurements have not played important roles in the models and (2) Deleting infrared LED and 90° measurements would reduce the number of LEDs from three to two and reduce the number of PT from nine to four. This would result in a simpler and more feasible

Using these models, final $R^2$ values of 0.99, 0.99, 1.00, 1.00 and 0.99 for sandy $loam_1$, sandy $loam_2$, loam, clay loam and silty clay loam, respectively were achieved. When all texture types were combined, the $R^2$ value was 0.88. This indicates that neither color indices, nor angle

indices were capable of completely removing the effects of particle size or size distribution on SSC measurement.

**Effect of Soil Texture on Sediment Measurement**

In order to understand the incapability of the color and angle indices in reducing the measurement errors caused by texture differences, predicted soil concentrations were plotted against actual concentrations using prediction models that included the blue-green vs. orange color index and the 180° vs. 45° angle index as independent variables (Figures 3.6-4 and 3.6-5).

Figure 3.6-4 uses five separate prediction models developed for five individual soil texture types, whereas Figure 3.6-5 uses the model developed across five soil texture types for trial 1. When soil texture types were not mixed, the prediction models developed using proper color and angle indices were capable of predicting the concentration with a high accuracy. However, when soil texture types were mixed, the prediction accuracy was greatly reduced (Figure 3.6-5).

Figure 3.6-5 also indicates the impact of sand content on the predicted concentration. The actual concentration seen by the sensor was in general lower for soils with a higher sand content, indicating that the increase in sand within the soil/water mixture either made it more difficult for the particles to be suspended by the mixer or made the mixture less uniform and, thus, giving different readings at different locations within the mixture.

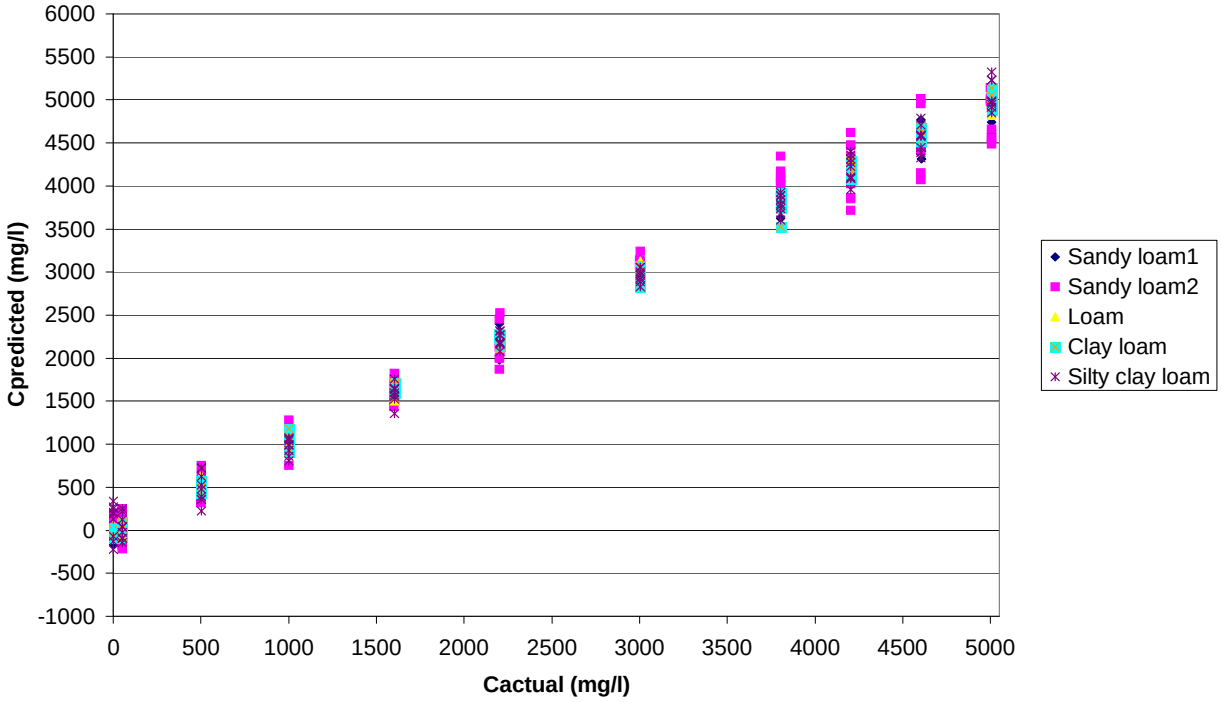


**Figure 3.6-4. Actual vs. predicted concentration for trial 1 using five separate prediction models, each developed for an individual soil texture.**

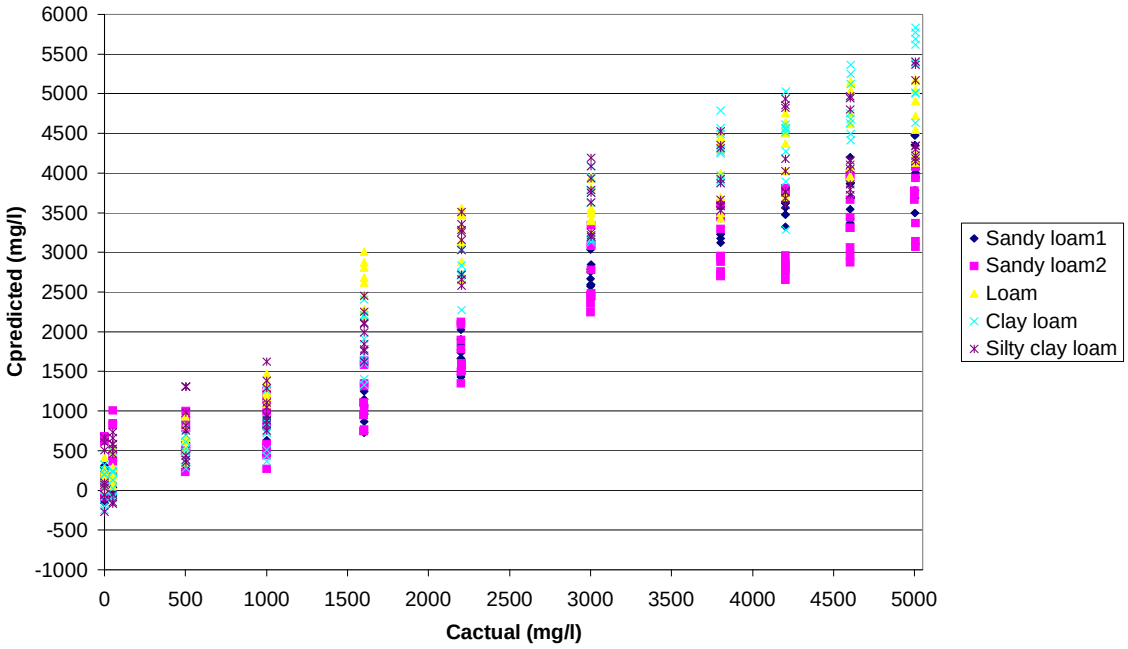


**Figure 3.6-5. Actual vs. predicted concentration for trial 1 using prediction model developed across all five soil types.**

## Final Models

The final models used for validation selected only three variables – the calculated values for $BG_{180}$, the color index $Index_{BG\_OR}$, and the angle index $Index_{BG180\_45}$. These simplified models were selected to minimize the complexity of the model and to avoid model overfitting. This also allows for much simpler sensor design, which only requires the use of two LEDs and three PTs. Model overfitting can occur when too many variables are used. An overfitted model can have a very good fit to the training data; however, when it is applied to different data sets, large errors may occur.

The final models included a model developed across all texture types and five individual models, each developed for a specific soil texture type. Figure 3.6-6 displays the predicted concentration against actual concentration using the all-texture model for trial 1. The $R^2$ value and RMSE are 0.85 and 699 mg/L, respectively. When this model was validated using data from trials 2 and 3, the $R^2$ values were reduced to 0.83 and 0.83, and the RMSE increased to 742 and 725 mg/L, respectively.

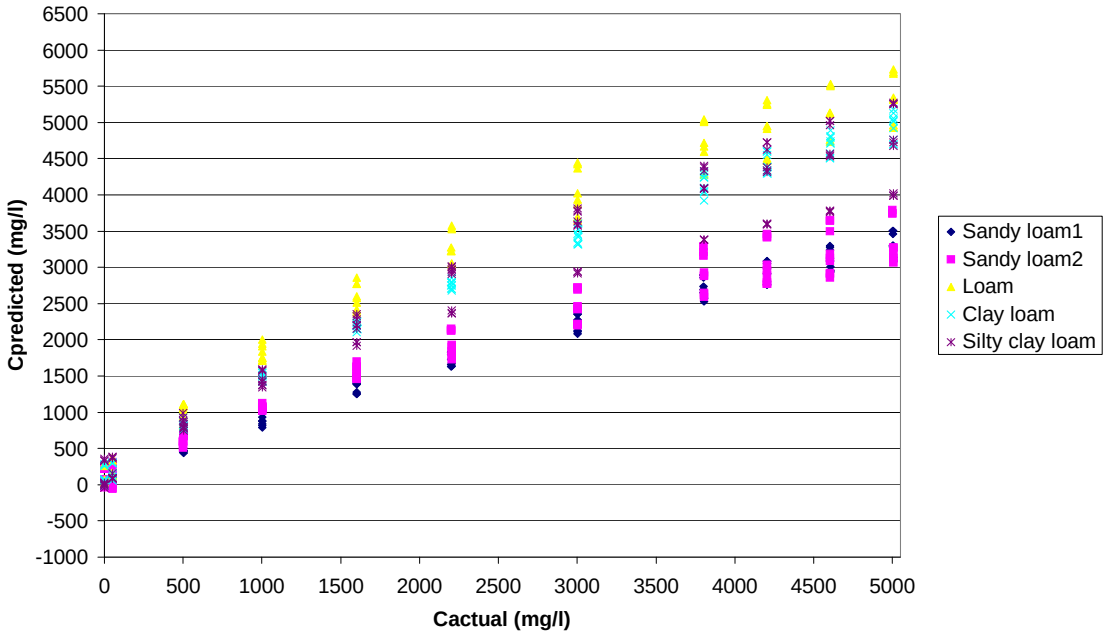


**Figure 3.6-6. Actual vs. predicted concentration for trial 1 (calibration), all soil textures, using the simplified model.**

Single-texture models were also evaluated. $R^2$ values for trial 2 validation data of 0.97, 0.96, 0.92, 0.97 and 0.90 were achieved for sandy $loam_1$, sandy $loam_2$, loam, clay loam and silty clay loam soils, respectively. These values for trial 3 validation data were 0.97, 0.98, 0.97, 0.95 and 0.90, respectively. Larger predicted errors for trials 2 and 3 were seen for soils with lowest sand content such as loam, clay loam and silty clay loam soils. The reasons for these results are still unknown.

Although many precautions were taken to minimize the error during the experiment, multiple factors can be identified as possible sources of error in the results due to the nature of the study. Errors caused by the mixing apparatus or settling of larger particles may have resulted in non-uniform solutions. Errors caused by noise from external light and electrical sources also may have affected the readings. Furthermore, inconsistency in measurement timing among tests may have caused variations in soil particle settling time before measurement, resulting in errors.

### 3.6.e. CONCLUSIONS

Through this research discoveries were made in the impact of soil texture on the accuracy of optical sediment sensors. Both angle of measurement and wavelengths of light sources were critical in negating the effects of water type on measurement accuracy. More accurate sediment concentration measurement can be obtained through the use of multiple wavelengths and multiple angles of measurement.

Signals obtained at the $90^o$ measurement angle were generally weak and noisy. This was especially true when higher sediment concentrations were present. However, at lower concentrations, measurement obtained at the 90° angle may still be useful. In general, use of

multiple measurement angles can help achieve more accurate measurement of suspended sediment concentration.

The sensor has been proven accurate when measuring sediment concentration in various types of water. However, conclusions cannot be made concerning the accuracy of this sensor in determining concentration among various soil textures. $R^2$ values ranging from 0.90 to 0.97 were achieved for two independent validation data sets across all water types when separate models were developed for individual soil texture types. When soil types were combined, the $R^2$ values were reduced to 0.85 and 0.83 for the training and validation data sets, respectively.

### 3.6.f. MODIFYING SENSOR DESIGN BASED ON FIELD CONDITIONS

#### Sensor Design Simplification

Statistical study of the of the laboratory test data have indicated (1) The infrared LED and 90° measurements did not play an important role in the prediction models and (2) Deleting infrared LED and 90° measurements would reduce the number of LEDs from three to two and reduce the number of PT from nine to four. This would result in a simpler and more feasible design for the sensor. Based on these results, the "three-ring" design of the sensor (Figure 3.6-7) was simplified to a "two-ring" design (Figure 3.6-8).

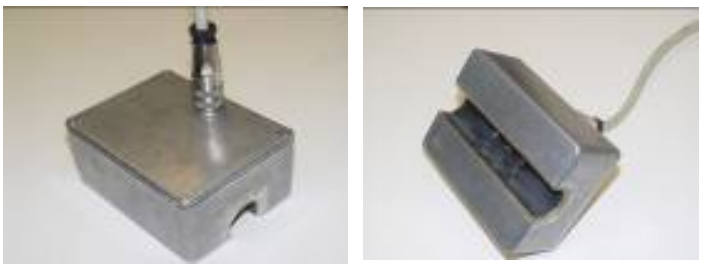

**Figure 3.6-7. A three-ring, waterproof sensor prototype**

**Figure 3.6-8. A simplified two-ring sensor prototype**

#### Laboratory Tests

Figure 3.6-9 displays the laboratory test setup for the prototype sensor. It consists of the sensor, a Campbell Scientific CR5000 datalogger, a signal conditioning and processing board, a power supply, and a personal computer.

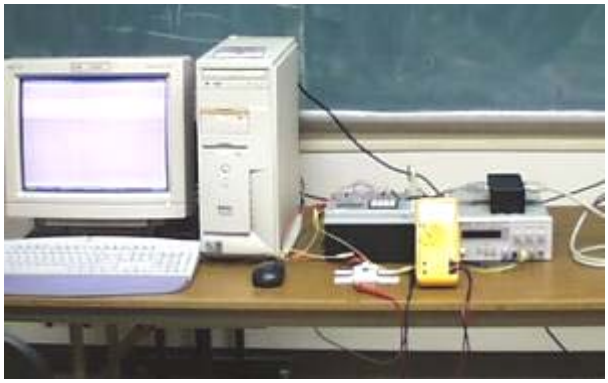

**Figure 3.6-9. Laboratory Setup for the Prototype Sensor.**

The datalogger was programmed to turn on and off each LED in a predefined sequence, while reading and processing the signals from the phototransistors associated with the LED being pulsed. The prototype sensor was tested at combinations of four water types (Three Mile Creek at Fort Riley, Wildcat Creek in Manhattan, KS, Tuttle Creek Reservoir in Pottawatomie County, KS, and distilled water) and five soil types (sandy loam1, sandy loam2, clay, clay loam and silty clay loam). The experiment was carefully designed to produce three statistically independent data sets, one of which was used to train statistical and neural-network models for predicting soil sediment concentration, whereas the remaining two sets were used to validate the models.

Eleven soil concentrations were tested at each soil-water combination. At each soil concentration, three repeated measures were taken. Figure 3.6-10 shows a pump-driven circulation system designed for maintaining uniform concentrations in the laboratory test.

**Figure 3.6-10. A circulation system providing uniform sediment concentrations.**

**Removal of Ambient Light Effect**

In order to reduce the influence of ambient light on the measurement, a relative index of "LED-on minus LED-off" was used in the prediction models. In addition, an outdoor experiment was conducted to test the sensor under different ambient light conditions, from noon to dusk to night, using another pump-driven circulation system (Figure 3.6-11). Gains of the signal conditioning circuits for each sensor were adjusted to cover a wide range of ambient light intensity. Calibration models were once again established using the outdoor test data. To ensure the statistical correctness, the test data were divided into three statistically independent data sets for calibration, validation and test purpose, respectively. Twelve concentrations were used in the experiment.

**Figure 3.6-11. Circulation system used in outdoors experiment.**

**Long-Term Monitoring in Stream**

Three prototype sensors in water-proof packages were fabricated and were placed in the downstream location of a low-water stream crossing at Fort Riley on August 16, 2005. The sensors were placed at three depths to provide the vertical profile of sediment concentrations during and after storm events with and without vehicle crossing. A solar panel is used to power the sensors, the signal conditioning unit, and the data-acquisition/storage equipment so that long-term monitoring becomes possible. Figure 3.6-12 showed the sensors placed in the stream bed.

**Figure 3.6-12. Installation of sensors, solar panel, and control circuitry. The photos were taken during the dry season.**

### 3.6.g. RESULTS

#### Laboratory Tests

Both statistical and neural-network models were developed based on test data obtained at combinations of four water types and five soil types. Models for individual soil types in all waters provided very accurate sediment concentration measurements with $R^2$ values of higher than 0.99, indicating almost complete elimination of the influence of water color on measurement accuracy (Table 3.6-2). When all soil types were combined, the $R^2$ values derived for the training and the two validation data sets were 0.974, 0.951, and 0.958, respectively, indicating partial removal of the influence of soil type on sediment concentration measurement.

**Table 3.6-2. $R^2$ Values Achieved Across Four Water Types.**

| Soil type | Sandy loam 1 | Sandy loam 2 | Loam | Clay loam | Silty clay loam |
|---|---|---|---|---|---|
| $R^2$ value | 0.9968 | 0.9894 | 0.9992 | 0.9985 | 0.9983 |

#### Outdoor Tests

An outdoor experiment was conducted to verify the effectiveness of light modulation in reducing the influence of ambient light variation on measurement. In Figure 3.6-13, signals acquired with "LED on" were strongly affected by the ambient light; whereas the relative signals ("LED-on minus LED-off") were rather stable within a wide range of ambient light intensity.

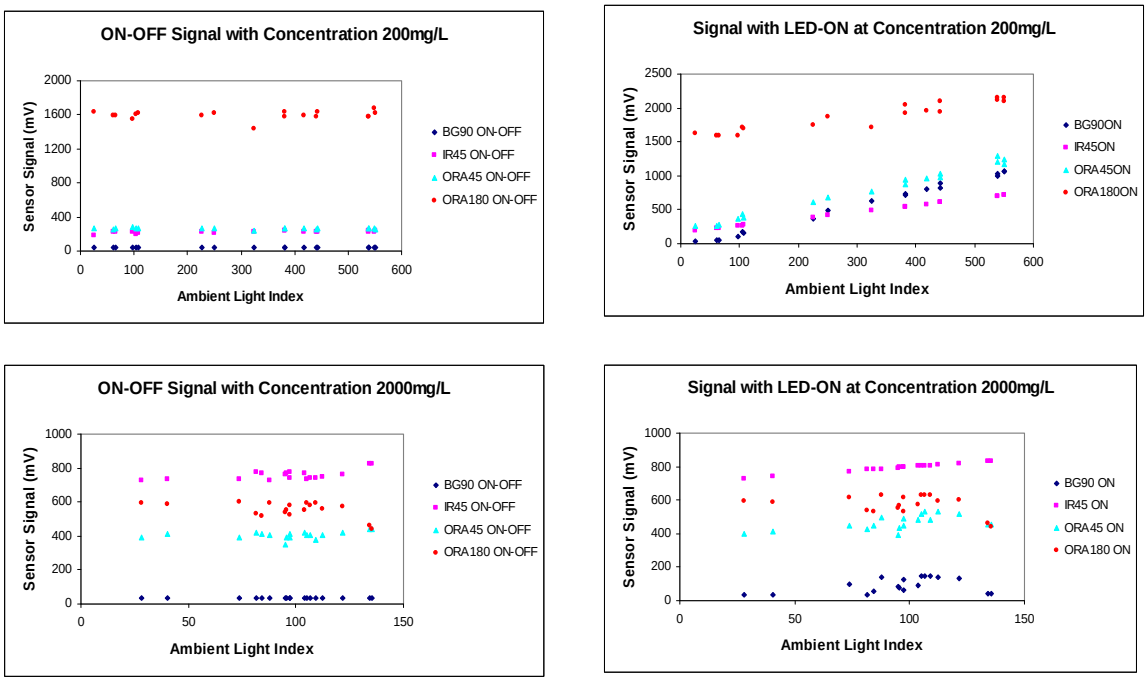


**Figure 3.6-13. Effect of light modulation in reducing the influence of ambient-light variation on measurement.**

The light modulation algorithm resulted in accurate concentration measurement under variable, outdoor light conditions. Table 3.6-3 shows that the calibration and validation data sets, which were randomly selected from 18 tests conducted at different times in the day over a two-week periods, all achieved $R^2$ values of 0.99. Predicted model was developed based on the calibration dataset and then it was applied to two validation datasets. Figure 3.6-14 gives "predicted vs. actual" concentrations curves for calibration and validation datasets.

**Table 3.6-3. Results of Outdoor Test Using Light Modulation.**

| Dataset | Calibration | Validation 1 | Validation 2 |
|---|---|---|---|
| R Square Value | 0.995 | 0.999 | 0.992 |
| RMS Error (mg/L) | 181.1 | 220.4 | 249.9 |

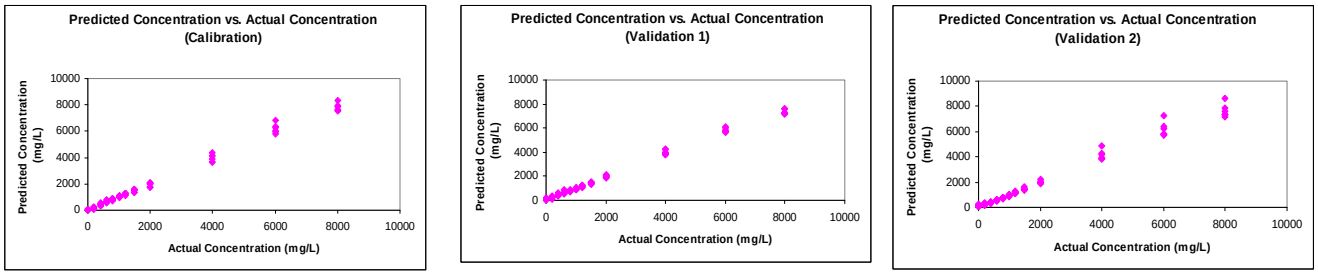


**Figure 3.6-14. Predicted vs. actual sediment concentration for outdoor test.**

**Field Tests**

After the three sensors were installed in the stream on August 16, 2005, there have been two rainstorm events that led water into the stream. However, during both events, water in the stream only covered the sensor at the lowest position. 3.6-15 gives signals recorded over a 50-minute period on August 25th, including signals from the four phototransistors and the sediment concentration calculated based on these signals.

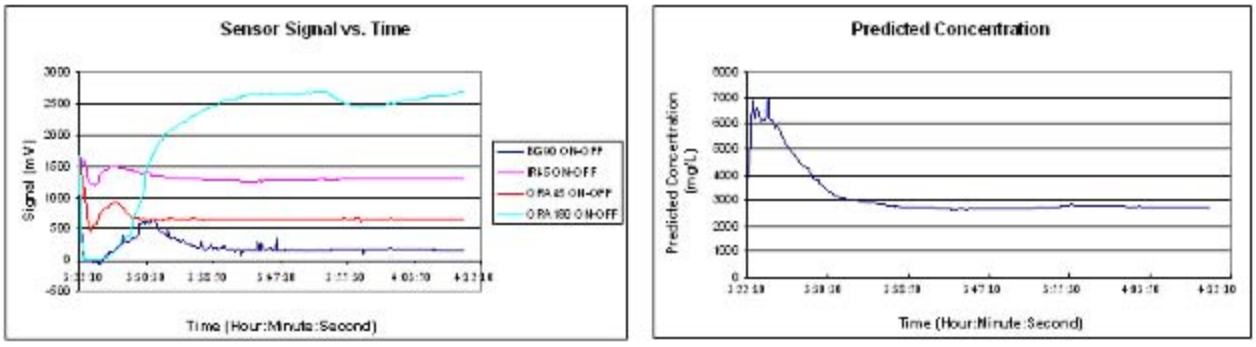


**(a)** **(b)**

**Figure 3.6-15. Recorded sediment concentration during a rainstorm event on August 25, 2005: (a) Signals measured by four phototransistors, (b) Calculated sediment concentration.**

### 3.6.h. CONCLUSIONS

- The sediment concentration sensor developed in this study measures pure soil sediment concentrations in water. It differs from traditional turbidity sensors in:
    - The optical filters selected based on a spectral analysis of different water types helped remove the effect of water color on sediment concentration measurement.
    - The geometric design of the optical components helped reduce the effect of soil texture on sediment concentration measurement.
    - Light modulation helped remove the effect of ambient light variation on measurement.
- Statistical and neural-network prediction models successfully predicted sediment concentrations of various types of soils in various types of waters under variable ambient light conditions with $R^2$ values of no lower than 0.95.
- The sensor has been installed at a low-water stream crossing and has started to monitor actual sediment concentrations after rainstorm events.

### 3.6.i. Field Test of Multiple Sensors

*Multiple SSC sensors have been tested at several experimental sites since 2006. The experiments at Little Kitten Creek, Manhattan, Kansas, and Fort Benning, Georgia, lasted for the longest time.*

**Little Kitten Creek, Manhattan, Kansas**
One prototype sensor has been installed at Little Kitten Creek in Manhattan, Kansas, since August, 2006. The SSC measurement system comprises an optical sediment sensor, a signal conditioning circuit box, a CR10X datalogger manufactured by Campbell Scientific, Inc., a 15 W solar panel, and a 12 V deep cycle battery. A datalogger program developed using PC208W software (PC208W, 2000) controls and takes measurement every 10 seconds.

The sensor was installed in the middle of the creek about 0.2 m (8 inches) above the creek bed to make sure it was submerged under water all the times (Figure 3.6-16). It was mounted by U-clamps and bolts on a galvanized steel pipe. A 12 meter-long cable that transmitted electrical current signals was enclosed in PVC pipes for protection. The PVC pipes were secured by reinforcing steel bars along the creek bed and bank. A protection fence was built at the upstream side using metal stakes to protect the sensor from floating logs or other flotsam. The datalogger, the battery, and the signal conditioning box were placed in a waterproof plastic enclosure.


**Figure 3.6-16. Sensor installation in Little Kitten Creek, Manhattan, KS.**

**Upatoi Creek, Fort Benning, Georgia[1] Sensor Deployment**

Studies have indicated that military training activities on ranges are adversely impacting the environment. For example, installations have many miles of unimproved roads and tank trails. Vehicle traffic on these roads and trails typically causes extensive erosion that results in reduced water quality because of increased sediment loads. This is especially true at locations where an unimproved road or trail must traverse a stream or creek. Continued erosion can make trails impassable at crossing sites, and also result in environmental penalties for the installations.

In order to test the ability of an articulated roadbed system (cable concrete) in reducing soil erosion caused by military training, such a structure was built at a LWSC of the Upatoi Creek at Fort Benning, Georgia. The construction started on August 22, 2006 and was completed on October 22, 2006. To monitor changes in SSC before, during, and after the construction, four optical sediment sensors, which were developed and fabricated at Kansas State University, were installed in June 2006 at the downstream side of the LWSC on both sides of the creek, about 30 m from the crossing site. The sensors were modified several times based on clogging and fouling problems observed during the test. Real-time monitoring continued for eight months, from June 2006 to February 2007.

The following four prototype sensor design variations were tested during the monitoring period:

- June 2 - June 30, 2006: closed-bottom sensors without filter screens
- June 30 - July 26, 2006: closed-bottom sensors with filter screens installed at both ends of the sensors.
- July 28 - September 7: closed-bottom sensors with filter screens installed only at the front ends.
- September 7, 2006 – February 7, 2007: open-bottom sensors

A datalogger was programmed to turn each LED on and off in a predefined sequence while reading and processing the signals from the PT associated with the LED. SSC values were then calculated from the signals using pre-trained calibration models. The SSC measurements were taken every minute. Data from the datalogger was downloaded approximately every 30 days by field personnel.

Four prototype sensors were installed about 30 meters downstream from the crossing. Two sensors were installed on each side of the creek (the “North” side and the “South side”) (Figure

[1] This is a collaborative project with the U.S. Army Aberdeen Test Center, Aberdeen Proving Ground, MD.

3.6-17), about 15 m from the creek center, with the “bottom” sensor mounted about 4 inches above the creek bed, and the top sensor about 10 inches above the bottom sensor. The overall water depth and creek flow rate varied from day to day depending on storm events in the creek watershed. The optical sensors were securely mounted with U-clamps and bolts on 8-foot long metal stakes that had been driven several feet into the creek bed. A datalogger (Campbell Scientific Inc., model CR 10) was mounted on each bank to collect data from two sensors. The dataloggers were mounted in weatherproof enclosures purchased from the same manufacturer. The enclosures were mounted on 10 foot long, pressure treated lumber posts that had been buried several feet deep into the banks. A 12 V (35 ah CA) deep cycle battery to power each datalogger was mounted on a wooden platform next to the datalogger enclosure. Deep cycle batteries were used instead of starter batteries since they have greater “depth of discharge” capability then either starter batteries or hybrid batteries. A large depth of discharge capability was necessary to ensure a reliable power supply to the dataloggers, since the batteries were being charged by solar panels. A 100W solar panel to charge the batteries was mounted above each datalogger enclosure at a 45 degree angle to capture sunlight. Tree branches and foliage were cut away from around the solar panels to ensure sufficient exposure to sunlight. All components were mounted sufficiently high on the posts to prevent water from reaching the dataloggers, batteries, and solar panels in the event creek levels rose during storm events. Wiring from the sensors to the dataloggers was contained in 1-1/2 inch schedule 40 PVC pipe runs along the creek bottom. The PVC pipe runs were anchored to metal stakes driven securely into the creek bed with plastic wire ties. The purpose of the PVC pipe was to protect wiring from flotsam in the creek and from the current. The installation is shown in Figure 3.6-18.

**a)** **b)**

**Figure 3.6-17. Sensor installation showing enclosures containing the dataloggers and the solar panels at the crossing site: a) North side; b) South side.**


**Figure 3.6-18. Sensor mounting method.**

The first trip to the site was made on May 3, 2006. During the installation, it was found that some of the sensor signals exceeded the laboratory calibration ranges. Loose connections in the signal-conditioning circuits were also detected. In order to solve these problems, it was decided to take all sensors back to the laboratory at Kansas State University, and recalibrate them using water and soil samples taken from the site. The open-bottom design was also replaced with a closed-bottom design to avoid the impact of reflected or refracted light from the river bed on the signals. After it was determined later that the closed-bottom design caused clogging problems, the open-bottom design was again installed at the site in September 2006. There was also a problem with biofouling of the LED and PT lenses. Although the clogging problem improved significantly with the open-bottom design, the biofouling problem for optical lenses persisted.

The dataloggers were set to execute the data collection program every minute. Because it took the datalogger only 11.3ms to turn the LED on or off, and 4.4ms to take one measurement, the datalogger spent most of the time in the idle state, waiting for the next execution. Within a 4.4 ms program execution time, changes in TSS due to water flow can be ignored. The datalogger used at Fort Benning had a 2 megabyte flash memory. With a 1-minute execution interval, it could hold at least one month of TSS data collected at 1 minute intervals without losing data due to overwriting.

**Data Correction for Clogging and Fouling**

A MATLAB program was developed to correct the clogging and fouling effects on the signals. The basic assumption for the clogging correction was that there should not be a sudden rise in the light signal unless materials covering the lenses are washed away within a short period of time. Based on this assumption, the clogging correction was done by removing sustained steep rises in the signals using a set of carefully selected thresholds, including 1) a threshold for the width of a moving-average window that smoothed the raw signals, 2) a signal rise/fall contrast threshold that detects the occurrence of sudden signal rises, and 3) a threshold for the width of a moving-average window that smoothed the clogging-corrected signals as a preparation for a regression analysis that determines the fouling trends. The signal rise/fall contrast was defined as the signal up-slope/down-slope ratio. Lower threshold values were used for the closed-bottom design because clogging occurred more frequently on the closed-bottom sensors.

The biofouling effect was corrected by removing the fouling trend found through a regression analysis on peak signal values measured during no-rain periods. Although no significant difference in biofouling was found between the closed-bottom and open-bottom designs, biofouling trends for individual sensors differed greatly. Thus, correction of biofouling was done on individual sensors. It should be noted that signal smoothing through moving-average filters is only used to determine the thresholds and fouling trends. Actual clogging and biofouling corrections were still done on original signals so that details of the signals were not lost. Using the orange signal measured at an 180°angle as an example, Figure 3.6-19 compares the signals before and after clogging and fouling corrections.

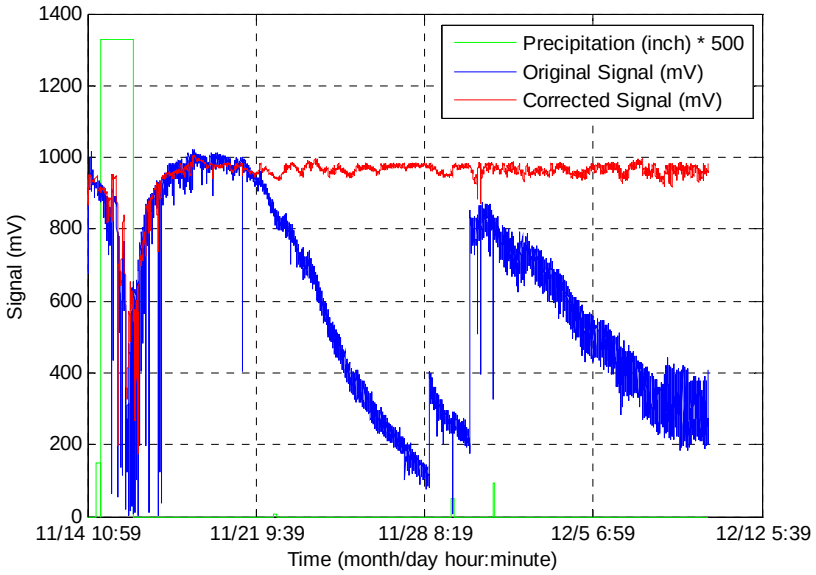


**Figure 3.6-19. Original signal and signal corrected for clogging and fouling.**

**Comparison of Sediment Concentrations before, during, and after the Construction**

Comparing sediment concentration data measured before, during, and after the construction of the stream crossing was difficult because the frequencies and intensities of rain events occurring within each period are different. Thus, simply comparing total, peak, or average sediment concentrations measured during each period is not meaningful. For effective comparison, two relative indices were established in two steps:

A. Firstly, two parameters were introduced – "*cumulative sediment concentration*" ($S_c$) and "*precipitation intensity*" ($I_p$). The cumulative sediment concentration (with a unit of "mg/L·minute") is defined as the integration of sediment concentration S measured by a sensor over the recorded rain event period T (Equation 3.6-5).

$$S_C = \int_T S(t)\,dt \qquad \text{[Eq. 3.6-5]}$$

The precipitation intensity (with a unit of "inch/minute") is defined as the ratio between the recorded precipitation $P_r$ (inch) for a rain event and the recorded length T (minutes) of the rain event (Equation 3.6-6). These two parameters use either recorded whether data or measured sediment concentrations that have been corrected for clogging and fouling and, thus, are independent of sensor design and location.

$$I_p = \frac{P_r}{T} \qquad \text{[Eq. 3.6-6]}$$

B. Secondly, two relative indices were developed using these parameters. The first relative index, "*cumulative index*", $I_{cum}$, is the slope of the linear regression line of the cumulative sediment concentration ($S_c$) measured by a sensor against the precipitation recorded within each rain events ($P_r$) that took place during an evaluation period (Equation 3.6-7). The evaluation periods studied are the pre-, during-, and post-construction periods. This index is considered a representation of the cumulative effect of rain events on sedimentation within an evaluation period.

$$S_C = I_{cum} P_r + b + \varepsilon \qquad \text{[Eq. 3.6-7]}$$

where b is the intercept of the regression line and ε is the error term.

The second relative index, "*intensity index*", $I_{int}$, is the slope of the linear regression line of the peak sediment concentration measured by a sensor ($S_{p)}$ against the precipitation intensity recorded for each storm event ($I_p$) that took place during an evaluation period (Equation 3.6-8). Again, the evaluation periods studied are the pre-, during-, and post-construction periods. This index reflects the instantaneous effect of rain events on sediment surge within an evaluation period.

$$S_p = I_{\text{int}} I_p + b + \varepsilon \qquad \text{[Eq. 3.6-8]}$$

Construction work at the LWSC to "harden" the crossing site using an articulated roadbed system (cable concrete) started on August 22, 2006 and was completed on October 22, 2006. From June, 2006, to March, 2007, four optical sediment sensors continuously measured sediment concentrations at the site to study the effectiveness of the structure on reducing soil erosion caused by military training. Figure 3.6-20 shows the completed construction work at the crossing site. Each SSC measurement system comprises two optical sediment sensors, two signal conditioning circuit boxes, a CR10X datalogger manufactured by Campbell Scientific, Inc., a 12 V deep cycle battery powered by a 15 W solar panel manufactured by Brunton, Inc. Dataloggers were programmed to control and take a measurement every 1 minute. Two sensor designs (closed-bottom and open-bottom) were tested. Sampling continued while construction work was ongoing.

**Figure 3.6-20. Completed LWSC site.**

Four sensors were installed about 30 meters downstream of the crossing, about 15m on each side of the centerline of the crossing. On each side of the creek, two sensors were installed with the "bottom" sensor about 0.1 m (4 inches) above the creek bed, and the top sensor about 0.25 m (10 inches) above the bottom sensor. The optical sensors were securely mounted with U-clamps and bolts on 2.44m - long (8 feet) green metal stakes that had been driven about 1 meter into the creek bed. Both dataloggers were mounted in weatherproof enclosures. The enclosures were mounted to pressure treated lumber posts that were buried about 1 meter deep into the banks. The 12 V deep cycle batteries for the power dataloggers were mounted on a wooden platform next to datalogger enclosures. The solar panel to charge the batteries was mounted above each data logger enclosure at a 45 degree angle to capture sunlight. Tree branches and foliage were removed from around the solar panels to ensure that sufficient sunlight would reach the solar panels. The measurement system on each bank was mounted sufficiently high to ensure that water levels would not submerge the data loggers, batteries, or solar panels in the event creek levels rose during storm events. Wiring from the sensors to the data loggers was contained in the PVC pipe which runs along the creek bottom. The PVC pipes were anchored to metal stakes driven securely into the creek bed with plastic wire ties. The purpose of the PVC pipe was to protect wiring from flotsam in the creek and from the current.

### 3.6.j. RESULTS

#### Little Kitten Creek, Manhattan, Kansas

The SSC changes rapidly in small creeks such as Little Kitten Creek. The optical sediment sensor developed in this study was able to quickly respond to rapid intermittent flushes of suspended sediment during storms. Figure 3.6-21 shows sediment concentrations measured during three storm events within a 31-hour period. Rainfall data was provided by the NSF Long Term Ecological Research Program at Konza Prairie Biological Station. The station is 8 miles away from the test site.

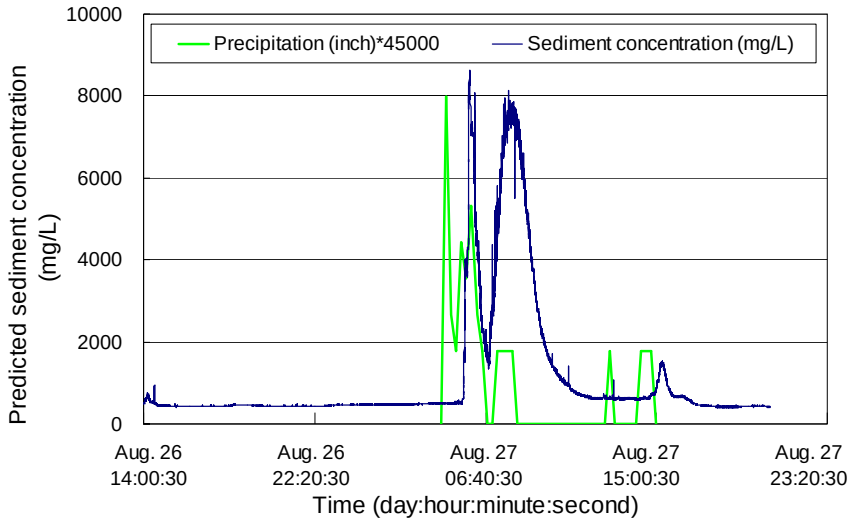


**Figure 3.6-21. Three storm events recorded within a 31-hour period.**

Fouling, including biofouling, on optical lenses has been a common problem for optical sensors exposed to various pollutants in water. Field tests at Little Kitten Creek showed that fouling effect caused signal deterioration (Figure 3.6-22). This can be determined by the observation that signals went back to their reasonable level after the sensor was cleaned. The measured signals shown in Figure 3.6-22 also indicated that fouling of the sensor lenses caused the transmitted signal to decrease and the backscattered signal to increase. It is easy to explain that the signal from the transmittance angle measurement decreases. However, the reason that the backscattered signal is increasing due to fouling effect needs to be investigated in the future. In order to maintain meaningful signals, the lenses need to be cleaned periodically. Various methods have been used to remove fouling effect, e.g. antifoulant coatings (Manov et al., 2004), Wiper mechanism (Ridd and Larcombe, 1994), and ultrasonic methods (WTW, 2007). During data post-processing, some correction algorithms may be applied to restore the signals. In this study, a correction algorithm was developed by determining the fouling trend found through a regression analysis on peak signal values taken during no-rain periods. The fouling trend was then removed to restore the sensor signals. A MATLAB (MATLAB, 2006) program was developed to complete the signal correction. Examples of signal deterioration due to fouling and sediment concentration data restored by a regression analysis were shown in Figure 3.6-22 and Figure 3.6-23, respectively.

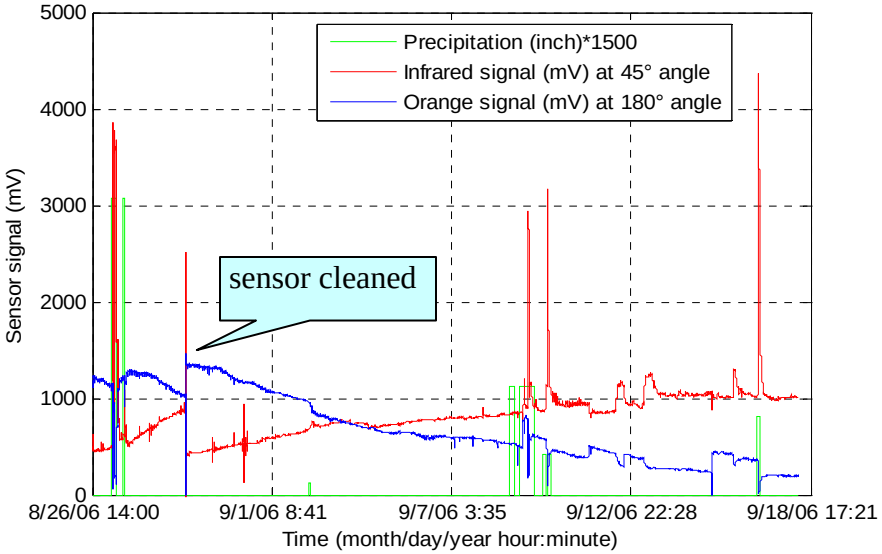


**Figure 3.6-22. Signal deterioration due to fouling.**

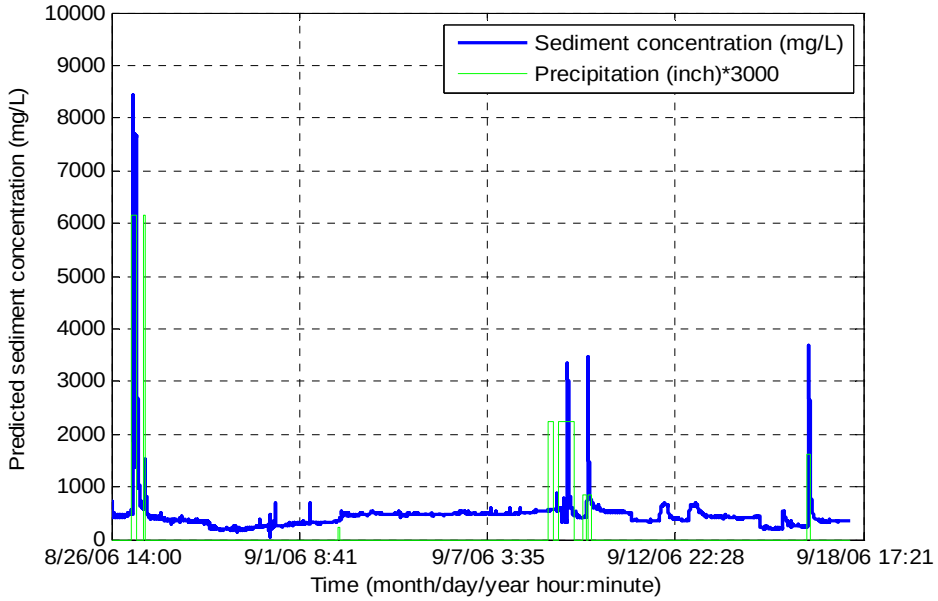


**Figure 3.6-23. Sediment concentration data restored with a regression analysis. Daily precipitation data source: www.weatherunderground.com.**

Upatoi Creek, Fort Benning, Georgia

After eight months of field deployment, the sensors and their installations have sustained various weather conditions, including several strong storm events, and have operated normally. No water leakage was found on any of the sensors, indicating good waterproof packaging.

Table 3.6-4 gives the intensity indices obtained using the data collected before, during, and after the construction. Effectiveness of the construction in reducing sediment concentration surge due

to stormwater runoff is clearly demonstrated by the decrease in the intensity index values. It should be noted that only the data taken in June was used for the "pre-construction" period. This is because, during the July-August period, filter screens installed in the sensors caused severe clogging problems, making the sensors insensitive to many sediment concentration changes. In Table 3.6-4, the intensity index during construction is not the largest number. With all the construction work going on at the site, there would be more sediment going into the creek. However, the intensity index is only calculated during rain events. Sediment spikes not occurring during rain events would not contribute to the intensity index.

**Table 3.6-4. Comparison of intensity indices obtained for the pre-, during-, and post-construction periods. Only the data collected in June, 2006, was used for the pre-construction period.**

| Period | Intensity Index ((g/L)/(in./min)) |
|---|---|
| Pre-construction | 845 |
| During-construction | 407 |
| Post-construction | 161 |

Table 3.6-5 compares the cumulative indices obtained for the three evaluation periods. With a heavy rain storm event (2.66 in) on November 15 excluded, the data indicate the effectiveness of the new LWSC in reducing the cumulative sedimentation at the site. When the heavy rainstorm event is included, however, the comparison becomes unclear. A possible explanation is that, for long-lasting, heavy storm events, more sediment from upstream would be brought to the crossing site and, thus, increasing the cumulative index. The LWSC was designed to reduce soil erosion caused by vehicles crossing the stream, not erosion occurring upstream.

**Table 3.6-5. Comparison of cumulative indices obtained for the pre-, during-, and post-construction periods. Only the data collected in June, 2006 was used for the pre-construction period.**

| Period | | Cumulative Index ((g/L·min)/inch) |
|---|---|---|
| Pre-construction | | 901 |
| During-construction | | 1,556 |
| Post-construction | Including a 2.66 inch rainstorm in November | 1,473 |
| | Excluding a 2.66 inch rainstorm in November | 531 |

Table 3.6-6 gives a comparison of the maximum TSS concentration levels measured during four storm events with similar precipitation before (June 6), during (October 11), and after (January 7 and January 22) the construction, respectively. The obvious decreasing trend in TSS clearly indicated the effectiveness of the construction in reducing soil erosion at the crossing.

**Table 3.6-6. Comparison of maximum TSS concentration levels measured during similar storm events before, during, and after construction.**

| Period | Date | Precipitation (inch) | Max. TSS concentration (mg/L) |
|---|---|---|---|
| Pre-construction | June 6th | 0.61 | 21,400 |
| During-construction | October 11th | 0.81 | 16,500 |
| Post-construction | January 7th | 0.88 | 8,100 |
| | January 22nd | 0.87 | 2,850 |

The data from January 2007 (Figures 3.6-24) indicate that, for some rainstorm events, measured sediment concentration peaks lag behind the raining periods. These peaks probably were caused by sediment runoff originating upstream, some distance away from the crossing. Since the precipitation data obtained does not provide spatial distribution of precipitation within the Upatoi Creek watershed, no further analysis is possible.

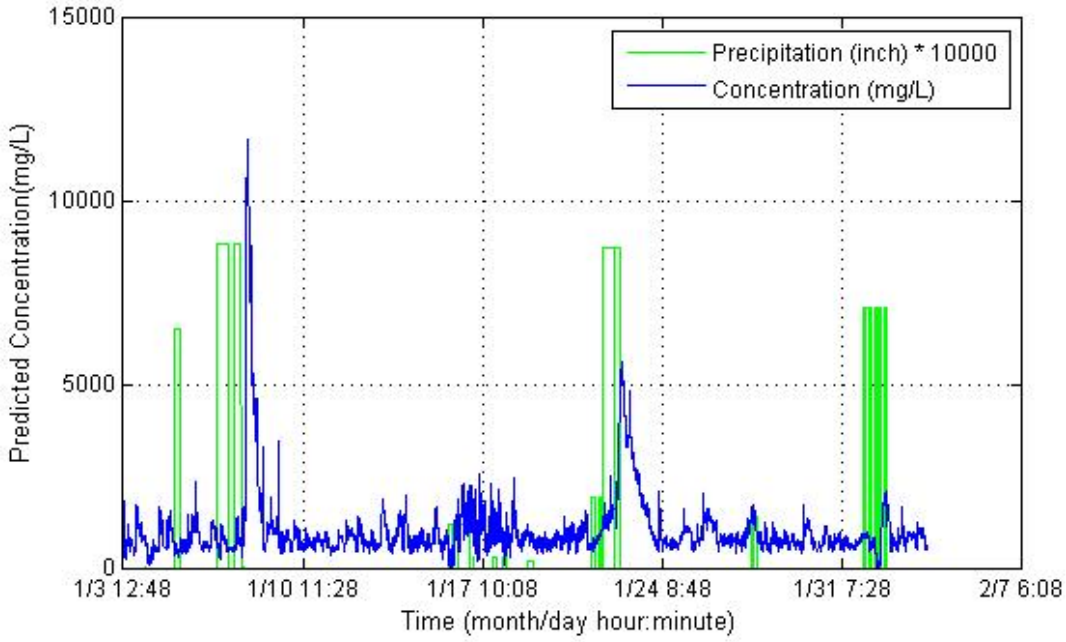


**Figure 3.6-24. TSS concentration predicted by the top sensor at the North side. Data after 2/4 were deleted because of the fouling effect.**

The data acquired within the eight month period indicated that the open-bottom design provided higher-quality signals than the closed-bottom design. This is mainly because the open bottom design did not allow sediment to settle out within the sensor, thus reducing the clogging problem. Visual inspections of the sensors after they were deployed in water for a long time also indicated that the bottom-open design had less biofouling problems, probably because of less direct contact between the lenses and the flotsam that was “snagged and hung up” by the closed bottom design.

Comparisons between the signals acquired during summer and winter months clearly indicated that the fouling effect was greatly reduced during the winter months. This observation probably

is related to the fact that, during winter, plant and animal growth and activities slow down significantly. Thus, it can probably be concluded that the fouling problem observed on the sensors is mainly a bio-fouling problem.

An obvious weakness of the experimental study conducted at the Upatoi Creek was the lack of accurate precipitation data for the site. In many cases, the differences in precipitation between the weather station at the Columbus Airport and the Upatoi Creek site may have caused inconsistencies in data analyses. For future studies, a rain gauge will be installed at each sediment-monitoring site. It should be noted that, while an on site rain gauge will allow better correlation between sediment concentration spikes and precipitation events, some inconsistencies will still remain since the site is essentially an open system with sediment flux from upstream areas of the watershed.

Another weakness was that data analysis had to be limited to the effect of rainstorms on sedimentation. The effect of military vehicles crossing Upatoi Creek could not be assessed in greater detail since an infrared vehicle counter installed at the crossing site did not reliably function, which made it very difficult to correlate actual timings of military vehicle crossings with TSS readings from the data loggers. For any future studies, a more reliable method of detecting vehicle crossing will need to be implemented.

### 3.6.k. CONCLUSIONS

The following conclusions can be drawn from the experimental work jointly conducted by Kansas State University and U.S. Army Aberdeen Test Center at the LWSC of the Upatoi Creek at Fort Benning during the period of June 2006 – February 2007:

- The sediment sensors with waterproof packaging and the sensor installation methodology used at the LWSC of Upatoi Creek at Fort. Benning are proven effective for long-term, in-situ sediment monitoring.

- The sediment sensor and associated signal conditioning/processing circuitry are capable of accurately measuring the dynamic changes of TSS in natural water.

- The open-bottom design of the sediment sensor is much less susceptible to lens clogging and biofouling than the closed-bottom design.

- Biofouling has stronger effects on the measurement during the summer season than during the winter season.

- Signal deterioration due to lens clogging and biofouling can be corrected through post-processing using statistical methods.

- With post-processing, long-term sediment monitoring can be achieved if the lenses on the sediment sensors are manually cleaned once per month.

- The TSS data obtained by the sediment sensors before, during, and after the "hardened" structure was constructed at the LWSC of the Upatoi Creek using an articulated roadbed system (cable concrete) proved that the structure is effective in significantly reducing sediment loads to the stream.

### 3.6.l. FACILITATING REMOTE MONITORING VIA WIRELESS SENSOR NETWORK AND INTERNET

**Existing Technologies**

Wireless communication currently is one of the most active areas of technology development. As stated by Wang et al. (2003), this development is driven primarily by the transformation of what has been largely a medium for supporting voice telephony into a medium for supporting other services, such as transmission of video, images, text, and data. Current research describes many approaches for achieving wireless communication. Wang et al. (2006) classified wireless network technologies by communication ranges.

Short-range approaches for wireless personal area networks include Bluetooth, ZigBee, and Ultra-wideband (UWB). Bluetooth is a protocol designed for low power consumption in a short range. Kim et al. (2006) developed a system for automated irrigation using Bluetooth. ZigBee protocols are intended for use in embedded applications requiring low data rates and low power consumption. Atmel Corporation (2008) has a low-power 2.4-GHz transceiver designed for low-cost ZigBee applications. Yang et al. (2004) mentioned that UWB is a technology for transmitting large amounts of data over a wide spectrum of frequency bands with low complexity, low cost, and low power consumption. This technology has an enhanced capability to penetrate through obstacles. Gemtek's (2008) USB Dongle WUWBD-101 is designed based on UWB technology. Other short-range methods including Crossbow's (2008) MICA2 provide high-level functional integration designed to optimize the addition of wireless mesh networking technology to a wide variety of sensing applications. Hartung et al. (2006) implemented a multi-hop wireless sensor network using MICA2 to monitor wildfire behavior and enhance safety considerations.

Wireless local area networks (WLAN) are one example of a mid-range technology implemented to extend or substitute for a wired LAN (Chan, 2007). WLAN also is referred to as the IEEE 802.11 family of standards. It consists of access points that provide access to different WLAN users.

Broadband wireless access (BWA) is a long-range communication technology. As specified in IEEE standard 802.16, BWA is an interface specification aimed at providing high-speed wireless access for wireless metropolitan area networks (Eklund et al., 2002). Nortel (2007) offers an end-to-end WiMAX solution, which is an example product for this broadband technique.

Cellular phone systems also are categorized as long-range technologies. Chan (2007) clarified the evolution of the mobile network for major wireless systems. The second generation ("2G") systems include GSM, launched in 1991, and IS-95 CDMA, first deployed in 1995. These two technologies evolved to General Packet Radio Service (GPRS) and CDMA2000 1xRTT,

respectively, to provide data service that exceeds the second generation ("2.5G"). Enhanced Data-rate GSM Evolution (EDGE), a third generation ("3G") standard, reached a higher data rate with minimal modifications in GPRS. GPRS and CDMA2000 1xRTT then continuously evolve to Universal Mobile Telecommunication System and CDMA2000 3x (or CDMA2000 EV-DO Rev. B), respectively.

Microwave link radio frequency technology also is included in the long-range transmission category. Although not well known by end-users in a network, it is an important component of wireless communication. One example is Campbell Scientific's CR200 series datalogger, which has a communication range up to 16 km. MaxStream (2008) also has many kinds of radio frequency modems for indoor or outdoor ranges up to 22 km.

Methods for global range, such as satellite and meteor burst communications, also exist. SatWest (2008) offers a satellite network system ideal for small teams or individuals with high data requirements. Using the ionized trail of gases left from a meteor, satellite network systems can create communication networks between different points by reflecting a signal up and back down to a receiver station located up to 1600 km away (Brown, 1985). MeteorComm (2008) has a product that provides communication in meteor burst networks and offers wireless data solutions for environmental monitoring, the railroad industry, maritime vessel tracking, and emergency services such as flood warning systems.

Adopting wireless sensor network (WSN) technology in precision agriculture is intriguing and practicable. Zhang (2004) investigated a WSN for precision agriculture using Bluetooth. Although challenges such as battery life and transmission latency exist in his application, it reveals a hopeful future for WSN in agriculture applications. Liu et al. (2007) presented a method for measuring environmental parameters in a greenhouse using WSN. After sinking data to a terminal, this terminal transfers data by short message service from a GSM system. However, the small size of the WSN device is a double-edged sword. The battery-powered sensors and wireless devices enable flexibility in deployment but shorten the useful lifetime of the system. The existing WSN systems did not give a long-term, low cost solution for areas far away from Internet access and power supply.

With these ideas and problems in mind, the objective of our research was to build an unattended, robust, and remote real-time monitoring system; and provide the design details and configuration of this remote WSN, specifically emphasizing system reliability, battery lifetime, transmission range, and cost effectiveness.

**Two-Layer Wireless Sensor Network Configuration**

The system configuration including sensor, communication components, and monitoring backbone servers is illustrated in Figure 3.6-25. The whole system is divided into two parts: a remote system and an indoor system. Anything inside the remote area belongs to the remote system.

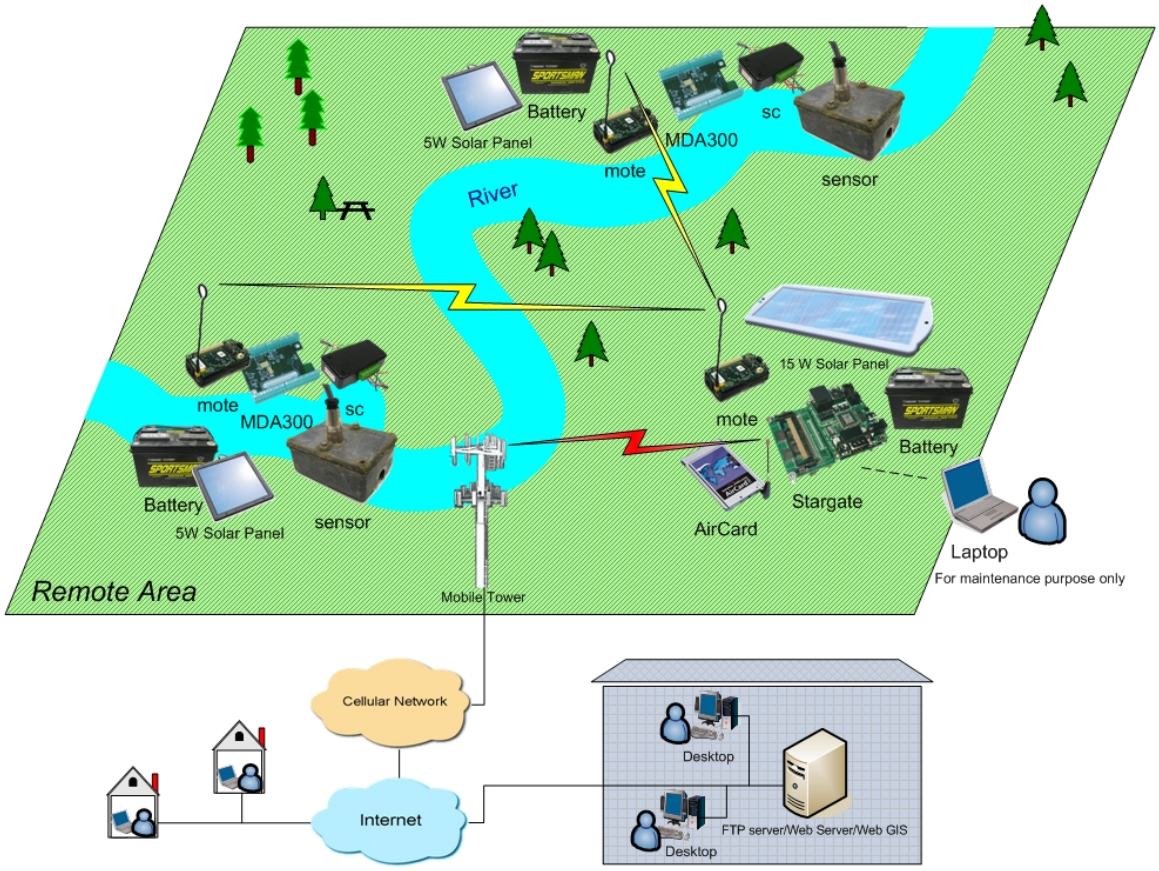


**Figure 3.6-25. Conceptual configuration of a two-layer WSN for real-time sediment runoff monitoring.**

**System Components**

A signal conditioner was used to amplify the sensor data. The signal conditioner also provides a 5V regulated power and control signal for the optical soil sediment sensor. A DAQ board (MDA300, Crossbow Technology Inc., San Jose, CA) was used to obtain the analog output from the signal conditioner. It has a 12-bit onboard ADC, seven single-ended analog channels, and six digital I/O ports. The maximum measurable input signal is 2.5V.

Wireless motes enable a low-power wireless sensor network. The third generation motes (MICA2; MPR400, Crossbow Technology Inc., San Jose, CA) are used to achieve an ad-hoc mesh network. A 900-MHz FSK modulated radio frequency in an unlicensed ISM band is used for MICA2 wireless communication. The maximum data transfer rate is 38.4 kbps, which is greater than the required rate for the application in this study. The outdoor line of sight range is 150 m. With a proper driver program installed, adequate power supply, and mounting the MICA2 to the MDA300 board through a 51-pin expansion connector, the measured sensor data are ready for broadcast. In recent experiments, we also used a new mote product MICAZ. Functionalities of MICAZ are the same as or enhanced from MICA2, but they use a direct sequence spread spectrum 2.4GHz radio for communications. The maximum data rate for MICAZ increased to 250 kbps.

We used nesC language to write the driver program for the motes. Every 30 seconds, the mote starts to turn on and off different LED; each LED is turned on 6 ms and then turned off. Samples are taken in the middle of each on or off interval. This ensures correct measurement without interference from other lights. The sampling timing scheme is illustrated in Figure 3.6-26.

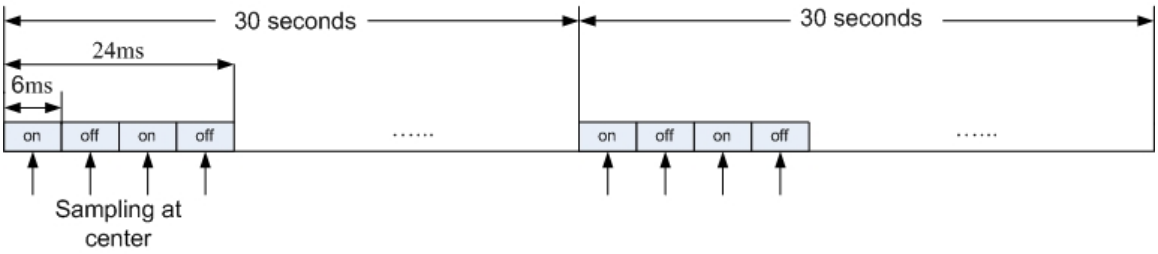


**Figure 3.6-26. Sampling timing scheme.**

As a high-performance processing platform designed for sensor, signal processing, controlling, Stargate can be used for many wireless sensor networking applications. We use a Stargate (SPB400, Crossbow Technology Inc., San Jose, CA) as an unattended remote control and communication center. It has a standalone, open-source Linux operating system, compact flash (CF) and PCMCIA connectors. A 512-MB CF card (SDCFH-512-901, SanDisk, Milpitas, CA) was installed on the Stargate to store application programs and sensor data. It can store one year's worth of data. This guaranteed that backup data always will be available in the worst wireless transmission scenario. With an additional daughter card (SDC400CA, Crossbow Technology Inc., San Jose, CA), the Stargate also supports a variety of interfaces, including RS-232, 10/100 Ethernet, USB port, and JTAG. A mote attached on the daughter card serves as a base station that can receive wireless data from one or multiple remote motes.

The AirCard (AirCard 750, Sierra Wireless, Richmond, BC, Canada) is essentially a cell phone built into a PCMCIA card. There are many different types of aircards for mobile phone systems from different carriers, such as CDMA from Verizon Wireless and GSM from T-Mobile. We chose the AirCard 750 based on the availability of the required data transfer service in the study area. The AirCard greatly improved the mobility of our system, extending it, theoretically, to anywhere with cell phone connection capability. This is especially important to rural areas, where little or no Internet access is available.

A 12 V car battery was used as a power source for the remote system. Efficient power usage is vital for longevity of outdoor systems. This study required appropriate power management for both sensor and wireless data communication.

For sensor data scanning, we turn each optical light sensor on and off every 30 seconds. Within this period, the light is turned on for only 6 ms, and this length can be controlled by the mote. This scheme minimizes sensors' power consumption.

As programmed, the mote always stays in a sleeping mode after finishing the control and data transfer tasks. With a 30-second data scanning interval, two AA batteries lasted an average of 4.5 days in the test. Instead of using AA battery, a 3.3 V voltage regulator can be used for mote power supply. A 12 V car battery used for mote and sensor scanning lasted more than one

month. In a recent study, we used a 5 W solar panel to recharge the battery, extending its lifetime to a few months.

The Stargate and AirCard are the two main power consumers in the entire system. The current drained by Stargate can reach up to 500mA while AirCard is in operation. Because we used a 12 V battery as the power supply and Stargate needs only a 5 V power supply, in the worst case, 3.5 W power was wasted on the voltage regulator's heat sink. This also generated a heating dissipation problem in the small enclosure used to protect the Stargate and AirCard for outdoor operation. To solve this problem, in addition to adding a fan and holes, we used a switching voltage regulator (DE-SW050, Dimension Engineering, Akron, OH). The benefit of the switching voltage regulator is that it drains current only when necessary. Thus, no heat is built up and no energy is wasted on the regulator while it supplies the 5 V power constantly. This significantly increased the battery life.

GPRS is a mobile data service. The maximum speed of a GPRS connection is comparable to a modem connection in an analog telephone network (about 32-40 kbps). In today's market, all mobile service providers offer data service as well as voice service. We chose T-Mobile's GPRS simply because their data service has the same coverage as their voice service. Therefore, we easily can use an ordinary cell phone to check signal strength in our field testing area.
An FTP server was set up on the indoor hosting computer to receive remote files transferred through GPRS. Received data files are stored in a database. Both Java and C languages are used to ensure data are processed in a timely manner. Raw data are processed and converted to engineering unit automatically using an SQL program in the database. An Internet information service was established for real-time data access on the Internet. Web server-side programming helped to realize the real-time web access from anywhere in the world.

**WSN at Fort Riley**

A preliminary experiment was conducted at Fort Riley, Kansas in August 2006. One demo sensor was connected to a water pipe. A water pump propels the water with soil sediment from a nearby water tank into the pipe. The sensor measures the sediment concentration in the running water. The MDA300 attached to MICA2 collects data from the sensor, and a Stargate transfers data via the AirCard 750. A laptop was used for debugging and temporary on-site monitoring. A LabView program was used to obtain and display real-time data on the laptop.
We established transmission and received data from both the in-field remote computer and the indoor hosting computer. However, at that time, we encountered several problems—the data transfer signal was sometimes weak, the power source was overheated, and the Stargate occasionally stopped responding. These problems reduced system reliability, which is detrimental for an unattended remote system.

Due to the weakness of the GPRS data transfer signal in rural areas, the AirCard 750 on the Stargate can lose its signal and disconnect from the system. The AirCard 750 used in this study cannot restore connection by itself. To solve this problem, we mounted a range extender antenna (YSC-RE1905U-SNP, Sharper Concepts Inc., Boca Raton, FL) on a 1-m pole to improve the signal power level. We also added a checkpoint in the Stargate control program to determine whether the FTP connection is still alive every 30 seconds. If the connection is not maintained,

the program rechecks the FTP link two more times before it restarts the AirCard to restore the connection. Data transfer traffic congestion, mainly due to high traffic volume in the service area, also disrupts communications. When congestion occurs, the program will try to restore the connection every $2 \times i$ second, where $i$ is the previous Time of Waiting for Restart (TWR). The initial TWR value is 10 seconds.

We solved the overheating problem by using a power management algorithm in both the nesC program on the mote and the shell-script program on the Stargate. Basically, we put those devices on "sleep" whenever possible. Also, as explained previously, using a switching voltage regulator significantly reduced the heating problem and increased the battery life.

The Stargate is a single-board computer. Like most computers, it can stop responding after operating for an extended time. We started a watchdog timer (WDT), a hardware timing device that triggers a system reset if the program hangs or neglects regular services. During Stargate's restarting period, sensor data are saved on the remote mote's 512-Kb flash memory, which, in this study, can save up to 40 hours of data without sending them out. Therefore, restarting the Stargate will not cause data losses.

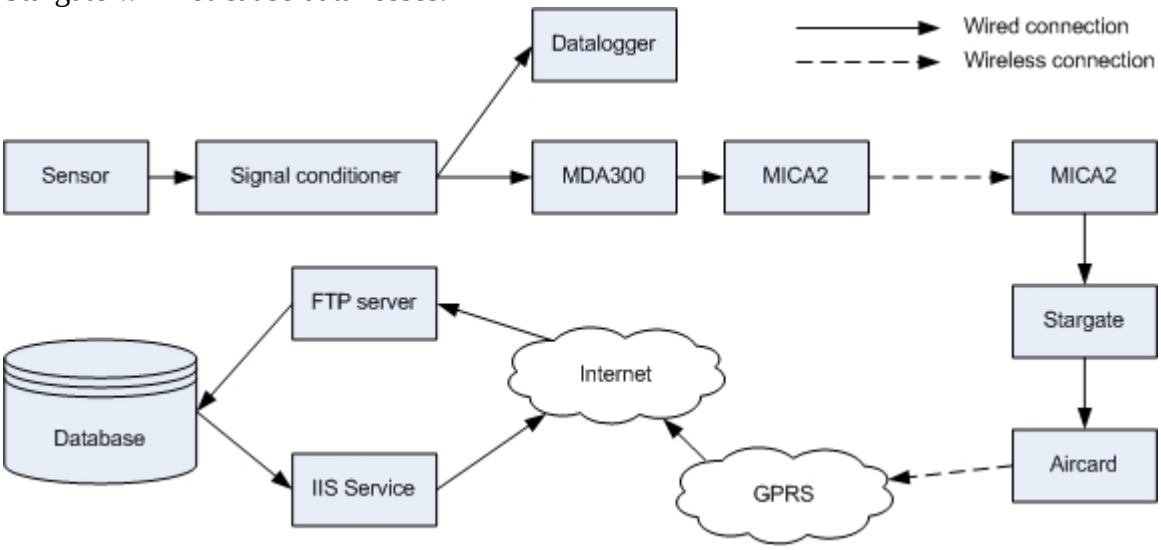


**Figure 3.6-27. Block diagram for sensor and remote system at the Little Kitten Creek site in Manhattan, Kansas.**

**WSN at Little Kitten Creek, Manhattan, Kansas**

We conducted a second experiment in Little Kitten Creek (Manhattan, Kansas) from August 2006 to March 2007. System components are illustrated in Figure 3.6-27. A sensor is located in the creek, and the wireless communication system is located on the bank. A 12-m cable connects the signal conditioner on the shore to the sensor in the creek. It is necessary to provide appropriate protection for the sensor. In this study, protection included a waterproof enclosure for the sensor and data cable. A protective fence is used to protect the sensor and cable from damage by floating logs or other debris. We used a datalogger (CR10, Campbell Scientific Inc., Logan, UT) to control optical sensor scanning. Sensor data are stored in this datalogger every 10 seconds. Saved data can be used later to verify the accuracy of data transmitted from the wireless system during the same period. The datalogger also sends a synchronization digital signal to the

MDA300 board to initiate its onboard sampling every 30 seconds. Thus, the sampling rate for the MDA300 was set at one third the rate of the CR10 datalogger. Data are sent immediately from MICA2 to the Stargate and transferred to an indoor hosting computer through GPRS using an FTP service. We observed a 10 to 12 second transmission latency due to FTP connection and data transfer. After implementing the resuming algorithm with the checkpoint in the mote program and the WDT for the Stargate, data transmission became more reliable and robust. The system sent data continuously for 15 days and stopped due to battery failure. The system was powered by a 12 V car battery. Voltage levels at the battery and each MICA2 in the system can be monitored in real time via the Internet. In several tests, we found that the battery life for this system ranged from 11 to 15 days. A solar panel is a possible solution for prolonging the battery life. During the test, we had to go to the field and manually change the battery whenever the voltage level went low.

**WSN in Mission, Kansas**

We applied solar panels in our most recent experiment. The experiment was set up in Mission, Kansas. On August 17, 2007, we installed two sensors and a two-layer wireless sensor network to measure sediment concentrations in storm drainage water. Two MICAZ sensor stations collected and sent data to a central station. As the second infrastructure layer, the central station can store data and communicate with a cell phone system, enabling us to use an FTP protocol to retrieve data at our backbone computer system. We did not use a datalogger in this experiment. Backup data are stored on a CF memory card that can store one year's worth of data. Real-time monitoring data are published on the Internet. Figure 3.6-28 shows the deployment map of those stations.


**Figure 3.6-28. Map of the wireless network deployed in Mission, Kansas (Map from Google Imagery, Digital Globe, Sanborn, Map Data)**

Power supply was enhanced by installing a 15 W solar panel (Northern Tool Equipment) for the central station and 5 W solar panels for each sensor station. Reprogramming the software to further reduce the activation time on remote devices also improved power conservation. We tested the system from Jan. 16 to March. 19, 2008, and observed that the power supply was sufficient under normal weather conditions.

Radio-hostile environments are another challenge we experienced in this study. Signal loss due to absorption by nearby water and lawns greatly reduced the transmission range. Trees and vehicles also impeded signals. Moreover, interference caused by obstacles near the path of transmission, usually referred to as a “Fresnel Zone” (2008) problem, also hindered the stability of data transmission. The system suffered from either no signal or a severe packet loss.

We tried to use different carrier frequencies (433 MHz, 900 MHz and 2.4 GHz ) to compare the radio transmission range under the same environmental conditions. The effective radio transmission ranges for 433 MHz, 900 MHz and 2.4 GHz were found to be approximately 30 m, 10 m and 20 m, respectively. The distance between one of the sensor stations to the central station is 96 m; therefore, changing carrier frequency did not satisfy the requirement for this study. Ultimately, we decided to use a 2.4 GHz MICAZ mote which, compared with its previous counterpart, has a higher data rate, lower power consumption, cheaper external antenna, and better anti-interference ability.

We also tested multi-hopping relays by adding additional motes between sensor stations and the central station. However, this makes the system more complicated, and the implementation cost is high. We finally solved the transmission range problem by using both omni-directional and Yagi directional antennas. An omni-directional antenna (HyperLink Technologies Inc.) with 8.5 dBi gain was used at the central station. Each sensor station has a Yagi directional antenna (HyperLink Technologies Inc.) with gain of 14.5 dBi. Proper selection of the tower height places the transmitter and receiver antennae within the “first Fresnel Zone,” where the signal strength is maximized. Setting antennae at a height of 3 m (Figure 3.6-29) minimized packet loss. For more than two months of continuous observation, the packet loss rate was reduced to 3.1%.


**Figure 3.6-29. Two sensors and a remote system in Mission, Kansas.**

### 3.6.m. RESULTS

**Web Interface**

After setting up the system, we transferred sensor data to a database on an indoor hosting computer. Those data can be observed on the Internet and are updated every 3 minutes. One example of the real-time monitoring interface on the Internet is shown in Figure 3.6-30.

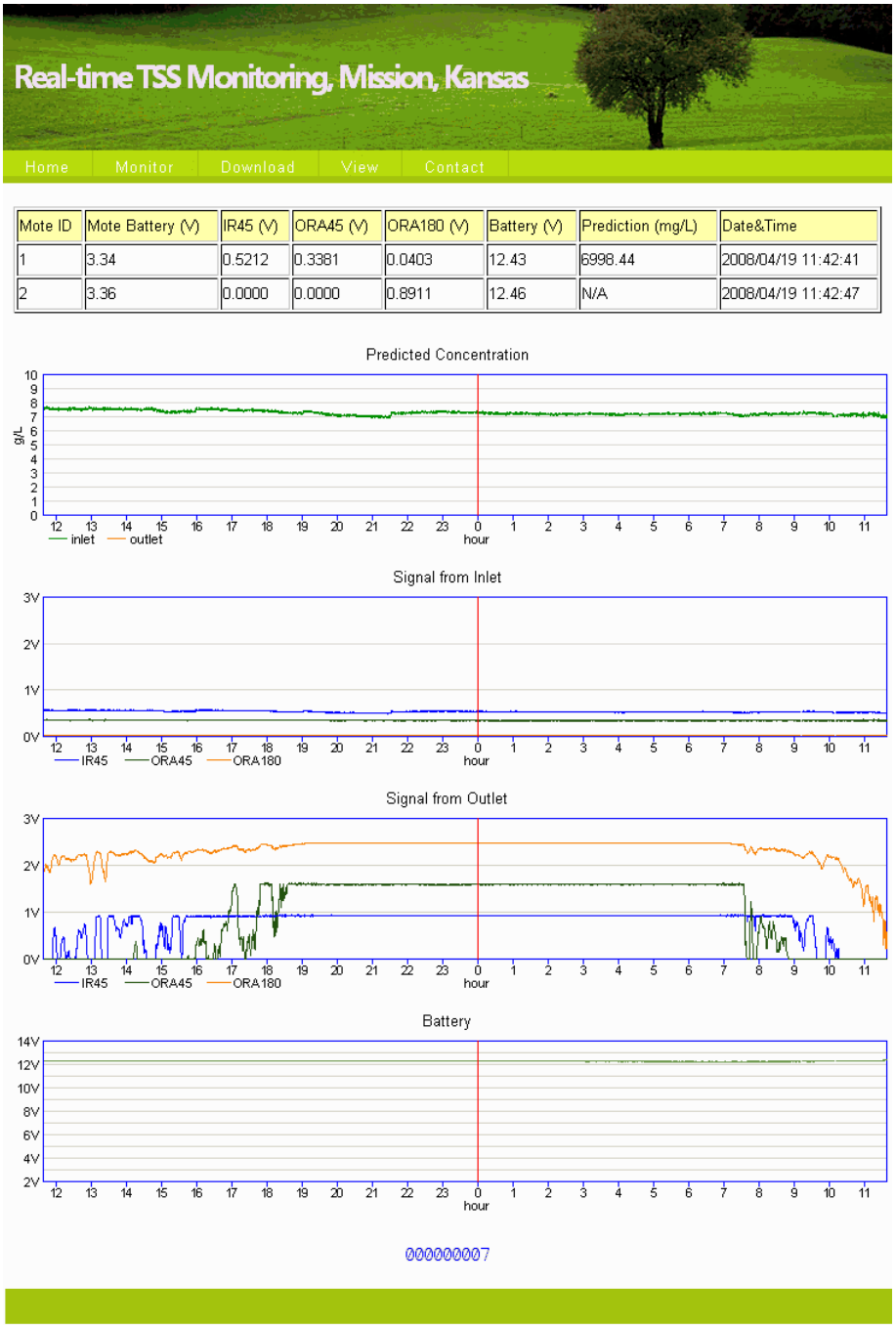


| Mote ID | Mote Battery (V) | IR45 (V) | ORA45 (V) | ORA180 (V) | Battery (V) | Prediction (mg/L) | Date&Time |
|---|---|---|---|---|---|---|---|
| 1 | 3.34 | 0.5212 | 0.3381 | 0.0403 | 12.43 | 6998.44 | 2008/04/19 11:42:41 |
| 2 | 3.36 | 0.0000 | 0.0000 | 0.8911 | 12.46 | N/A | 2008/04/19 11:42:47 |

**Figure 3.6-30. A screenshot of the real-time monitoring interface at the Website.**

**Packet Loss**

After collecting data from January 24 to February 15, 2007, we compared wireless-transferred data with data stored in a datalogger. Results are illustrated in Figure 31 (wireless transferred data) and Figure 3.6-32 (data stored in the datalogger).

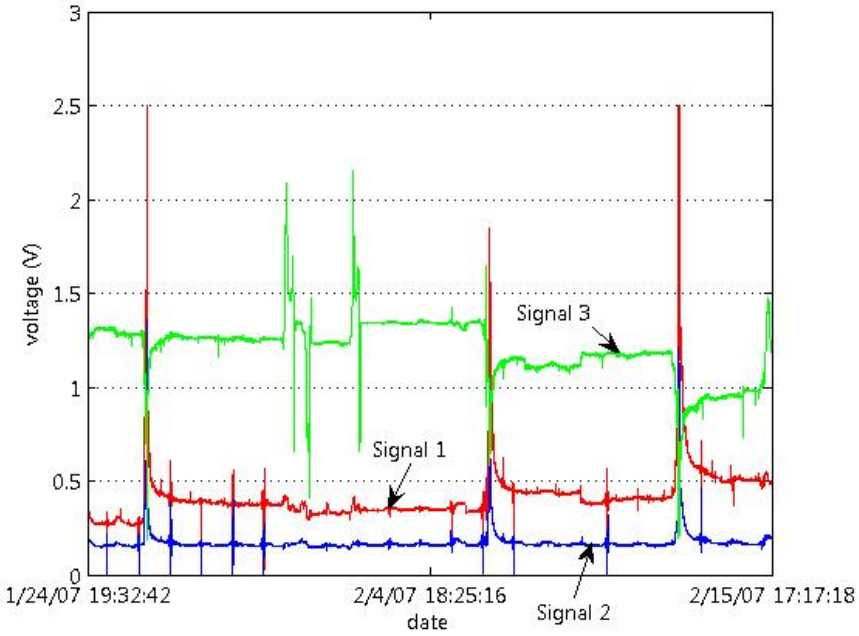


**Figure 3.6-31. Wireless-transferred data extracted from the indoor computer database.**

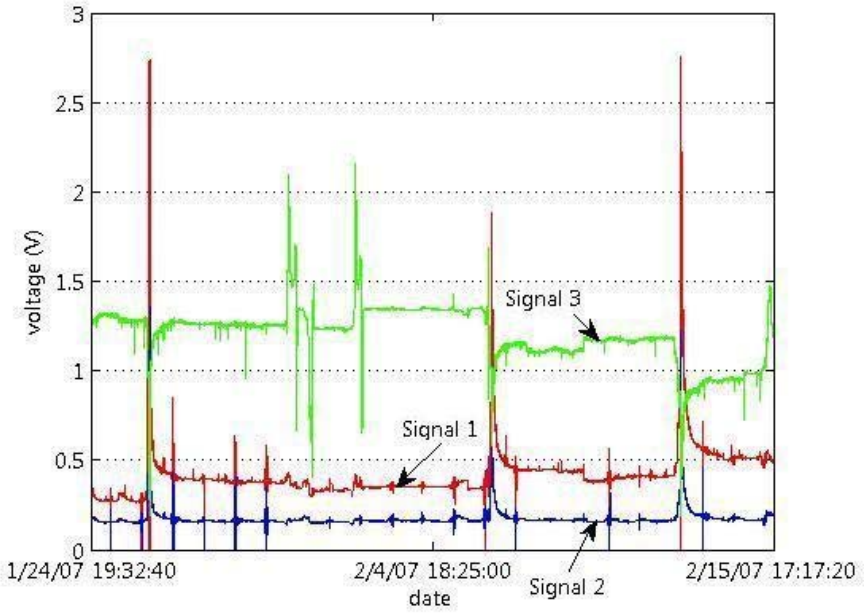


**Figure 3.6-32. Sensor data logged by CR10.**

The analog to digital convertor (ADC) on the data-acquisition board mounted on the wireless mote and the datalogger were different. This dissimilarity was reduced by establishing a regression model of the datalogger data against the wirelessly received data. Using this model, data received from the WSN are first converted to "equivalent" datalogger data and then compare with the actual datalogger data. The result is shown in Table 3.6-7.

**Table 3.6-7. Percentages of Outliers in Transmitted Signals.**

| | Signal 1 | Signal 2 | Signal 3 |
|---|---|---|---|
| Mean of absolute difference between signals (mV) | 4.2 | 1.8 | 1.8 |
| Confidence interval ($2\sigma$) (mV) | 16.3 | 9.5 | 5.7 |
| Number of outliers | 673 | 527 | 1959 |
| % of outliers in data | 1.09 | 0.85 | 3.16 |

In Table 3.6-7, the "outliers" are defined as the transmitted signals that are outside of the confidence interval of the datalogger-recorded signals. The confidence interval is defined by $\pm 2\sigma$ from the datalogger-recorded values, where $\sigma$ is the standard deviation of the difference between the wireless-transmitted and datalogger-recorded signals, which is assumed to have a normal distribution. As can be observed in Table 3.6-7, signal 3 presented the worst case, where 3.16% of the wirelessly transmitted data are considered the "outliers". Further observation of these outliers revealed that most of them occurred around 10:40 AM each day, which is the time when the ambient light condition for the sensor optics experienced a sharp change from shadow to direct sun light. This transition takes place within a very short period of time. Due to the fact that the sampling times of the mote and the datalogger were not completely synchronized, a small difference in sampling time may yield significantly different signal readings within this transition period. Thus, the outliers may not necessarily represent wireless transmission errors.

From the most recent experiment in Mission, Kansas, we have continuously recorded wireless data since Jan. 16, 2008. In order to study the data loss during wireless signal transmission, we defined the packet loss rate as follows:

$$\text{Loss Rate } L_R = \left( \frac{N_T - N_S}{N_T} \right) \times 100\% \qquad \text{[Eq. 3.6-9]}$$

where

$N_S$ is the actual number of data packets received during a period.

$N_T$ is the number of data packets theoretically transmitted during the same period, and

$$N_T = \left\lceil \frac{T_D}{T_S} \right\rceil \qquad \text{[Eq. 3.6-10]}$$

where

$\lceil x \rceil$ is the ceiling function that returns the smallest integer not less than $x$,

$T_D$ is the duration of the observation period in seconds, and

$T_S$ is the sampling interval in seconds.

From March to May, 2008, we received 197,650 data packets from the wireless system. The actual data packet loss rate is 3.1%.

A severe ice storm occurred in mid-December 2007, during our most recent experiment in Mission, Kansas. The equipment survived without damage and data loss. However, due to a power outage, we could not retrieve data from the backbone database on the indoor computer. After the power is resumed, we were able to recover the data and completely return to normal operation of the entire system.

**Cost Analysis**

Long-range wireless communications using microwave link or satellite are expensive. In this study, we explored the use of a commercial cell phone service to achieve low-cost, long-range transmission. The cost for the two-sensor system is summarized in Table 3.6-8.

**Table 3.6-8. Hardware Cost for Two Sensors in a Real-Time Sediment Runoff Monitoring System.**

| Components | Price |
|---|---|
| Wireless devices | $1,300.00 |
| Antenna devices | $350.00 |
| Power supply devices | $650.00 |
| Cellular service | $620.00 |
| Total | $2,920.00 |

## 3.6.n. CONCLUSIONS

In this study, we developed a remote, real-time, wireless sediment runoff monitoring system and addressed several challenges associated with the system. The following conclusions can be drawn from this study:

- We used a commercial GPRS mobile phone system to provide long-range wireless data transfer in an area where wired or wireless Internet access was not available. The use of an extendible antenna enhanced GPRS signal power and reduced abrupt FTP disconnection to a low level.
- Wireless transmission was achieved in a radio-hostile environment by using omni-directional and directional antennae with proper heights.
- We provided reliable power supply in the testing area with solar panels. Hardware redesign and software algorithm modifications also extended the battery life.
- We developed software for both the remote system and the indoor hosting computer. An auto-resuming algorithm was used to improve reliability of the system, which is essential for success of remote, real-time systems.
- The sensor successfully monitored in-field soil sediment concentration and transferred data to an indoor computer. With this system, real-time soil sediment concentration can be observed from any location with Internet access, and no software installation is required for monitoring at the user-end.
- We reduced costs by using appropriate antennae to achieve long-range wireless coverage. The total price for a two-sensor WSN is around US $3,000.

- This system is a promising, low-cost wireless solution for remote, real-time monitoring and has many potential applications.

## 3.7 TASK 7: ENVIRONMENTAL DECISION SUPPORT TOOL

### 3.7.a. BACKGROUND

The 2000 National Water Quality Inventory reported that 40% of the nation's water bodies do not meet water quality standards and identified non-point source pollution (NPS) as the leading cause of surface water degradation (USEPA 2000). Over 290,000 miles of river, almost 7,900,000 acres of lake, and 12,500 square miles of estuary failed to meet water quality standards. Military training maneuvers have the potential to significantly alter land surfaces, reduce quality and promote NPS pollution, resulting in a reduction of training land quality and the inability of military installations to meet water quality standards as defined by current, and future, total maximum daily loads (TMDLs) mandated in Section 303(d) of the 1972 Clean Water Act.

Military readiness depends upon high quality training. A prerequisite of effective maneuver training is repetition and a large land base. This creates intense stress on land. Environmental protection requirements place additional restrictions on land use and availability. Because military training schedules are set well in advance to make the best use of installation training facilities and National Training Centers, there is little flexibility to modify training events and maintain readiness. Management practices that allow for intensive military training tempos while protecting surface water quality and reducing NPS pollution generation are required.

Since the passage of the National Environmental Policy Act of 1969 (NEPA) and the publication of U.S. Army Regulation 200-2 (Department of Army 1988), the military has been required to minimize or avoid both short and long-term environmental impacts caused by military training. Because there is a limited amount of available land for military training, it is in the Army's best interest to protect these areas to fulfill their mission requirements for realistic training and testing. In order to meet this need the military initiated the Integrated Training and Management (ITAM) program with the overall goal to achieve optimum sustainable use of military lands. The ITAM program provides Army range officers with the capability to manage and maintain training lands and support mission readiness.

ITAM integrates mission requirements with environmental requirements and environmental management practices, and establishes the policies and procedures to achieve optimum, sustainable use of training and testing lands. There are multiple components of ITAM including Training Requirements Integration (TRI), Range and Training Land Assessment (RTLA), Land Rehabilitation and Maintenance (LRAM), Sustainable Range Awareness (SRA), and Geographic Information Systems (GIS).

TRI is the component of the ITAM Program that provides a decision support procedure for integrating training requirements with land management, training management, and natural and cultural resources management processes and data derived from RTLA and Army Conservation Program components. TRI supports the Army's requirements for environmentally sustainable training lands. The goals for TRI are twofold: (1) to ensure sustained accessibility to adequate

training lands to support training to standards under realistic natural conditions, and (2) to provide military trainers and land managers with the necessary technical and analytical information to integrate doctrinally based training and testing with land constraints and quantify training land carrying capacity.

RTLA programs are focused on training support and training land management, and may be used to support NEPA and other compliance and planning efforts related to Army transformation, restationing, and realignment. Current policies allow installation-level land managers and range operations staffs to determine how they can best collect and use resource data to support foundational/long-term and site-specific land management decisions such as training area allocation, training area use and land rehabilitation effectiveness. Analyzing the impact of military training on soil erosion is part of the RTLA program. Over the past decade a great deal of effort has been given to collecting data and modeling soil erosion from track vehicle activity. The Tri-Service CADD/GIS Technology Center recently released a technical report (Doe et al., 1999) that evaluated the applicability of several soil erosion models for use on military lands. The report recommends four models for consideration by military land managers: AGNPS, CASC2D, RUSLE, and USPED. Each of these models has strengths to consider. However, none of the models is capable of predicting the initiation point of soil erosion and locating potential gully sites.

Currently, Range managers send personnel out to survey the training lands and locate gullies. This is a constant and labor intensive process because gullies develop as a result of maneuver intensity and location, intense rainfall events, soil moisture content of soils, vegetation type and health, and topographic relief (e.g. slope). Gullies not only contribute to soil erosion and water quality problems, but are a cause of injury to soldiers and damage to equipment when a gully of sufficient depth is encountered during maneuvers, especially at night.

### 3.7.b. APPROACH

Predicting water erosion locations within a given drainage area is difficult because the initiation point of erosion is related to where overland flow transitions from sheet flow to concentrated flow (Figure 3.7-1) (Meyer et al. 1999). Determining the overland flowpath of surface water runoff – and the precise location where concentration takes place – is a key process in erosion modeling (Abrahams and Atkinson 1993, Bennett et al. 2000). The efficiency of BMPs for preventing or minimizing NPS pollution (e.g., vegetated buffer systems) is significantly affected by overland flow conditions (Abraham and Atkinson 1993, Abraham et al. 1999). However, the ability to classify varying flow regimes, from sheet flow to concentrated flow, is problematic because it is difficult to quantify the energy content of runoff water.

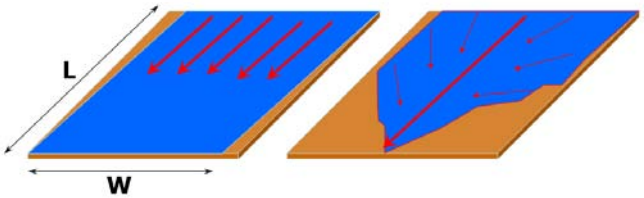


**Figure 3.7-1. Illustration highlighting the difference between sheet and concentrated flows. Controlling the mode of overland flow transport is key to preventing gully formation and NPS pollution.**

Many researchers have shown that the kinematic wave theory is a useful tool for assessing the process of overland flow at varying flow regimes (i.e., sheet to concentrated flow) (Laguna and Giraldez 1993, Wong and Chen 1999, Singh 2001). Based on this theory, McCuen and Spiess (1995) showed that the relationship of nL/S0.5 (abbreviated nLS) effectively categorized hydrological flow regimes into sheet flow or concentrated flow, where n is Manning's coefficient for overland flow (L) is the length of overland flow (feet), and S is the slope. In work conducted at the Flint Hills ecoregion of Kansas (in which Fort Riley is located), overland flow transitioned from sheet to concentrated flow at nLS values near 100 (a unitless value).

The nLS model was developed for the ArcGIS 9.x (ESRI, Redlands, CA) suite of GIS software applications that are routinely utilized across DoD agencies and installations. Because of this, the model itself can be delivered in a variety of forms, including as an ArcToolbox "tool", a Python script, or as a ModelBuilder graphic model. In addition, the model and necessary data will be made available to end users through multiple clients (e.g., Internet browsers, desktop GIS software) over the Internet as a GIS "service" or web application. This delivery method simplifies model use, facilitates access to required input datasets, and eliminates the need to physically distribute executable files and updates.

The $nL/S^{0.5}$ equation established by McCuen and Spiess (1995) is operationalized as a three layer raster calculation in a GIS using classified LULC data and DEMs (Figure 3.7-2). Slope (S) is calculated from a DEM using 3 x 3 cell neighborhood and the average maximum technique (Burrough and McDonnell 1988). Length of overland flow (L) is a fixed value based on the grid cell size of the DEM. LULC data provides the relevant Level I or Level II landcover type (Anderson et al. 1976) on a cell-by-cell basis for the entire study area. This nominal data is then reclassified into quantitative estimates of Manning's n (n) by using a look-up table of coefficient values (Table 3.7-1) (Engman 1983, Foster et al. 1985, McCuen and Spiess 1995).

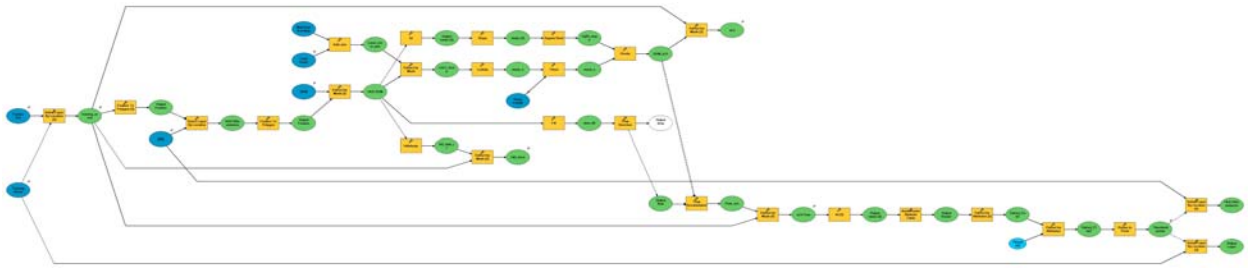

**Figure 3.7-2. Graphic representation of ArcGIS tool version of the nLS model developed using ArcGIS ModelBuilder.**

**Table 3.7-1. Landuse/landcover classes used in model development in Kansas and their associated values for Manning's coefficient (n).**

| *Land cover* | *n* | *Land cover* | *n* |
|---|---|---|---|
| Cultivated Land | 0.045 | Sandsage Shrubland | 0.06 |
| Conservation Reserve Program | 0.045 | Urban Areas | 0.01 |
| Mixed Prairie | 0.03 | Cattail Marsh | 0.05 |
| Tallgrass Prairie | 0.03 | Deciduous Woodland | 0.07 |
| Sand Prairie | 0.03 | Shortgrass Prairie | 0.03 |
| Cottonwood Floodplain Woodland | 0.1 | Freshwater Marsh | 0.05 |
| Water | 0.0001 | Low or Wet Prairie | 0.03 |
| Cottonwood Floodplain Forest | 0.1 | Willow Shrubland | 0.06 |
| Bulrush Marsh | 0.05 | Pecan Floodplain Forest | 0.1 |
| Ash/Elm/Hackberry Floodplain Forest | 0.1 | Playa Lake | 0.0001 |
| Non-Native Grassland | 0.23 | Salt Cedar or Tamarisk Shrubland | 0.06 |
| Weedy Upland | 0.03 | Western Wheatgrass Prairie | 0.03 |
| Mixed Prairie – Disturbed | 0.04 | | |

The computed nLS output grid represents a unitless estimate of the energy of surface runoff water as it flows downslope. These individual cell-based energy estimates, linked by the direction of overland flow, can then be summed. The relationship between actual gully locations and accumulated energy are then compared to develop a predictive model. To accomplish this, the D8 algorithm (O'Callaghan and Mark 1984) is used to create a flow direction grid that estimates the direction of water flow from cell-to-cell (i.e., "upstream" to "downstream") based upon topographic slope and aspect from a DEM input. Individual cell values from the previous nLS calculation are then summed to generate a weighted flow accumulation grid where each output cell is populated with a value equal to the summed energy of cells flowing into it from the "upstream" direction.

After the initial nLS model is run, a point file of gully head locations, acquired in the field or digitized from digital orthophotography, is overlaid with model results to extract the accumulated energy value at each gully location. The three statistical intervals of mean ($\mu$) and standard deviations ($\pm 0.5\sigma$, $\pm 1.0\sigma$, and $\pm 1.5\sigma$) of energy accumulation values are calculated and used to characterize the critical threshold value where overland sheet flow is expected to transition to concentrated flow.

Model performance is evaluated using a classification error matrix (Story and Congalton 1986, Lillesand and Kiefer 1994). Error matrices compare the relationship between known and predicted data. Here, known data is the location of gullies collected in the field using differential global positioning system (DGPS) receivers or digitized from high resolution digital orthophotography using standard aerial photo interpretation techniques (Arnold 1997). Predicted data are those locations (e.g., the threshold value $\pm 0.5\ \sigma$) where the nLS model indicates the likely formation of gullies, or the transition from sheet to concentrated flow data. Overall model accuracy is calculated by dividing the total number of correctly classified locations (both gulley

and non-gulley sites) by the total number of modeled locations. An addition benefit of the classification error matrix is that is allows both model errors of omission and errors of commission to be quantified, along with overall model accuracy.

### 3.7.c. RESULTS AND DISCUSSION

The erosion potential model developed for Fort Riley, referred to here as the "nLS" model, is capable of determining areas of high erosion potential and, therefore, the optimal locations for siting erosion-preventing BMPs. Because the nLS model has few input requirements, for which easily accessed datasets are available nationwide, data acquisition and preparation times are minimal compared to existing erosion models (e.g., AGNPS, CASC2D, RUSLE, USPED). The nLS model has been successful in predicting gully locations in two separate watersheds in the Flint Hills ecoregion in which Fort Riley, Kansas is located. Based upon an accumulated nLS value of 100 (± 0.5 SD), overall model accuracy was calculated at 88% using a classification error matrix. The critical threshold value of 100 may vary at different installation locations. Quantifying the amount of that variation, and determining its significance in the context of nLS model performance, is a critical task.

Currently, locating gully points is a time-consuming and potentially dangerous task if conducted on the ground, and very expensive if completed via air survey. The application of the methods embodied in the user-friendly tools to be demonstrated in this project will permit land managers to reduce the size of and prioritize their search area by focusing their attention on sites most likely to develop gullies in accordance with the biophysical characteristics of the training area. Because of the model's flexible GIS format, additional spatial data layers such as troop movement and vehicle tracking could be incorporated into the model design to enhance performance and usability. The tangible dollar value is time saved in locating gullies. The unknown savings comes in reduction of injuries to soldiers and repairs to damaged equipment. The nLS modeling approach also promises to be the premier tool for siting BMPs designed to reduce soil erosion, thereby assisting installations in meeting current or future sediment TMDLs for streams leaving federal lands.

The ability to predict future erosion potential with the nLS model offers several significant advantages to military installations including, (1) the ability to assess training land impacts from scheduled training exercises given current environmental conditions, (2) providing a sound scientific basis to estimate LRAM costs to repair and prevent gully erosion on current, future, or rental training lands, and (3) the ability to estimate and compare environmental impacts due to training events associated with installation realignment or mission change. Financial considerations can be expanded from analyzing the expected expense of only one exercise to predicting annual and/or reoccurring costs by simulating multiple training exercises.

The model described above might also be used to predict the impact of future training events on overland flow and the formation of new gully incision points. The ecological impact of military vehicle maneuvers has been well studied (Ayers et al. 2005b, Rice et al. 2006, Liu et al. 2007). The relationships quantified by these studies between vehicle turning radius and both vegetation damage and rut depth can be seamlessly integrated with the nLS modeling framework using standard GIS data processing and manipulation techniques. By incorporating vehicle tracking

data, from field training or simulator-based exercises, the anticipated environmental damages such as vegetation loss and vehicle rutting can be simulated and used as the basis to modify current representations of installation terrain (Ayers et al. 2005b, Rice and Ayers 2005, Rice et al. 2006, Liu 2007). The validated nLS model can then be run using modified vegetation and topographic input to identify likely sites of future gully initiation. Information derived in this manner will benefit installations by making training areas safer for people and equipment, and ITAM coordinators for purposes of estimating costs associated with post-exercise training area repairs.

A calibrated and validated nLS model can be delivered to end users as an ArcGIS model for use in desktop ESRI GIS software. A follow-on project funded by ESTCP is also facilitating the use and as a fully functional ArcGIS Server application with geoprocessing, data extraction, and geodatabase editing capability. A significant part of this proposal includes development of an ArcGIS Server application to deliver nLS modeling capability to a large number of users over networks through a single shared system. Central management of modeling tools benefits end users by rendering much of the analytical complexity transparent while ensuring they adhere to best practices and techniques defined by GIS professionals. Further, this system can support remote geodatabase creation and editing through clients such as Internet browsers, mobile GIS platforms, and traditional desktop GIS programs. Because ArcGIS Server is an enterprise GIS system, multiple offices across the organizational hierarchy (e.g., from ERDC to the local ITAM office) can have immediate on-demand access to spatial data as soon as it is saved on the central server. This approach also offers the potential for greater efficiency as models and data developed once can be used by the entire organization. Alternatively, end users can utilize Web services based on ArcGIS Server on their own desktop systems and infuse their own data or supplement new applications with existing models and data. By delivering an effective and user friendly GIS server application in this project, the potential for using server applications as an integrative analysis platform with other biological, hydrological, and engineering models within the DoD enterprise will be demonstrated.

## 3.8. TASK 8: STREAM CROSSING EVALUATION

### 3.8.a. METHODS AND MATERIALS

#### Study Sites

The bedrock in the study areas (which is fairly shallow) is composed of shale and limestone of Pennsylvanian and Permian age (Jewett, 1941 and Ingrisano, 2005). Mudstone formations of Permian age occur in some parts of the study sites (Ingrisano, 2005). According to Ingrisano, 2005, the Flint Hills are characterized by the presence of bench and slope topography. As shown in Figure 3.8-1, the bedrock formations in the study areas are Permian in age and belong to the Council Grove and Chase groups. These groups are composed of different types of shale and limestone as shown in Figure 3.8-2. The limestone formations in the study areas are of two types: flint and non-flint bearing formations. The non-flint limestone formations are more resistant to weathering (forming extensive plateaus), while the flint bearing limestone formations are easily eroded forming steep slopes and rounded knobs (Jewett, 1941 and Ingrisano, 2005). Stream

channels in the area reflect the underlying geology and bed material formations are composed of clay, silt and gravel.

The soils in the study watersheds belong to the following soil series: Benfield (Udic Argiustolls), Florence (Udic Argiustolls), Wymore (Aquic Argiudolls), Irwin (Pachic Argiustolls), Clime (Udic Haplustolls), Sogn (Lithic Haplustolls) (Clark and Worley, 1975). These soils (Mollisols) are silty clay loams, cherty silt loams and silt loam. The Benfield-Florence association comprises of moderately deep, sloping and moderately steep silty clay loams and cherty silt loams. The Wymore-Irwin association comprises of silty clay loams that range from level to sloping. The Clime-Sogn association comprises of silty clay loams that are moderately deep and shallow, sloping and moderately steep.

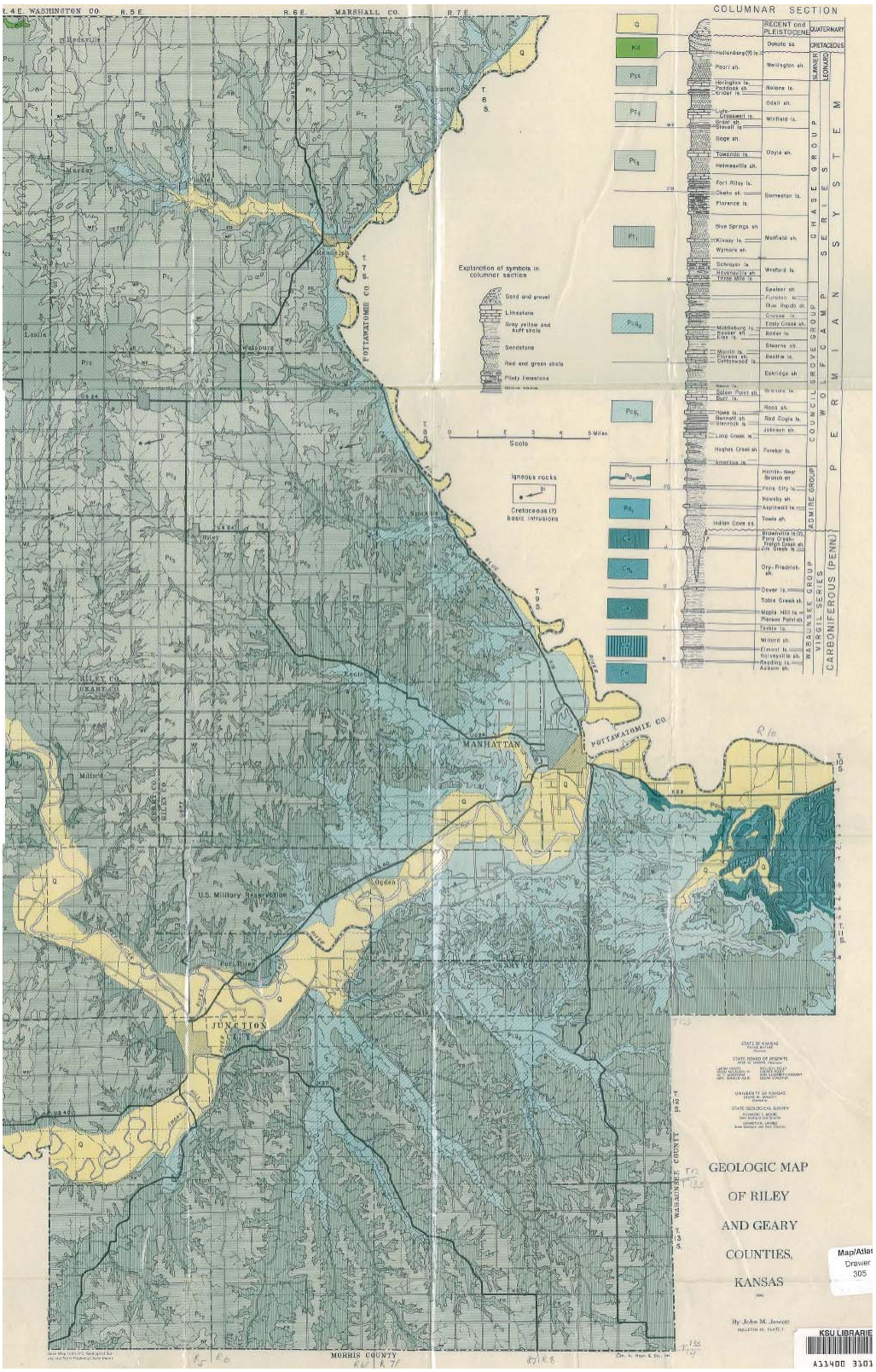


**Figure 3.8-1. Geologic map of Riley and Geary counties, Kansas. Adapted after Jewett, 1941.**

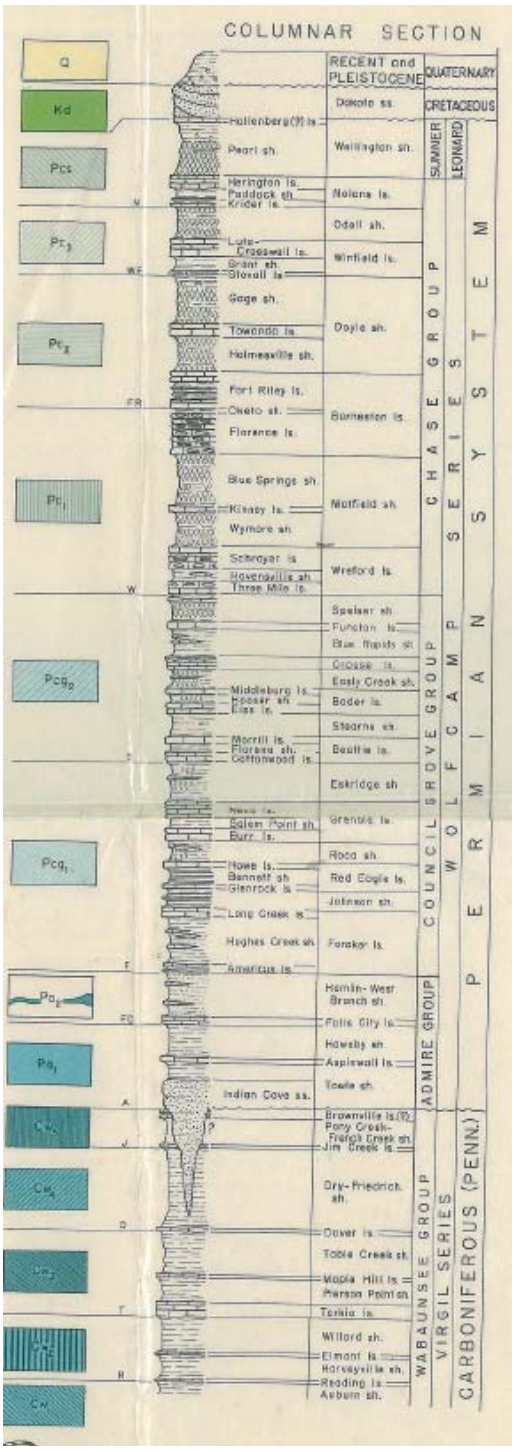


**Figure 3.8-2. Stratigraphic column of geologic formations in Riley and Geary counties, Kansas. Adapted after Jewett, 1941.**

Fort Riley has a continental climate which is characterized by warm to hot summers and cold winters (Brown, 1975). The region experiences abundant sunshine, moderate winds and low to moderate humidity (Brown, 1975). The average annual precipitation is approximately 800 mm (Ingrisano, 2005). The largest part of annual precipitation is received during the spring and early summer seasons (Brown, 1975 and Ingrisano, 2005). The mean annual temperature is 12.94 $^{o}$C (Ruffner, 1974).

The vegetation in the study areas is riparian woodland, and native tall grass prairie in the uplands. The main land use practice on Fort Riley is military maneuvers. These maneuvers take place in designated areas known as training areas and provide the mechanized infantry units the opportunity to practice (Figures 3.8-3 and 3.8-4). In addition, the training areas are co-used for agriculture and as a habitat for wildlife (Ingrisano, 2005). Fort Riley occasionally leases out approximately 200 km$^2$ of land to the public for farming. These areas under agriculture serve as buffer zones against fire around firing ranges (Ingrisano, 2005).

**Figure 3.8-3. Military maneuvers on Fort Riley.**

**Figure 3.8-4. Mechanized infantry units training on Fort Riley.**

The study sites represent a wide range of stream conditions and types.
Selection of study sites was based on the following criteria:

1. Size of stream and type of stream bed.
2. Presence of low water fords and frequency of their use.
3. Location of a stream reach within a watershed, i.e. reaches in the upland and lowland areas.
4. Size of drainage area of the study reaches.

The study areas are located at Fort Riley in the Flint Hills physiographic province of Kansas (Figure 3.8-5).

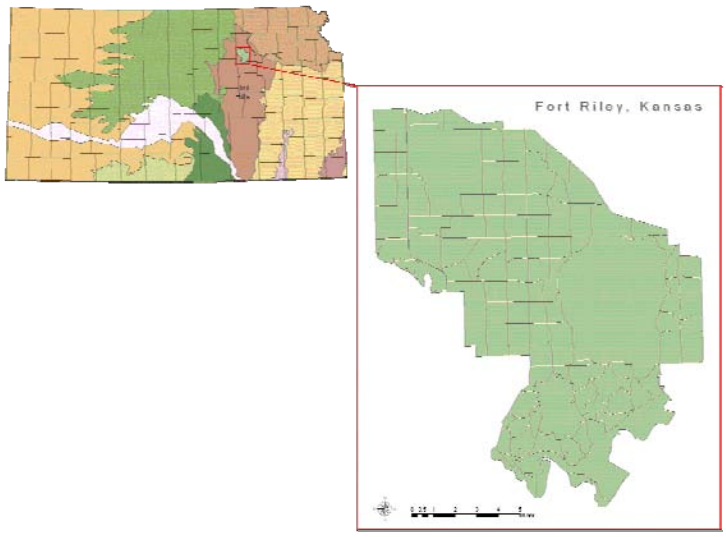


**Figure 3.8-5. Map of Kansas showing different eco-regions. Inset is a map of Fort Riley. Adapted after Ingrisano (2005).**

Six separate study reaches were established. Some were ephemeral streams and others were perennial. For the purpose of this final report a detailed discussion of data collected on the lowland reach of Wind Creek (Figure 3.8-6) will be discussed. The complete data are in the thesis "Analyzing Effects of Low Water Fords on Stream Stability at Fort Riley, Kansas" (Malinga, 2007). Wind Creek is a perennial stream which flows into Wildcat Creek which flows into the Kansas River. The drainage area of the lowland reach of Wind Creek is 20.30 $km^2$.

Figure 3.8-7 shows the location of the study sites on Fort Riley. All the study sites, except for Silver Creek, have hardened low water fords located along the study stream reaches. The Silver Creek site was included in this study because the military plans to construct a low water ford at this study site. Monitoring the Silver Creek study site, before and after a low water ford is constructed provides a basis for tracking changes to the stream brought about by construction and use of a low water ford.

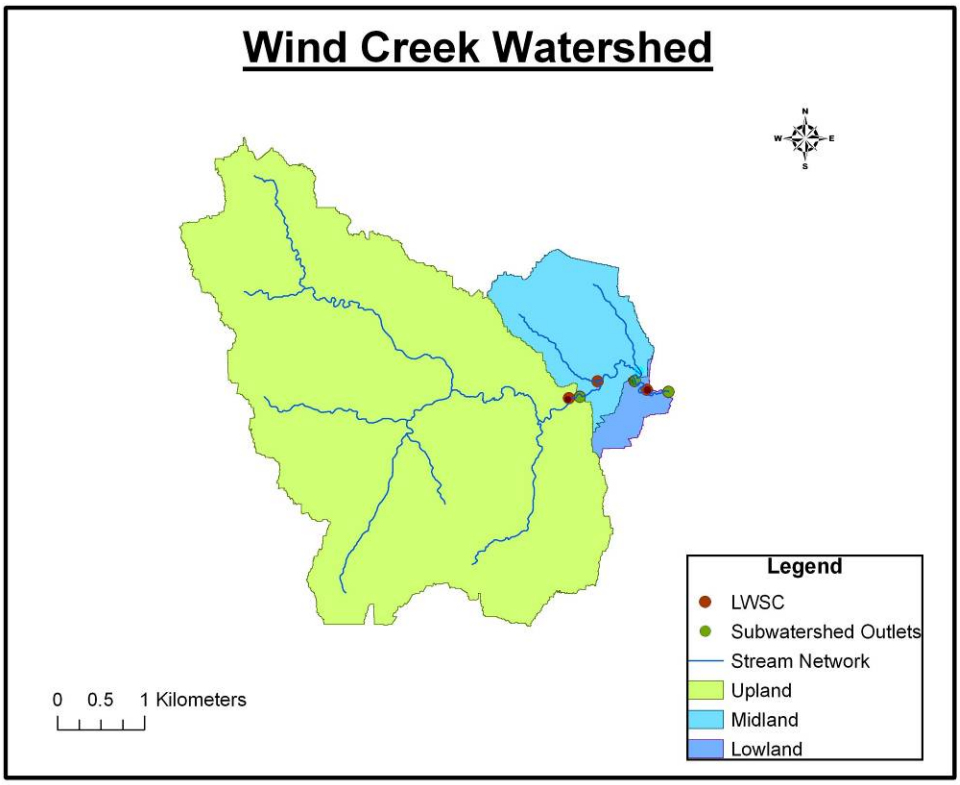


**Figure 3.8-6. Wind Creek watershed, Fort Riley, Kansas.**

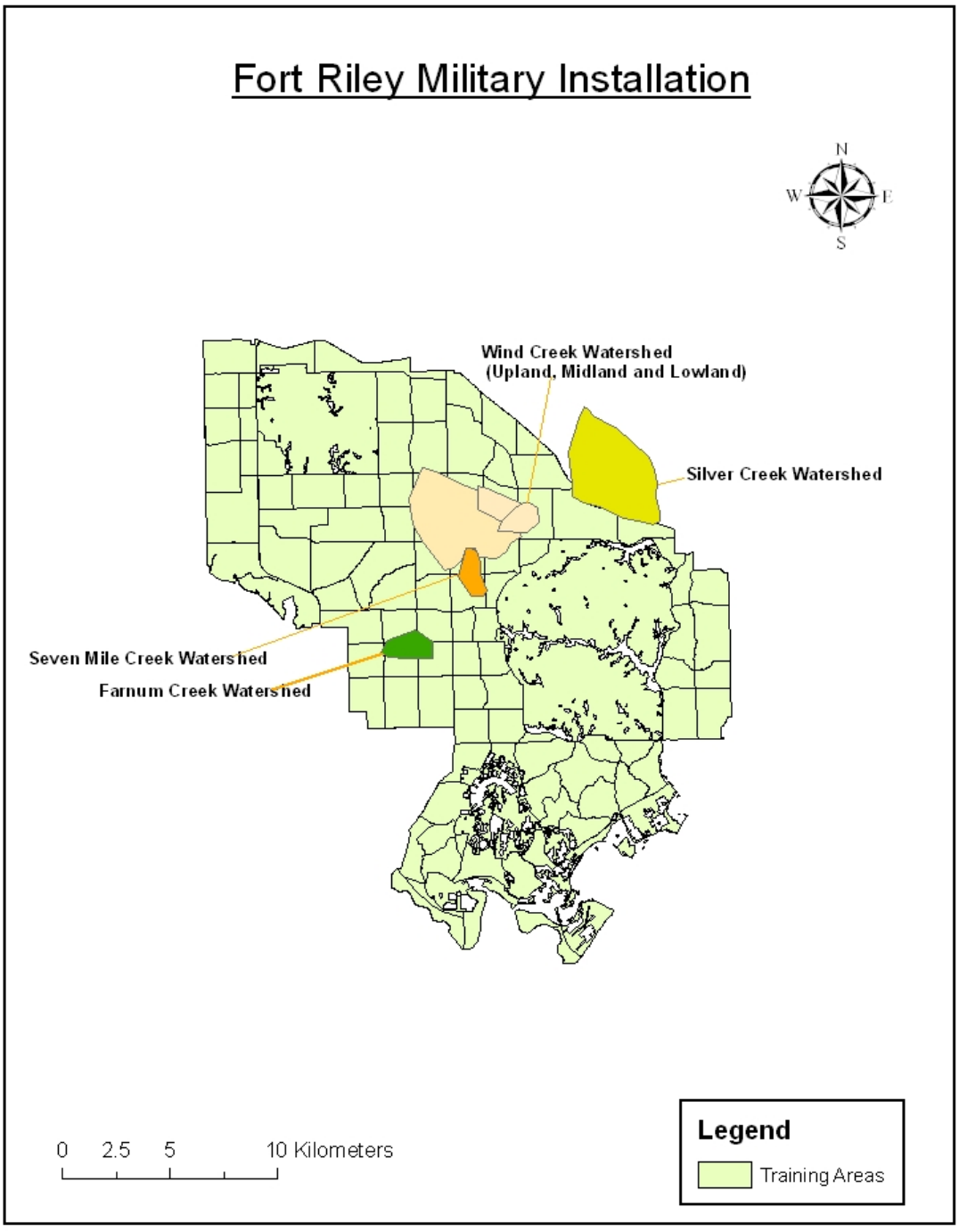


**Figure 3.8-7. Location of study reaches at Fort Riley, Kansas.**

## Stream Classification

Stream reaches selected for the study were surveyed and classified using the Rosgen stream classification system (Rosgen, 1996). The Rosgen stream classification system is a hierarchical methodology that consists of four levels of stream classification. Level I classification provides a broad description of streams based on geomorphic characteristics. Level II classification, characterizes streams with a more detailed morphological description of stream type from field measurements of channel dimensions and bed composition. Level III assessment considers current conditions of the stream by characterizing streams according to stability, potential and function. At Level IV, predicated stream conditions are verified through analysis of stream flows, sediment loads, and additional geomorphic parameters (Rosgen, 1996). The first three levels of the Rosgen stream classification system are used in this study.

## Stream Surveys

### Longitudinal Profile Surveys

A systematic survey of each study reach was performed using conventional survey methods (Harrelson et al., 1994). Longitudinal profile surveys began and ended at riffle crests (head of riffle). Stationing along the longitudinal profile was conducted at 6.1 m intervals or where the stream bed had a change in slope. Sharp changes in channel slope were always observed at transition points (Figure 3.8-8) between the different stream features (i.e. pool, glide, riffle and run). Pools are generally considered the deepest points within a stream, while riffles are the shallow points. Glides and runs are transition features between pools and riffles. Stream bed, water surface and bankfull elevations were established using a laser level and leveling rod with an attached receiver. Stream bed elevations were taken at the deepest points (thalweg) along each stream reach, while bankfull elevations were taken on the active floodplain. Elevations are based on permanent benchmarks established within each study reach. Selected study reaches were approximately 20-30 bankfull widths long. Morphometric parameters determined from the longitudinal profile survey were: bankfull slope, water surface slope (S), channel slope and channel sinuosity (K). Bankfull slope was determined as ratio of the difference in bankfull elevation (between the beginning and end point of each study reach), and the length of the study reach. Channel slope was determined as a ratio of the difference in elevation of the channel bed (between the beginning and end point of each study reach) and the length of study reach. Water surface slope was determined as a ratio of the difference in elevation of the water surface (between the beginning and end point of each study reach) and the length of study reach. Channel sinuosity (K) was determined by computing the ratio between stream reach length and valley length. Repeat longitudinal profile surveys of each reach were conducted to quantify changes in stream bed elevation and slope.

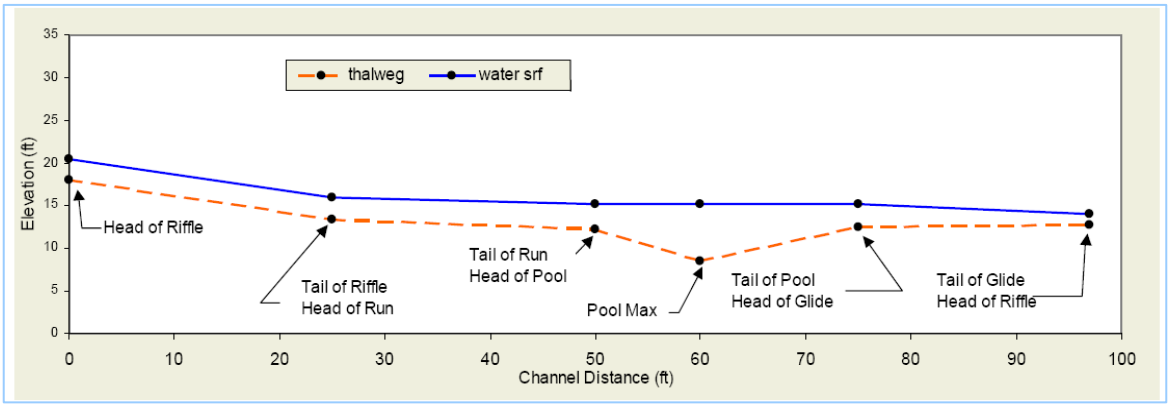


**Figure 3.8-8. Longitudinal profile along a stream reach. Source: Vermont Stream Geomorphic Assessment Phase 3 Handbook, 2003.**

## Cross Section Surveys

Cross section transects were selected along each study reach. The selected cross section transects were at riffles and pools (and sometimes at runs and glides) on each study reach. Cross section transects were monumented with iron rebar on the left and right bank of the channel. With a cam line strung across the channel for stationing, elevation measurements were established across the channel, and tied to benchmarks on the left and right banks of the channel as well as to the longitudinal profile survey. Cross section profiles were then plotted from channel bed elevations and distance measurements (Figure 3.8-9). Bankfull stage (Figure 3.8-10) was identified at each channel cross section surveyed; bankfull stage was taken as the elevation of the active floodplain (Wolman and Leopold, 1957).

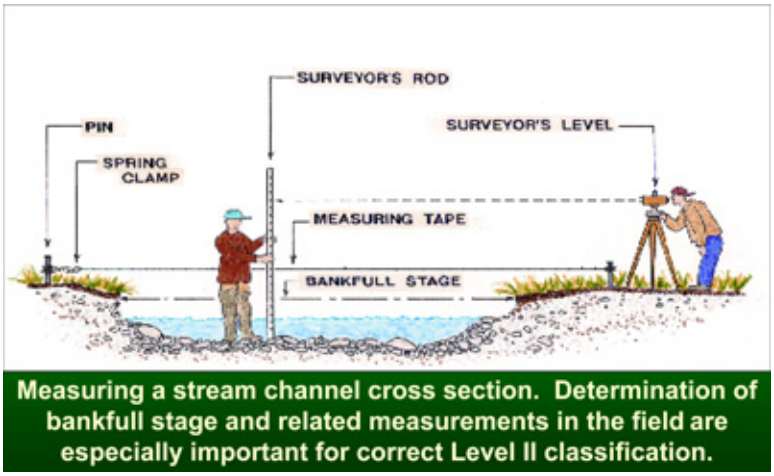


**Figure 3.8-9. Cross section profile. Adapted from Rosgen, 1996.**

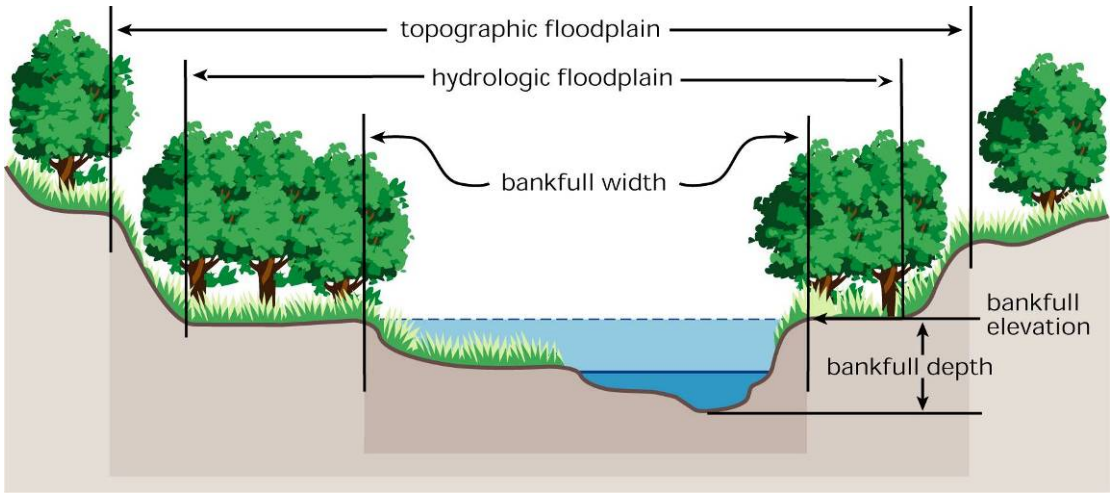


**Figure 3.8-10. Cross section profile showing bankfull stage. Source: Stream Corridor Restoration: Principles, Processes, and Practices, FISRWG (10/1998).**

Morphometric indices computed from the cross section survey data include: bankfull width ($W_{bkf}$), mean bankfull depth ($D_{bkf}$), bankfull area ($A_{bkf}$), width of flood prone area ($W_{fpa}$), bankfull velocity (u), bankfull discharge ($Q_{bkf}$), entrenchment ratio (ER) and width-depth ratio (W/D). Bankfull area was computed as the area of the channel below bankfull stage, while the width of flood prone area was determined at an elevation corresponding to twice the maximum bankfull depth, and entrenchment ratio was computed as a ratio of width of flood prone area ($W_{fpa}$) to bankfull width ($W_{bkf}$). Bankfull width was considered as the channel width corresponding to bankfull stage. Mean bankfull depth was computed by dividing bankfull area by bankfull cross section width. In order to calculate bankfull velocity, a Manning's roughness coefficient of the channel was determined using a relationship (developed by Rosgen, 2006) between channel friction factor (computed from Equation 3.8-1) and Manning's roughness coefficient. Bankfull velocity was computed using Manning's roughness (Equation 3.8-2), while bankfull discharge was computed using Equation 3.8-3. The width-depth ratio indicates the shape of channel cross section while the entrenchment ratio indicates degree of vertical containment of the stream channel (Rosgen, 1996). Bankfull parameters determined from field data were validated using regional curves (Leopold, 1953) developed for the Kansas Flint Hills (Kansas State Conservation Commission, 2005).

$$\frac{u}{u^*} = \left[ 2.83 + 5.66 \times Log\left( \frac{R}{D_{84}} \right) \right] \qquad \text{[Eq. 3.8-1]}$$

$$u = \frac{1}{n} \times R^{2/3} \times S^{1/2} \qquad \text{[Eq. 3.8-2]}$$

$$Q = u \times A_{bkf} \qquad \text{[Eq. 3.8-3]}$$

where:

$\frac{u}{u^*}$ = friction factor
u = Bankfull velocity (m/s)
$A_{bkf}$ = Bankfull Area ($m^2$)

R = Hydraulic radius of the channel (R = $A_{bkf}$/ bankfull channel wetted perimeter (P)) (m)
S = Channel slope (m/m)
$D_{84}$ = Bed material size of a particle size of the $84^{th}$ percentile (mm).
n = Manning's roughness coefficient for the channel
Q = Bankfull discharge ($m^3/s$)

Repeat surveys of the cross section transects were conducted in the summer of 2007 (June-July) to determine rates of lateral and vertical migration of the stream channels. These rates of migration were quantified by measuring the net percentage change in channel cross section area (determined using Equation 3.8-4). A negative value indicates aggradation, while a positive value indicates degradation.

$$(\Delta A\%) = \frac{A_{after} - A_{before}}{A_{before}} \times 100 \qquad \text{[Eq. 3.8-4]}$$

where:

$\Delta$ A% = Net percentage change in channel cross section area
$A_{after}$ = Channel cross section area from 2007 survey
$A_{before}$ = Channel cross section area from 2006 survey

**Bed Material Characterization**

**Reach Pebble Count**

A modified Wolman pebble count (Wolman, 1954) was conducted at each study site to determine the particle size distribution in each study reach. The reach pebble count (detailed procedure is presented in Rosgen, 2007) was stratified such that a representative sample was collected from each reach. One hundred particles were collected and their median axis measured and recorded. A particle size distribution curve was plotted using the data collected. Information derived from the particle size distribution curve (from the reach pebble count) was later used during classification of the streams.

**Active Bed Pebble Count**

The active bed pebble count characterizes bed material at a riffle (Rosgen, 2007). One hundred particles were collected (from the active bed at the riffle) and their median axis measured and recorded. A particle size distribution curve was plotted using the data collected. Information derived from the particle size distribution curve (from the active bed pebble count) was later used in velocity and sediment competence calculations.

**Bar Core Sample**

Additionally, bar core samples were collected from point bars (at a position on the downstream third of a point bar between bankfull stage and thalweg), (Figure 3.8-11) at the Farnum Creek, Silver Creek, and Wind Creek study sites to determine the size of sediment particles available for entrainment at bankfull discharge. According to Rosgen, 2006, the bar core sample represents the size gradation of bedload at bankfull stage. Data from the bar core sample was analyzed to

determine sediment transport competence of each reach. A detailed procedure used for the bar core sample collection and analysis is presented by Bunte and Abt (2001), US EPA (2006), and Rosgen (2006). A brief description of the procedure is presented below:

1. The bar sample was collected from a location, on the downstream third of a point bar, between the thalweg and bankfull stage (Figure 3.8-11).
2. Two largest particles on the surface of the bar sample location were collected, and their median axes and weights were measured and recorded.
3. Using a bottomless bucket, to define the area where the sample would be collected, bed materials were excavated up to a depth of twice the diameter of the largest surface particle measured in step 2 above.
4. Excavated materials were collected and weighed. Materials were then wet sieved (Figure 3.8.-12) using sieves of sizes 63 mm, 31.5 mm, 16 mm, 8 mm, 4 mm and 2 mm. Net weights of materials retained on each sieve were measured and recorded.
5. Particle size distribution curve was then developed by plotting cumulative weights of materials (passing each sieve) against particle size. The particle size class index $D_{50}$ was then determined from the curve.

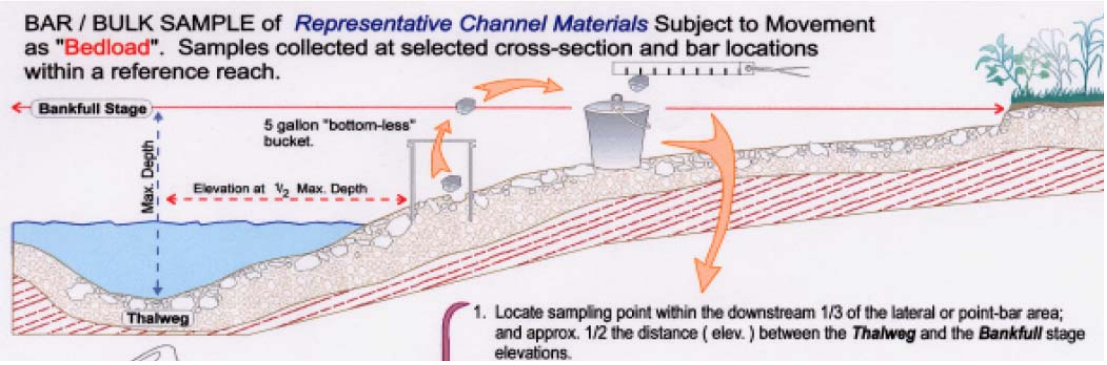


**Figure 3.8-11. Bar sample collection and analysis. Source: Rosgen (2006).**

**Figure 3.8-12. Sieve analysis of a bar core sample at Silver Creek, Keats.**

**Scour Chain Surveys**

Scour chains can be used to measure the amount of scour or fill at riffles and glides. In order to measure the amount of scour or fill along a reach, chains were installed into the stream bed at a riffle, upstream and downstream within each study reach. The scour chains were driven flush with the stream bed (Figure 3.8-13) and elevations of scour chain locations were taken. The two largest particles in the vicinity of each chain were measured and recorded. Repeat surveys (Figure 3.8-14) of the chains were conducted to measure the amount of scour or fill at a particular riffle along a study reach. Chains were resurveyed by measuring the length of chain exposed or buried into the stream bed, after major flow events. Again, the two largest particles in the vicinity of the chains were measured.

**Figure 3.8-13. Installing a scour chain at riffle on Wind Creek, upland reach.**

**Figure 3.8-14. Repeat survey of scour chains at Wind Creek upland reach.**

**Stream Bank Surveys**

Stream bank erosion monitoring was conducted at each study reach. Bank erosion monitoring was conducted by establishing permanent bank transects along each study reach. These bank transects were established in the summer of 2006. The bank transects were selected to represent a range of stream bank conditions along each study reach. At each transect, erosion pins (12.7mm diameter and 0.61m long) were installed in the bank (Figure 3.8-15), with the bottom most pin at an elevation of 0.30 m above a toe pin (installed into stream bed) and subsequent pins at elevations of 0.61 m apart. The erosion pins were driven into the stream bank with a hammer until the pins were flush with the stream bank. By placing a plumb survey rod on top of the toe pin (Figure 3.8-15), horizontal distance measurements (between the stream bank and the edge of the vertical survey rod) were determined using a pocket rod (with a spirit level attached to the pocket rod). The process was repeated at incremental elevations of 0.15 m along the vertical survey rod placed on the toe pin, each time the vertical distance and corresponding horizontal distance was measured and recorded. A bank profile of each transect was developed by plotting the vertical distance against horizontal distance. Using the same procedures above, repeat surveys of the bank transects were conducted (in the summer of 2007) to measure the actual rates of lateral migration of the stream bank transects surveyed in 2006. The length of erosion pins exposed (at each bank transect) was also measured and recorded. The pins were then pounded flush with the stream bank.

In order to estimate the amount of annual erosion generated from stream banks in each of the study reaches, the Bank Erosion Hazard Index (BEHI) and Near Bank Stress (NBS) ratings (Rosgen, 1996, 2001a, 2006, and US EPA, 2006) of each bank transect surveyed were determined. The BEHI characterizes stream banks according to following variables: stream bank height, bankfull height, root depth, root density, surface protection, bank materials, and bank angle. The NBS is the stress placed on near bank region associated with the stream bank transects being evaluated (Rosgen, 2001a, 2006, and US EPA, 2006). The NBS rating characterizes a stream bank transect according to its location within the reach. The BEHI variables and NBS condition for each bank transect were evaluated and recorded. Using the methods presented in Level III of the Rosgen stream classification system (1996, 2001a, and 2006), cumulative BEHI and NBS ratings were determined for each bank transect. Bank erosion rates were estimated using Colorado data, Rosgen (1996) and the computed BEHI and NBS ratings at each bank transect. The Colorado rating curves were used to estimate bank erosion rates because of the lack of bank erosion prediction curves for the Flint Hills region.

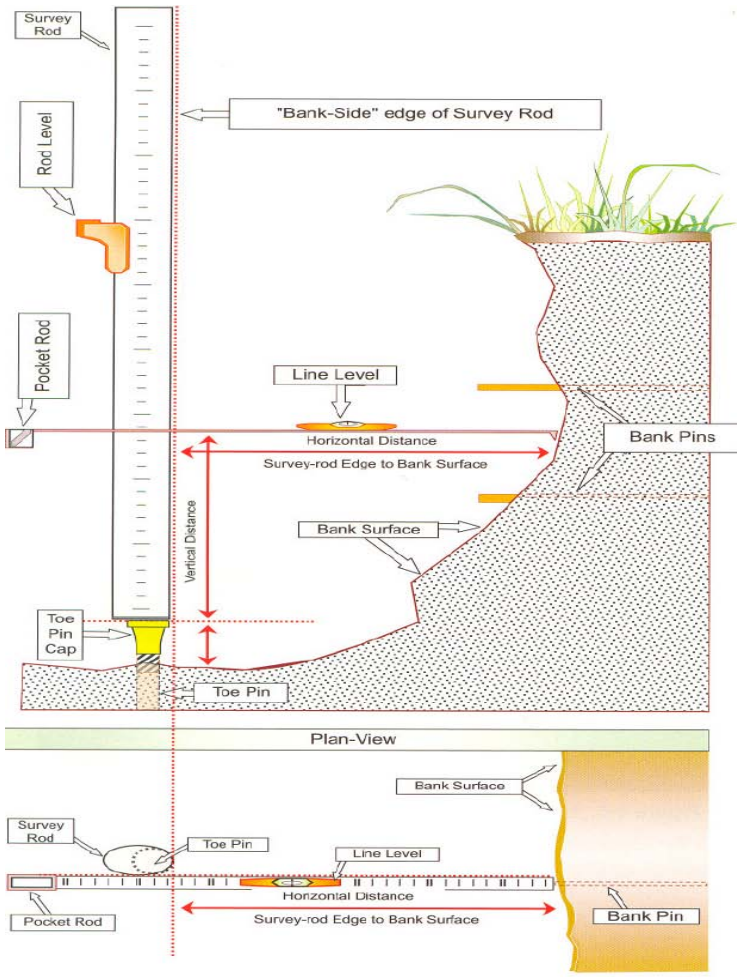


**Figure 3.8-15. Measurement of stream bank profile. Source: Rosgen (1996).**

**Sediment Competence**

A stream in equilibrium is able to move its sediment and discharge in such a manner that it maintains its pattern, profile and dimension, without aggrading or degrading (Rosgen, 1996). Entrainment calculations were performed to determine the stability of each study reach. This was accomplished by determining the channel depth and slope necessary for the entrainment of the largest particle on the downstream a third of a point bar at a location between bankfull stage and the thalweg. The critical dimensionless shear stress ( $\tau_c$ ), (Andrews, 1984; Rosgen, 2006) was computed at bankfull stage from Equation 3.8-5 while bankfull shear stresses were computed using Equation 3.8-6. The bankfull mean depth and water surface slope (necessary for entrainment of the largest particle on the downstream third of a point bar at a location between bankfull stage and the thalweg) are calculated from Equations 3.8-7 and 3.8-8, respectively. Equation 3.8-9 was used to calculate the size of the largest particle entrained by bankfull shear stress.

$$\tau_c = 0.0384 \times \left[ \frac{D_{50}}{Db_{50}} \right]^{-0.887} \quad \text{[Eq. 3.8-5]}$$

$$\tau_b = \rho_w \times g \times R \times S \quad \text{[Eq. 3.8-6]}$$

$$D_r = \tau_c \times \gamma \times \frac{D_i}{S} \quad \text{[Eq. 3.8-7]}$$

$$S_r = \tau_c \times \gamma \times \frac{D_i}{D_{bkf}} \quad \text{[Eq. 3.8-8]}$$

$$D_{ib} = 152.02 \times \tau_c^{0.7355} \quad \text{[Eq. 3.8-9]}$$

where:

$\tau_b$ = Bankfull shear stress ($N/m^2$)

$\tau_c$ = Critical shear stress

g = Gravitational acceleration ($m^2/s$)

$\gamma$ = Submerged specific weight of sediment

$\rho_w$ = Density of water ($kg/m^3$)

R = Hydraulic radius (m)

$S_b$ = Existing bankfull water surface slope (m/m)

$S_r$ = required bankfull water surface slope (m/m)

$D_{50}$ = Median size particle from reach pebble count (mm)

$D_{A50}$ = Median size particle from active bed pebble count (mm)

$D_{s50}$ = Median particle size from bar sample (mm)

$D_l$ = Largest particle from bar sample (mm)

$D_{le}$ = Largest particle entrained by available bankfull shear stress (mm)

$D_{Rbkf}$ = Bankfull mean depth required for entrainment of largest particle (m)

$D_{bkf}$ = Existing bankfull mean depth (m)

**Mapping of Roads and Stream Crossings**

Approach roads are critical areas that often act as conduits for sediment laden storm runoff generated from upland areas and delivered to stream channels. Fort Riley has approximately eighty hardened fords across the training ranges. Fords are considered sources of sediment (Figures 3.8-16 and 3.8-17) delivered into streams through approach roads leading to stream crossing locations (Milauskas, 1988; Thompson et al., 1989; Brown, 1994; Sample et al., 1998; Blinn et al., 1999). Due to the poor state of some of the approach roads, sediment is generated from the roads and deposited at stream crossing sites. Roads were surveyed to develop a better understanding of erosion dynamics on these roads. Road slopes, vegetation and erosion variables were determined at each of the study sites. Stream crossings were also mapped to determine the area of the stream prone to traffic disturbance.

**Figure 3.8-16. Gully forming on a road leading to stream crossing site.**

**Figure 3.8-17. Approach roads can be a source of sediment.**

## 3.8.b. RESULTS AND ACCOMPLISHMENTS

Six separate study reaches were established. For the purpose of this final report a detailed discussion of data collected on the lowland reach of Wind Creek will be discussed. The complete data are in the thesis "Analyzing Effects of Low Water Fords on Stream Stability at Fort Riley, Kansas" (Malinga, 2007).

### Wind Creek, Lowland Reach

### Stream Classification

Morphometric variables listed in Table 3.8-1 were used for classifying the Wind Creek, lowland study reach Wind Creek lowland reach was classified as an F4 stream type. Streams of F4 classification have gentle channel slopes and are entrenched channels (with high width-depth ratio) with gravel dominated beds. A stream of F4 classification has well developed pool-riffle morphology. This stream reach, like any unstable F4 stream has accelerated rates of stream bank erosion at locations below the stream crossing. Locations above the stream crossing experienced moderate bank erosion rates due to the good stability of the stream banks in these locations. The dense vegetation on these banks plays a role in reducing the amount of bank erosion at these locations. This reach is located in valley type VIII, considered to have a wide and gentle slope with well developed floodplain adjacent to river terraces (Rosgen, 1996). Table 3.8-2 shows the variables used in the calculation of bankfull velocity and discharge at this reach.

**Table 3.8-1. Stream Classification Protocol for Wind Creek Lowland Reach.**

| Morphometric Variable | Magnitude | Units |
|---|---|---|
| **Bankfull Width ($W_{bkf}$)**<br>Width of the stream channel at bankfull stage elevation, in a riffle section. | 10.07 | m |
| **Bankfull Depth($d_{bkf}$)**<br>Mean depth of the stream channel cross-section, at bankfull stage elevation, in a riffle section ($d_{bkf}$ = A / $W_{bkf}$). | 0.80 | m |
| **Bankfull Cross Section Area ($A_{bkf}$)**<br>Area of the stream channel cross-section, at bankfull stage elevation, in a riffle section. | 8.09 | $m^2$ |
| **Width/Depth Ratio ($W_{bkf}$ /$d_{bkf}$)**<br>Bankfull width divided by bankfull mean depth, in a riffle section. | 12.52 | m/m |
| **Maximum Depth($d_{mbkf}$)**<br>Maximum depth of the bankfull channel cross-section, or distance between the bankfull stage and Thalweg elevations, in a riffle section. | 1.22 | m |
| **Width of Flood-Prone Area ($W_{fpa}$)**<br>Twice maximum depth, or (2 x $d_{mbkf}$) = the stage/elevation at which flood-prone area width is determined in a riffle section. | 13.73 | m |
| **Entrenchment Ratio (ER)**<br>The ratio of flood-prone area width divided by bankfull channel width ($W_{fpa}$ / $W_{bkf}$) (riffle section). | 1.36 | m/m |
| **Channel Materials (Particle Size Index ) $D_{50}$**<br>The $D_{50}$ particle size index represents the mean diameter of channel materials, as sampled from the channel surface, between the bankfull stage and Thalweg elevations. | 52 | mm |
| **Water Surface Slope (S)**<br>Channel slope = "rise over run" for a reach approximately 20–30 bankfull channel widths in length, with the "riffle-to-riffle" water surface slope representing the gradient at bankfull stage. | 0.0032 | m/m |
| **Channel Sinuosity (k)**<br>Sinuosity is an index of channel pattern, determined from a ratio of stream length divided by valley length (SL / VL); or estimated from a ratio of valley slope divided by channel slope (VS / S). | 1.89 | m/m |
| ***Stream Type*** | **F4** | |

**Table 3.8-2. Bankfull Discharge Variables at Wind Creek, Lowland Reach.**

| Variable | Magnitude |
|---|---|
| $W_{bkf}$ (m) | 10.07 |
| $D_{bkf}$ (m) | 0.80 |
| $W_{pbkf}$ (m) | 11.67 |
| $A_{bkf}$ (m) | 8.09 |
| R (m) | 0.69 |
| $D_{84}$ (mm) | 89 |
| $R/D_{84}$ | 7.80 |
| S (m/m) | 0.0032 |
| u* | 0.148 |
| u (m/s) | 1.20 |
| u/u* | 7.40 |
| n | 0.0380 |
| $Q_{bkf}$ ($m^3/s$) | 9.40 |

**Changes in Stream Geometry**

Tables 3.8-3 through 3.8-4 show channel geometry data collected. Figure 3-8.18 shows a comparison of changes in channel cross section area for cross section transects above and below the stream crossing. The changes at these cross section transects indicate fill or/and scour. The changes in cross section area at the Wind Creek lowland reach ranged from moderate to large. As shown in Figure 3.8-18, the cross section transects above the stream crossing indicated moderate change while the transects below the stream crossing indicated fairly large change. Cross section transect 7, immediately below the stream crossing, indicated a 5.1% change in cross sectional area due to bank erosion (average of 0.39 m/yr) on the left bank. Further downstream, cross section transect 8 indicated 18.6% increase in channel cross section area. These changes were associated with scour at the stream bed and bank erosion on the left bank. Cross section transect 9 indicated moderate scour at the thalweg (0.61m increase in thalweg depth) and deposition on the left bank. Cross section transects 10 and 11 indicated moderate fill and slight scour respectively. Results from the scour chains at cross section transects 1, 9 and 11 corroborate the findings from the cross section survey. The major changes in cross section area observed at cross section locations immediately below the stream crossing suggest that the stream crossing could be causing some of this change. The stream crossing at this reach is located in a meander bend, between cross section transects 6 and 7. The stream crossing at this location changes the alignment of stream flow during high flow events. This change in flow alignment has increased the energy slope along locations below the stream crossing. The altered energy slope has increased the magnitude of available stream power thereby increasing the rates of channel bed scour and bank erosion at locations in the vicinity and below the stream crossing. The results from the longitudinal profile survey corroborate findings from the cross section survey. Moderate changes in stream bed elevation were observed at locations above the stream crossing, while locations below the stream crossing indicated significant change. No appreciable change in channel slope was observed at this reach.

**Table 3.8-3. Changes in cross sectional area between the original survey (2006) and the resurvey in 2007 at Wind Creek, Lowland Reach.**

| Study Reach | Cross section number | Cross section designation | Change in cross section area ($m^2$) | Percent change in cross section area (%) |
|---|---|---|---|---|
| Wind Creek (Lowland) | 1 | Riffle | 0.62 | 1.7 |
| | 2 | Pool | 0.05 | 0.2 |
| | 3 | Riffle | 0.28 | 0.9 |
| | 4 | Pool | 1.27 | 3.1 |
| | 5 | Riffle | 0.73 | 2.5 |
| | 6 | Run | 1.66 | 5.5 |
| | 7 | Riffle | 2.25 | 5.1 |
| | 8 | Pool | 5.28 | 18.6 |
| | 9 | Run | 0.14 | 0.5 |
| | 10 | Pool | -0.96 | -2.7 |
| | 11 | Riffle | 0.78 | 1.6 |

[Negative values indicate fill while positive values indicate scour].

**Table 3.8-4. A summary of channel geometry variables at Wind Creek, Lowland Reach.**

| Study Reach | Number of cross section transects | Range of width (m) | Range of depth (m) | Number of cross sections | |
|---|---|---|---|---|---|
| | | | | Fill | Scour |
| Wind Creek, lowland | 11 | 12.8-16.8 | 2.9-4.4 | 1 | 10 |

**Table 3.8-5. A comparison of changes in channel cross section area between cross section transects above and below stream crossing at Wind Creek, Lowland Reach.**

| Study Reach | Average change in cross section area (above ford), ($m^2$) | | Average change in cross section area (below ford), ($m^2$) | | Average change in cross section area for whole reach ($m^2$) | |
|---|---|---|---|---|---|---|
| | Riffle | Pool | Riffle | Pool | Riffle | Pool |
| Wind Creek, lowland | 0.82 | 0.66 | 1.06 | 2.16 | 0.94 | 1.41 |

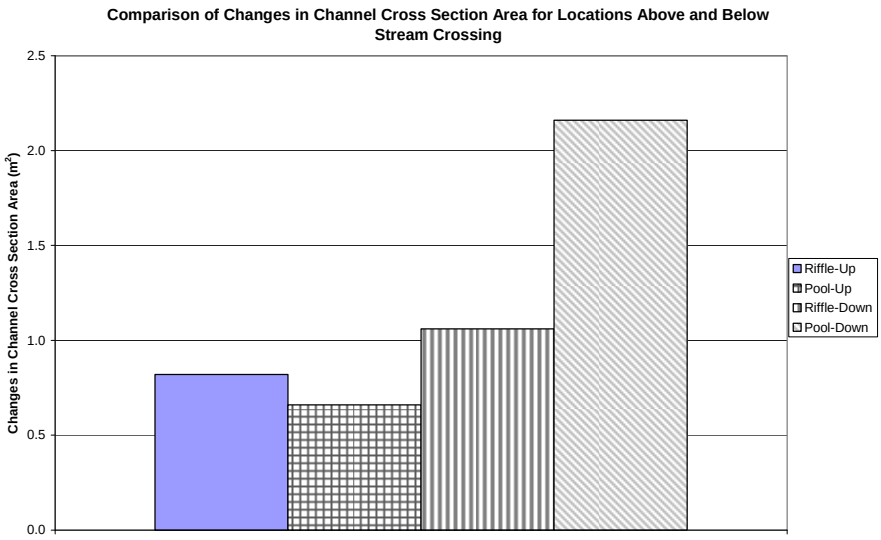


**Figure 3.8-18. A comparison of changes in channel cross section area for cross section transects above and below stream crossing at Wind Creek, lowland reach.**

## Changes in Bed Material Composition

Results of the reach pebble count (Table 3.8-6) indicated a significant shift towards more coarse sediment. This shift in sediment size is due to the replacement of finer sediment (previously stored in pools) with coarse sediment transported from the upstream locations. Results from the active bed count at cross section transects 1 and 11 also indicated a shift towards coarser sediment at the riffles.

**Table 3.8-6. Changes in particle size distribution from reach pebble count at Wind Creek, Lowland Reach.**

| | Particle Size (mm) | | | | |
|---|---|---|---|---|---|
| Year | $D_{35}$ | $D_{50}$ | $D_{84}$ | $D_{95}$ | $D_{100}$ |
| 2006 | 2 | 22.6 | 82 | 140 | 180 |
| 2007 | 28 | 54 | 150 | 220 | 512 |

## Stream Bank Surveys and Bank Erosion Prediction

The BEHI and NBS ratings developed for the Wind Creek lowland study reach are shown in Table 3.8-7. There was a difference in BEHI ratings between the bank transects above and below the stream crossing at this study reach. The NBS rating was the same for bank transects upstream and downstream from the stream crossing. High and extreme BEHI and NBS ratings indicate increased potential for stream bank erosion as well as stream bank instability. Table 3.8-8 shows the predicted and measured bank erosion rates and annual sediment yield. The predicted bank erosion rate (using Figure 3.8-19) lies within the range of the bank erosion rates measured at this study reach.

**Table 3.8-7. BEHI and NBS ratings of bank transects at Wind Creek, Lowland Reach.**

| Study Reach | BEHI Rating | | NBS Rating | |
|---|---|---|---|---|
| | Upstream | Downstream | Upstream | Downstream |
| Wind Creek, Lowland | High | Very High | Extreme (6) | Extreme (6) |

**Table 3.8-8. Predicted and measured bank erosion rates at Wind Creek, Lowland Reach.**

| Study Reach | Predicted Annual Bank Erosion Rates (m/yr) | Actual Annual Bank Erosion Rates (m/yr) | Actual Annual Sediment Yield (kg/m/yr) |
|---|---|---|---|
| Wind Creek, lowland | 0.40 | 0.23-0.65 | 880 |

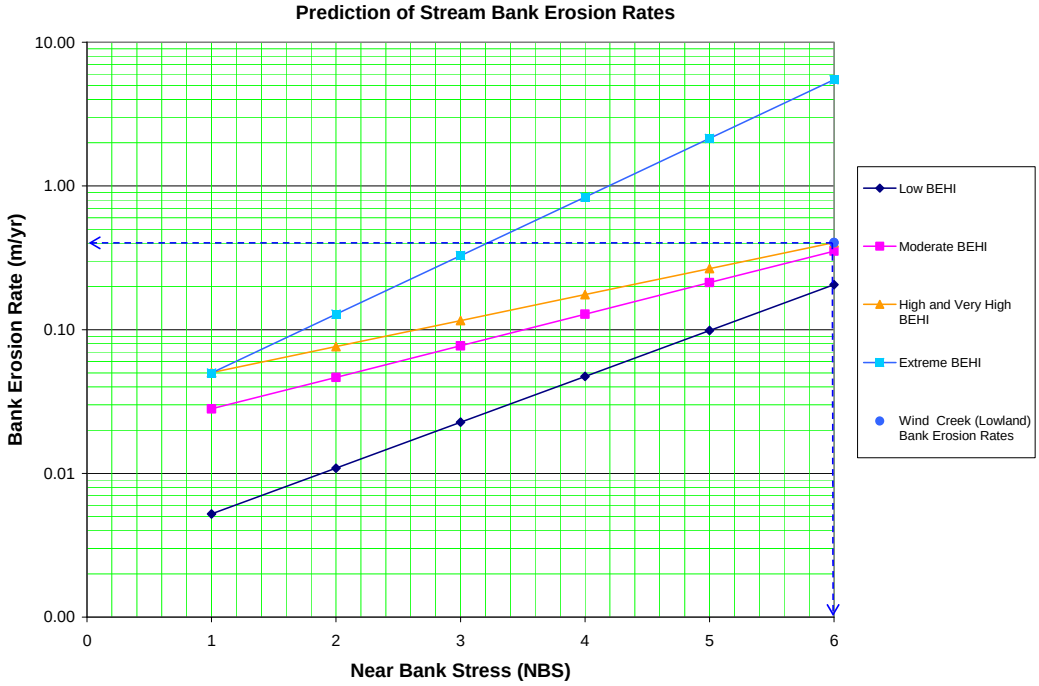


**Figure 3.8-19. Relationship of BEHI and NBS ratings used to predict annual stream bank erosion rates on Wind Creek, lowland reach. Adapted after Rosgen (1996 & 2006).**

The measured bank erosion rates and annual sediment yield (Table 3.8-8) at Wind Creek lowland reach were quite high due to the increased stream discharge (attributed to increase in drainage area), high frequency and magnitude of flow events experienced in March-June, 2007 period. The stream crossing also contributes to the increase in bank erosion rates in the downstream locations of this study reach. Based on runoff estimates (Figure 3.8-21) from March-June 2007 precipitation data, it is shown that this stream reach experienced at least three bankfull events (with 1.4 year return interval) and two events higher than bankfull stage (each with approximately a 4 year return interval). Figure 3.8-22 shows a relationship between the peak flow rates and their corresponding percent non exceedance for the Wind Creek lowland reach. In comparing precipitation totals (Figures 3.8-20) over the previous eleven years, it is indicated that the 2007 rainfall season had significantly higher precipitation totals due to the high frequency and magnitude of precipitation events observed. Given the high magnitude, frequency and duration of the precipitation events observed during the 2007 rainfall season, bank erosion rates of a high magnitude were observed.

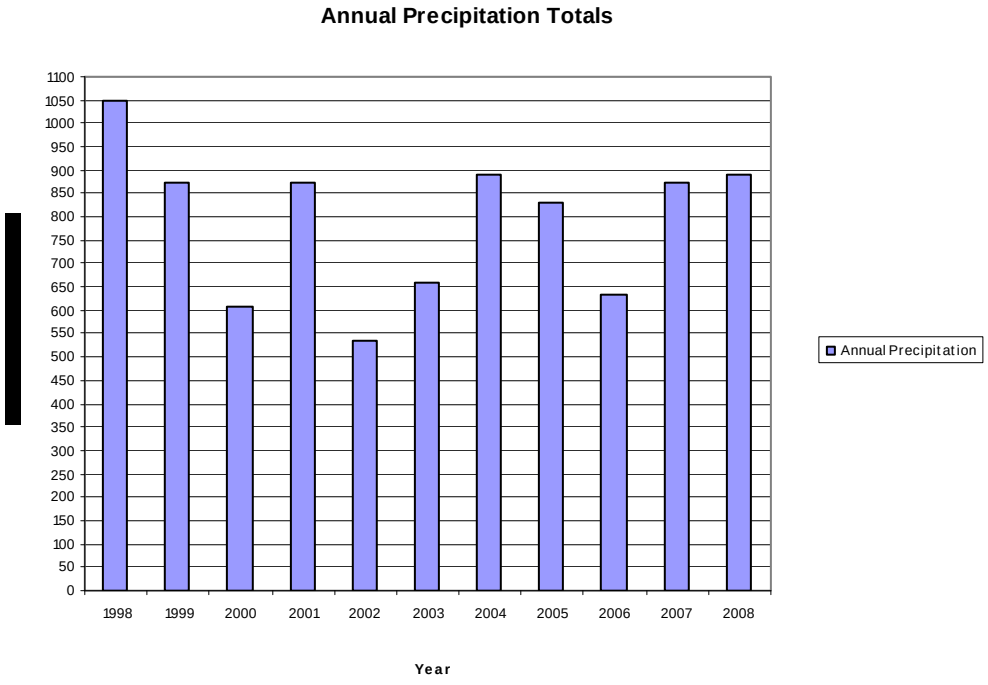


**Figure 3.8-20. Annual precipitation totals at Manhattan Airport, Kansas. Source: Knapp (2008).**

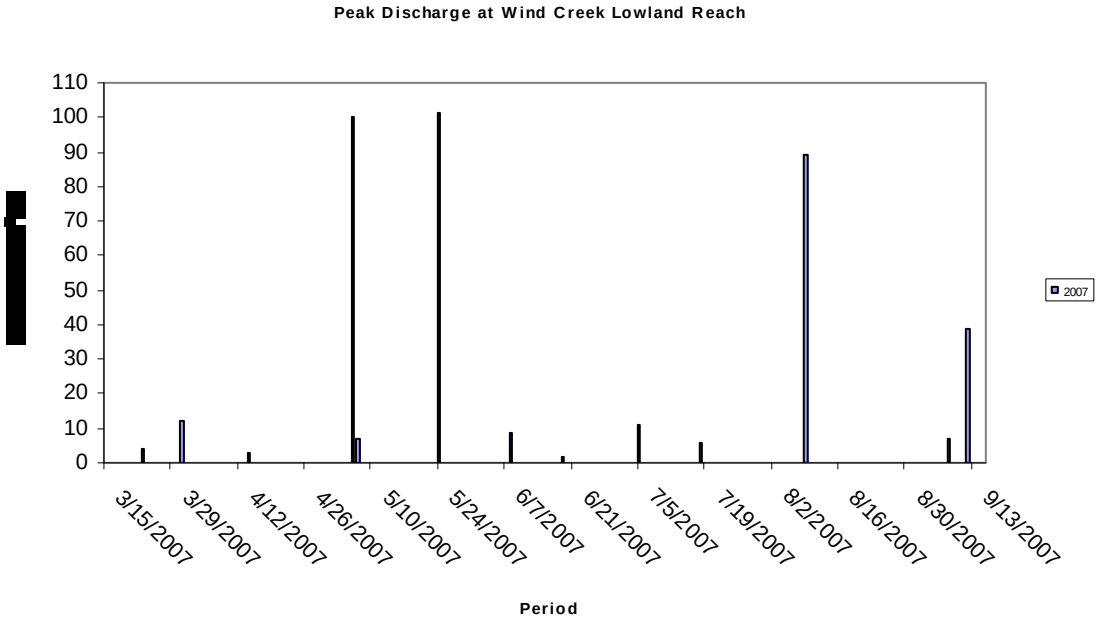


**Figure 3.8-21. Estimated peak stream discharge observed during March-June, 2007 at Wind Creek lowland watershed.**

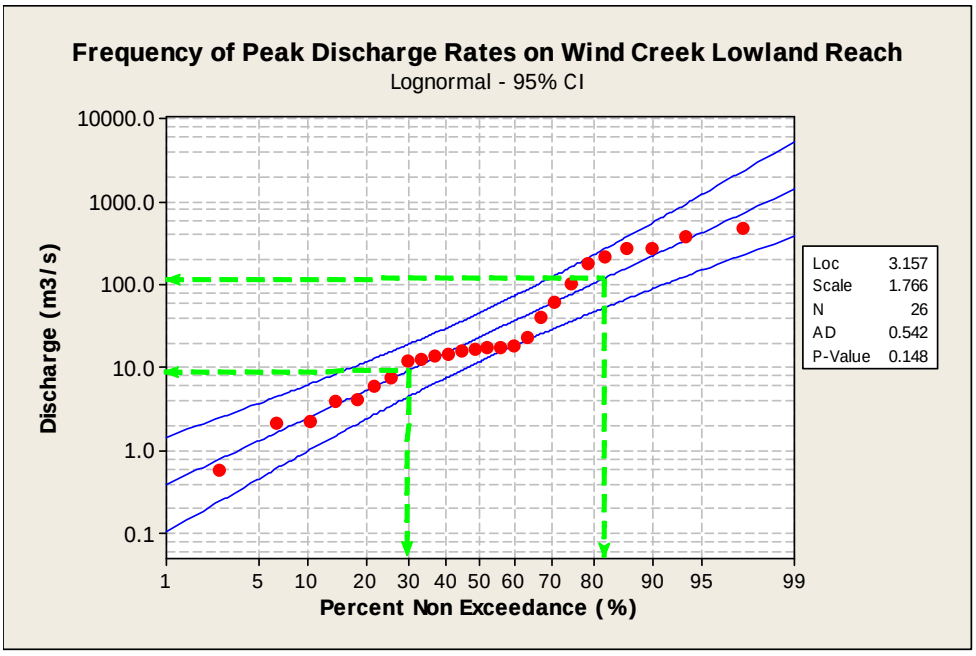


**Figure 3.8-22. Frequency of peak stream flow rates at Wind Creek Lowland reach.**

Figure 3.8-23 shows a comparison of sediment yield from stream segments upstream and downstream of a low water ford at this study reach. The sediment yield generated from locations below the stream crossing at this study reach was approximately three times greater than the sediment yield generated from the stream segments above the stream crossing. As mentioned previously, the stream crossing at this study reach could potentially be causing the high rates of bank erosion at locations below the stream crossing. However, erosion rates generally increase in the downstream direction because discharge (and stream power) increases in the downstream direction. This trend (downstream increase in erosion rates) has a tendency to mask the impact of any other factors contributing to the increase in bank erosion rates in the downstream direction. A poorly constructed low water ford for example, can alter the direction of stream flow in such a manner that stream banks immediately below the crossing are subjected to increased shear stresses. Increased shear stresses on the stream banks leads to high rates of bank erosion. Because of the downstream increase in erosion rates, it is therefore difficult to apportion the magnitude of bank erosion (along the downstream location of a reach) caused by poorly located constructed stream crossings. It is also worth noting that stream crossings concentrate runoff from upland areas, increasing the amount of runoff and sediment discharged into streams. Increased runoff and sediment entering streams poses a potential of causing stream instability. Increased sediment in streams has adverse impacts on aquatic life as well as water quality.

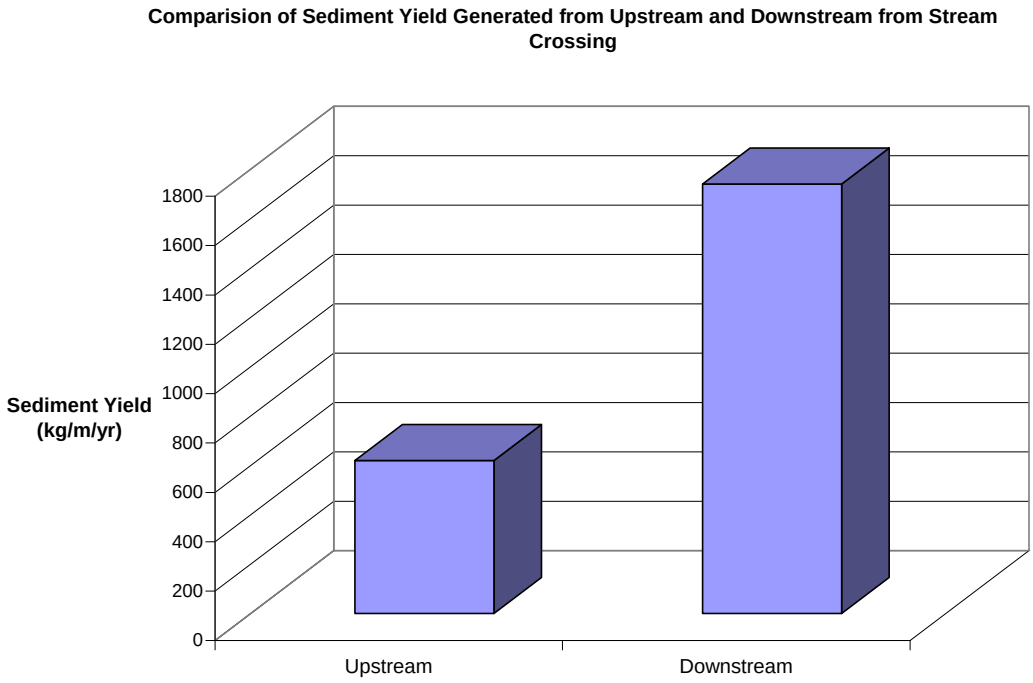


**Figure 3.8.-23. A comparison of sediment yield between upstream and downstream locations from stream crossing at Wind Creek, lowland reach.**

It is also interesting to note that the Wind Creek lowland reach generated a higher sediment yield compared to Silver Creek which is also an F4 stream type draining a large area. The different land use types on these two watersheds, partly explain the difference in bank erosion rates at the two sites. Silver Creek has no stream crossings and drains an agricultural watershed (with best management practices) while Wind Creek lowland reach drains areas heavily disturbed by military training exercises and has stream crossings. Military training exercises disturb soil and vegetation, making the land susceptible to high rates of runoff and as well as soil erosion. Increased runoff from military training areas and stream crossings has an impact on the Wind Creek lowland reach, possibly causing the increased stream instability.

## Sediment Competence

The results of sediment competence calculations at the Wind Creek lowland reach are shown in Table 3.8-9. These results suggest that this reach lacks adequate slope and mean bankfull depth required to entrain the largest particle on the downstream a third of the point bar at a location between the thalweg and bankfull. This implies that the reach lacks adequate stream power to transport its sediment and channel aggradation is predicted to occur as the stream tries to adjust its slope and depth to a stage where stream equilibrium is restored. However, field observations indicate that this stream reach has the potential to transport its sediment without any adverse impacts on the stream. Furthermore, results from the longitudinal profile and channel geometry surveys show no signs of major aggradation along the stream reach. Additional field studies are required to resolve these discrepancies.

**Table 3.8-9. A summary of sediment competence variables at Wind Creek lowland study reach.**

| Variable | $S_b$ (%) | $S_r$ (%) | $D_{bkf}$ (m) | $D_{Rbkf}$ (m) | $D_{s50}$ (mm) | $D_{A50}$ (mm) | $D_{50}$ (mm) | $D_l$ (mm) | $D_{le}$ (mm) | $T_c$ | $T_b(N/m^2)$ |
|---|---|---|---|---|---|---|---|---|---|---|---|
| Magnitude | 0.32 | 0.41 | 0.80 | 1.03 | 29 | 48 | 52 | 100 | 95 | 0.020 | 25.39 |

**Stream Channel Successional Changes**

The Wind Creek lowland reach classified as an F4 stream type shows signs of channel adjustment in the lower locations of the study reach. This reach is probably at the end of the F4 to C4 transition sequence (Figure 3.8-24). However, increased supply of sediment from the stream banks and upland areas is likely to cause increased stream instability. The stream crossing at this reach is another concern from a stream stability standpoint. Continued monitoring of this study reach will provide additional information required to verify the above the predictions

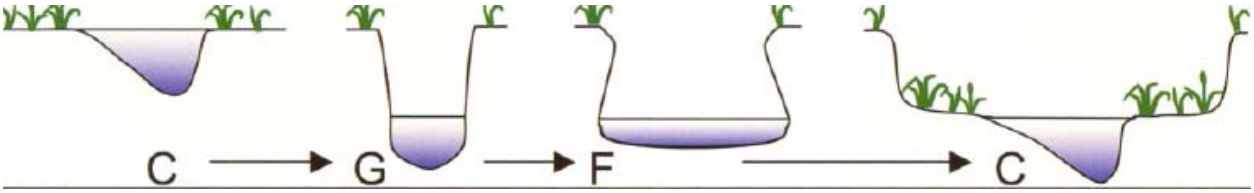


**Figure 3.8-24. Stream channel successional changes (adapted from Rosgen, 1996).**

### 3.8.c. GENERAL DISCUSSION: ROADS AND STREAM CROSSINGS

Characteristics of approach roads at each study site were measured and recorded as shown in Table 3.8-10. Approach roads to stream crossing locations are critical areas that often act as conduits for sediment laden runoff generated from upland areas and deposited into streams at stream crossing locations. This sediment is a water quality concern and again poses the potential of disrupting stream equilibrium. A stream in equilibrium shows a balance between its sediment discharge (Qs), sediment particle size ($D_{50}$), stream flow (Qw) and stream slope (S), (Lane, 1955; Rosgen, 1996). Lane (1955) showed this relationship (Figure 3.8-25) qualitatively as [Qs x $D_{50}$] $\propto$ [Qw x S]. A change in one or more of these stream variables triggers a change in stream equilibrium. Extra sediment introduced into the stream through the approach roads is likely to disrupt the equilibrium of the stream in the long run. As a consequence, channel aggradation and a shift in bed material composition to finer particles is predicted to follow stream channel alterations. Erosion dynamics and hillslope hydrology on these approach roads is still not well understood. Future studies should be focused at addressing these concerns.

**Table 3.8-10. Summary of variables measured on approach roads to stream crossings at the study reaches.**

| Variable/Reach | SR (%) | SL (%) | Hg (m) | Av (%) | Hv (m) |
|---|---|---|---|---|---|
| Seven Mile Creek | 2.4 | 8.5 | 0.15 | 83 | 0.58 |
| Farnum Creek | 13.3 | 13.6 | 0.40 | 73 | 0.55 |
| Wind Creek (upland) | 6.1 | 8.9 | 0.35 | 100 | 0.96 |
| Wind Creek (midland) | 7.7 | 7.4 | 0.0 | 90 | 0.69 |
| Wind Creek (lowland) | 8.1 | 12.2 | 0.61 | 20 | 0.31 |

SR –slope of road ,right side; SL-slope of road, left side; Hg-average depth of gully; Av-percentage of road area covered by vegetation; Hv-average height of vegetation on road.

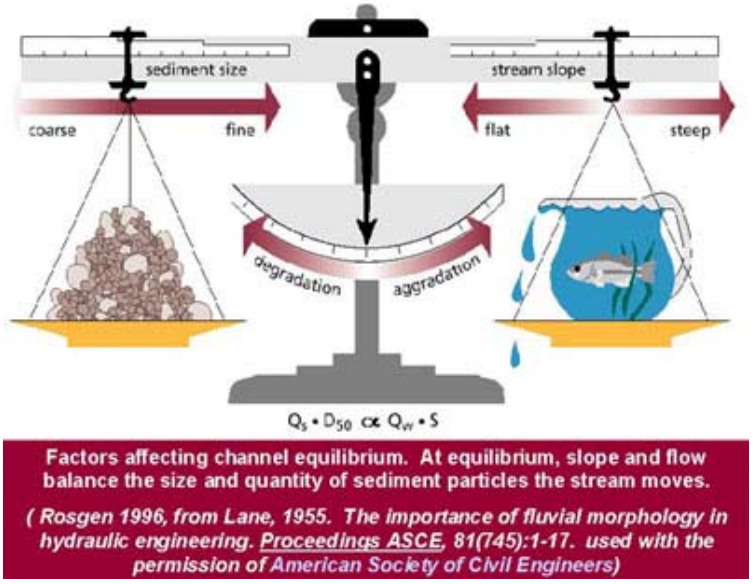


**Figure 3.8-25. A generalized relationship between factors affecting stream equilibrium. Adapted after Lane, 1955. Source: Stream Corridor Restoration: Principles, Processes, and Practices, FISRWG (10/1998).**

Furthermore, during low flow events, stream velocities at stream crossing sites are often reduced due to the widening of the channel at these locations. The reduced flow velocity at stream crossings often leads to sediment deposition at the stream crossings. It is also worth noting that poorly designed or constructed low water fords can act as dams, disrupting transport of sediment downstream. At poorly constructed stream crossings, back water pools usually form immediately upstream of the stream crossing site. During low flow events, backwater pools upstream of the ford act as sinks for sediment, which disrupts transport of sediment to the downstream reaches of the stream. During high flow events, the sediment deposited in the backwater pools and stream crossing locations is flushed downstream causing spikes in turbidity and suspended sediment in the stream. Increased turbidity and suspended sediment in the water is a concern from a water quality standpoint. In addition, high levels of turbidity and suspended sediment in the streams are a threat to aquatic life, especially the Topeka Shiner, an endangered species which resides in Flint Hills streams (Sample et al., 1998; Ingrisano, 2005).

## 3.8.d. SITE SELECTION, DESIGN AND CONSTRUCTION OF LOW WATER FORDS.

### Low Water Fords: Development Process

Observations made and data collected during stream surveys should be applied to designing and constructing low water fords. Constructed fords should be designed to mimic natural stream features (i.e. riffles) in form, materials, and function as closely as possible. Ford designs based on stream function can mitigate some of the environmental impacts associated with constructed low water fords. The design of low water fords is site specific, and depends on a number of factors such as soil types, topography, stream type, size and size of drainage area. It is therefore important to conduct a site assessment study in order to collect data required before any designs can be developed. Figure 3.8-26 shows a sequence of the process that should be followed during the development of low water fords.

### Data Collection

This step involves collecting all the data required during the design process. Data collected includes stream data, soil types, topographical variables (slope and nature of terrain) and size of drainage area. The stream data collected should include channel slope, dimensions and stream type. The size of drainage area gives an indication of the magnitude of stream flows routed through a proposed stream crossing location. Information on soil types gives an idea on soil strength and susceptibility of the soils to erosion. Once channel dimensions and the range of flows at the proposed site are determined, dimensions of the stream crossing and flow velocities can be determined.

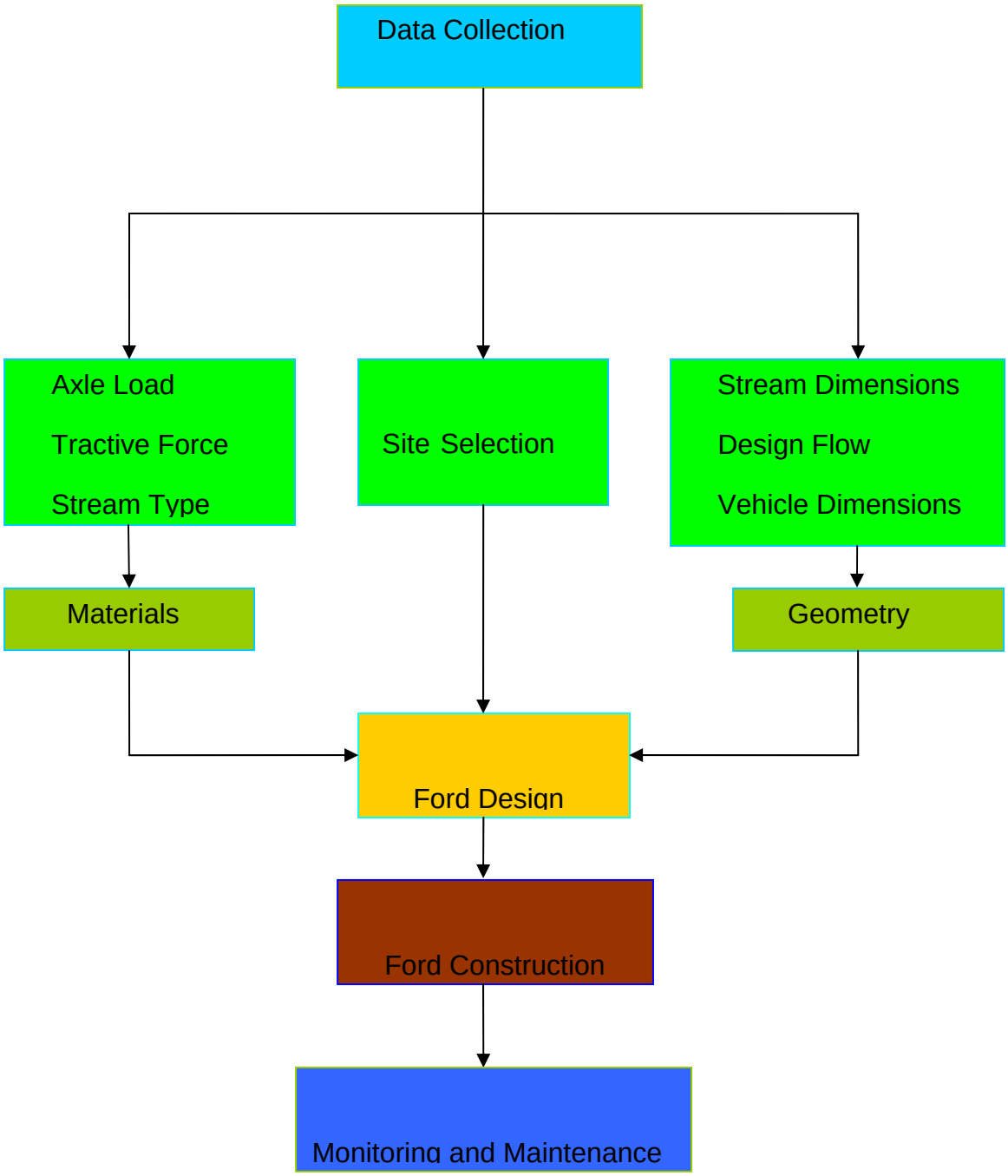


**Figure 3.8-26. Development process for low water fords.**

**Site Selection**

The location of a low water ford determines if a ford will successfully function as designed or fail. Based on observations of constructed fords on Fort Riley, some fords are performing well while others are not. The successfully performing fords are those that were well located while the failing fords are those that were located poorly. The following site selection criteria will help avoid some of the problems associated with poorly located stream crossings.

1. It is desirable to locate stream crossings on riffles. Riffles (Figure 3.8-27 and 3.8-28) are shallow places along a stream and are generally considered to be stable. Riffles provide a strong foundation for stream crossing since there is plenty of gravel at these locations.
2. In all cases, pools and meander bends (Figure 3.8-29) along a stream reach should be avoided when selecting a location for a stream crossing. These areas are prone to be unstable. A stream crossing in a pool or a meander bend can instigate stream instability. Bends tend to receive large quantities of both fine and coarse sediment which can act as an obstacle to vehicular traffic if located in the vicinity of a stream crossing (Figure 3.8-30 to Figure 3.8-35).
3. Tributary entry points (Figure 3.8-35 and 3.8-36) along streams should be avoided because of the large quantities of sediment carried by tributaries. This sediment often gets deposited at these entry locations along the main stream. In addition, these locations experience high turbulent conditions during high flow events and have a potential of compromising the stability of any constructed structure in the vicinity of the stream crossing location.
4. Stream crossings should be located perpendicular to the direction of stream flow. Locating a stream crossing structure in a skew direction to the stream flow has a tendency of changing the alignment of flow in a stream. The misalignment of flow path of a stream can cause undesirable effects on the reach downstream of the crossing structure.
5. Areas with gentle bank slopes provide excellent sites to locate approach roads to a stream crossing. However, all the above factors must be taken into account.
6. The above site selection criteria demonstrate the importance of adequately locating a suitable site for a stream crossing structure. The performance of a stream crossing structure is totally dependant on the choice of site, among other considerations.

**Figure 3.8-27. A riffle (in the foreground) is a relatively stable point along a stream reach (downstream view).**

**Figure 3.8-28. Properly functioning low water ford, located on a riffle (stream flow from left to right).**


**Figure 3.8-29. A stream crossing site located on a meander bend at Wind Creek, lowland reach (stream flow from left to right).**

**Figure 3.8-30. Wind Creek lowland stream crossing site, before May 5, 2007 flood event (stream flow from left to right).**

**Figure 3.8-31. Sediment deposited on road at Wind Creek lowland stream crossing site, after May 5, 2007 flood event (stream flow from right to left).**

**Figure 3.8-32. Sediment bar deposited on road at a stream crossings site, upstream view.**

**Figure 3.8-33. Sediment bar deposited on road at a stream crossings site, downstream view.**

**Figure 3.8-34. Sediment bar deposited on road at a stream crossings site, a view from left bank to right bank (flow from right to left).**

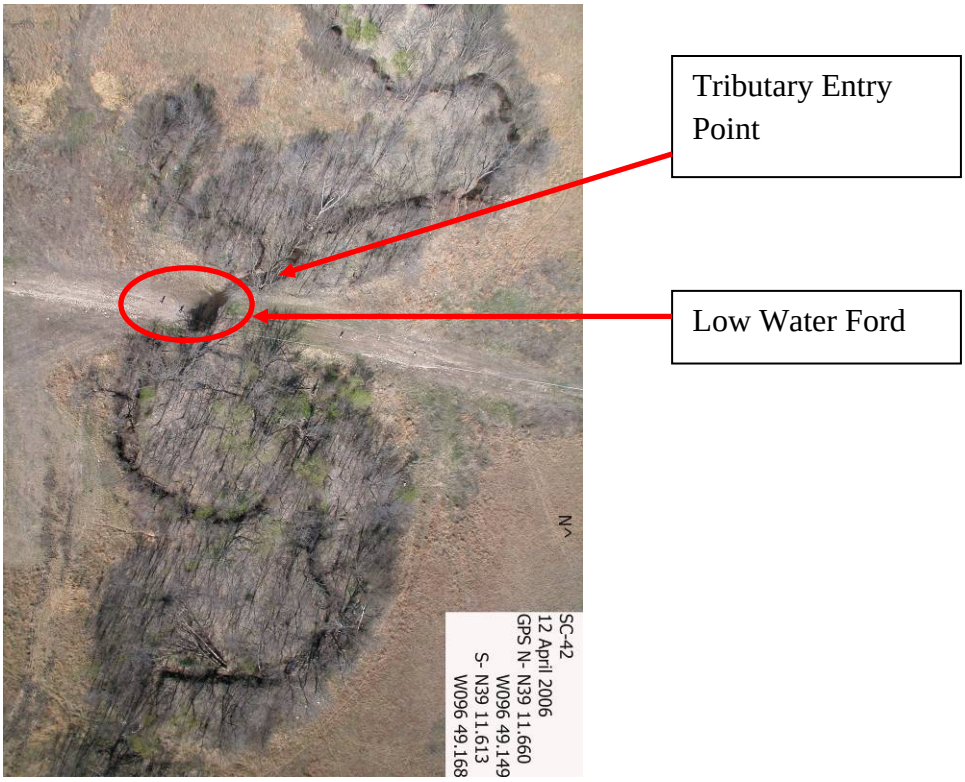


**Figure 3.8-35. Tributary entry point at a location upstream of a stream crossing site at Seven Mile Creek, an aerial view.**

**Figure 3.8-36. Tributary entry point upstream of stream crossing site at Seven Mile Creek reach, upstream view.**

**Design and Construction Guidelines**

Dimensions of the stream crossings should be developed based on a compromise between dimensions required for adequate vehicle ingress and egress, and stream stability. The stream crossing dimensions should be sized to allow easy crossing conditions for traffic but still be able to adequately convey stream flow through the stream crossing site without any adverse impacts on the stream. Tendency to oversize a stream crossing should be avoided. Overly sized stream crossings cause a reduction in flow velocities (and stream power) which leads to sediment deposition at the crossing site (see Figures 3.8-31 through 3.8.34). The original stream bed elevation at the crossing site should be maintained to allow flow, sediment transport and migration of fish through the crossing site during periods of low stream flow. Materials used at the stream crossing should be adequately selected to mimic natural riffles and also withstand large axle loads of the traffic crossing these streams. The stream crossing should be built with a range of rock sizes. The largest rocks (usually placed in the lower layers beneath the stream crossing) should be selected to withstand both high flow events and large axle loads due to traffic. Size of the largest stable rock should be determined by analyzing tractive forces at the proposed site (Newbury et al., 1997). According to Newbury et al., 1997 and Chow, 1959, tractive force at a riffle site can be estimated from Equation 3.8-10, while the diameter of the largest stable rock can be determined from Equation 3.8-11.

$$T = 1000 \times D \times S \quad \text{[Eq. 3.8-10]}$$

$$\theta = 1500 \times D \times S \quad \text{[Eq. 3.8-11]}$$

where:

T = Tractive force ($kg/m^2$)
D = Flow depth (m)
S = Slope of the downstream face of the riffle.
θ = Diameter of stable rock size (cm).

Geotextile materials (non-woven recommended) should be used to provide additional stability and structural strength to the stream crossing. Geotextile materials are especially helpful when working with streams with clayey or silty bottoms that are susceptible to movement. Construction guidelines discussed here are based on modifications of earlier recommendations presented by Sample et al., 1998. Fort Riley is investigating two design options for approach roads. This chapter discusses one of the design options described above. The stream crossing and approach road construction process follows a sequence of steps listed below:

1. Cut or fill the approach roads to the stream crossing site to a suitable grade. Grades of less than or equal to 12% (Figure 3.8-37) are recommended. The minimum recommended roads widths are 5.5m (Figure 3.8-38).
2. Water bars (Figure 3.8-39) shall be constructed on approach roads. Spacing of water bars will depend on the slopes of the approach roads.
3. Excavate the stream crossing bed to a depth of 0.9-1.2m. The width and length of excavation (Figure 3.8-39) should conform to the stream crossing dimensions determined during the design phase.
4. A geotextile material (Amoco 2016) shall be laid down on the excavated stream bed. The excavated stream bed area should be back filled in 3 layers of rocks (Figure 3.8-40) until the original bed elevation is reached. The bottom most layer shall be composed of rock of diameter 46-61 cm. The preceding layer shall be filled with rock of diameter determined from Equation 9, while the top most layer shall be filled with rock of the same diameter as the $D_{84}$ particle size on the riffle upstream of the stream crossing at the proposed crossing site. As shown in Figure 3.8-41, the longitudinal profile along the low water ford should conform to the original longitudinal profile of the stream.
5. Geotextile material (Amoco 2006) shall be laid on the graded approach roads (Figure 3.8-37). Rock is placed over the geotextile material in 2 layers of 0.30 m. Rock of 20-30 cm and 7.5- 10 cm diameter shall be placed in the bottom and upper layers respectively of the road base. Table 3.8-11 shows an estimate of materials required for the construction of a hardened low water ford.
6. Provide adequate drainage on the sides of the roads to funnel runoff to the surrounding vegetation close to the road sides (Figure 3.8-38 and 3.8-39).
7. Best management practices shall be employed during and after the construction phase.

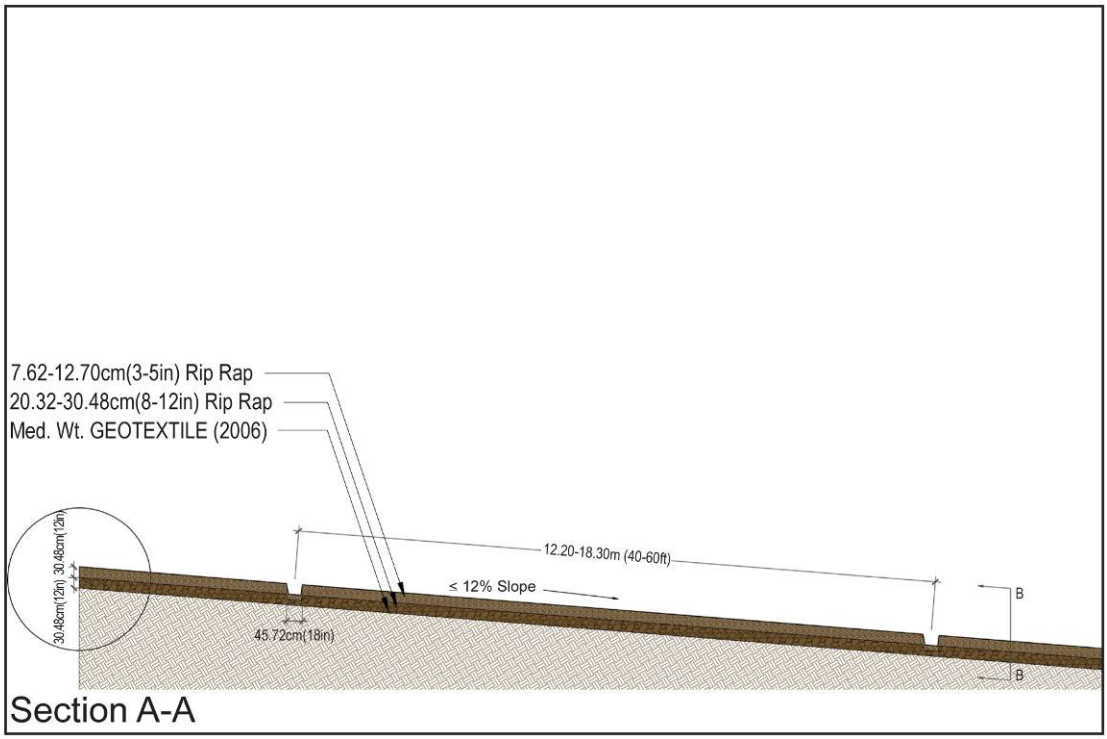


**Figure 3.8-37. Longitudinal profile along approach road leading to a stream crossing site.**

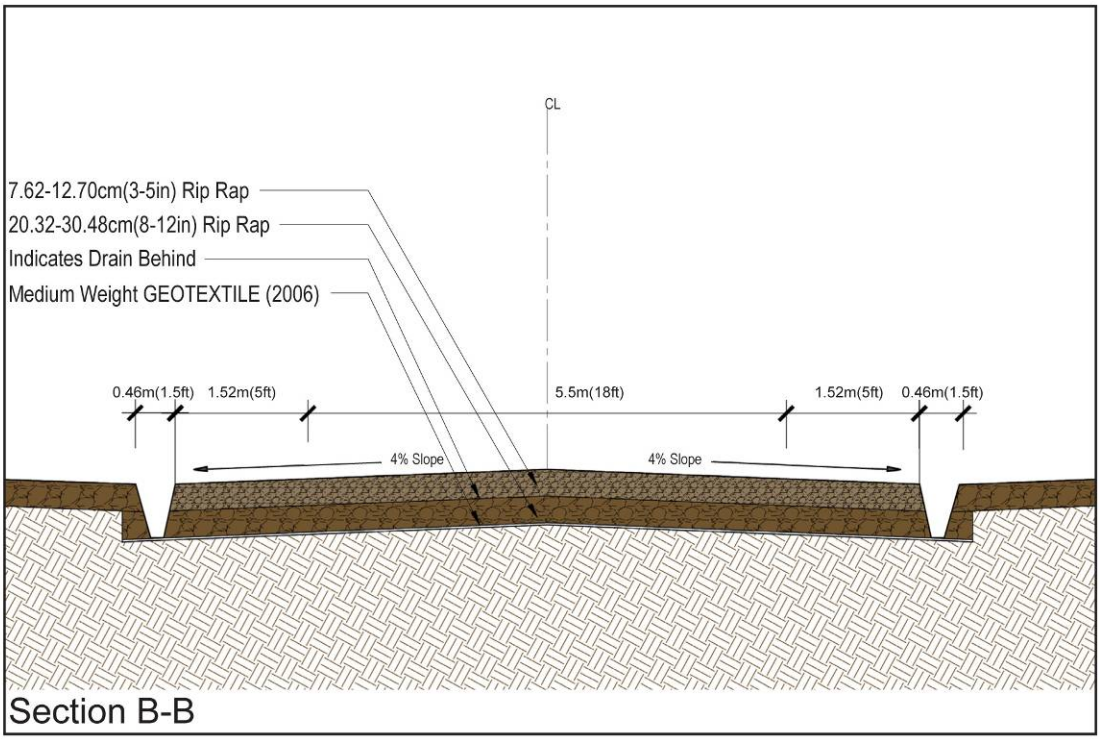


**Figure 3.8-38. Cross section across approach road leading to a stream crossing site.**

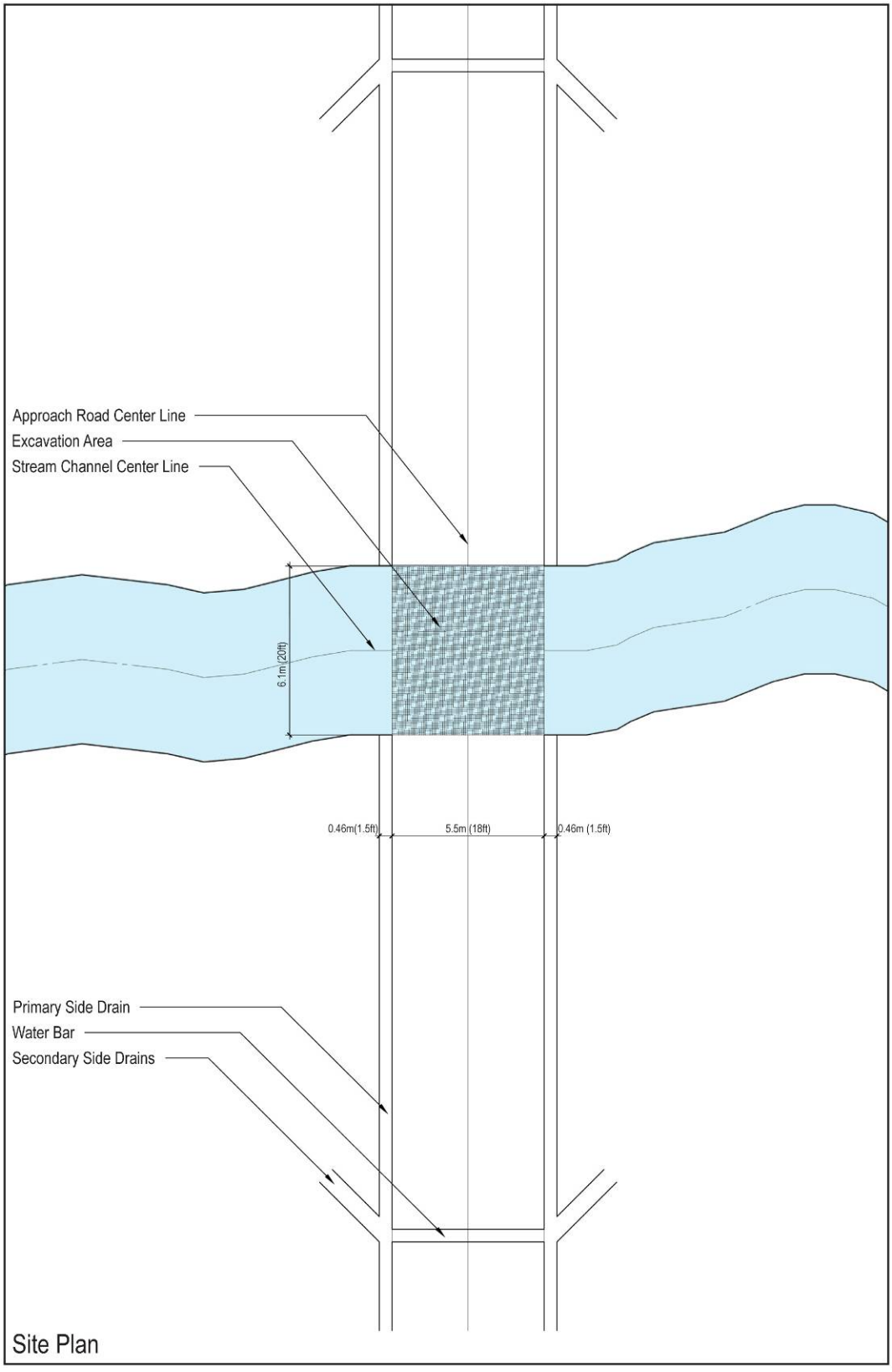


**Figure 3.8-39. Plan of a stream crossing site.**

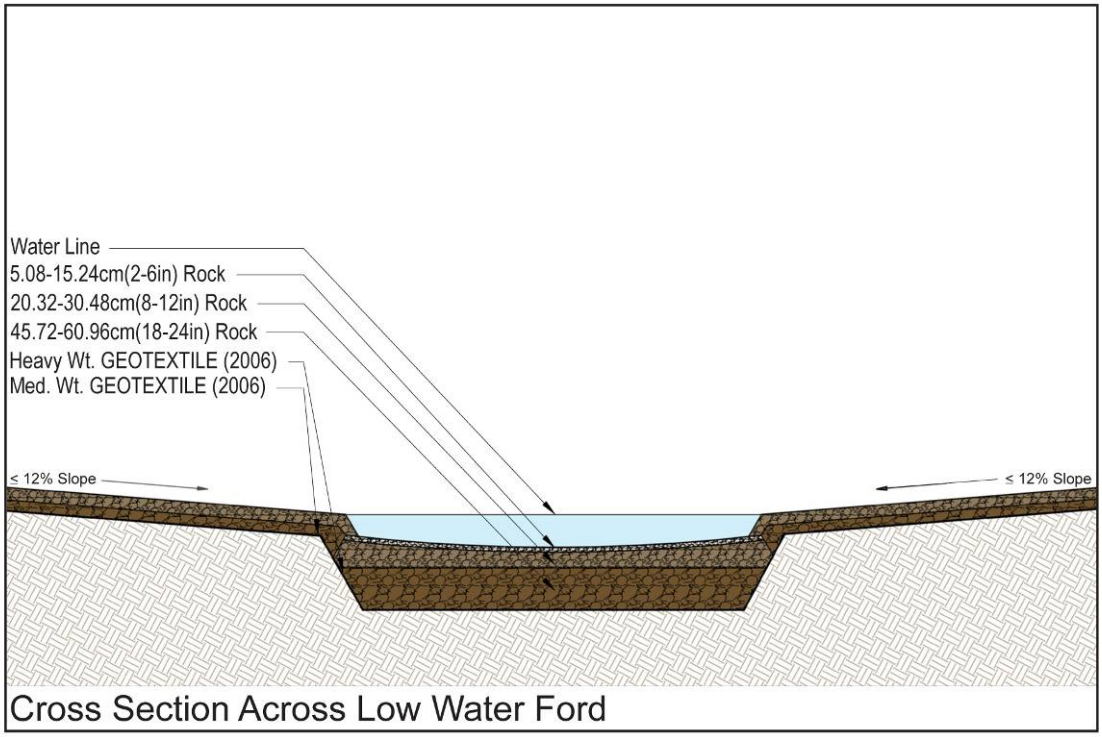


**Figure 3.8-40. Cross section across a low water ford.**

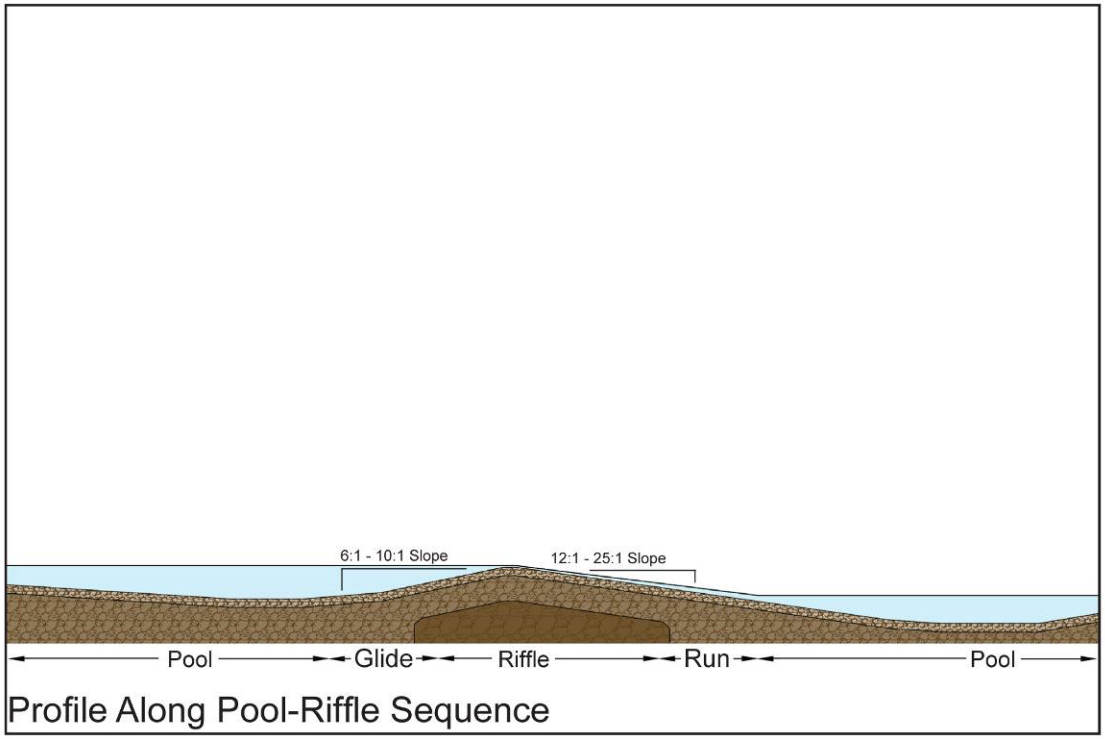


**Figure 3.8-41. Longitudinal profile along a low water ford.**

**Table 3.8-11. Estimates of quantities of material required for construction of a hardened low water ford. Source: Sample et al., 1998.**

| Material | Quantity |
|---|---|
| Largest rock (e.g. 30-46 cm diameter) | 54 $m^3$ |
| 20-30 cm diameter | 69 $m^3$ |
| 7.5-10 cm diameter | 200 $m^3$ |
| Geotextile (Amoco 2006) | 1000 $m^2$ |
| Geotextile (Amoco 2016) | 42 $m^2$ |

**Monitoring and Maintenance**

Structural integrity and function of low water fords should be regularly monitored. The regular monitoring can help assess the performance of the structures and their effect on stream stability and aquatic life. In addition, the data gathered from this monitoring process can be used to develop an excellent maintenance plan for the low water fords. This data can also be used to improve the designs of low water fords. Adequately designed and maintained low water fords will provide the military with better stream crossing conditions as well as mitigate environmental impacts associated with crossing streams.

**Best Practices and Maintenance Considerations**

Adequately located, designed and constructed low water fords can address some of the environmental concerns associated with use of stream crossings. The following are some of the best practices and maintenance considerations associated with low water fords:

1. Fords should be constructed during periods of low stream flow to minimize the impact on water quality and aquatic life in streams.
2. Stabilize approach roads by using non-erodible material (geotextile and gravel). Hardened and stabilized roads have a higher life span and require less maintenance.
3. Minimize modifications made to the stream dimensions at crossing sites. Overly modifying stream dimensions at crossing site can cause undesirable impacts on the stream.
4. Locate the stream crossing site on a riffle and in a direction perpendicular to stream flow. Maintain original stream bed elevation to allow free passage of aquatic life and stream flow during low flow events.
5. Minimize removal of vegetation adjacent to crossing site. Vegetation provides protection against erosion.
6. Maintenance of stream crossings is important. Stream crossings should be regularly maintained in order to provide better conditions for crossing streams as well as mitigate any undesirable environmental impacts associated with poorly maintained stream crossings. Regular maintenance also increases the life span of stream crossings.

### 3.8. e. CONCLUSIONS AND RECOMMENDATIONS

Poorly located and constructed low water fords pose a potential for causing stream instability through accelerated bank erosion at locations in the vicinity of the stream crossing, and possibly further downstream. The accelerated bank erosion at these sites can be caused by a low water ford which alters stream flow alignment and therefore accelerating flow in the downstream direction causing increased erosion downstream. Stream crossings in a poor location can be unstable and therefore pose a safety threat to military personnel and equipment crossing these streams. This demonstrates the need to locate and construct stream crossings in proper locations along a stream. Furthermore, poorly designed stream crossings may act as dams, trapping sediment in backwater pools created upstream of stream crossing locations. With high stream flows, trapped sediment in backwater pools is flushed downstream generating high levels of turbidity and suspended sediment in the streams. High levels of sediment and turbidity in streams is a threat to aquatic life as well as a water quality concern. Poorly designed or/and constructed stream crossings can also act as a migration barrier to aquatic life affecting breeding cycles of fish and other aquatic life. This emphasizes the need for proper design and construction techniques for low water fords.

Military maneuvers on training lands have a potential of causing undesirable impacts on the environment. These impacts include increased runoff (rich in sediment) generated from upland areas and delivered to streams often through roads leading to stream crossing locations. Need still exists to study hillslope hydrology and erosion dynamics on approach roads (to stream crossing locations). The impact of runoff and sediment (from upland areas) transported through approach roads to stream crossing sites is still unknown. Future studies should be conducted to assess the impact of runoff and sediment (from upland areas) on stream stability. Furthermore, the sediment introduced into these streams is generally considered a water quality issue as well as a problem to aquatic life in streams. This extra sediment can offset the balance of sediment in a stream system triggering instability in the stream.

Residual effects of past land use practices such as agriculture and grazing may still be felt in the study watersheds on Fort Riley, however, these effects may be minimal. As mentioned earlier, military maneuvers on Fort Riley rangelands are destructive to vegetation and cause soil compaction increasing runoff and soil erosion rates in the study watersheds. Increased runoff and upland erosion rates in these watersheds affect the streams because of the excess sediment delivered to the streams. Some of the streams in the study watersheds show signs of stream transition from the current stream types to different stream types. These stream successional changes involve change in stream dimensions such as channel deepening which is usually followed by widening. These stream changes have direct implications on the low water fords on Fort Riley. As a consequence, there will be constant need to modify the design and construction techniques of these fords in order to accommodate changes in the stream morphology. Benefits of doing so include better stream crossing conditions for the military and less impacts on the environment.

Some of the streams investigated show signs of instability which may compromise or threaten the stream functions in these streams. Continued monitoring of these streams will provide additional information required for decision making. Furthermore, need still exists to implement and monitor the performance of the modified designs of stream crossings. Through adaptive management, better designs of stream crossings can be developed. Better designs of low water

fords will provide the military with better stream crossing conditions as well as mitigate any environmental impacts associated with crossing streams. Finally, need still exists to develop bank erosion rating curves for the state of Kansas, especially for the Flint Hills region. Continued monitoring of the study sites will provide some of the data required for the development of erosion rating curves for the Flint Hills region.

## LITERATURE CITED


Abernethy, B., and Rutherfurd, I.D., 2000, The effect of riparian tree roots on the mass-stability of riverbanks: Earth Surface Processes and Landforms, v. 25, p. 921-937.

Abrahams, A.D. and J.F. Atkinson. 1993. Relation between grain velocity and sediment concentration in overland flow. *Water Resources Research* 29(9):3020-3028.

Abrahams, A.D. and J.F. Atkinson. 1993. Relation between grain velocity and sediment concentration in overland flow. *Water Resources Research* 29(9):3020-3028

Abrahams, A.D., L. Gary, C. Krishnan, and J.F. Atkinson. 1999. Predicting sediment transport by interrill overland flow on rough surfaces. *Earth Surface Processes and Landforms* 23(12):1087-1099

Abu-Zreig, M., R. P. Rudra, H. R. Whiteley, M. N. Lalonde and N. K. Kaushik. 2003. Phosphorus removal in vegetated filter strips. *Journal of environmental quality* 32(2): 613-619.

Abu-Zreig, M., R. P. Rudra, M. N. Lalonde, H. R. Whiteley and N. K. Kaushik. 2004. Experimental investigation of runoff reduction and sediment removal by vegetated filter strips. *Hydrological Processes* 18(11): 2029-2037.

Allen, R. G., L. S. Pereira, D. Raes, M. Smith. 1998. Crop evapotranspiration – guidelines for computing crop water requirements. Food and Agricultural Organization of the United Nations. FAO Paper 56.

Althoff, D. P., P. S. Gipson, J. S. Pontius and P. B. Woodford. 2006. Plant community and bare ground trends on Fort Riley, Kansas: Implications for monitoring of a highly disturbed landscape. *Transactions of the Kansas Academy of Science* 109(3): 101-119.

Anderson, A., Sekscienski, S., Sydelko, P., Winters, L., Brown, M., Colosky, C., Shirinia, T., and Weith, G. 1999. U.S. Army Training and Testing Area Carrying Capacity (ATTAC) Handbook for Installations. Version 1.1 United States Environmental Center

Anderson, J., E. Hardy, J Roach, and R. Witmer. 1976. A land use and land cover classification system for use with remote sensor data. Geological Survey Professional Paper 964, U.S. Geological Survey. Washington, D.C.: U.S. Government Printing Office.

Andrews, E.D. 1984. Bed-material entrainment and hydraulic geometry of gravel-bed rivers in Colorado. Geol. Soc. of Am. Bull., 95, 371-378.

APHA (American Public Health Association), American Water Works Association, and Water Environment Federation. 1998. *Standard Methods for the Examination of Water and Wastewater*. 20th edition. Washington, DC: APHA.

Arnold, R.H. 1997. Interpretation of Airphotos and Remotely Sensed Imagery. Upper Saddle River, NJ: Prentice-Hall.

Atmel Corporation, 2008. Low cost ZigBee applications. Available at: www.atmel.com Accessed 20 Feb. 2008.

Ayers, P. C. Butler, A. Fiscor, C. Wu, Q. Li, and A. Anderson. 2005b. Vehicle Impact Study, Fort Riley, Kansas, October 2004. Submitted to ITAM, Fort Riley Military Installation, Kansas (March 2005).

Ayers, P. D., A. B. Anderson, and C. Wu. 2005a. Analysis of vehicle use patterns during field training exercises. *Journal of Terramechanics* 42(3-4) 321-338.

Barfield, B. J., R. L. Blevins, A. W. Fogle, C. E. Madison, S. Inamdar, D. I. Carey and V. P. Evangelou. 1998. Water quality impacts of natural filter strips in karst areas. *Transactions of the ASAE* 41(2): 371-382.

Barling, R. D., I.D. Moore, and R.B. Grayson. 1994. A quasi-dynamic wetness index for characterizing the spatial distribution of zones of surface saturation and soil water content. *Water Resources Research* 30:1029-1044.

Bartsch, K.P., Miegroet, J., Boettinger, J., and Dobrowolski, J.P. 2002. Using empirical erosion models and GIS to determine erosion at Camp Williams, Utah. *Journal of Soil and Water Conservation.* 57(1): 29-37.

Beche, L. A., S. L. Stephens and V. H. Resh. 2005. Effects of prescribed fire on a Sierra Nevada(California, USA) stream and its riparian zone. *Forest Ecology and Management* 218(1/3): 37-59.

Bennett, S. J., J. Casali, K.M. Robinson, and K. C. Kadavy. 2000. Characteristics of actively ephemeral gullies in an experimental channel. *Transactions of the ASAE* 43(3):641-649.

Bennett, S.J., C.V. Alonso, S.N. Prasad, M.J.M. Romkens. 2000. Experiments on headcut growth and migration in concentrated flows typical of upland areas. *Water Resources Research* 36(7):1911–1922.

Bennett, S.J., C.V. Alonso, S.N. Prasad, M.J.M. Romkens. 2000. Experiments on headcut growth and migration in concentrated flows typical of upland areas. *Water Resources Research* 36(7):1911–1922.

Beven, K., Lamb, R., Quinn, P., Romanowicz, R., and Freer, J. 1994. `TOPMODEL.' In: V. P. Singh (Ed.). Computer Models of Watershed Hydrology, Water Resources Publications, Littleton, CO.

Blanco-Canqui, H., C. J. Gantzer and S. H. Anderson. 2006. Performance of grass barriers and filter strips under interrill and concentrated flow. *Journal of environmental quality* 35(6): 1969-1974.

Blanco-Canqui, H., C. J. Gantzer, S. H. Anderson and E. E. Alberts. 2004. Grass Barriers for Reduced Concentrated Flow Induced Soil and Nutrient Loss. *Soil Science Society of America Journal* 68(6): 1963-1972.

Blinn, C. R., R. Dahlman, L. Hislop and M. A. Thompson. 1998. Temporary stream and wetland crossing options for forest management. Gen. Tech. Rep. NC-202. St. Paul, MN.: USDA, Forest Service, North Central Forest Experiment Station.

Bouwer, H. 1966. Rapid field measurement of air entry value and hydraulic conductivity of soil as significant parameters in flow system analysis. *Water Resources Research* 2(4): 729-738.

Brown, D.W., 1985. A physical meteor burst propagation model and some significant results for communications and systems design. IEEE Journal on Selected Areas in Communications. 5 (3), 745-755.

Brown, K.J. 1994. River-bed sedimentation caused by off-road vehicles at river fords in the Victorian Highlands, Australia. Water Resources Bulletin 30(2):239-249.

Brown. M.J. 1975. Climate. United States Department of Agriculture (USDA)-Natural Resources Conservation Service (NRCS). *Soil Survey of Riley County and Part of Geary County, Kansas*. Washington, DC. : USDA.

Buchanan, P., C.A. Ruhl and D. Schoellhamer. 2001. Continuous monitoring in San Francisco Bay and delta: 13 June 2001: Available at: http://sfports.wr.usgs.gov/Fixed_sta/DataCollection/data_collect.html. Accessed 8 Jan. 2003.

Bunt, J. A. C., P. Larcombe, C. F. Jago. 1999. Quantifying the response of optical backscatter devices and transmissometers to variations in suspended particulate matter. *Continental Shelf Research* 19: 1199-1220.

Bunte, K. and S. R. Abt. 2001. Sampling surface and subsurface particle-size distribution in gravel and cobble-bed streams for analyses in sediment transport, hydraulics, and streambed monitoring. Gen. Tech. Rep. RMRS-GTR-74. Rocky Mtn., CO.: USDA, Forest Service, Rocky Mtn. Research Station.

Burrough, P. A. and R.A. McDonnell. 1998. Principles of Geographical Information Systems. New York: Oxford University Press.

Campbell Scientific Inc., 2003. CR10X measurement and control system operator's manual. Campbell Scientific Inc., Logan, UT.

Campbell Scientific, 2008. CR200 series brochure. Available at: www.campbellsci.com Accessed 20 Feb. 2008.

Carlson, T.N. 1986. Regional-scale Estimates of Surface Moisture Availability and Thermal Inertia using Remote Thermal Measurements. Remote Sensing Reviews 1: 197-247.

Carlson, T.N., Gillies, R.R., and T.J. Schmugge. 1995. An Interpretation of Methodologies for Indirect Measurement of Soil Water Content. Agricultural and Forest Meteorology 77: 191-205.

Carlson, T.N., R.R. Gillies, and E.M. Perry. 1994. A Method to Make use of Thermal Infrared Temperature and NDVI Measurements to Infer Soil Water Content and Fractional Vegetation Cover. Remote Sensing Reviews 52: 45-59.

Carr, G. M. and J. P. Neary. 2006. Water Quality for Ecosystem and Human Health. *Hydrol. Process.* 21.

Chan A.H. Comparing wireless data network standards. AFRICON 2007, Windhoek, Namibia, 2007.

Chow, V.T.1959. *Open Channel Hydraulics*. New York, NY. McGraw Hill Book Company, Inc.

Clar, M. L., B. J. Barfield and T. P. O'Connor, eds. 2004. *Stormwater Best Management Practice Design Guide*. Washington, DC: United States Environmental Protection Agency.

Clark. N and H.E. Worley. 1975. Classification of soil. United States Department of Agriculture (USDA)-Natural Resources Conservation Service (NRCS). *Soil Survey of Riley County and Part of Geary County, Kansas*. Washington, DC. : USDA.

Clesceri, L. S., A. E. Greenberg, and A. D. Eaton. 1998. Standard methods for the examination of water and wastewater. American Public Health Association.

Cochrane, T. A. and D. C. Flanagan. 2005. Effect of DEM resolution in the runoff and soil loss predictions of the WEPP watershed model. *Transactions of the ASAE*. 48 (1): 109-120.

Cochrane, T. A., L. D. Norton, C. Castro-Filho, J. H. Caviglione. 2004. Development of a river sediment transport monitoring system for large reservoirs. *Applied Engineering in Agriculture* 20(6):771-781.

Coffey, S.W., and M.D. Smolen. 1990. The Nonpoint Source Manager's Guide to Water Quality Monitoring - Draft. Developed under EPA Grant Number T-9010662. U.S. Environmental Protection Agency, Water Management Division, Region 7, Kansas City, MO.

Crossbow Technology, 2008. Stargate and mote. Available at: www.xbow.com Accessed 20 Feb. 2008.

Curran, P.J. and E.M.M. Novo. 1988. The relationship between suspended sediment concentration and remotely sensed spectral radiance: A review. *Journal of Coastal Research.* 4: 351-368.

Daly, C., W.P. Gibson, G.H. Taylor, G.L. Johnson, and P. Pasteris. 2002. A knowledge-based approach to the statistical mapping of climate. *Climate Research*, 22:99-113.

Daly, C., W.P. Gibson, G.H. Taylor, G.L. Johnson, and P. Pasteris. 2002. A knowledge-based approach to the statistical mapping of climate. *Climate Research*, 22:99-113.

Daraigan, S. G., M. Z. Matjafri, K. Abdullah, L. H. San, W. C. Jeng. 2006. Multi-spectral optical sensor based on light scattering for measuring total suspended solids. In *Proceedings of SPIE - The International Society for Optical Engineering 6201*, 62010W-1-62010W-6. Bellingham, WA: SPIE.

Daraigan, S.G., M. Z. Matjafri, K. Abdullah, A. Abdul-Aziz, A. A. Tajuddin. 2005. A simple instrument for measuring total suspended solids in polluted marine waters. In *Proceedings of 2005 Asian Conference on Sensors and the International Conference on New Techniques in Pharmaceutical and Biomedical Research*, 219-221. New York, NY: IEEE.

Davies-Colley, R. J., and D. G. Smith. 2001. Turbidity, suspended sediment, and water clarity: A review. *Journal of the American Water Resources Association* 37(5): 1085-1101.

Davies-Colley, R.J. and D.G. Smith. 2001. Turbidity, suspended sediment and water clarity: A review. Jour. Amer. Water Resour. Assoc. 37:1085-1101.

Davies-Colley, R.J., and D.G. Smith. 2001. Turbidity, suspended sediment, and water clarity: A review. J. American Water Resources Association 37(5): 1085-1101.

Desmet, P.J.J. 1997. Effects of Interpolation Errors on the Analysis of DEMs. Earth Surface Processes and Landforms 22(6):563-580

Desmet, P.J.J. and Govers, G. 1996. A GIS procedure for automatically calculating the USLE LS factor on topographically complex landscape units. *Journal of Soil and Water Conservation*. 51(5):427-433.

Dillaha, T. A., R. B. Reneau, S. Mostaghimi and D. Lee. 1989. Vegetative filter strips for agricultural nonpoint source pollution control. *Trans. ASAE* 32(2): 513-519.

Dressing, S. A. 2003. National Management Measures to Control Nonpoint Pollution from Agriculture-USEPA. EPA 841-B-03-004.

Duda, R. and P.E. Hart. 1973. Pattern Classification and Scene Analysis. New York: Wiley.

Dunne, T., and L.B. Leopold. 1978. Water in Environmental Planning. W.H. Freeman and Company, NY.

Dunne, T., and Leopold, L. B., 1978, Water in environmental planning: San Francisco, W.H. Freeman and Company, 818 p.

Egbert, S.L., D.L. Peterson, A.M. Stewart, C.L. Lauver, C.F. Blodgett, K.P. Price, and E.A. Martinko. 2001, The Kansa GAP Land cover map: final report. Kansas Biological Survey Report #98. University of Kansas. Lawrence, KS.

Egbert, S.L., D.L. Peterson, A.M. Stewart, C.L. Lauver, C.F. Blodgett, K.P. Price, and E.A. Martinko. 2001, The Kansa GAP Land cover map: final report. Kansas Biological Survey Report #98. University of Kansas. Lawrence, KS.

Eklund, C., Marks, R.B., Stanwood, K.L., Wang, S. 2002. IEEE standard 802.16: a technical overview of the WirelessMAN™ air interface for broadband wireless access. IEEE Communications Magazine. 40 (6), 98 – 107.

Elliott, W.J., A.M. Liebenow, J.M. Laflen and K.D. Kohl. 1989. A compendium of soil erodibility data from WEPP cropland soil field erodibility experiments 1987 and 1988. NSERL Report No. 3. USDA-ARS National Soil Erosion Research Lab., West Lafayette, IN.

Emmerich, W. E. and J. R. Cox. 1992. Hydrologic characteristics immediately after seasonal burning on introduced and native grasslands. *Journal of Range Management* 45; 476-479.

Emmert, B.E., 2004, Regional curve development for Kansas, in Proceedings of the ASAE Conference: Self-sustaining solutions for streams, watersheds, and wetlands conference: St. Paul, Minnesota, p. 27-34.

Engel, B. 2003. Estimating Soil Erosion Using RUSLE (Revised Universal Soil Loss Equation) using ArcView. Purdue University. http://pasture.ecn.purdue.edu/~abe526/resources1/gisrusle/gisrusle.html

Engman, E.T. 1983. Roughness coefficients for routing surface runoff. In Proceedings. Spec. Conf. Frontiers of Hydraulic Engineering.

Engman, E.T. 1983. Roughness coefficients for routing surface runoff. In Proceedings. Spec. Conf. Frontiers of Hydraulic Engineering.

Engman, E.T. 1983. Roughness coefficients for routing surface runoff. In Proceedings. Spec. Conf. Frontiers of Hydraulic Engineering.

Engman, E.T. and N. Chauhan. 1995. Status of microwave soil moisture measurements with remote sensing. Remote Sensing of the Environment 51:189-198.

Environmental Sensitivities Research Institute. 2002. *ArcGIS 9.1: Using ArcGIS Spatial Analyst*. ESRI Press, Redlands, CA.

EPA. 1999. Guidance manual for compliance with the interim enhanced surface water treatment rule: Turbidity provisions. Washington, D.C.: United States Environmental Protection Agency.

Fay, P.A. 1997. Plant Communities at Fort Riley, Kansas: Assessing Species Composition, Land Management, and Disturbance using Land Condition Trend Analysis Data. Champaign, IL: U.S. Army Construction Engineering Research Laboratory (CERL).

FISRWG. 1998. Stream Corridor Restoration: Principles, Processes, and Practices. By the Federal Interagency Stream Restoration Working Group (FISRWG) (15 Federal agencies of the US Government). GPO Item No. 0120-A; SuDocs No. A 57.6/2: EN 3/PT.653. ISBN-0-934213-59-3.

Florinski. I.V. 1998. Accuracy of local topographic variables derived from digital elevation models. *International Journal of Geographic Information Science* 12(1):47-61.

Foster, G.R. 1986. Understanding ephemeral gully erosion. Soil Conservation: an assessment of the National Resources Inventory, Vol. 2. The National Academy of Science. Washington D.C.

Foster, G.R. 1986. Understanding ephemeral gully erosion. Soil Conservation: an assessment of the National Resources Inventory, Vol. 2. The National Academy of Science. Washington D.C.

Foster, G.R., R. A. Young, and W.H. Neibling. 1985. Sediment composition for nonpoint source pollution analysis. *Transactions of the ASAE* 28(1):133-139.

Foster, G.R., R. A. Young, and W.H. Neibling. 1985. Sediment composition for nonpoint source pollution analysis. *Transitions of the ASAE* 28(1):133-139.

Foster, G.R., R. A. Young, and W.H. Neibling. 1985. Sediment composition for nonpoint source pollution analysis. *Transitions of the ASAE* 28(1):133-139.

Fresnel Zone, 2008. Wireless – Fresnel Zones and their effect. Available at: www.zytrax.com/tech/wireless/fresnel.htm Accessed 2 Feb. 2008.

Fuat, I. 1987. Maximum likelihood classification, optimal or problematic? A comparison with the nearest neighbor classification. *International Journal of Remote Sensing* 8(12):1829-1838.

Gao, J. 1997. Resolution and accuracy of terrain representation by grid DEM at a micro scale. *International Journal of Geographical Information Science* 11(2):199-212.

Garbrecht, J., F.L. Ogden, P.A. DeBarry, and D.R. Maidment. 2001. GIS and distributed watershed models I: data coverages and sources. *Journal of Hydrologic Engineering* 6(6):506-514.

Gareth, H. O., G.J.L. Leeks, D. Cooper, D. McNeil and P. Smith. 2002. Two technological advances in continuous monitoring of suspended sediment transport and particle characteristics. 2002: Available at: http://www.nve.no/iahs_ws_oslo2002/p2601d_et_al.pdf. Accessed 22 Feb. 2003.

Garg, V. and I. Chaubey. 2003. Effects of suspended sediment distribution on spectral reflectance. Pp. 136-140 in Total Maximum Daily Load (TMDL) Environmental Regulations II, Conference Proceedings (8 November 2003, Albuquerque, New Mexico, USA), ed. Ali Saleh. ASAE paper #701P1503. Nov. 2003: Available at: http://asae.frymulti.com/request2.asp?JID=1&AID=15549&CID=tmdl2003&T=1. Accessed 10 Aug. 2004.

Gay, D., Levis, P., Culler, D., Brewer, E. 2003. nesC, 2003. nesC 1.1 Language Reference Manual. Available at: nescc.sourceforge.net/papers/nesc-ref.pdf Accessed 18 Mar. 2008.

Gemtek, 2008. UWB technology. Available at: www.gemtek.com.tw Accessed 20 Feb. 2008.

Gharabaghi, B., R. P. Rudra, H. R. Whiteley and W. T. Dickinson. 2001. Sediment-Removal Efficiency of Vegetative Filter Strips. *ASAE Meeting Paper*, Paper Number: 01-2071, Sacramento, California.

Gillies, R.R. and T.N. Carlson. 1995. Thermal Remote Sensing of Surface Soil Water Content with Partial Vegetation Cover for Incorporation into Climate Models. Journal of Applied Meteorology 34: 745-756.

Gippel, C.J. 1989. The Use of Turbidity Instruments to Measure Stream Water Suspended Sediments Concentration. Department of Geography and Oceanography, University College, Australian Defense Force Academy. Monograph Series No. 4.

Gippel, C.J. 1995. Potential of Turbidity Monitoring for Measuring the Transport of Suspended Solids in Streams. *Hydrological Processes*. 9: 83-97.

Goward, S.N., C.J. Tucker, and D.G. Dye. 1985. North American Vegetation Patterns observed with the NOAA-7 Advanced Very High Resolution Radiometer. Vegetation 64: 3-14.

Grant, D. M. and B. D. Dawson. 2001. *ISCO Open Channel Flow Measurement Handbook.* Lincoln, Nebraska, ISCO.

Green, W. H. and G. A. Ampt. 1911. Studies on soil physics, 1. The flow of air and water through soils. *J. Agric. Sci* 4(1): 1-24.

Gribbin, J. E. 2007. *Introduction to hydraulics and hydrology with applications for stormwater management.* third ed. Clifton Park, NY: Thomson Delmar Learning.

Hach company. Oxygen demand, chemical method 8000 DR/2400. Hach Company. Hach Company. Available at: http://www.hach.com/fmmimghach?/CODE%3AOXYGENCOD_NONE_MID_R7566%7C1. Accessed 02/25 2008.

Han, L., D.C. Rundquist, L.L. Liu, R.N. Fraser and J.F. Schalles. 1994. The spectral responses of algal chlorophyll in water with varying levels of suspended sediment. *International Journal of Remote Sensing*. 15(18): 3707-3718.

Hancock G..R. and K.G. Evans. 2005. Channel head location and characteristics using digital elevation models. *Earth Surface Processes and Landforms* 31(7):809-824.

Hancock G..R. and K.G. Evans. 2005. Channel head location and characteristics using digital elevation models. *Earth Surface Processes and Landforms* 31(7):809-824.

Harrelson, C.C., C.L. Rawlins, and J.P. Potyondy. 1994. Stream channel reference sites: An illustrated guide to field technique. Gen. Tech. Rep. RM-245. Rocky Mtn., CO.: USDA, Forest Service, Rocky Mountain Forest and Range Experimental Station.

Hartung, C., Han, R., Seielstad, C., Holbrook S. 2006. FireWxNet: A multitiered portable wireless system for monitoring weather conditions in wildland fire environments. MobiSys 06 Paper, Uppsala, Sweden.

Haugen, L. 2002. Design and testing of a vehicle tracking system for monitoring environmental impact at U.S. Army training installations. MS Thesis. Colorado State University, Fort Collins, CO.

Haugen, L. B., P. D. Ayers, and A. B. Anderson. 2003. Vehicle Movement Patterns and Impact During Military Training Exercises. *Journal of Terramechanics* 40(2):83-95.

Haugen, L., P. Ayers, M. Vance, A. Anderson. 2000. Using GPS for vehicle tracking and dynamic property monitoring. Paper No. 001071 presented at the 2000 ASAE Annual International Meeting, ASAE, 2950 Niles Rd., St. Joseph, MI 49085-9659.

Haydon, B. P. 1998. Chapter 2: Regional climate and the distribution of tallgrass prairie. In *Grassland dynamics: Long term ecological research in tallgrass prairie,* 19-34. ed. A. K. Knapp, Briggs, J. M., Hartnett, D. C. and Collins, S. L., Oxford: Oxford University Press.

Hayes, J.C., E.E. Godbold and B.J. Barfield. 2001. Turbidity based on sediment characteristics for southeastern U.S. soils. Soil Erosion Research for the 21st Century, Proc. Int. Symp. (3-5 January 2001, Honolulu, HI, USA). Jan. 2001: Available at: http://asae.frymulti.com/request2asp?JID=1&AID=44978-CID=se2001&T=1. Accessed 7 May 2004.

Helmers, M. J., D. E. Eisenhauer, M. G. Dosskey, T. G. Franti, J. M. Brothers and M. C. McCullough. 2005. Flow pathways and sediment trapping in a field-scale vegetative filter. *Transactions of the ASAE* 48(3): 955-968.

Helmers, M. J., T. Isenhart, M. Dosskey, S. Dabney and J. Strock. 2006. Buffers and vegetative filter strips. Available at: http://www.epa.gov/msbasin/taskforce/2006symposia/4BuffersVegHelmers.pdf. Assessed 03/10/2008

Holmes, K.W., O.A. Chadwick, and P.C. Kyriadkidis. 2000. Error in a USGS 30-meter digital elevation model and its impact on terrain modeling. *Journal of Hydrology* 233:154-173.

Holmes, K.W., O.A. Chadwick, and P.C. Kyriadkidis. 2000. Error in a USGS 30-meter digital elevation model and its impact on terrain modeling. *Journal of Hydrology* 233:154-173.

Hosomi, M. and R. Sudo. 1986. Simultaneous determination of total nitrogen and total phosphorus in freshwater samples using persulfate digestion. International Journal of Environmental Studies. 27:267-275.

Houston, Stephen T., Doe, William W., and Shaw, Robert B. 2001. Environmental risk of Army ranges and impact areas: an ecological framework for assessment. *Federal Facilities Environmental Journal.* 11(1): 93-111.

http://edcdaac.usgs.gov/modis/pdf/mod13q1.pdf

Hubbard, R. K., G. L. Newton and G. J. Gascho. 2003. Nutrient removal by grass components of vegetated buffer systems receiving swine lagoon effluent. *Journal of Soil and Water Conservation (Ankeny)* 58(5): 232-242.

Huntley, D. A., and D. M. Hanes. 1987. Direct measurement of suspended sediment transport. In *Proceedings of a Specialty Conference on Advances in Understanding of Coastal Sediment Processes*, 723-737. New York, NY: ASCE.

Hutchinson, J.M.S. 2003. Estimating Near Surface Soil Moisture using Active Microwave Satellite Imagery and Optical Sensor Inputs. Transactions of the American Society of Agricultural Engineers 46(2):225-236.

Hutchinson, M.F. 1989. A new procedure for gridding elevation and stream line data with automatic removal of pits. *Journal of Hydrology* 106:211-232.

Idso, S.B., R.J. Reginato, D.C. Reicosky, and J.L. Hatfield. 1981. Determining Soil-induced Plant Water Potential Depressions in Alfalfa by Means of Infrared Thermometry. Agronomy Journal 73: 826-830.

Ingrisano, M.A., 2005, Geomorphic differences between similar streams with contrasting anthropogenic influence in the Kansas Flint Hills: M.S. thesis, Kansas State University, Manhattan, 154 p.

Jaber, F.H. and R.H. Mohtar. 2002. Dynamic time step for one-dimensional overland flow kinematic wave solution. *Journal of Hydrologic Engineering* 7(1):3-11.

Jackson, R.D., S.B. Idso, R.J. Reginato, and P.J. Pinter Jr. 1981. Canopy Temperature as a Crop Water Stress Indicator. Water Resources Research 17(4): 1133-1138.

Jantz, Donald R., Harner, Rodney F., Rowland, Harold T., and Gier, Donald A. 1975. Soil survey of Riley County and part of Geary County, Kansas. United States Department of Agriculture, Soil Conservation Service.

Jensen, J.R. 1996. *Introductory digital image processing: a remote sensing perspective*. Prentice Hall, Upper Saddle River, NJ.

Jensen, J.R. 1996. *Introductory digital image processing: a remote sensing perspective*. Prentice Hall, Upper Saddle River, NJ.

Jenson, S.K. and J. O. Domingue. 1988. Extracting Topographic Structure from Digital Elevation Data for Geographic Information System Analysis. *Photogrammetric Engineering and Remote Sensing* 54(11):1593-1600.

Jewett, J.M.1941. The Geology of Riley and Geary Counties, Kansas. Kansas State University Geological Survey Bulletin 39.

Jin, C. X., M. J. M. Roemkens and F. Griffioen. 2000. Estimating Manning's roughness coefficient for shallow overland flow in non-submerged vegetative filter strips. *Transactions of the ASAE* 43(6): 1459-1466.

Johansen, M. P., T. E. Hakonson and D. D. Breshears. 2001. Post-fire runoff and erosion from rainfall simulation: contrasting forests with shrublands and grasslands. *Hydrological Processes* 15(15): 2953-2965.

Jones, D.S., Kowalski, D.G., and Shaw, R.B. 1996. Calculating Revised Universal Soil Loss Equation (RUSLE) Estimates on Department of Defense Lands: A Review Of RUSLE Factors and U.S. Army Land Condition-Trend Analysis (LCTA) Data Gaps. Center for Ecological Management of Military Lands. CEMML TPS 96-8. Department of Forest Science, Colorado State University, Fort Collins, Colorado

Juracek, K.E. and D.M. Wolock. 2002. Spatial and statistical differences between 1:25000- and 1:24000 scale digital soil databases. *Journal of Soil and Water Conservation* 57 (2):89-64.

Kansas Department of Health and Environment. 2002. Kansas Bureau of Water, Watershed Planning Section, Total Maximum Daily Load (TMDL). http://www.kdhe.state.ks.us/tmdl.

Kansas State Research and Extension. 2008. Kansas State Research and Extension-Weather Data Library. Kansas State Research and Extension. Kansas State University. Available at: http://av.vet.ksu.edu/webwx/. Accessed 01/21 2008.

Kenward, T., D.P. Lettenmaier, E.F. Wood, and E. Fielding. 2000. Effects of digital elevation model accuracy on hydrologic predictions. *Remote Sensing Environments* 74:432-444.

Kim, I. J. 2006. Identifying the Roles of Overland Flow Characteristics and Vegetated Buffer Systems for Nonpoint Source Pollution Control. PhD diss. Kansas State University.

Kim, Y., Evans, R. G., Iversen, W., Pierce, F. J. 2006. Instrumentation and control for wireless sensor network for automated irrigation. ASABE Paper No.061105. ASABE, Portland, Oregon.

Knapp. M. 2007. Precipitation data for Riley county. Kansas State University, Weather Data Library. Manhattan, KS.

Komor, S. C. and D. S. Hansen. 2002. Attenuation of Runoff and Chemical Loads in Grass Filter Strips at Two Cattle Feedlots, Minnesota, 1995-98. *Water Resources Investigations Report. United States Geological Survey*24.

Konza Prairie Biological Station. Prairie Fires. Konza Prairie Biological Station. Konza Prairie Biological Station. Available at: http://www.konza.ksu.edu/keep/firemgt.asp#Konza. Accessed 02/05 2008.

Kuchler, A.W. 1974. A New Vegetation Map of Kansas. Ecology 55: 568-604.

Kuenstler, W. 1998. C factor: Cover-Management in Guidelines for the use of the Revised Universal Soil Loss Equation (RUSLE) version 1.06 on Mined Lands, Construction Sites, and Reclaimed Lands. Terrence Toy and George Foster eds. Office of Technology Transfer, Office of Surface Mining and Reclamation (OSM), Western Regional Coordinating Center, Denver, Colorado

Kuo, W.L., T.S. Steenhuis, C.E. McCulloch, C.L. Mohler, D.A. Weinstein, S.D. DeGloria, and D.P. Swaney. 1999. Effect of gird size on runoff and soil moisture for a variable-source-area hydrology model. *Water Resources Research* . 35 (11):3419-3428.

Kuo, W.L., T.S. Steenhuis, C.E. McCulloch, C.L. Mohler, D.A. Weinstein, S.D. DeGloria, and D.P. Swaney. 1999. Effect of gird size on runoff and soil moisture for a variable-source-area hydrology model. *Water Resources Research* . 35(11):3419-3428.

Laguna, A. and J.V. Giraldez. 1993. The description of soil erosion through a kinematic wave model. *Journal of Hydrology* 145:65-82.

Laguna, A. and J.V. Giraldez. 1993. The description of soil erosion through a kinematic wave model. *Journal of Hydrology* 145:65-82.

Lee, K. H., T. M. Isenhart, R. C. Schultz and S. K. Mickelson. 1999. Nutrient and sediment removal by switchgrass and cool-season grass filter strips in Central Iowa, USA. *Agroforestry Systems* 44(2): 121-132.

Leeds, R., L. C. Brown, M. R. Sulc and L. VanLieshout. 1994 Vegetative Filter Strips: Application, Installation and Maintenance. FactSheet AEX-467–94, Ohio State University Extension, Food, Agricultural and Biological Engineering. Ohio state university. Available at: http://ohioline.osu.edu/aex-fact/0467.html. Accessed 05/10 2007.

Leopold, L. B., Wolman, G. M., and Miller, J. P., 1964, Fluvial processes in geomorphology: Toronto, General Publishing Company Ltd., 522 p.

Leopold, L.B., and T.J. Maddock. 1953. The hydraulic geometry of stream channels and some physiographic implications. U.S. Geol. Survey Paper 252.

Lewis, Jack and Rand Eads. 1996. Turbidity-controlled suspended sediment sampling. Available at www.watershed.org/news/sum_96/turbid.html. Accessed April 1, 2007.

Lillesand, T.M. and R.W. Keifer, 1994. Remote Sensing and Image Interpretation (3rd ed). New York: Wiley.

Lim, T. T., D. R. Edwards, S. R. Workman, B. T. Larson and L. Dunn. 1998. Vegetated filter strip removal of cattle manure constituents in runoff. *Transactions of the ASAE* 41(5): 1375-1381.

Liu H., Meng, Z., Cui, S. 2007. A wireless sensor network prototype for environmental monitoring in greenhouses. WiCom 2007, Shanghai, China. 2007.

Liu, K., P. Ayers, H. Howard, and A. Anderson. 2007 Influence of turning radius on military vehicle induced rut formation. Proceedings of the Joint North America, Asia-Pacific ISTVS Conference and Annual Meeting of the Japanese Society for Terramechanics, Fairbanks, Alaska.

Liu, Q.Q. and L. Chen, J.C. Li, and V.P. Singh. 2004. Two-dimensional kinematic wave model of overland flow. *Journal of Hydrology* 291:28-41.

Loughlin, W. P. 1991. Principal Component Analysis for alteration mapping. *Photogrammetric Engineering and Remote Sensing* 57: 1163-1169.

Maa, J. P.-Y. 1988. Laboratory measurements of instantaneous sediment concentration under waves. *IEEE Journal of Oceanic Engineering* 13(4):299-302.

Maffione, R. A., and D. V. Dana. 1997. Instruments and methods for measuring the backwardscattering coefficient of ocean waters. *Appl. Opt.* 36(24): 6057-6068.

Malinga, G.A. 2007. Analyzing Effects of Low Water Fords on Stream Stability at Fort Riley, Kansas. M.S. Thesis, Kansas State University, Manhattan. 247 p.

Manov, D.V., G.C. Chang, and T. D. Dickey. 2004. Methods for reducing biofouling of moored optical sensors. *Journal of Atmospheric and Oceanic Technology* 21(6): 958-967.

Marcos, E. 2000. Comparative Analysis of Runoff and Sediment Yield with a Rainfall Simulator After Experimental Fire. *Arid Soil Research and Rehabilitation* 14(3): 293-307.

Martínez-Casasnovas, J.A. 2003. A spatial information technology approach for the mapping and quantification of gully erosion. *Catena* 50:293-308.

Martínez-Casasnovas, J.A., C. Antón-Fernández, and M. C. Ramos. 2003. Sediment production in large gullies of the Mediterranean area (NE Spain) from high-resolution digital elevation models and geographical information systems analysis. *Earth Surface Processes and Landforms* 28(5):443-456.

Martínez-Casasnovas, J.A., M.C. Ramos, and J. Poesen. 2004. Assessment of sidewall erosion in large gullies using multi-temporal DEMs and logistic regression analysis. *Geomorphology* 58:305-321.

Martínez-Casasnovas, J.A., M.C. Ramos, and J. Poesen. 2004. Assessment of sidewall erosion in large gullies using multi-temporal DEMs and logistic regression analysis. *Geomorphology* 58:305-321.

Martínez-Casasnovas, J.A., M.C. Ramos, and M. Ribes-Dasi. 2002. Soil erosion caused by extreme rainfall events: mapping and quantification in agricultural plots from very detailed digital elevation models. *Geoderma* 105: 125–140.

MATLAB. 2006. M*atrix Laboratory*. Ver. 7.3.0.267 (R2006b). Natick, MA: The MathWorks, Inc.

Mau, D.P. 2001. Sediment deposition and trends and transport of phosphorus and other chemical constituents, Cheney Reservoir watershed, south-central Kansas. USGS Water-Resources Investigations Report 01-4085. Lawrence, KS.

MaxStream, 2008. RF Modem. Available at: www.maxstream.net Accessed 20 Feb. 2008.

McCabe, J.M., and C.L. Sandretto. 1985. Some Aquatic Impacts of Sediment, Nutrients, and Pesticides in Agricultural Runoff. Publication No. 201. Limnological Research Laboratory, Dept. of Fisheries and Wildlife, Michigan State University.

Mccuen, R. H. 1998. *Hydrologic analysis and design*, second edition. Prentice-Hall. Englewood Cliffs, Upper Saddle Rive, NJ.

McCuen, R.H. and J.M. Spiess. 1995. Assessment of kinematic wave time of concentration. *Journal of Hydrologic Engineering* 121(3):256-266.

McCuen, R.H. and J.M. Spiess. 1995. Assessment of kinematic wave time of concentration. *Journal of Hydrologic Engineering* 121(3):256-266.

McCuen, R.H. and J.M. Spiess. 1995. Assessment of kinematic wave time of concentration. *Journal of Hydrologic Engineering* 121(3):256-266.

McMaster, K.J. 2002. Effects of digital elevation model resolution on derived stream network positions. *Water Resources Research* 38(4):13-1~13-9.

McMaster, K.J. 2002. Effects of digital elevation model resolution on derived stream network positions. *Water Resources Research* 38(4):13-1~13-9.

Mendez, A., T. A. Dillaha and S. Mostaghimi. 1999. Sediment and nitrogen transport in grass filter strips. *Journal of the American Water Resources Association* 35(4): 867-875.

MeteorComm, 2008. Wireless communications for a changing world. Available at: www.meteorcomm.com Accessed 20 Feb. 2008.

Meyer, A. and J.A. Martínez-Casasnovas. 1999. Prediction of existing gully erosion in vineyard parcels of the NE Spain: a logistic modeling approach. *Soil and Tillage Research* 50:319-331.

Meyer, A. and J.A. Martínez-Casasnovas. 1999. Prediction of existing gully erosion in vineyard parcels of the NE Spain: a logistic modeling approach. *Soil and Tillage Research* 50:319-331.

Meyer, L.D., S.M. Dabney, C.E. Murphree, W.C. Harmon, and E.H. Grissinger. 1999. Crop production systems to control erosion and reduce runoff from upland silty soils. *Transactions of the ASAE* 42(6):1645-1652.

Meyer, L.D., S.M. Dabney, C.E. Murphree, W.C. Harmon, and E.H. Grissinger. 1999. Crop production systems to control erosion and reduce runoff from upland silty soils. *Transactions of the ASAE* 42(6):1645-1652.

Milauskas, S.J.1988. Low water stream crossing options for haul roads. Southern J. Applied Forestry.12 (1):11-15.

Mitasova, H., Hofier, J., Zlocha, M., and Iverson, L.R. 1996. Modeling topographic potential for erosion and deposition using GIS. *International Journal Geographical Information Systems*. 10(5): 629-641.

Mizaikoff, B. 2003. Infrared optical sensors for water quality monitoring. *Water Science and Technology* 47(2): 35-42.

Moglen, G.E. and G.L. Hartman. 2001. Resolution effects on hydrologic modeling parameters and peak discharge. *Journal of Hydrologic Engineering* 6:490-497.

Montgomery, D.R. and W.E. Dietrich. 1988. Where do channels begin? *Nature* 336:232-234.

Montgomery, D.R. and W.E. Dietrich. 1989. Source areas, drainage density, and channel initiation. *Water Resources Research* 25(8):1907-1918.

Montgomery, D.R. and W.E. Dietrich. 1989. Source areas, drainage density, and channel initiation. *Water Resources Research* 25(8):1907-1918.

Montgomery, D.R. and W.E. Dietrich. 1992. Channel Initiation and the Problem of Landscape Scale. *Science* 255:826-830.

Moore, I.D., G.J. Burch, and D.H. Mackenzie. 1988. Topographic effects on the distribution of surface soil water and the location of ephemeral gullies. *Transactions of the ASAE* 31(4):1098-1107.

Moore, I.D., R.B. Grayson, and A.R. Ladson. 1991. Digital terrain modeling: a review of hydrological, geomophological, and biological applications. *Hydrological process* 5:3-30.

Moran, S.M., T.R. Clarke, Y. Inoue, and A. Vidal. 1994. Estimating Crop Water Deficit using the Relationship between Surface-Air Temperature and Spectral Vegetation Index. Remote Sensing of the Environment 49: 246-263.

Murren, C. 1993. Turbidity and particles in water and waste. *Control and Instrumentation* 25(6): 35-36.

Myers, T.J., and Swanson, S., 1992, Variation of stream stability with stream type and livestock bank damage in Northern Nevada: Water Resource Bulletin, v. 28, no. 4, p. 743-754.

Nearing, M.A., Lane, L.J., Lopes, V.L. 1994. in Soil Erosion Research Methods. *Modeling Soil erosion*. ed. Lal, R., Ch. 6:127-158, 2nd ed. St. Lucie Press, Delray, Florida.

Neary, D. G., K. C. Ryan and L. F. DeBano. 2005. Wildland Fire in Ecosystems: Effects of Fire on Soil and Water, USDA Forest Service, Ogden, Utah.

Nebel, B. J. and R. T. Wright. 1998. *Environmental Science: The Way the World Works.* Prentice Hall PTR, 102-103.

Nemani, R., L. Pierce, and S. Running. 1993. Developing Satellite-derived Estimates of Surface Moisture Status. Journal of Applied Meteorology 32: 548-557.

Nemani, R.R. and S.W. Running. 1989. Estimation of Regional Surface Resistance to Evapotranspiration from NDVI and Thermal-IR AVHRR Data. Journal of Applied Meteorology 28: 276-284.

Newbury. R.W, M.N. Gabor and D.J. Bates. 1997. Creating habitats in channelized or uniform streams using riffles and pools. Stream Restoration Manual, British Columbia Forest Renewal Program, Victoria, BC.

Newcombe, C.P. and D.D. MacDonald. 1991. Effects of Suspended Sediments on Aquatic Ecosystems. North American Journal of Fisheries Management. 11: 72-82.

Newham, L. T. H., J. C. Rutherford and B. F. W. Croke. 2005. A conceptual model of particulate trapping in riparian buffers, CSIRO Land and Water Technical Report, Canberra, Australia.

Nortel 2007: Nortel WiMAX 802.16e Portfolio. Available at: telstarint.com/Nortel%20Wimax_files/Nortel%20mobile.pdf Accessed 18 Mar. 2008.

O'Callaghan, J.F. and D.M. Mark. 1984. The extraction of drainage networks from digital elevation data. *Computer Vision, Graphics, and Image processing* 28:323-344.

Omernik, J. M. 1987. Ecoregions of the continuous United States. Map (scale 1:7,500,000). *Annals of the Association of American Geographers* 77(1): 118-125.

Omernik, J. M. 1995. *Ecoregions*: A spatial framework for environmental management. In: Biological Assessment and Criteria: Tools for Water Resource Planning and Decision Making. Edited by Davis, W.S. and T.P. Simon. Lewis Publishers, Boca Raton, FL.

Omernik, J.M. 1987. Ecoregions of the Conterminous United States. Map (scale 1:7,500,000). Annals of the Association of American Geographers 77(1):118-125.

O'Neill, P.E., N.S. Chauhan, and T.J. Jackson. 1996. Use of Active and Passive Microwave Remote Sensing for Soil Moisture Estimation through Corn. International Journal of Remote Sensing 17(10):1851-1865.

O'Neill, P.E., T.J. Jackson, N.S. Chauhan, and M.S. Seyfried. 1993. Microwave Soil Moisture Estimation in Humid and Semi-humid Watersheds. Advances in Space Research 13(5):115-118.

OPTIMO. 2004. Fundamental science: Characterization of coloured suspensions using scattered light - clarifying diagnostics in process production and quality control: Available at: http://optimo.lboro.ac.uk/science.html. Accessed 10 Aug. 2004.

Owensby, C. E. and J. Wyrill. 1973. Effects of range burning on Kansas Flint Hills Soil. *Journal of Range Management* 26(3): 185-188.

Papadopoulou, A.A., A.A. Mouza, S.V. Paras and A.J. Karabelas. 1998. A new turbidity meter for monitoring the quality of water. July 1998: Available at: http://philon.cheng.outh.gr/sites/docs/s19.pdf. Accessed 10 July 2003.

PC208W. 2000. *PC208W*. Ver. 3.1a. Logan, UT: Campbell Scientific, Inc.

Pfankuch, D.J., 1975, Stream reach inventory and channel stability evaluation: USDA Forest Service, Washington DC, US Government Printing Office, no. 696, 26 p.

Pierson, F. B., P. R. Robichaud, K. E. Spaeth and C. A. Moffet. 2003. Impacts of fire on hydrology and erosion in steep mountain big sagebrush communities. *Proceedings of the First Interagency Conference on research in the Watersheds* 625-630.

Pope, L.M., and C.R. Milligan. 2002. Sources and concentrations of phosphorus in the Cheney Reservoir watershed, south-central Kansas. USGS Fact Sheet 010-02. Lawrence, KS

Postolache, O., P. Girao, M. Pereira, H. Ramos. 2002. An IR turbidity sensor: Design and application. In *Proceedings of the 19th IEEE,* 535- 539. New York, NY: IEEE.

Quist, M.C., Fay, P.A., Guy, C.S., Knapp, A.K., Rubenstein, B.N. 2003. Military training effects on terrestrial and aquatic communities on a grassland military installation. *Ecological Applications.* 13(2): 432-442.

Quist, M.C., P.A. Fay, S.G. Christopher, A.K. Knapp, and B.N. Rubensteini. 2003. Military training effects on terrestrial and aquatic communities on grassland military installation. *Ecological Applications* 13(2), 2003, pp. 432–442

Quyang D. and Bartholic, J. 2001. Web-Based Application for Soil Erosion Prediction. Proceedings of an International Symposium – Soil Erosion Research for the 21st Century. Honolulu, Hi. American Society of Agricultural Engineers Paper. Institute of Water Research, Michigan State University.

Ragan, R.M. and J.O. Duru. 1972. Kinematic wave nomograph for times of concentration. *Journal of Hydrologic Engineering* 98(10):1765-1771.

Ravens, T.M. and P.H. Gschwend. 1999. Flume measurement of sediment erodibility in Boston Harbor. *Journal of Hydrologic Engineering* 125(10):998-1005.

Rawls, W. J., D. L. Brakensiek and B. Soni. 1983a. Agricultural Management Effects on Soil Water Processes; Part I: Soil Water Retention and Green and Ampt Infiltration Parameters. *Transactions of the American Society of Agricultural Engineers* 26(6): 1753-1759.

Rawls, W. J., D. L. Brakensiek and N. Miller. 1983b. Green-Ampt Infiltration Parameters from Soils Data. *Journal of Hydraulic Engineering* 109(1): 62-70.

Renard, K.G., Foster, G.R., Weesies, G.A., McCool, D.K., Yoder, D.C. 1997. Predicting Soil Erosion by Water: A Guide to Conservation Planning with the Revised Universal Soil Loss Equation (RUSLE). Agricultural Handbook 703. United States Department of Agricultural.

Renard, K.G., Laflen, J.M., Foster, G.R., and D.K. McCool. 1994. in Soil Erosion Research Methods. *The Revised Universal Soil Loss Equation*. ed. Lal, R., Ch. 5:105-124, 2nd ed. St. Lucie Press, Delray, Florida..

Rice, M. K., and P. D. Ayers. 2005. Evaluation of Tracking Study for Maneuvers performed at Fort Riley, Kansas Military Installation in May of 2005. Research Report Submitted to Fort Riley Military Installation.

Rice, M., P. Ayers, A. Anderson, and L. Randolph. 2006. Assessment of ecological impacts of military maneuvers in training areas. Paper No. 067013 presented at the 2006 ASABE Annual International Meeting. ASABE, 2950 Niles Rd., St. Joseph, MI 49085-9659.

Ridd, P., and P. Larcombe. 1994. Biofouling control for optical backscatter suspended sediment sensors. *Marine Geology* 116(1994): 255-258.

Riley, S. J. 1998. The sediment concentration-turbidity relation: its value in monitoring at Ranger Uranium Mine, Northern Territory, Australia. *Catena* 32(1): 1-14.

Riley, S.J. 1998. The sediment concentration-turbidity relation: Its value in monitoring at Ranger Uranium Mine, Northern Territory, Australia. Cantena. 32: 1-14.

Ritchie, J.C. and C.M. Cooper. 2001. Remote sensing techniques for determining water quality: applications to TMDLs. pp. 367-373. In: TMDL Science Issues Conference, Water Environment Federation, Alexandria, VA: Available at: http://www.wef.org/pdffiles/TMDL/Ritchie.pdf. Accessed 1 Sept. 2004.

Ritchie, J.C., F.R. Schiebe, C.M. Cooper and J.A. Harrington, Jr. 1994. Chlorophyll measurements in the presence of suspended sediment using broad band spectral sensors aboard satellites. *Journal of Freshwater Ecology*. 9: 197-206.

Robichaud, P. R. 2000. Fire effects on infiltration rates after prescribed fire in Northern Rocky Mountain forests, USA. *Journal of Hydrology(Amsterdam)* 231(1): 220-229.

Rockers, J.J., I. Ratcliff, L.W. Doed, and E.F. Bouse. 1966, Soil survey of Reno County, Kansas: U.S. Department of Agriculture, Soil Conservation Service. Washington D.C.

Roo, A.P.J. 1998. Modelling runoff and sediment transport in catchments using GIS. *Hydrological Processes* 12(6):905-922.

Rosenblatt, A.E., A.J. Gold, M.H. Stolt, P.M. Groffman, and D.Q. Kellog. 2001. Identifying riparian sinks for watershed nitrate using soils surveys. *Journal of Environmental Quality* 30:1596-1604.

Rosgen, D. L., 1996, Applied river morphology: Pagosa Springs, Wildland Hydrology, 343 p.

Rosgen, D.L. 2001. A practical method of computing stream bank erosion rate.7th Federal Interagency Sediment Conference, March 24-29, Reno, Nevada.

Rosgen, D.L. 2006. Watershed Assessment of River Stability and Sediment Supply (WARSSS). Fort Collins, CO.: Wildland Hydrology Books.

Rosgen, D.L. 2007. River Morphology Applications: Field Course, Bend, Oregon. Fort Collins, CO.: Wildland Hydrology.

Ruffner. J.A and F.E. Bair. 1974. The weather almanac, a reference guide to weather and climate of United States and its key cities. Detroit MI. Gale Research Company.

Sadar, M. 2002. Turbidity Instrumentation – An Overview of Today's Available Technology. Reston, VA: USGS, Office of Surface Water. Available at: water.usgs.gov/osw/techniques/TSS/sadar.pdf. Accessed 20 April 2007.

Sadar, M. 2002. Turbidity instrumentation – an overview of today's available technology. May 2002: Available at: http://water.usgs.gov/osw/techniques/ TSS/sadar.pdf. Accessed 16 Feb. 2003.

Sadar, M. J. and T. L. Engelhardt. 2003. Determining correlation of nephelometric turbidity measurement to suspended solids in industrial samples: Available at: http://www.hach.com/cs/knowledge-pdfs/TurbidityandSuspendedSolids.pdf. Accessed 10 July 2003.

Sadar, M. J., and T. L. Engelhardt. 1993. Determining Correlation of Nephelometric Turbidity Measurements to Suspended Solids Measurements in Industrial Samples. Cesena, Italy: Communication Technology. Available at: www.comm-tec.com/. Accessed 20 April 2007.

Sample, L. J., Steichen, J., and Kelley, J. R. Jr., 1998, Water quality impacts from low water fords on military training lands: Journal of the American Water Resources Association, v. 34, no. 4, p. 939-949.

Sanderson, M. A., R. M. Jones, M. J. McFarland, J. Stroup, R. L. Reed and J. P. Muir. 2001. Nutrient movement and removal in a switchgrass biomass-filter strip system treated with dairy manure. *Journal of environmental quality* 30(1): 210-216.

SAS Institute. 2002. SAS 9.0 Users guide. SAS Institute, Inc., Cary, NC.

SatWest, 2008. Satellite network systems. Available at: www.satwest.com Accessed 20 Feb. 2008.

Schmid, F. J. 1996. Assessment of Nonpoint Source (NPS) pollution Potential at Military Bases. Public Works Technical Bulletin 420-46-5A1-C5.

Schmitt, T. J., M. G. Dosskey and K. D. Hoagland. 1999. Filter strip performance and processes for different vegetation, widths, and contaminants. *Journal of environmental quality* 28(5): 1479-1489.

Schwab, A.P., P. Splichal, and L.S. Solon. 1993. Factors affecting the soil extraction and preconcentration by $C_{18}$ solid-phase enrichment of alachlor, atrazine, and atrazine dealkylation products. P. 86-92. *In* K.B. Hoddinott and T.A. O'Shay (eds.) Application of agricultural analysis in environmental studies. ASTM Publication STP 1162. Philadelphia, PA.

Sharpley, A. and P. Kleinman. 2003. Effect of Rainfall Simulator and Plot Scale on Overland Flow and Phosphorus Transport. *Journal of Environmental Quality* 32:2172-2179.

Sherwani, J.K., and D.H. Moreau. 1975. Strategies for Water Quality Monitoring. Report No. 107. Water Resources Research Institute of the University of North Carolina, Raleigh, NC.

Shields, A., 1936. Application of similarity principles and turbulence research to bed- load movement. In: Ott, W.P. and Unchelen, J.C. (Translators), Mitteilungen der preussischen Nersuchsanstalt fur Wassed Brau end Schiffbuar. Report 167. Pasadena, CA. California Institute of Technology.

Singh, V. P. 2001. Kinematic wave modelling in water resources: a historical perspective. *Hydrological Processes.* 15(4):671-706

Singh, V. P. 2001. Kinematic wave modelling in water resources: a historical perspective. *Hydrological Processes.* 15(4):671-706

Smith, R.L. 1990. Ecology and Field Biology. 4th ed. Harper Collins Publishers, NY.

Soil Testing Laboratory at Kansas State University. 2005. Procedures for analysis of water samples. Department of Agronomy, Kansas University. Kansas State University. Available at: http://www.oznet.ksu.edu/Agronomy/SoilTesting/w_analysis_offered.htm. Accessed 02/05 2008.

Spooner, J., S.W. Coffey, J.A. Gale, A.L. Lanier, S.L. Brichford, and M.D. Smolen. 1991. NWQEP Report: Water Quality Monitoring Report for Agricultural Nonpoint Source Pollution Control Projects - Methods and Findings from the Rural Clean Water Program. North Carolina State University, Biological and Agricultural Engineering Department, Raleigh.

St. Clair, A. K. 2007. Suitability of tallgrass prairie filter strips for control of non-point source pollution originating from military activities. Masters diss. Manhattan, Kansas, USA: Kansas State University.

State Conservation Commission (SCC) and Tetra Tech Inc. 2005. Assessment of geomorphic definition and documentation of Kansas stream corridor reference reaches. Kansas City, KS.

Stoll, Q. M. 2004. Design of a real-time, optical sediment concentration sensor. MS thesis. Manhattan, Kansas: Kansas State University, Department of Biological and Agricultural Engineering.

Stoll, Quentin. 2004. Design of a real-time optical sediment concentration sensor. MS thesis. Manhattan, Kansas: Kansas State University, Department of Biological and Agricultural Engineering.

Story, M., and R. Congalton. 1986. Accuracy assessment: A user's perspective. *Photogrammetric Engineering & Remote Sensing* 52(3):397-399.

Strategic Environmental Research and Development Program (SERDP). 2006. SERDP home page. http://www.serdp.org. Last accessed May 19, 2006.

Striffler, W.D. 1965. The Selection of Experimental Watersheds and Methods in Disturbed Forest Areas. In Publication No. 66 of the I.A.S.H. Symposium of Budapest.

Tarboton, D.G., R.L. Bras, and I. Rodriguez-Iturbe. 1991. On the extraction of channel networks from digital elevation model. *Hydrological Processes* 5:81-100.

Teledyne ISCO. 2005. *730 Bubbler module-Installation and operation guide.* Teledyne ISCO.

Thompson, J.D., S.E. Taylor, J. E. Gazin, R.B. Rummer, and R. A. Albright. 1996. Water quality impacts from low water stream crossings. Technical Paper No.96-5015. ASABE, 2950 Niles Road, St. Joseph, MI 49085-9659 USA.

Trame, Ann-Marie. 1997. Known and potential impacts of physical disturbance from maneuver training on threatened and endangered species. *USACERL Technical Report 97/70*, US Army Corps of Engineers. Construction Engineering Research Laboratories, Champaign, Illinois.

Tucker, C.J. 1979. Red and Photographic Infrared Linear Combinations for Monitoring Vegetation. Remote Sensing of the Environment 8: 127-150.

Tucker, G.E. and R.L. Bras. 1998, Hillslope processes, drainage density, and landscape morphology. *Water Resources Research*, 34:2751-2764.

Tufekcioglu, A., J. W. Raich, T. M. Isenhart and R. C. Schultz. 1999. Fine root dynamics, coarse root biomass, root distribution, and soil respiration in a multispecies riparian buffer in Central Iowa, USA. *Agroforestry Systems* 44(2): 163-174.

Tweddale, Scott A., Echlschlaeger, Charles R., Seybold, William F. 2000. An improved method for spatial extrapolation of vegetation cover estimates (USLE/RUSLE C factor) Using LCTA and remotely sensed imagery. *USAEC Report #SFIM–AEC-EQ-TR-200011* U.S. Army Environmental Center.

U.S. EPA, 2006. Watershed Assessment of River Stability and Sediment Supply (WARSSS). Version 1.0. Washington, DC. U.S EPA. Available at www.epa.gov/warsss. Accessed on 02 April 2007.

Ulaby, F.T., P.C. Dubois, and J. van Zyl. 1996. Radar Mapping of Surface Soil Moisture. Journal of Hydrology 184:57-84.

United States Forest Service, 1994, Stream channel reference sites: An illustrated guide to field technique: United States Department of Agriculture General Technical Report RM-245, 61 p.

United States Geological Service (USGS). 2005. Land Processes Distributed Active Archive Center. MODIS/Terra Vegetation Indices 16 Day L3 Global 250m ISIN Grid.

USDA. Web Soil Survey. USDA-NRCS. Kansas State University. Available at: http://websoilsurvey.nrcs.usda.gov/app/WebSoilSurvey.aspx. Accessed 11/23 2007.

USDA-NRCS. 2003. Filter strip CODE 393. In *National Conservation Practice Standards,* ed. Anonymous , USDA-NRCS.

USDA-NRCS. 2004. Illinois Native Plant Guide. USDA-NRCS. Available at: http://www.il.nrcs.usda.gov/technical/plants/npg/index.html. Accessed 12/10 2007.

USDA-NRCS. National Conservation Practice Standars. USDA-NRCS. Available at: http://www.nrcs.usda.gov/technical/Standards/nhcp.html. Accessed 01/29 2008.

USEPA. 2000. National Water Quality Inventory. Available at: http://www.epa.gov/305b/2000report. Last accessed May 16, 2007.

USEPA. 1991b. Watershed Monitoring and Reporting for Section 319 National Monitoring Program Projects. U.S. Environmental Protection Agency, Office of Water, Washington, DC.

USEPA. 2003. Introduction to clean water act. USEPA. USEPA. Available at: http://www.epa.gov/watertrain/cwa/index.htm. Accessed 01/29 2008.

USEPA. 2007. National Water Quality Inventory: 2002 Report. Office of Water, Washington DC.

Vandekerckhove, L., J. Poesen, D.O. Wijdenes, J. Nachtergaele, C. Kosmas, M.J. Roxo, and T. Figueiredo. 2000. Thresholds for gully initiation and sedimentation in Mediterranean Europe. *Earth Surface Processes and Landforms* 25(11):1201 – 1220.

Vermont Agency of Natural Resources. 2003. Vermont Stream Geomorphic Assessment, Phase 3 Handbook, Survey Assessment, Field and Data Analysis Protocols. Waterbury, VT.

Walker, J.P. and G.R. Willgoose. 1999. On the effect of digital elevation model accuracy on hydrology and geomorphology. *Water Resources Research* 35(7):2259-2268.

Wang, N., Zhang, N. Wang, M. 2006. Wireless sensors in agriculture and food industry – Recent development and future perspective. Computers and Electronics in Agriculture. 50 (1), 1-14.

Wang, X., Poor, H.V., 2003. Wireless Communication Systems: Advanced Techniques for Signal Reception. Prentice Hall.

Ward, A. D. and S. W. Trimble. 2004. Chapter 9: Soil conservation and sediment budgets. In *Environmental Hydrology,* 255-290.CRC Press.

Ward, Andy D. and William J. Elliot. 1995. Environmental Hydrology. New York: Lewis Publishers.

Wardlow, B.D. and S.L. Egbert. 2003. A State-level comparative analysis of the GAP and NLCD Land-cover data sets. *Photogrammetric Engineering and Remote Sensing* 69(12):1387-1397.

Wardlow, B.D. and S.L. Egbert. 2003. A State-level comparative analysis of the GAP and NLCD Land-cover data sets. *Photogrammetric Engineering and Remote Sensing* 69(12):1387-1397.

Warren, S.D. and C.F. Bagley. 1992. SPOT imagery and GIS in support of military land management. *GeoCarto International* 7(1): 35-43.

Willgoose, G. and G. Kuczera. 1994. Estimation of subgrid kinematic wave parameters for hillslopes. *Hydrological Processes* 9:469-482.

Wilson, J.P. and J.C. Gallant, ed. 2000. *Digital terrain analysis, Terrain analysis: principle and applications*: Edited by Wilson, J.P. and J.C. Gallant, John Wiley and Sons, New York, NY.

Wischmeier, W.H. and Smith, D.D. 1965. Predicting rainfall erosion losses from cropland east of the Rocky Mountains. Agricultural Handbook 282. Agricultural Research Service, United States Department of Agriculture, Washington DC, USA.

Wolman, J.G. and L.B. Leopold. 1957. River flood plains: some observations on their formation. U.S. Geological Survey Professional Paper 282-C.

Wolman, M.G. 1954. A method of sampling coarse river bed material. Transactions of the American Geophysical Union. 35(6): 651-956.

Wolman, M.G., 1954, A method of sampling coarse river-bed material, Transactions, American Geophysical Union, v. 35, no. 6, p. 951-956.

Wong, T.S.W. 2005. Assessment of time of concentration formulas for overland Flow. *Journal of Irrigation and Drainage Engineering* 131(4):383-387.

Wong, T.S.W. and C.N. Chen 1999. Time of Concentration Formula for Sheet Flow of Varying Flow Regime. *Journal of Hydrologic Engineering* 2(3):136-139.

Wong, T.S.W. and C.N. Chen 1999. Time of Concentration Formula for Sheet Flow of Varying Flow Regime. *Journal of Hydrologic Engineering* 2(3):136-139.

Wren, D. G., B. D. Barkdoll, R. A. Kuhnle and R. W. Derrow. 2000. Field techniques for suspended-sediment measurement. *Journal of Hydraulic Engineering* 126(2): 97-104.

WTW. 2007. Turbidity and Suspended Solids. West Wareham, MA: WTW, Inc. Available at: www.wtw.com. Accessed 13 January 2007.

Yang L., Giannakis, G.B., 2004. Ultra-wideband communications: an idea whose time has come. IEEE Signal Processing Magazine. 21 (6), 26-54.

Zaimes, G.N., Schultz, R.C., and Isenhart, T.M., 2004, Stream bank erosion adjacent to riparian forest buffers, row-crop fields, and continuously-grazed pastures along Bear Creek in central Iowa: Journal of Soil and Water Conservation, v. 59, no. 1, p. 19-27.

Zeverbergen, L.W. and C.R. Thorne. 1987. Quantitative Analysis of Land Surface Topography. *Earth Surface Processes and Landforms* 12:47-56.

Zeverbergen, L.W. and C.R. Thorne. 1987. Quantitative Analysis of Land Surface Topography. *Earth Surface Processes and Landforms* 12:47-56.

Zhang, W. and D. Montgomery. 1994. Digital elevation model grid size, landscape representation, and hydrologic simulations. *Water Resources Research* 30 (4):1019-1028.

Zhang, W., and D. Montgomery. 1994. Digital elevation model grid size, landscape representation, and hydrologic simulations, *Water Resources Research* 30(4): 1019-1028.

Zhang, Y., N. Zhang, Q. Stoll, D. Oard, J. Steichen, P. Woodford, P. Barnes, and S. Hutchinson. 2006. Monitoring sediment concentration at a low-water stream crossing using an optical sediment sensor. ASABE Paper No. 063091. St. Joseph, Mich.: ASABE.

Zhang, Y., Zhang, N., Grimm, G., Johnson, C., Oarrd, D. Steichen, J. 2007. Long-term field test of an optical sediment-concentration sensor at low-water stream crossings (LWSC). ASABE Paper No. 072137. St. Joseph, Mich.: ASABE.

Zhang, Z., 2004. Investigation of wireless sensor networks for precision agriculture. ASABE Paper No: 041154. ASABE, Ottawa, Ontario, Canada.